An Investigation into the Formation of a Variety of C_3 Organometallic Species via the Isomerisation of Alkynes by Ruthenium (II) and Rhodium (I) Complexes

Elizabeth J. Smith

PhD

University of York

Chemistry

April 2014

Abstract

A novel synthetic route for the formation of ruthenium complexes $[Ru(\kappa^2\text{-}OAc)_2(PR_3)_2]$ **1** has been developed. These complexes have been used to investigate the stoichiometric formation of geminal alkenes from the reaction of triphenylphosphine complex $[Ru(\kappa^2\text{-}OAc)_2(PPh_3)_2]$ **1a** with propargylic alcohols. It was found that the reaction was promoted by the use of the bulky, electron-rich triisopropylphosphine. This lead to the proposal that the mechanism involves a cationic intermediate and the suggested structure of this intermediate was vinyl carbene $[Ru(\kappa^2\text{-}OAc)(OC\{Me\}OCC\{H\}=CH_2)(PPh_3)_2][BF_4]$ **26**.

A series of analogues of **26** were synthesised and their reactivity investigated. Whilst no evidence was obtained of their being involved in the transformation of propargylic alcohols to alkenes, it was found that their reactivity can be tuned by changing the substituents on the vinyl moiety. Deprotonation leads to the formation of either the allenylidene complex $[Ru(\kappa^2\text{-}OAc)(\kappa^1\text{-}OAc)(PPh_3)_2(=C=C=CPh_2)]$ **30** or the vinyl vinylidene complexes $[Ru(\kappa^2\text{-}OAc)(\kappa^1\text{-}OAc)(PPh_3)_2(=C=CH\text{-}C(R)=CH_2)]$ **32** (R = Ph, Me). A theoretical investigation into this reaction has led to the suggestion that vinyl carbene complexes like **26** could be important reaction intermediates in the formation of allenylidenes from propargylic alcohols.

The reactivity of **1a** towards the triphenylphosphine-substituted alkyne $[HC{\equiv}CCH_2PPh_3]^+$ **39** has also been investigated. It has been found that this propargylic phosphonium is particularly prone to isomerisation to its allene isomer $[H_2C=C=CHPPh_3]^+$ **40** and, as a result, reaction with organometallic precursors leads primarily to the formation of the allene complexes $[Ru(\kappa^2\text{-}OAc)(\kappa^1\text{-}OAc)(\eta^2\text{-}H_2C=C=CHPPh_3)(PPh_3)_2][BF_4]$ **45a** and $[RhCl(\eta^2\text{-}H_2C=C=CHPPh_3)(P^iPr_3)_2][BPh_4]$ **60**. Experimental and theoretical investigations have concluded that the isomerisation is spontaneous (the allene is 37 kJ mol^{-1} more stable than the alkyne) and not metal promoted. It is however counter-ion dependant and use of the tetraphenylborate salt **39c** slows the process enough for novel vinylidene complexes $[Ru(\kappa^2\text{-}OAc)(\kappa^1\text{-}OAc)(C=C=CHCH_2PPh_3)(PPh_3)_2][BPh_4]$ **38** and $[RhCl(C=C=CHCH_2PPh_3)(P^iPr_3)_2][BPh_4]$ **63** to be synthesised.

.

Contents

List of Figures

List of Schemes

List of Tables

List of accompanying material

A CD is attached inside the back cover which contains the crystallographic information files (CIFs) for the crystallography and the XYZ coordinates for the theoretical calculations.

Acknowledgments

Thank you Jason! You have been the driving force behind this project, endlessly patient, understanding and, above all, enthusiastic. Your guidance and advice (even when it was Lego based) was always kindly given and invaluable. I cannot thank you enough.

I must also thank Christine for giving this project such a brilliant start in life, and for so graciously allowing me to take stewardship of it.

Then there are all the SLUGs around me who have made every day different and enjoyable. Thank you to Neets, Sharifa, Aimee, Dave, Richard, Lucy, Luisa, Sam, Iman, Chris, Sham, Lucia and all our project students for the advice, gossip, decorating my desk when I've been scooped, and generally putting up with me. And thanks to the non-SLUGs, Dan, Linda, Andy, Jon, Natalie, Danielle, Tom, Chris, Jess, Robs 1 & 2 and Ellis who made sure I took the occasional lunch break and fed me lots of cake.

Much of the work in this thesis would not have been possible without our experimental technicians. Thanks to Naser for running everything, Heather and Pedro in NMR, Karl and Helen in mass spec, Graeme for CHN and in particular to the wonderfully patient Adrian, Sam, Natalie and Rob in XRD. I must also thank those working in the departmental workshops; special thanks go to Abby and Brian in glassblowing for encouraging my interest in their work.

There are also those who have supported me outside of the chemistry department. Massive thanks go to Steve for taking me to the pub, Helen for showing me how the other half live and Debs for being my non-PhD friend, and for letting me beat her at Carcassonne.

Apologies go to my family for the lack of contact and visits, normal service will resume soon. I must however acknowledge my Mothers role in keeping me sane, thank you for letting me cry down the phone at you, rant about things you don't understand, posting me increasingly bizarre presents and for learning what a glovebox is.

Nick, thank you for everything. You have been so supportive and are probably the only person in the world, outside of my lab, who actually knows what I do. Thank you for caring about me, my project, my football team and for putting it all into perspective. I look forward to our thesis free future.

Author's Declaration

I hereby declare that the work described in this thesis was conducted in the Department of Chemistry at the University of York between October 2010 and March 2014 under the supervision of Dr Jason M. Lynam. The work described was conducted by myself. The research presented here is, to the best of my knowledge, original except where due credit has been given to fellow authors listed below. This work has not previously been presented for an award at this, or any other, university. Some of the work has been previously published in the following peer-reviewed articles:

- Computational Discovery of Stable Transition Metal Vinylidene Complexes; I. Khazal, O. J. S. Pickup, E. J. Smith, A. C. Whitwood, J. M. Lynam, K. Bolaky, T. R. King, B. W. Rawe and N. Fey, Organometallics, 2014, **33**, 1751-1761.

- Mapping the Elimination of Water from Hydroxyvinylidene Complexes of Ruthenium(II): Access to Allenylidene and Vinylvinylidene Complexes in a Stepwise Fashion; E. J. Smith, D. G. Johnson, R. J. Thatcher, A. C. Whitwood and J. M. Lynam, *Organometallics*, 2013, **32**, 7407-7417.

- Ruthenium Acetate Complexes as Versatile Probes of Metal–Ligand Interactions: Insight into the Ligand Effects of Vinylidene, Carbene, Carbonyl, Nitrosyl and Isocyanide; C. E. Welby, T. O. Eschemann, C. A. Unsworth, E. J. Smith, R. J. Thatcher, A. C. Whitwood and J. M. Lynam, *Eur. J. Inorg. Chem.*, 2012, 1493-1506.

Elizabeth J. Smith

1. Introduction

1.1 Alkyne isomerisation

The transformation of hydrocarbons into higher value chemicals containing useful functional groups has long been an aim of synthetic chemists. Alkanes are particularly unreactive, but the π-bonding present in unsaturated hydrocarbons leads to an increase in reactivity.[1] Alkenes and aromatic systems are produced in large volumes by the petrochemical industry and have become ubiquitous in synthetic chemistry. Alkynes have traditionally been viewed as being less common, both in the natural world and in synthetic chemistry.[2] The recent development of new synthetic methods which utilise alkynes as precursors is beginning to change this opinion (Scheme 1-1). The alkyne triple bond is one of the strongest covalent bonds known, with acetylene having a bond dissociation energy of 835 kJ mol^{-1} (cf. ethene = 611 kJ mol^{-1}, ethane = 376 kJ mol^{-1}).[2] As a result of this, the cleavage of alkyne is often viewed as a challenge.[3, 4] Alkynes however have a wide range of reactivity, far more so than the comparatively weak C-C bonds in alkanes. Courtesy of their π-electrons alkynes commonly undergo addition and oxidation reactions in a similar fashion to alkenes. Terminal alkynes can also be deprotonated to form acetylide species which have found widespread use in synthetic chemistry.[5]

Alkynes are excellent ligands for transition metals and exploration of this has led to a range of reactivities.[4] Some of the more famous examples revolve around previously mentioned acetylide chemistry, in particular copper acetylides. They are important intermediates in the Sonogashira palladium cross-coupling reaction[6] and copper catalysed azide-alkyne cycloaddition "click" reactions (Scheme 1-1).[7]

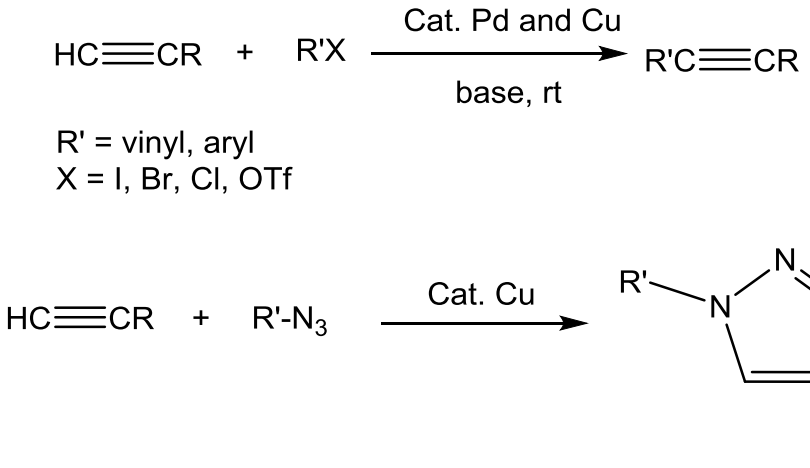

Scheme 1-1 Common Reactions involving Copper Acetylides, the Sonogashira Coupling (top) and "Click" Chemistry (bottom)

This thesis concentrates on the isomerisation of alkynes, in particular those containing a three-carbon backbone. Some of the more common C_3 hydrocarbon scaffolds possible in metal-free systems are shown in Figure 1-1. The range of structures possible show that seemingly simple rearrangements have huge potential for opening new reactions and synthetic routes.

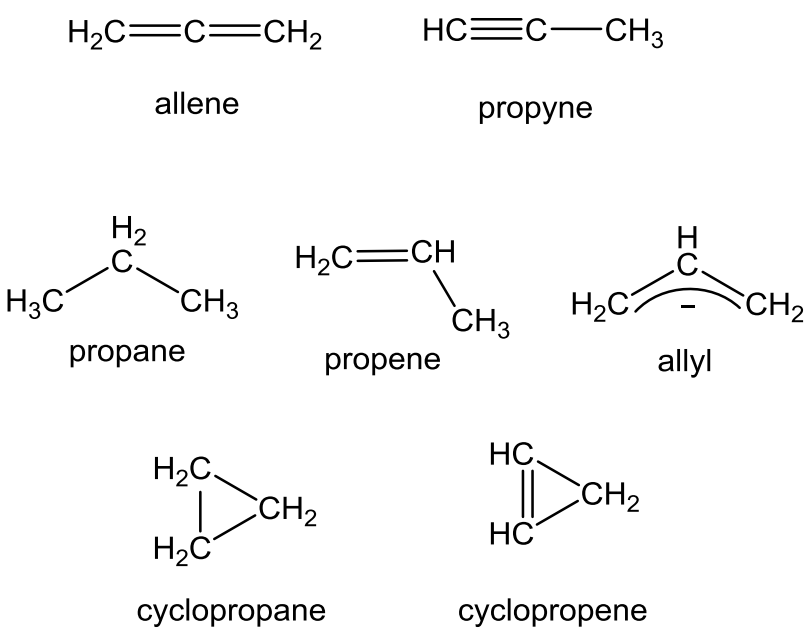

Figure 1-1 Important C_3 Isomers

With the involvement of transition metals more isomeric forms become available to the synthetic chemist (Figure 1-2). Some, such as the allyl and alkene complexes, are very similar to the metal-free forms, although the observed reactivity is often very different. Other structures, such as carbenes and allenylidenes, are generally only stable when coordinated to a metal centre. Complexes like this are known to be intermediates in important catalytic reactions like metathesis and propargylic substitution.[8, 9] The metal-carbon bond imparts important reactivity which is the source of much of the selectivity and activity observed in these catalytic systems.

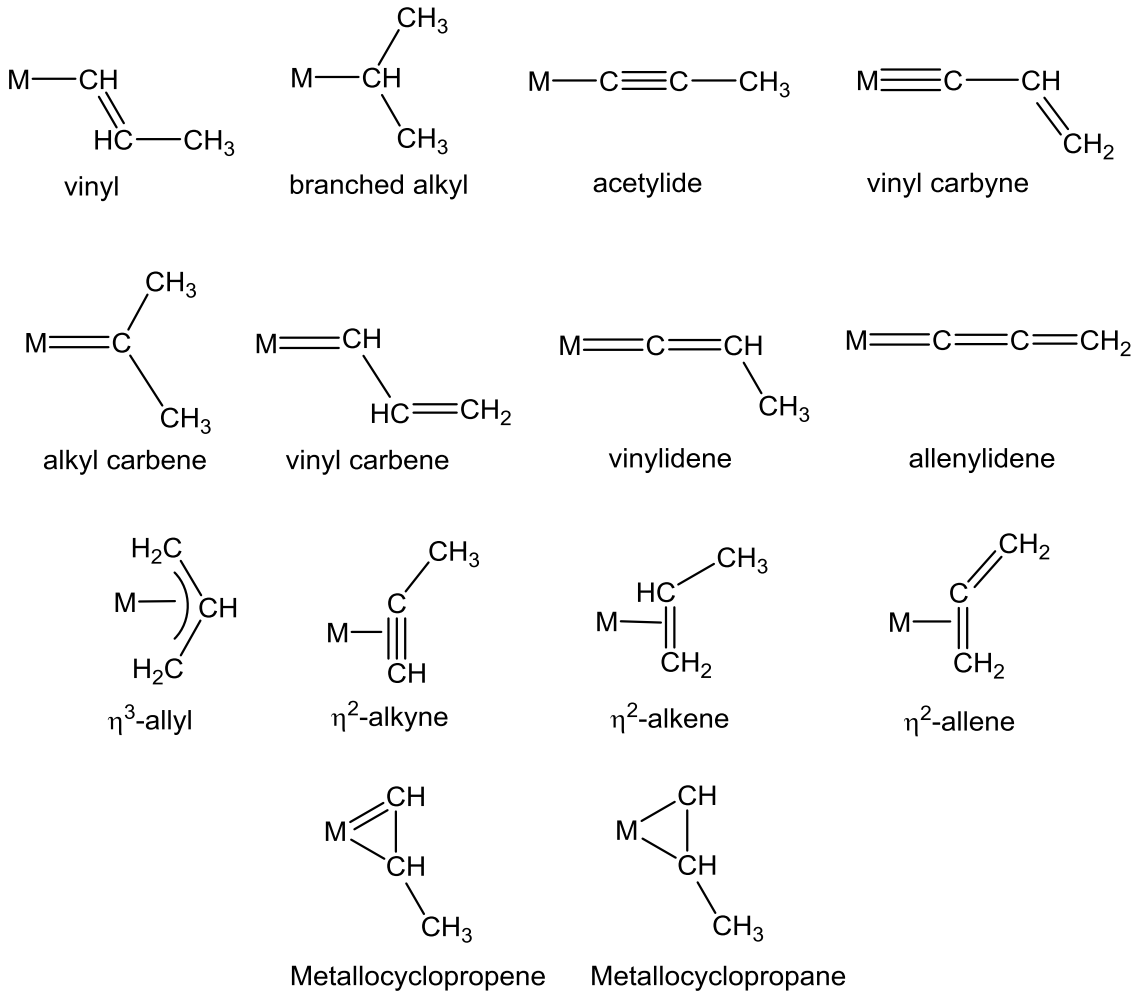

Figure 1-2 C_3 Metal Complexes

Much of the reactivity observed can be rationalised through an understanding of the orbital interactions involved in the bonding. The bonding and reactivity of these organometallic species will be the main topic of discussion for this introductory chapter. There will be an emphasis on organometallic species formed from alkynes or involved in alkyne catalysis.

1.2 Metal-Carbon σ-Bonds

1.2.1 Preamble

Transition metal carbon bonds generally display a high level of covalency, which is in contrast to the more ionic nature of the metal-carbon bonds observed for groups 1 and 2 metals. The bonding interaction consists primarily of the donation of electrons from a carbon orbital with σ-symmetry, into an empty metal orbital. The covalency levels increase across the periodic table, with early transition metals displaying stronger more polar bonds akin to C-O bonds.[10, 11] For the late transition metals the difference in

electronegativity is less pronounced (although the metals are still more electropositive than carbon) and the polarity of the bonds is comparable to C-N bonds.[11]

This σ-bonding is observed in alkyl, aryl, vinyl and acetylide complexes, amongst others. Complexes of this type are very common, particularly as intermediates in catalytic cycles. For example, all palladium cross-coupling reactions involve a transmetallation step to form an aryl, vinyl or alkyl complex. The Sonogashira reaction shown below (Scheme 1-2) also includes a copper-acetylide complex, although the true nature of the copper-cycle is poorly understood.[6]

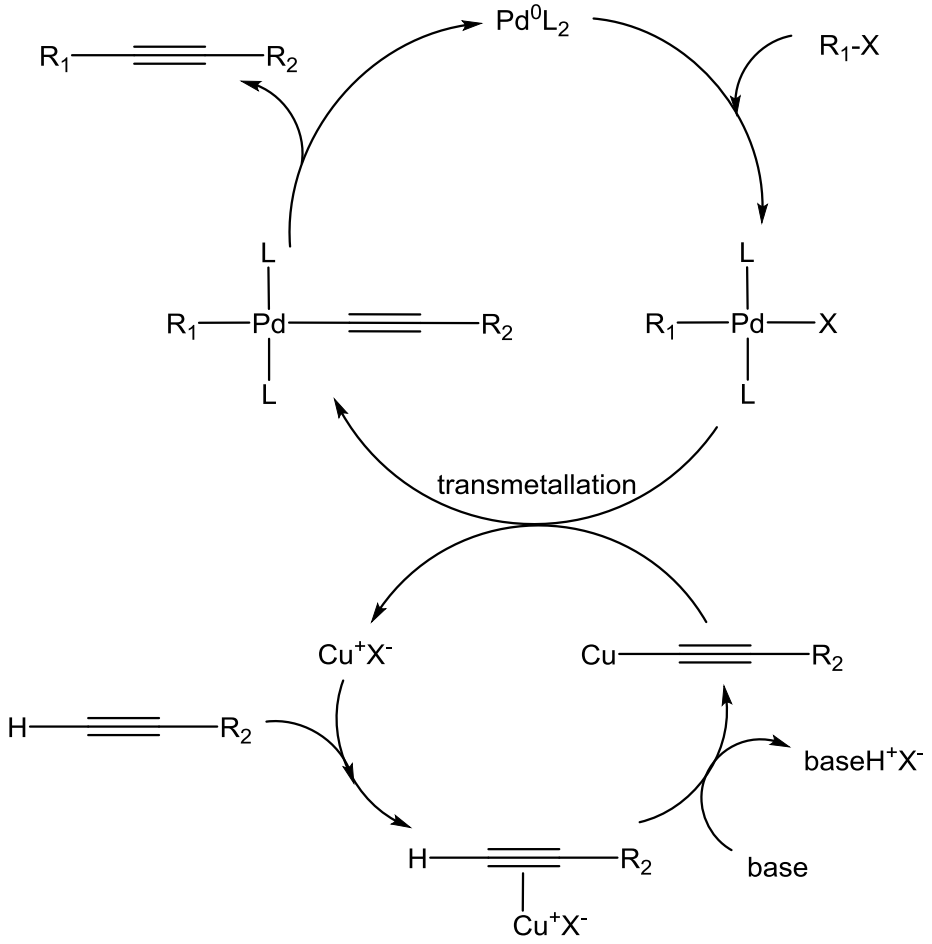

Scheme 1-2 Simplified Mechanism for the Sonogashira Reaction

Despite over a century of research, there is still a lot of interest in the fundamental understanding of alkyl ligands. Much of the recent research has centred around the topic of alkane C-H activation. Alkanes pose a particularly attractive challenge for synthetic modification as they are cheap, plentiful but unreactive substrates.[12]

It has been observed that the strongest C-H bonds are the easiest to activate. The formation of M-C bonds is dominated by the strength of the M-C bond being formed and fragments which stabilise stronger C-H bonds also result in strong M-C bonds.[13]

This has important selectivity implications with primary C-H bonds being easier to activate than secondary bonds, which are in turn more reactive than tertiary bonds.[14] Bond strengths are also important for determining the validity of catalytic systems. For example, the M-C bond strengths in 3rd row metals are often too strong to allow reductive elimination and therefore release of the product.[15]

1.2.2 Acetylide Complexes

Vinyl, aryl and acetylide ligands all display similar reactivity to alkyl complexes, but they can also interact with the metal centre through their π-electron system which can lend additional stability. The π-interaction is particularly strong in acetylide complexes and the electron delocalisation leads to many interesting properties. The properties being investigated include luminescence, electrical conductivity and liquid crystallinity.[16-18]

The orbitals present in an acetylide ligand are analogous to those present in CO, but the π-system is higher in energy. This means that donation from the metal into the π*-orbitals is often not accessible, and so back-bonding is less important than in CO systems. This higher energy π-system does however lead to good overlap between the metal orbitals and the π-bonding orbitals, making the acetylide ligand act more as a π-donor than a π-acceptor. However these π-bonding effects are small compared to the σ-donor interaction which dominates the overall bonding (Figure 1-3).[19]

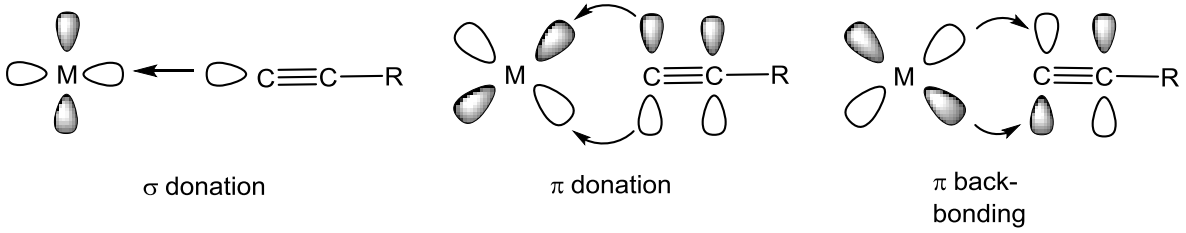

Figure 1-3 Acetylide Complex Bonding Interactions

The ease of formation and utility in synthesis of acetylide complexes has already been discussed in Section 1.1. The proton of terminal alkynes is relatively acidic and can be deprotonated with the use of strong bases. If however the alkyne is bound to a metal (see Section 1.9), the deprotonation can be achieved with relatively weak bases and so acetylide complexes are easily accessible.[7, 11] Transition-metal acetylide complexes have traditionally been synthesised from highly polarised organometallic acetylides such as lithium and copper salts as seen in the transmetallation step of Scheme 1-2Error! Reference source not found..[18] Another common route to transition metal acetylide complexes was pioneered by Bruce and involves the deprotonation of mono-substituted cationic vinylidene complexes (Scheme 1-3). It was also found that this

process could be reversed by treating the acetylide complex with an acid such as HPF_6 to form the vinylidene complex.[20]

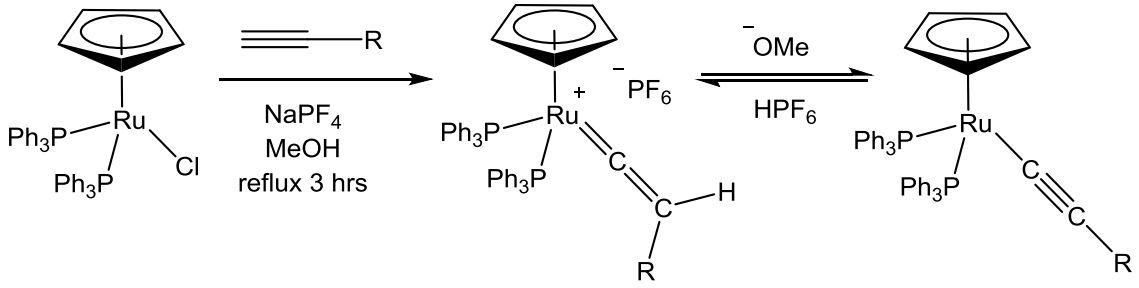

Scheme 1-3 Deprotonation of a Vinylidene Complex to form an Acetylide Complex

1.3 η^2-bound C_3 Species

1.3.1 Bonding

The simplest mode of coordination of an alkyne to a metal centre involves the use of the π-system and does not involve any isomerisation. It also applies to alkenes and involves the side-on binding of the alkyne/alkene moiety to the metal centre through its π-system. A σ-bond is formed by donation of electron density from the π-bond to an empty orbital on the metal. Back donation from the metal to the π*-orbital is also possible to form a π-bond between the metal and the alkene (Figure 1-4). This interaction weakens the C-C bond and can be observed through the lengthening of the C-C bond length.[11]

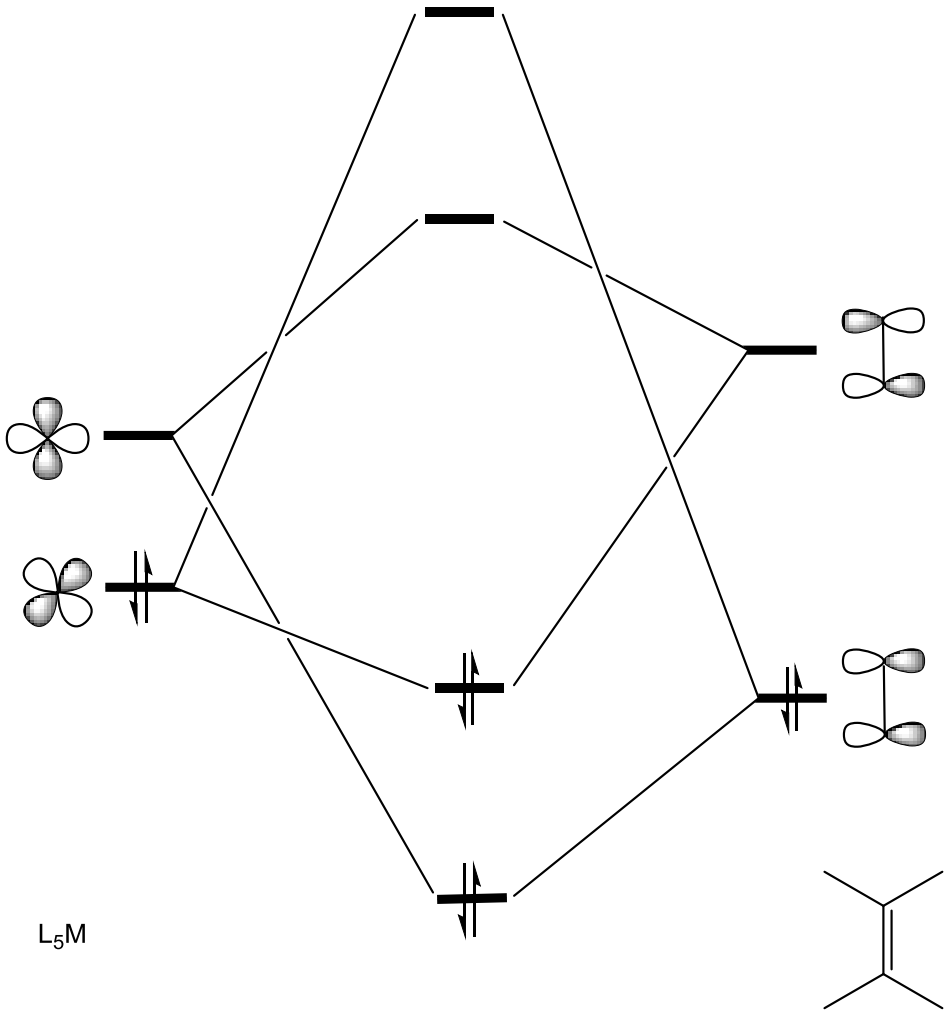

Figure 1-4 Molecular Orbital Diagram for an Alkene Complex

Alkynes have an additional π-bond and therefore an additional bonding interaction is possible. The π-bonding orbitals that are perpendicular to those forming the σ-bond can donate electron density to the metal and form a second π-interaction with the metal centre (Figure 1-5).

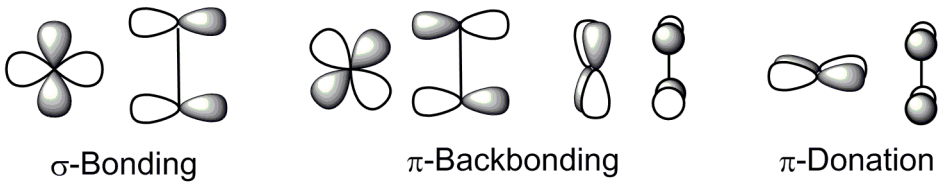

Figure 1-5 Bonding Modes in an Alkyne Complex

This bonding model for alkene complexes was first developed by Chatt, Dewar and Duncanson and it has important consequences for the reactivity of these species.[11, 21] Depending on the nature of the metal centre the bonding can vary from simple σ-bonding, leaving the alkene bonding and reactivity virtually unchanged, through to strong back-bonding leading to the formation of a metallocyclopropane (or metallocyclopropene in the case of an alkyne). This effectively leads to cleavage of the

π-bond and the substituents are now bent back away from the metal as the carbon atoms move from sp^2 to sp^3 (or sp to sp^2) hybridisation (Figure 1-6).

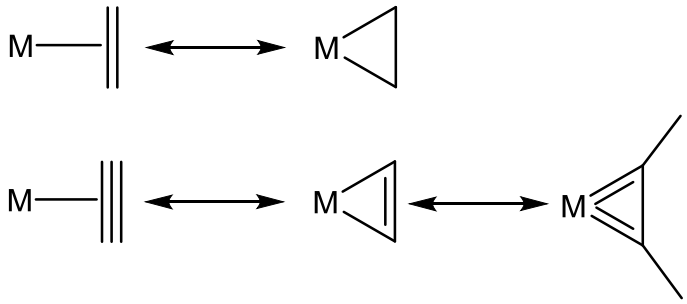

Figure 1-6 Alkene (top) and Alkyne (bottom) Complexes with their Metallocyclopropane (top) and Metallocyclopropene (bottom) Resonance Forms

Metal-mediated isomerisation of alkynes generally begins by the coordination of the alkyne in an η^2 fashion. Examples of this can be seen in Section 1.6.2 where the alkyne complex is isomerised to the vinylidene isomer via a proton migration. Much work has been done on these types of isomerisation, in particular by Casey who has demonstrated that treatment of alkyne complexes with acid leads to the selective formation of η^3-allyl and η^2-allene complexes (Scheme 1-4).[22, 23] Both of these transformations have been found to go via an intermediate metallocyclopropene complex.

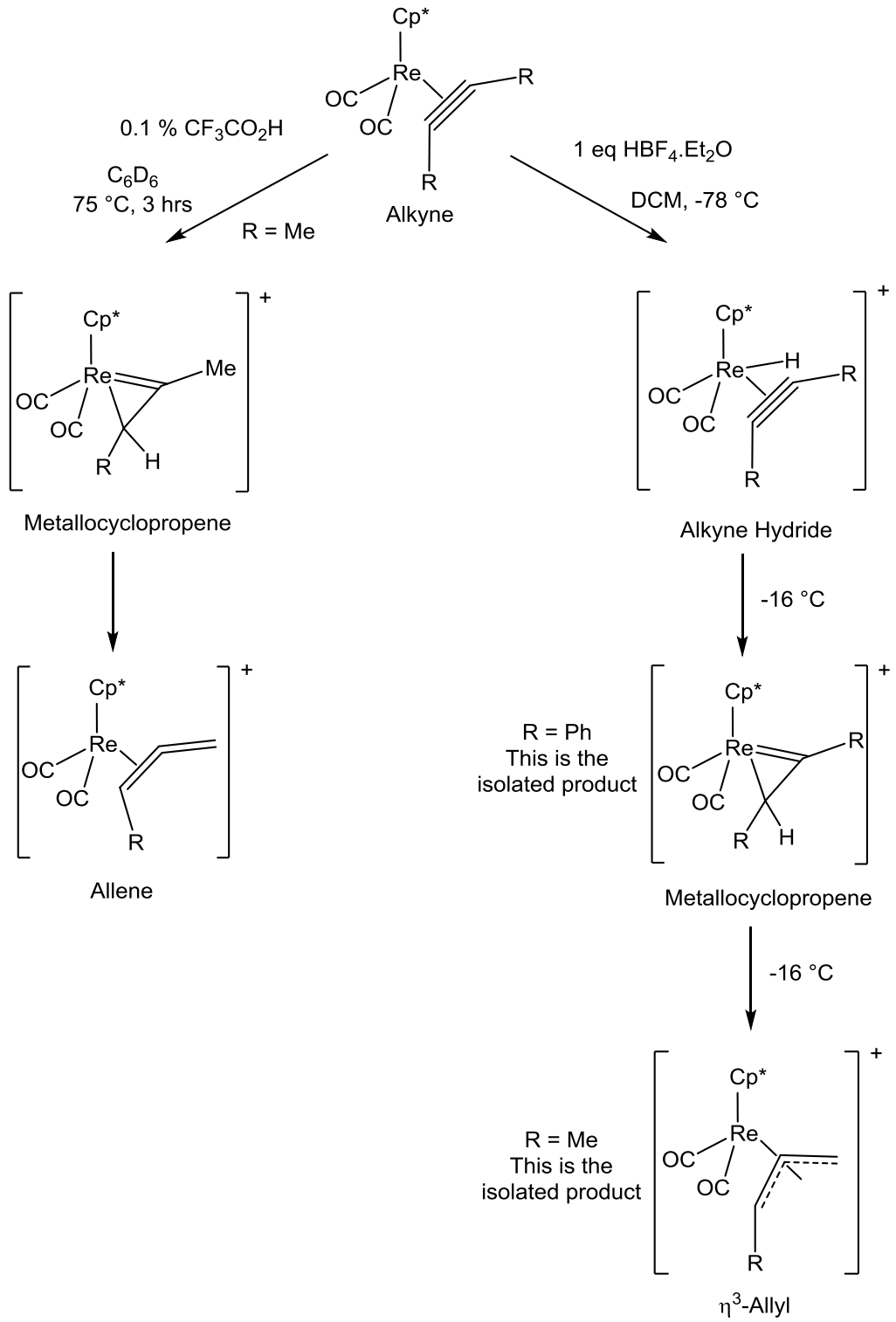

Scheme 1-4 Isomerisation of an Alkyne Complex to Allene and η^3-Allyl Complexes via a Metallocyclopropene Complex

1.3.2 Allene Ligands

In Section 1.1 (Figure 1-2) another η^2-ligand, the allene, was presented as a possible C_3 organometallic species. As a ligand, this can be viewed as an alkene, and the bonding models discussed in Section 1.3.1 apply here too. The allene functional group has been described as an "underutilized functional group",[24] despite the fact that the

chemistry of the allene allows access to alternative reactivity and selectivity to that seen in simple alkenes and that the allene is present in over 150 natural products.[25]

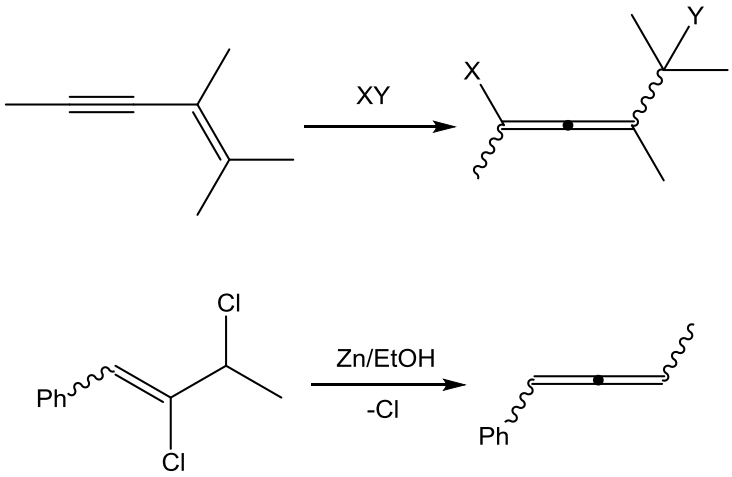

Scheme 1-5 Formation of Allenes via 1,4-Addititon to Enynes (top) and Dehalogenation (bottom)

Synthetic routes to allenes include 1,4-addition to enynes[5] and dehalogenation of di-chloro alkenes (Scheme 1-5).[26] Allenes with one or two substituents present at both ends of the functional group are optically active, and can be viewed in the same way as biphenyl systems with restricted rotation.[5] This was first demonstrated experimentally in 1935 by Maitland and Mills through the asymmetric synthesis of (+) or (-) allenes via the dehydration of enols using an enantiopure (+) or (-)-camphor-10-sulfoninc acid catalyst.[27]

Of relevance to this thesis is the formation of allenes through the rearrangement of propargylic systems.[5] This can be achieved via the [3,3]-sigmatropic transformation of propargyl vinyl ethers (known as the propargyl Claisen rearrangement) with the use of a catalyst or at high temperatures.[28] In a recent example this chemistry has been exploited in a rhodium-catalysed cascade reaction in which the five step synthesis of the substituted naphthalene shown in Scheme 1-6 could be completed in one pot.

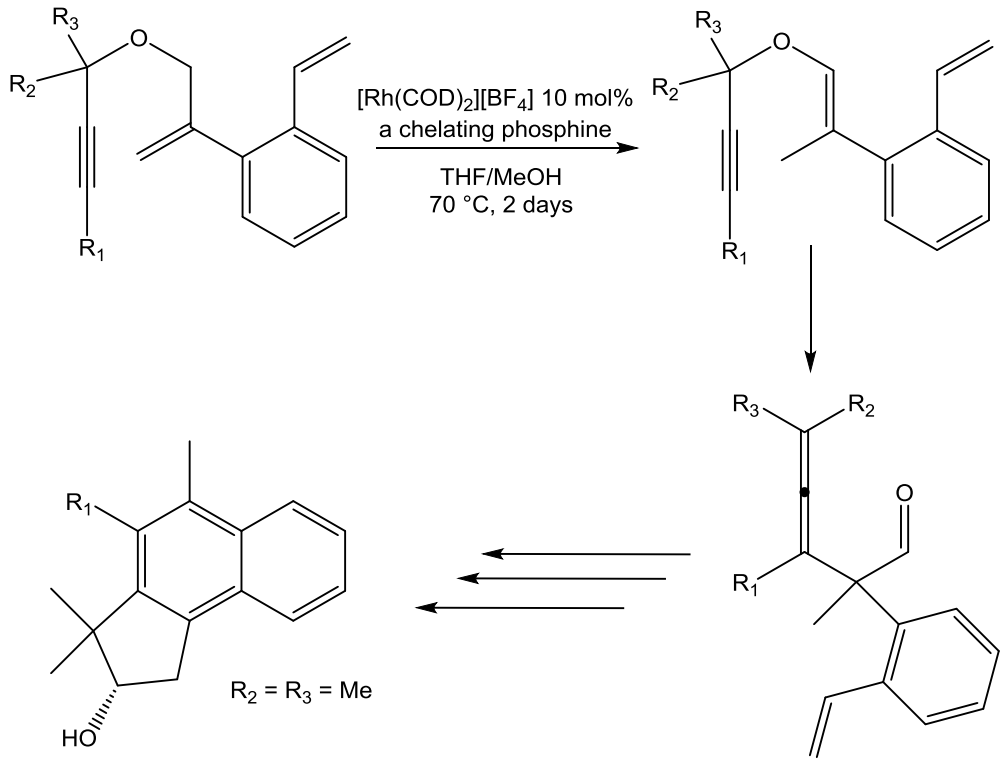

Scheme 1-6 A Rhodium Catalysed Cascade Reaction Involving a Propargyl Claisen Rearrangement. COD = 1,5-cyclooctadiene

Another route to allenes is the base-promoted rearrangement of propargylic systems which has been much studied over the last seven decades.[29] Theoretical studies have shown that the allene isomer is often more thermodynamically stable than the alkyne, particularly when an electron-donating heteroatom substituent is present such as in propargylic ethers. For example, a comparison of the relative energies of MeO-CH_2-C≡C-CH and MeO-CH=C=CH found that the allene isomer was 21 kJ mol^{-1} more stable than the alkyne (geometries were optimised at the RHF/6_31+G* level and energies were refined).[30]

In some systems, however, the rearrangement to form the allene is found to be spontaneous and occurs without the presence of strong base or a catalyst. An example of this is the rearrangement of propargylphosphonium species such as $[HC{\equiv}CCH_2PPh_3]^+$ (Scheme 1-7).

Scheme 1-7 Isomerisation of Triphenylpropargylphosphonium

In recent work, Hill has suggested that formation of the phosphino-allene complexes $[Ru(\eta^2\text{-}CH_2{=}C{=}CHPPh_3)(CO)_2(PPh_3)_2]Br$ and $[Pt(\eta^2\text{-}CH_2{=}C{=}CHPPh_3)(PPh_3)]PF_6$ from $[HC{\equiv}CCH_2PPh_3]^+$ was the result of a metal-mediated alkyne to allene isomerisation (Scheme 1-8).[31, 32] However it was observed that the isomerisation of the alkyne to the

allene occurred on standing in solution with no metal present, and a theoretical study showed the allene isomer to be significantly lower in energy than the alkyne (both in the gas phase and with solvent correction).[32] This suggests that the process may not be metal-mediated and further investigations into this alkyne to allene isomerisation will be presented in Chapter 4.

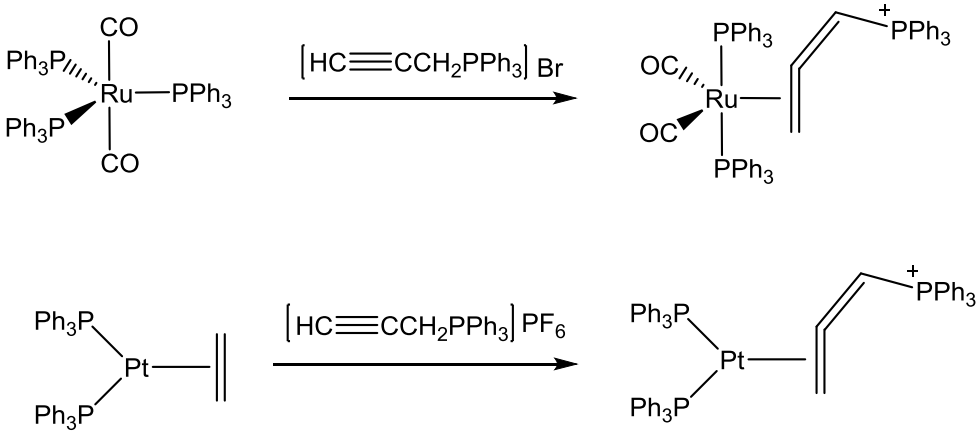

Scheme 1-8 Phosphino-Allenes from the Literature

Allene complexes are most commonly synthesised by the binding of an allene to a free coordination site on a metal centre. In a recent example, a gold η^2-allene complex, formed via the reaction of (P1)AuCl (P1 = P(^{t}Bu)$_2$*o*-biphenyl) with tetramethylallene, was found to undergo spontaneous rearrangement to a gold 1,3-diene complex. This observation then led to the development of a catalytic process in which a gold catalyst is used to form 1,3-dienes from allenes (Scheme 1-9).[33]

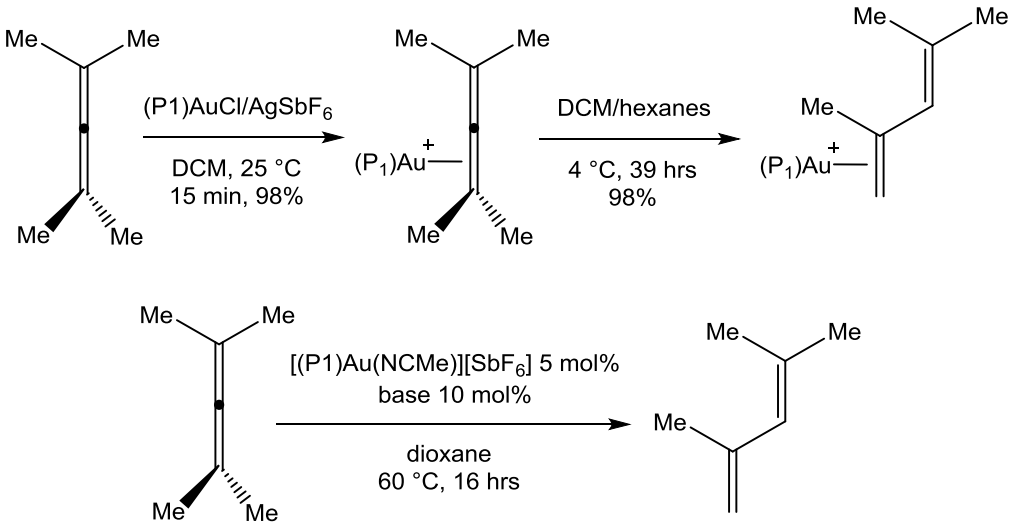

Scheme 1-9 Gold Allene Complexes in Catalysis. P1 = P(^{t}Bu)$_2$*o*-biphenyl

However, it is also possible to prepare the allene ligand within the coordination sphere of the metal, one example was discussed in Section 1.2. In these cases the precursor is often a propargylic system, just as in the metal-free syntheses discussed in the previous section.[34] An example of this is the photo-activation of [Cr(1,3,5-(CH$_3$)$_3$

$C_6H_3)(CO)_3$] in the presence of propargyl alcohol to form alkyne complex [Cr(1,3,5-$(CH_3)_3C_6H_3)(CO)_2(\eta^2$-$HC{\equiv}CCH_2OH)$]. Treatment of this alkyne complex with acid and triphenylphosphine lead to the formation of phosphino-allene complexes. The internal 1,2-allene complex **A** was found to be the most stable, with the 2,3-species **B** irreversibly converting to **A** upon standing (Scheme 1-10).[35]

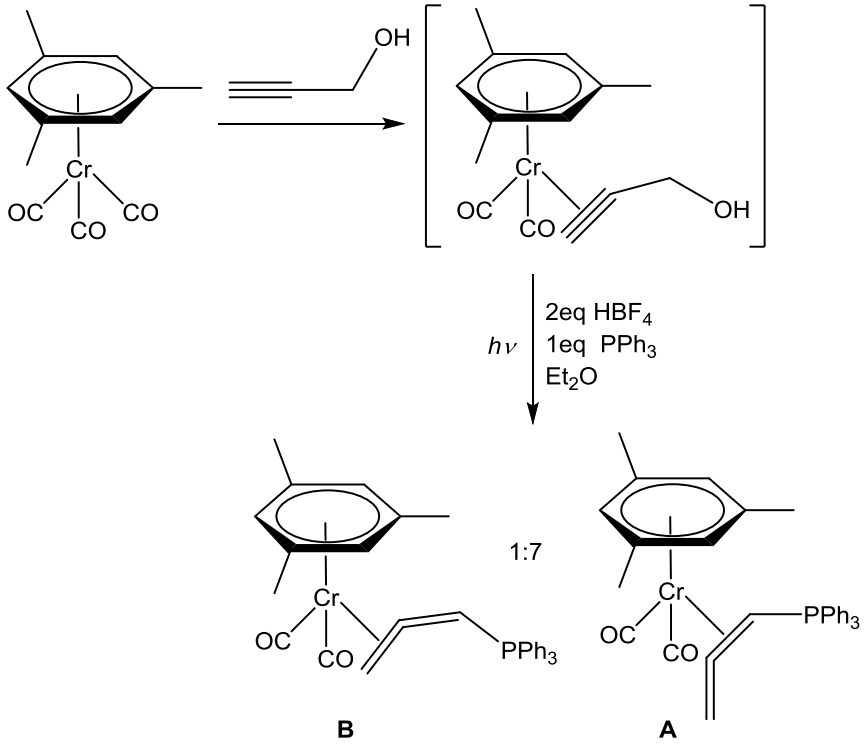

Scheme 1-10 Formation of Allene Complexes from an Alkyne Complex

1.4 Allyl Ligands

The allyl group is a C_3H_5 moiety which is a relatively common and well-studied organometallic ligand. It can bind in either an η^1 or an η^3-binding mode, and is also capable of forming bridging interactions (Figure 1-7). The η^1-form is an alkyl ligand, there is no interaction between the metal and the ligand π-electrons and the bonding can be viewed in the same way as that discussed in Section 1.2.

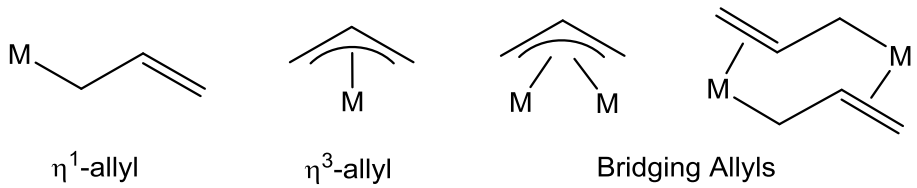

Figure 1-7 Possible Binding Modes for Allyl Complexes

The η^3-binding mode is the most common form and binds to the metal face-on, although it is often tilted so that the central carbon is closer to the metal that the

terminal carbon atoms.[11] The allyl moiety has three molecular orbitals (Figure 1-8); the bonding orbital Ψ_1, which is always doubly occupied, the empty anti-bonding orbital Ψ_3, and Ψ_2 which is doubly occupied when the ligand is viewed as having a negative charge ($C_3H_5^-$).[36]

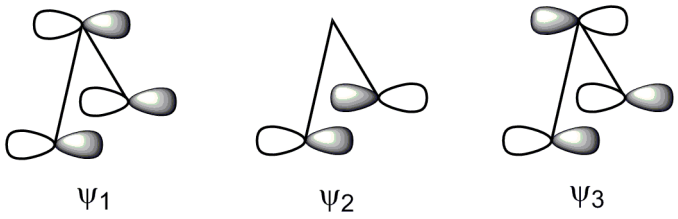

Figure 1-8 Molecular Orbitals of the Allyl Ligand

Allyl complexes are often formed through the displacement of a good leaving group by a nucleophillic vinyl compound such as a vinyl halide or vinyl Grignard.[37] Dienes are common precursors, leading to the formation of C_4 allyl complexes (Scheme 1-11).[38]

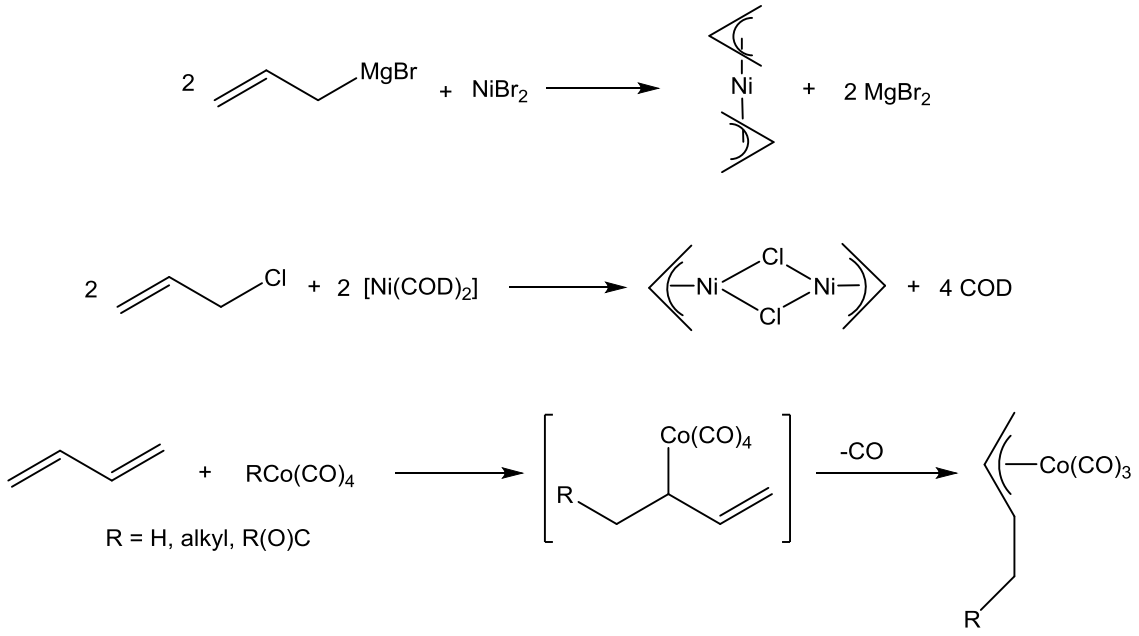

Scheme 1-11 Synthesis of Allyl Complexes from Vinyl Grignards (top), Vinyl Halides (middle) and Dienes (bottom).

In catalysis, allyl ligands are present as both spectator ligands and as key intermediates. One particularly important group of reactions in which they feature as intermediates is allylic substitution (Scheme 1-12).[11, 39]

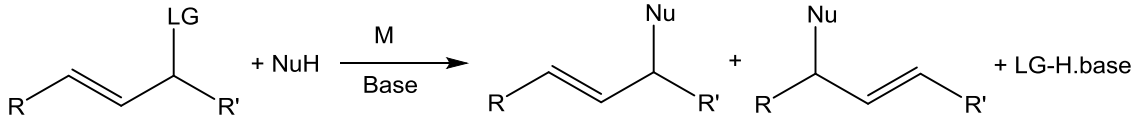

Scheme 1-12 General Catalytic Allylic Substitution Reaction

The commonly accepted mechanism involves the oxidative addition of the allylic starting material onto the metal centre. An η^3-allyl complex is then formed and the

leaving group becomes a weakly-coordinating counter ion. The nucleophile then attacks the allyl ligand (usually on the opposite face to the metal) with the subsequent formation of the two possible products (Scheme 1-13).

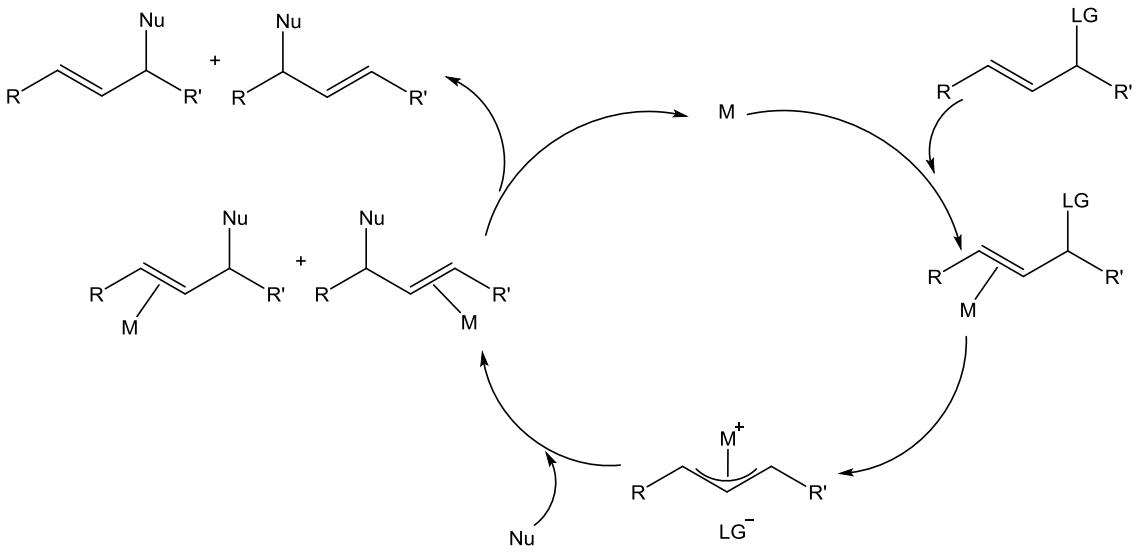

Scheme 1-13 A Simplified Mechanism for Catalytic Allylic Substitution

These reactions were first developed in the 1970s, and they have been subject to continual improvement since then. Allylic alkylation has attracted particular attention as a useful method for C-C bond formation, although it has been limited in the past by the scope of the nucleophiles available for use. There has been a recent report however of a general route for catalytic allylic alkylation using tertiary nucleophiles, which greatly extends the scope of this reaction. This reaction uses a palladium (II) catalyst with a bis(sulfoxide) ligand to produce products with excellent regio- and stereoselectivity (>20:1 linear:branched, >20:1 E:Z) (Scheme 1-14).[40]

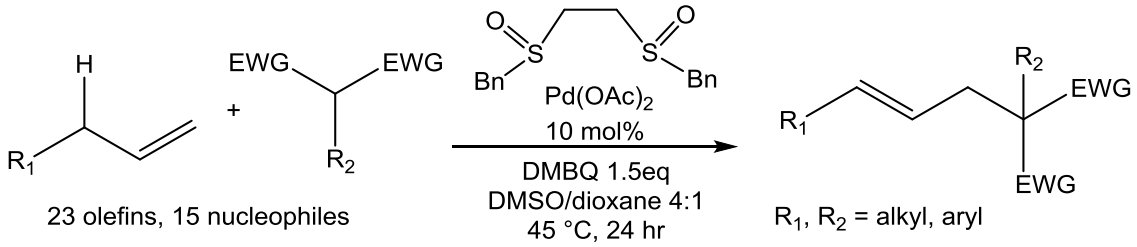

Scheme 1-14 Catalytic Allylic Alkylation. DMBQ = 2,6-Dimethoxy-1,4-benzoquinone

1.5 Carbene Ligands

1.5.1 Bonding

Carbenes are divalent carbon centres which can be stabilised by coordination to a metal centre. They can be classified in two ways, as either singlet or triplet, or as

Fischer or Schrock carbenes. They possess an orbital with σ-symmetry, and an orbital with π-symmetry (Figure 1-9).

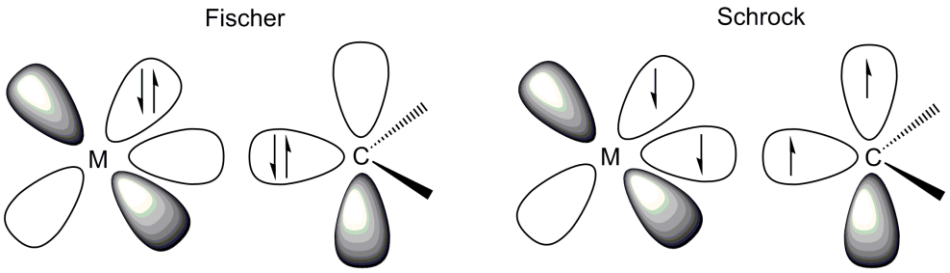

Figure 1-9 Bonding in Carbene Complexes

In a singlet carbene, the electrons are paired in the sp^2-hybrid orbital leaving the p-orbital empty. The electrons in the s-orbital can then act as a σ-donor to a metal centre, whilst the empty p-orbital can accept electron density from full metal d-orbitals (Figure 1-10). The overlap between the metal d-orbitals and the carbene p-orbital can be poor leading to an electron-deficient carbon atom which is susceptible to nucleophillic attack. In these Fischer carbenes additional stabilisation is gained from the donation of electron density from a +M substituent. These types of ligands are usually associated with late transition metals in low oxidation states, especially those with π-accepting ligands such as CO or phosphines.[11]

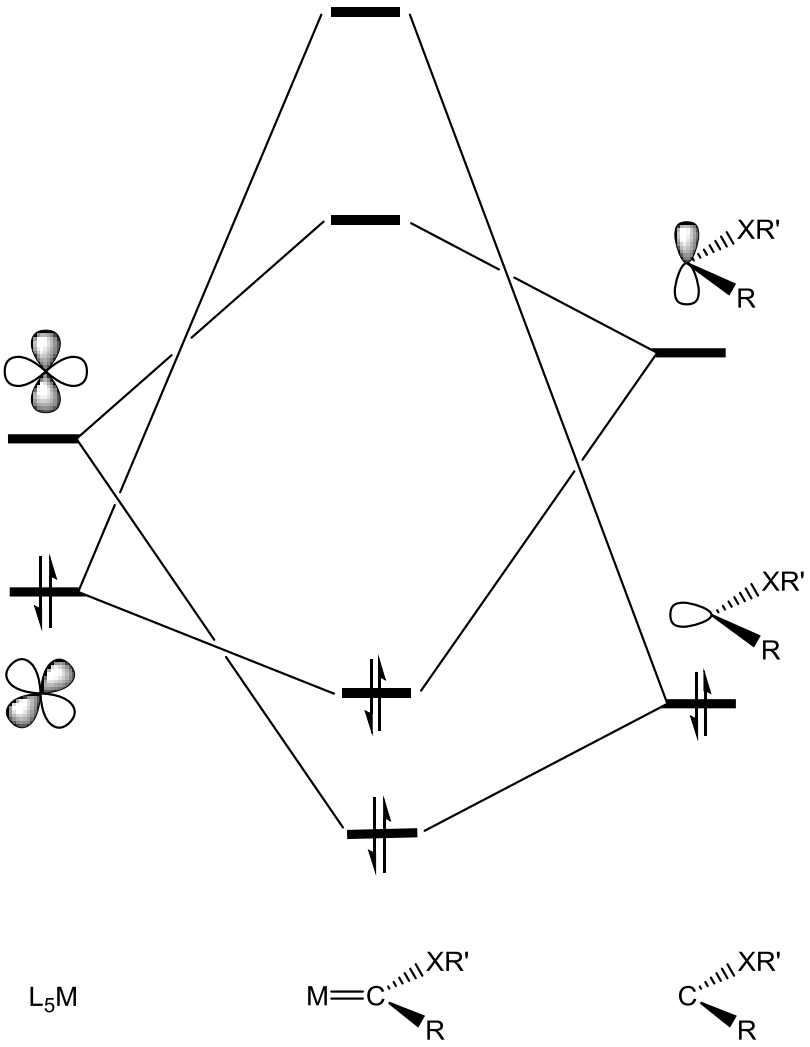

Figure 1-10 Simplified Molecular Orbital Diagram for Fischer-Type Carbenes

In a triplet carbene the two electrons are unpaired, with one residing in the sp^2-hybrid orbital, and one in the p-orbital (Figure 1-9). When bonded to a metal centre, strong back-bonding from the metal d-orbital to the p-orbital occurs and the carbon atom is found to be electron-rich and susceptible to electrophilic attack. These Schrock carbenes have only alkyl or hydrogen substituents and common for early transition metal complexes in high oxidation states.[11]

Carbene ligands are widespread in organometallic chemistry with many applications in catalysis, most notably in metathesis.[41] An important class of carbenes are the N-heterocyclic carbenes (NHCs) which are now widely used as ancillary ligands for altering the sterics and electronics of a system.[42] For the purposes of this introduction however, only C_3 carbenes will be discussed (Figure 1-2), with particular focus on those formed from alkynes.

1.5.2 Vinyl Carbene Complexes

Vinyl carbene complexes of ruthenium have attracted attention in the last couple of decades thanks to their role in olefin metathesis, Some of the very early metathesis catalysts developed by Grubbs were vinyl carbene complexes synthesised from 3,3-diphenylcyclopropene (Scheme 1-15).[43]

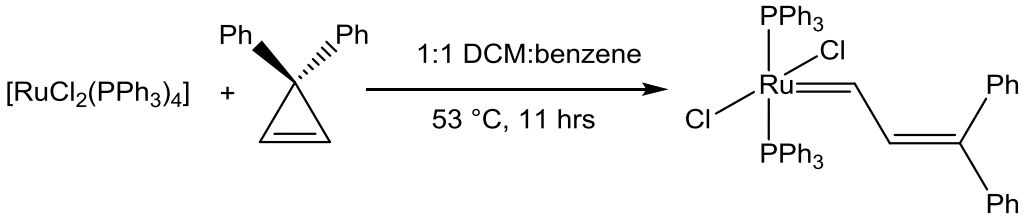

Scheme 1-15 Synthesis of an Early Vinyl Carbene Metathesis Catalyst

These early vinyl carbene catalysts were soon eclipsed by developments in the field and recent interest in vinyl carbene complexes has centred around their role as intermediates in catalytic enyne metathesis reactions.[44-47] The modern catalysts of choice in the area are the ruthenium carbenes developed by Grubbs (Figure 1-11). Grubbs' second generation catalyst is generally more reactive than his first generation system and has been found to catalyse the coupling of internal alkenes and alkynes.[44] This improved reactivity is attributed to the coordinatively unsaturated intermediate preferentially binding alkene over binding free phosphine. Therefore, more of the key vinyl carbene intermediate is formed.

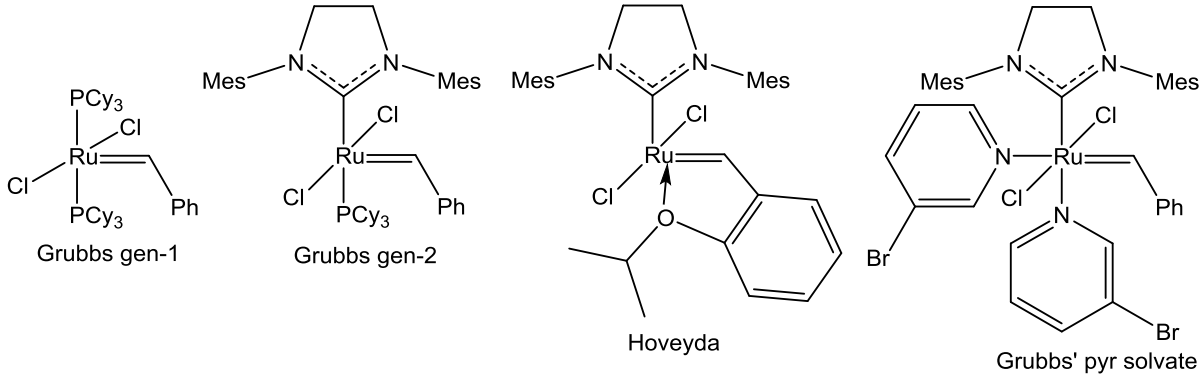

Figure 1-11 Ruthenium Carbene Catalysts used for Enyne Metathesis

Enyne metathesis involves the coupling of an alkene with an alkyne to produce a 1,3-diene. These reactions can be intramolecular (ring-closing enyne metathesis, RCEYM) or intermolecular (cross enyne metathesis) (Scheme 1-16).

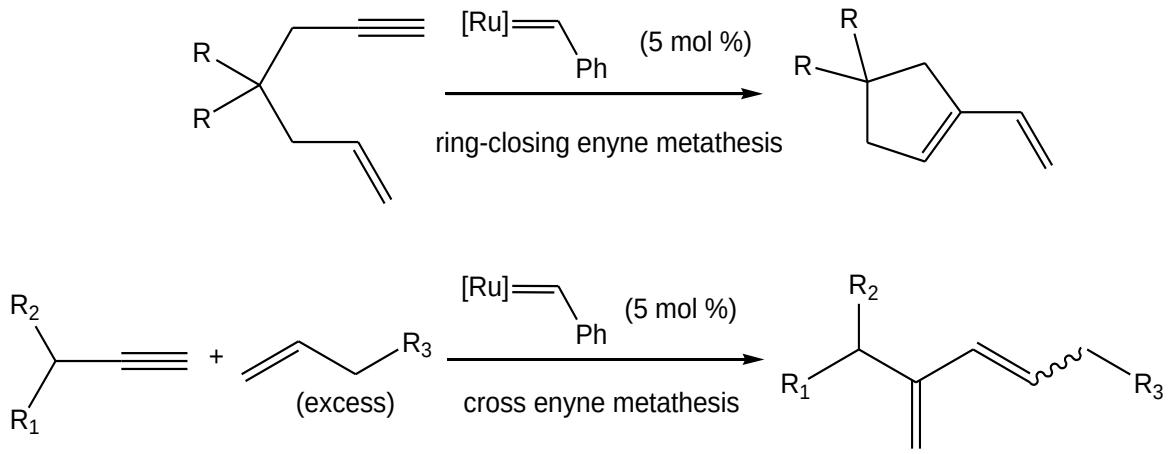

Scheme 1-16 Two Classes of Enyne Metathesis

The mechanism of enyne metathesis is not fully understood, but a key step in all forms of the reaction is the reaction of the alkyne with a metal carbene to form a vinyl carbene intermediate.[45] In parallel with alkene metathesis it is assumed that the desired alkene is introduced to the system via cycloaddition to the precursor carbene to form a ruthenacyclobutane. Cycloelimination then completes the initiation step to give the active catalytic species.

The alkyne then adds via cycloaddition and a ruthenacyclobutene. The cycloelimination step yields a vinyl carbene species which can be realised as product after another alkene substrate molecule has bound via cycloaddition (Scheme 1-17).

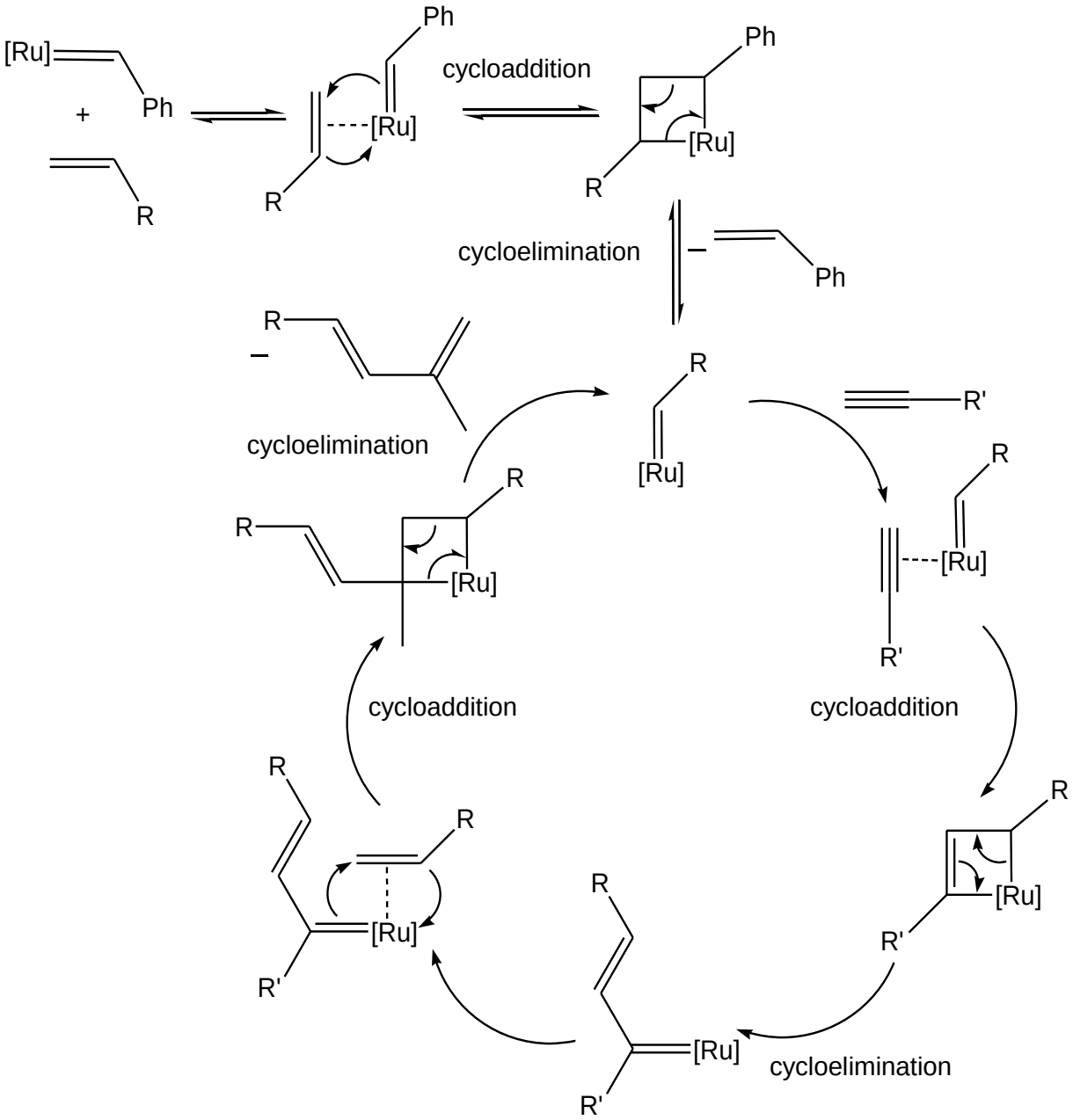

Scheme 1-17 Possible Mechanism for Enyne Metathesis

The vinyl carbene intermediates have been found to be relatively long lived and this longevity is thought to be the main rate limiting step. This has fuelled interest in vinyl carbenes and has led to the development of a number of synthetic routes, although only the most relevant will be discussed here.[45]

1.5.3 Synthesis of Vinyl Carbene Complexes from Alkynes

One of the more common methods of preparing vinyl carbenes uses metal hydride precursors which are then reacted with propargylic halides. This method was first developed by Grubbs as an improvement on the use of cyclopropenes as precursors and has been found to work in a variety of ligand environments, making it a versatile synthetic method.[48] It is thought that the mechanism involves insertion of the alkyne

into the ruthenium hydride bond, followed by elimination of the chloride. The chloride then ends up as an ancillary ligand on the metal centre (Scheme 1-18).

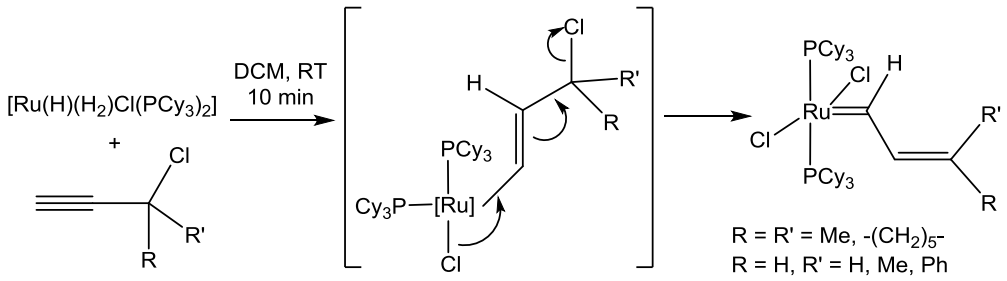

Scheme 1-18 Use of Metal Hydride Precursors to Form Vinyl Carbenes

A more recently developed method for isolating vinyl carbenes is to halt the enyne metathesis cycle after the insertion of an alkyne into the metal carbene. In order to do this, chelating carbenes are used as chelation gives the vinyl carbene kinetic stability and enables isolation. In this (Scheme 1-19) example from Fürstner's group,[49] Grubbs' generation-1 catalyst was used as the precursor and silver chloride used to sequester the liberated phosphine. Complexes of this type are of additional interest as it is thought that functional group chelation is a common catalyst deactivation pathway in enyne metathesis.[45]

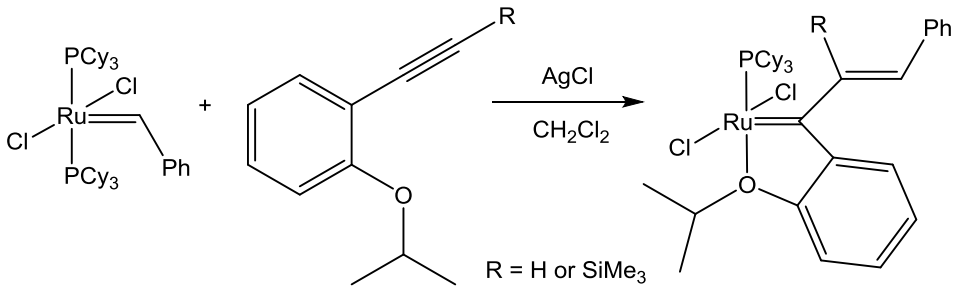

Scheme 1-19 Use of Chelation to Halt Metathesis and Enable Isolation of Vinyl Carbenes

An alternative method of preparation, which has been used extensively by Dixneuf and co-workers, is the addition of nucleophiles to allenylidenes. The allenylidenes can be generated *in situ* from propargylic alcohols, and a one-pot route to vinyl carbenes is available if a nucleophilic solvent such as methanol is used (Scheme 1-20).[50, 51]

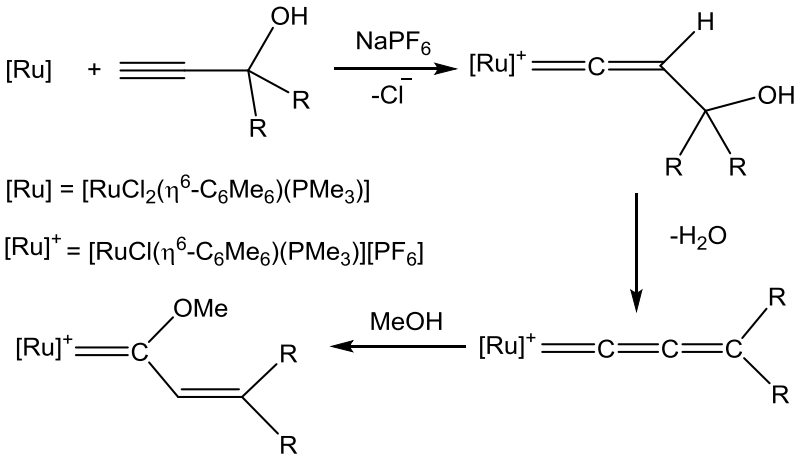

Scheme 1-20 Nucleophilic addition to Allenylidenes to form Vinyl Carbenes

Many of the vinyl carbene complexes synthesised were made specifically for screening as metathesis catalysts. As a result their stoichiometric reactivity (and indeed their catalytic behaviour in other systems) has barely been investigated, especially when compared to the wealth of knowledge available for other unsaturated ligand classes such as vinylidenes.[45]

1.6 Transition-Metal Vinylidene Complexes

1.6.1 Bonding in Vinylidenes

Interest in vinylidene ligands has intensified in recent years as their role as intermediates in many transformations such as the anti-Markovnikov addition of nucleophiles to alkynes has become increasingly apparent.[52-58] Vinylidenes are high energy tautomers of alkynes and theoretical studies (calculated using the DZ+P-SCEP methods) have calculated their relative stabilities to be ca. 188 kJ mol^{-1} in favour of the alkyne form.[57, 59, 60]

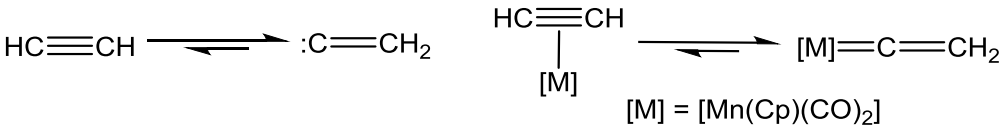

Figure 1-12 Relative Stabilities of Vinylidene and Acetylene Tautomers

However, coordination to certain metal fragments reverses this trend. Using the extended Hückle method, Hoffman has shown that [MnCp(=C=CH$_2$)(CO)$_2$] is 146 kJ mol^{-1} more stable than the corresponding η^2-acetylene tautomer (Figure 1-12).[61] This stabilisation allows metal bound vinylidenes to be isolated and their chemistry investigated.

Vinylidenes exhibit a range of interesting, yet selective, chemistry due to their alternating pattern of π-electron density. Like carbenes, vinylidene complexes can be

classified by this pattern. Complexes with an electrophilic α-carbon are of the Fischer-type (by far the most common type of isolated vinylidene complex), and those with a nucleophilic α-carbon of the Schrock-type (Figure 1-13).[62]

Figure 1-13 Classification of Metal Vinylidenes

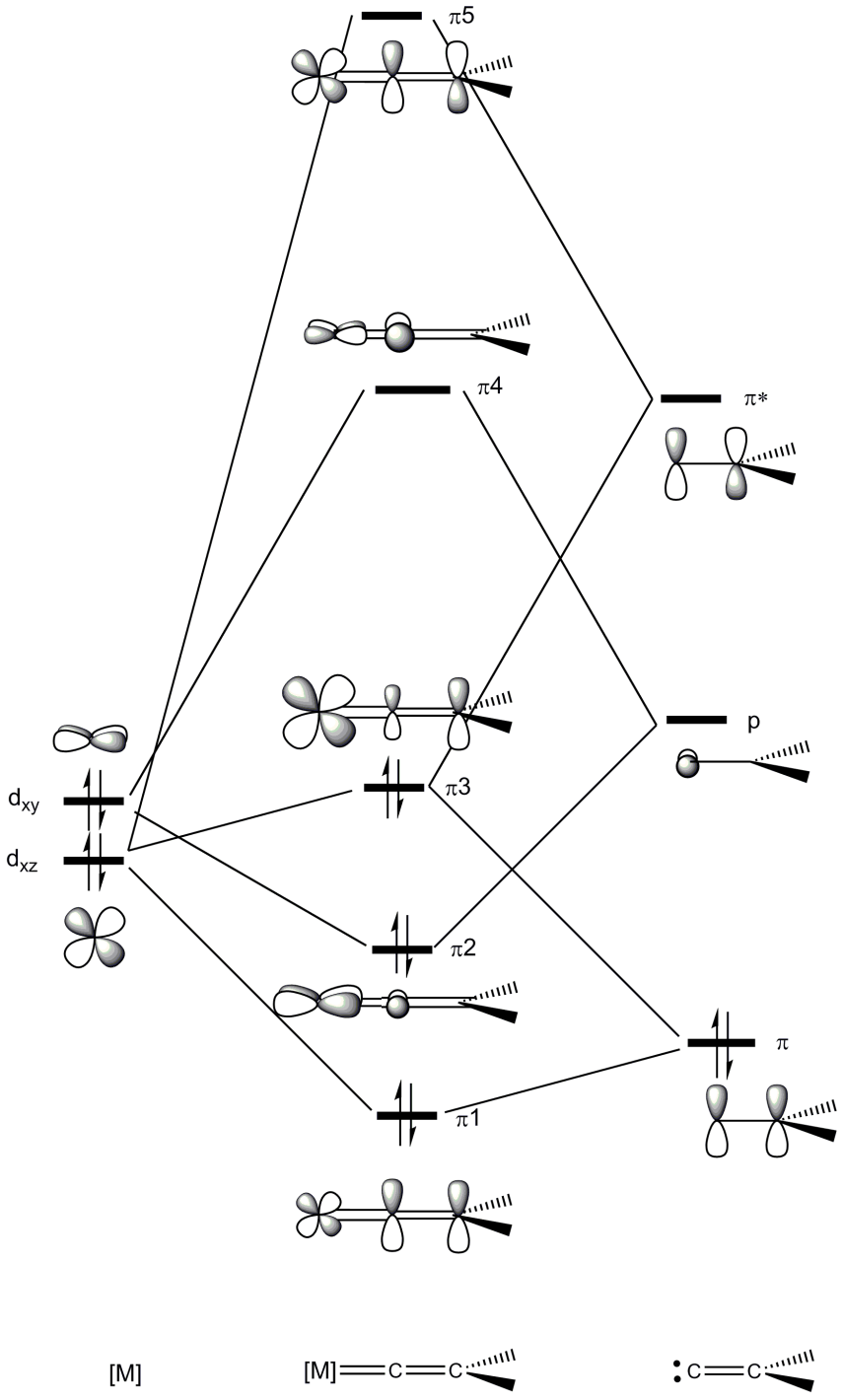

Figure 1-14 Simplified π-orbital Diagram for Fischer-type Vinylidenes

Much detailed work has been carried out towards understanding the bonding interactions behind this reactivity[61, 63, 64] and the simplified π-orbital interactions diagram (Figure 1-14) summarises some of the important points. For example, the LUMO (π4) receives its largest contribution from the empty p-orbital on the vinylidene α-carbon. Hence the α-carbon is electron-deficient and susceptible to nucleophilic attack. Both the metal centre and the β-carbon are known to undergo electrophilic attack. This is due to the HOMO (π3) corresponding to an anti-bonding interaction between a vinylidene π-bonding orbital and a metal d-orbital.[56, 62]

1.6.2 Mechanistic Insight into Vinylidene Formation

Since Antonova and co-workers reported the first acetylene-vinylidene rearrangement (AVR),[65, 66] (the mechanism had been first postulated by Chisholm and Clark in 1972)[67] synthesis of vinylidene complexes has been straightforward. After many studies into the area,[56, 58, 61, 62, 64, 68] three principal mechanisms for this transformation have been identified (Scheme 1-21).

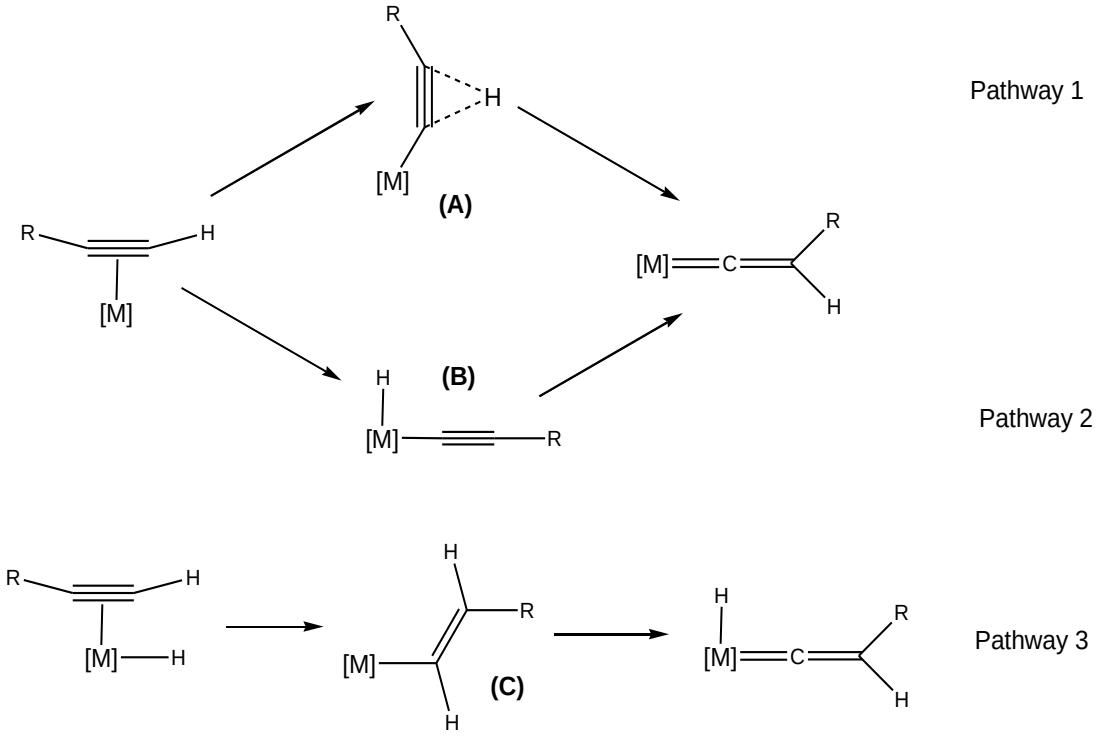

Scheme 1-21 Mechanisms for the Interconversion of Terminal Alkynes and Vinylidenes

All three pathways require initial complexation of the η^2-alkyne and therefore in order to form a vinylidene, any system must have the ability to form a vacant coordination site. Pathway 1 involves a 1,2-hydrogen shift, **(A)**, directly from the α-carbon to the β-carbon. In Pathway 2 however, a formal oxidative addition of the alkyne occurs and then the vinylidene is formed via a 1,3-hydrogen shift of the hydride intermediate **(B)**. A less common mechanism which relies on the starting complex containing a hydride

ligand is Pathway 3. This involves the insertion of the alkyne into the M-H bond forming an intermediate vinyl complex **(C)**.[69, 70]

The precise pathway by which a system undergoes interconversion between a terminal alkyne and a vinylidene depends on many factors. As a general rule it would appear that Pathway 1 (1,2-hydrogen shift) is more favoured for d^6 metal complexes,[61, 71, 72] but Pathway 2 (formal oxidative addition) becomes more favoured in electron-rich systems[73, 74] (and d^8 metal complexes, see below). Thus, variation of the electronic properties of ligands can induce conversion between the two pathways.[58] This effect was studied in a systematic fashion in 2004 when the mechanism was studied by DFT (6-31G**/BPW91) for five cationic Ru^{II} complexes, $[Ru(\eta^6\text{-}C_5Me_5)(dippe)]^+$, $[Ru(\eta^5\text{-}C_5Me_5)(dmpe)]^+$, $[Ru(\eta^5\text{-}C_5H_5)(PMe_3)_2]^+$, $[RuCl(\eta^5\text{-}C_6Me_6)(PMe_3)]^+$, $[Ru(\eta^5\text{-}C_5H_5)(CO)(PPh_3)]^+$ and $[Ru(\eta^6\text{-}C_6H_6)Cl(PMe_3)]^+$, with a wide range of electron density at the metal centre. The study found that whilst Pathway 1 was favoured for the majority, the energy for Pathway 2 decreased with increasing electron density with the most electron-rich complex, $[Ru(\eta^5\text{-}C_5Me_5)(HCCH)(dippe)]^+$, calculated to preferentially follow Pathway 2. [73]

Most of the evidence for Pathway 2 has been accumulated for d^8 complexes of Co,[75] Rh,[76-79] and Ir[80-82]. Not only do Group 9 metals have greater electron density than early transition metals, but the $d^8 \rightarrow d^6$ transition is more favourable than $d^6 \rightarrow d^4$.[73, 74] Bianchini reported a cobalt system $[Co(P(CH_2CH_2PPh_2)_3)L]^+$ that exhibited a temperature controlled stepwise conversion of L; η^2-HC≡CR → (H)(C≡CR) → C=C(H)R which was followed spectroscopically.[75] His group also worked on an analogous Rh system $[Rh(P(CH_2CH_2PPh_2)_3)L]^+$ [78, 79]which was found to halt at the hydride alkynyl stage with no conversion to the vinylidene, presumably due to the Rh-H bond being stronger than Co-H. Werner and co-workers have been able to isolate all three isomers (alkyne, alkynyl hydride and vinylidene) for the iridium fragment $[IrCl(P^iPr_3)_2L]$ and show that the conversion between them was facile.[80-82]

Many detailed studies in this area have focussed around the $[RhCl(P^iPr_3)_2]$ fragment and Werner was the first to investigate its ability to stabilise alkyne, alkynyl hydride and vinylidene ligands.[83] It was found that on warming to 50 °C in hexane, the alkyne complexes $[RhCl(\eta^2\text{-}HC{\equiv}CR)(P^iPr_3)_2]$ (R = H, Me, ^{t}Bu, Ph, CO_2Me) were converted to the vinylidene complexes $[RhCl(=C=CHR)(P^iPr_3)_2]$. When R = Ph or ^{t}Bu then the intermediate alkynyl hydride complexes $[RhH(\text{-}C{\equiv}CR)Cl(P^iPr_3)_2]$ could be isolated and characterised before being converted through to the vinylidene (Scheme 1-22).[80, 84]

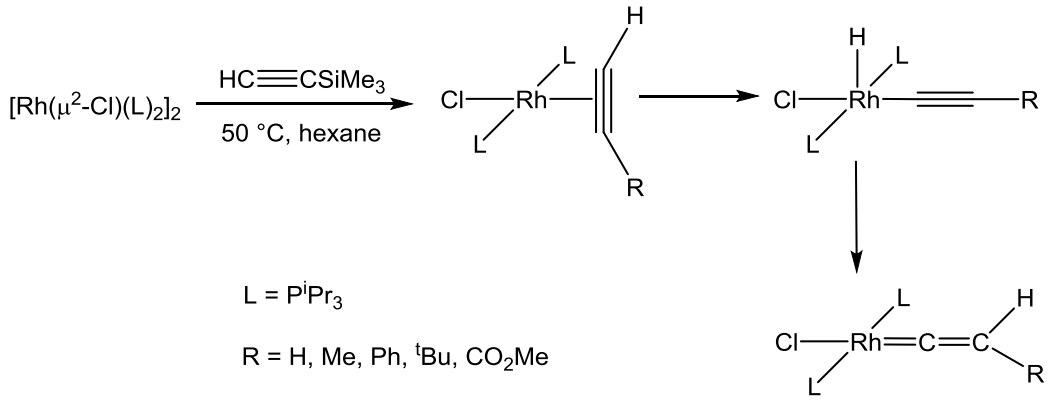

Scheme 1-22 Isolation of an Alkynyl Hydride Species: Evidence for Pathway 2

Calculations on this system were carried out by Wakatsuki et al. (using the MP2:MM3 method) which suggested that the proton migration in the alkynyl hydride to vinylidene rearrangement may occur via a bi-molecular pathway.[68] Grotjahn's group used a series of labelling experiments to test this hypothesis.[85, 86] Reaction of $[Rh(\mu^2\text{-}Cl)(P^iPr_3)_2]_2$ with a mixture of HC≡CH and $D^{13}C\equiv{}^{13}CD$ led to the formation of a mixture of $[RhCl(=C=CH_2)(P^iPr_3)_2]$ and $[RhCl(={}^{13}C={}^{13}CD_2)(P^iPr_3)_2]$ with no evidence for isotopic scrambling observed. No isotope exchange was observed in the formation of a mixture of $[RhCl(=C=CDBu)(P^iPr_2Ph)_2]$ and $[RhCl(=C=CH^iPr)(P^iPr_2Ph)_2]$ either (Scheme 1-23). Therefore it was concluded that the formation of these rhodium vinylidene complexes proceeds exclusively via a uni-molecular process.

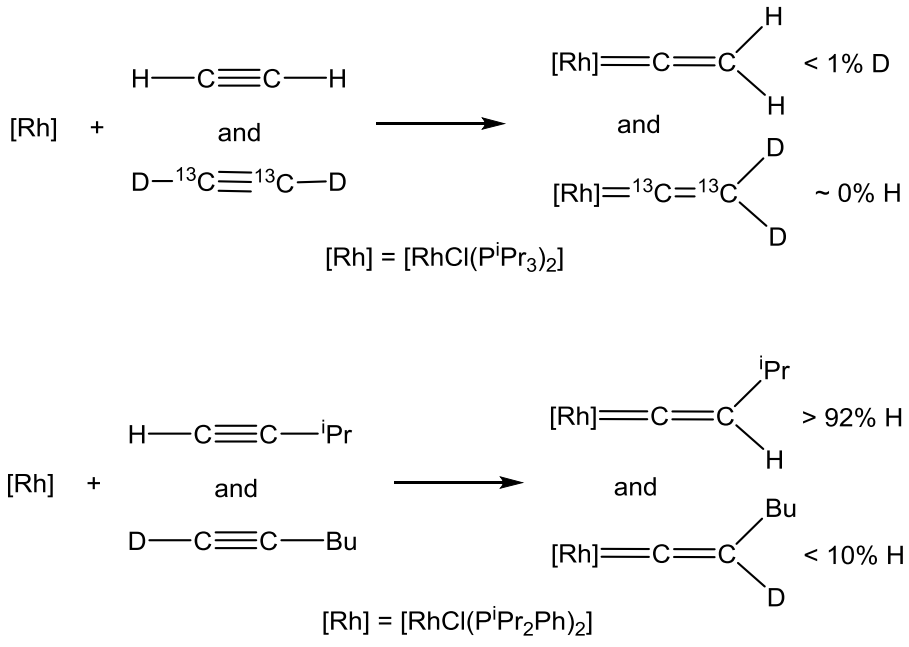

Scheme 1-23 No Isotopic Scrambling is Observed in These Labelling Studies Which Suggests a Uni-Molecular Pathway for Vinylidene Formation

The starting dimer $[Rh(\mu^2\text{-}Cl)(P^iPr_3)_2]_2$ is known to C-H activate DCM and as a result of this reactivity, levels of the intermediate alkynyl hydride were low and it was not observed in the kinetic experiments reported by Grotjahn.[86] Through a switch to d_8-THF

Lynam and co-workers were able to follow the reaction by ^{31}P-NMR spectroscopy and collect full kinetic data for the reaction. Signals corresponding to the intermediate alkynyl hydride were observed (a hydride resonance in the ^{1}H-NMR spectrum was also observed), before being replaced by those of the vinylidene product. With these data for the concentration of each component the reaction profile was successfully fitted to a kinetic pathway based on alkyne ⇌ alkynyl hydride → vinylidene.[87]

1.6.3 Vinylidene Formation from Internal Alkynes

Amongst the most interesting recent reports in this area are those demonstrating the formation of vinylidenes from internal alkynes. The vast majority of vinylidenes in the literature have been formed from isomerisation of terminal alkynes, though for a long time it has been known that heteroatom substituents such as SiR_3,[77, 88-92] SnR_3,[93, 94] SR[95] and I[96, 97] can also migrate. More recently the migration of carbon-based groups has been reported. The first example was a 1,2-CO_2Me shift which resulted in the formation of a bridging vinylidene species from the reaction of $MeO_2CC{\equiv}CCO_2Me$ with a diruthenium species.[98] This was then followed up by a similar C(O)Ph activation achieved by the complex [RuCl(η^5-C_5H_5)(PPh_3)$_2$] (with $AgPF_6$ used as a halide scavenger) converting PhC≡CCOPh into vinylidene complex [Ru(η^5-C_5H_5)(PPh_3)$_2$(=C=CHPh)]$^+$.[99] Migration of the Ph group was ruled out by the inactivity of the system with PhC≡CPh and indeed the mechanism was shown to proceed via a η^1-ketone species (Scheme 1-24), which proves the importance of the alkynone to the transformation.[100] More recent work in the area has shown that ruthenium *tris*(pyrazolyl)borate (Tp) complexes can also effect internal alkynone migration. Kinetic studies on the isomerisation process of this system have given activation parameters which are compatible with an intramolecular concerted mechanism (sigmatropic 1,2-C shift).[101]

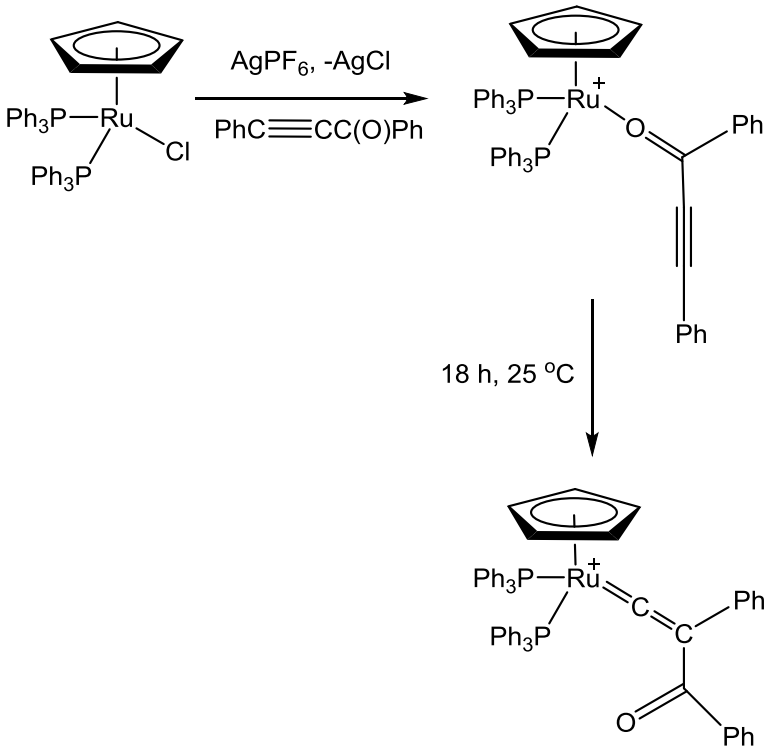

Scheme 1-24 Activation of a C(O)Ph Group by a CpRu Complex

A comparison carried out between Tp and Cp* ligands[102] has found that analogous Cp* complexes form π-alkyne species instead, despite the well-established similarities in the chemistry of these two ligands. Computational studies have suggested that this difference is due to the greater electron-donating abilities of Cp* over Tp and that this increased electron density on the metal encourages back-bonding to the alkyne, thus stabilising it over the vinylidene species.

However, this in contrast to recent work published by Lynam and Fey in which it was shown that the vinylidene tautomer was favoured over the alkyne complex in electron-rich metal systems. The ability of a wide range of metal fragments to stabilise vinylidene moieties was compared using ^{13}C-NMR shifts as a measure of the M-vinylidene interaction. Principle component analysis (PCA) was used to analyse the effect on the bonding of changing the vinylidene substituents, the ancillary ligands and the metal. Overall it was found that electron-rich ligand systems, and electron withdrawing substituents favour the formation of vinylidenes. It was suggested that the fragment $[RuCl_2(PR^2_3)(=C=CHR^1)]$, where R^1 is electron-withdrawing and R^2 electron-rich, would provide the ideal conditions favouring the vinylidene form thermodynamically.

More notable are the results from Ishii's group showing that migration of aryl, alkyl and acyl groups is promoted by the anionic complex $[Ru(P_3O_9)(dppe)(MeOH)]^-$ (P_3O_9 = trisodium trimetaphosphate). As a result of the wide functional group tolerance, it was

possible (using a ^{13}C labelling experiment) to establish the migratory aptitude of a range of substituents. The resultant order, $CO_2Et \approx C_6H_4CO_2Et$-*p* > Me > Ph > C_6H_4Me-*p* > C_6H_4OMe-*p*, suggests that electron-withdrawing groups have a greater migratory ability in this system. However the rate of vinylidene formation was typically shown to follow the opposite trend, suggesting the rate determining step is formation of the initial alkyne complex.[103, 104] Similar results were also obtained using the Ru and Fe half-sandwich complexes [MCl(η^5-C_5H_5)(dppe)] showing that the method has the potential to be widespread (see Scheme 1-25 for an example).[105, 106]

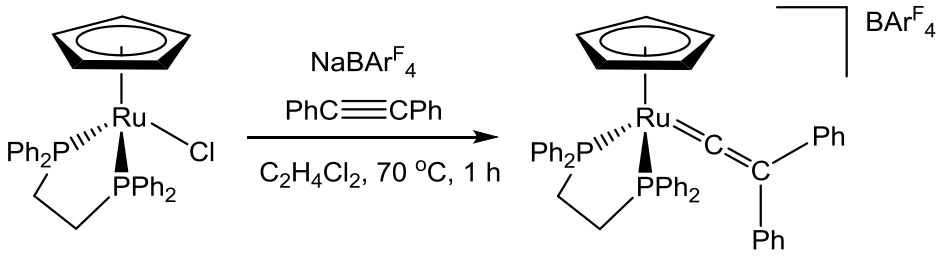

Scheme 1-25 Formation of a Di-Substituted Vinylidene by C-C Bond Activation (BAr^F_4 = [B[3,5-$(CF_3)_2C_6H_3]_4]^-$)

1.6.4 Anti-Markovnikov Addition to Terminal Alkynes

There are numerous examples of catalytic reactions involving intermediate vinylidenes, it is beyond the scope of this chapter to discuss them all. Many reviews have been published on the subject of vinylidenes in catalysis.[57, 58, 107-111] The example of anti-Markovnikov addition of nucleophiles to alkynes highlights the alternative selectivity available through use of intermediate vinylidenes (when compared to the parent alkynes).

The electron deficient nature of the α-carbon of coordinated vinylidenes favours the anti-Markovnikov addition of nucleophiles to terminal alkynes. This selectivity has proved useful in the synthesis of a wide range of organic products.[52, 112] Synthesis of enol esters (from the addition of carboxylic acids to alkynes) is a common use of this process as they are valuable organic intermediates and industrial precursors (as monomers in the polymer industry).[113] The anti-Markovnikov products from these reactions can have either E- or Z- stereochemistry and achieving this additional level of selectivity has often proved difficult. Dixneuf et al. reported a system in the 1990s[114-116] based on [Ru(methallyl)$_2$(dppe)] and [Ru(methallyl)$_2$(dppb)] which, as a result of the trans-addition of the carboxylic acid to the alkyne, afforded a wide range of Z-enol esters as the major product (see Scheme 1-26) .

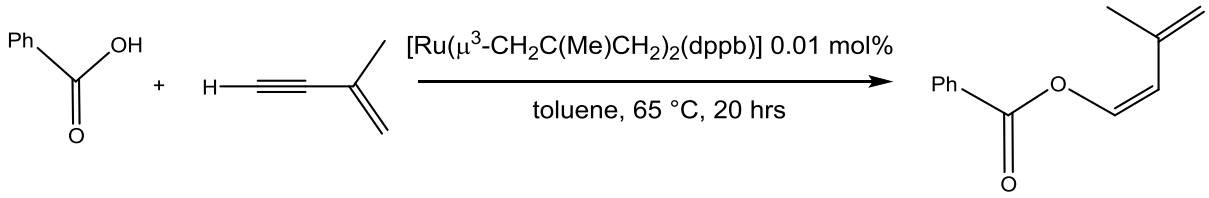

Scheme 1-26 Selective Synthesis of (Z)-Enol Esters by the Anti-Markovnikov Additon of a Carboxylic Acid to an Alkyne. dppb = 1,4-Bis(diphenylphosphino)butane

Another classic use of this atypical behaviour of vinylidene systems is the intramolecular addition of nucleophiles to give heterocyclic products.[107, 108] For the Group 6 metals this was first reported by McDonald and co-workers,[117] with photochemically-activated molybdenum hexacarbonyl (in the presence of triethylamine) being shown to catalyse the formation of vinylidene species from 3-butyn-1-ol derivatives. These species underwent a subsequent cyclisation to give indoles (Scheme 1-27).

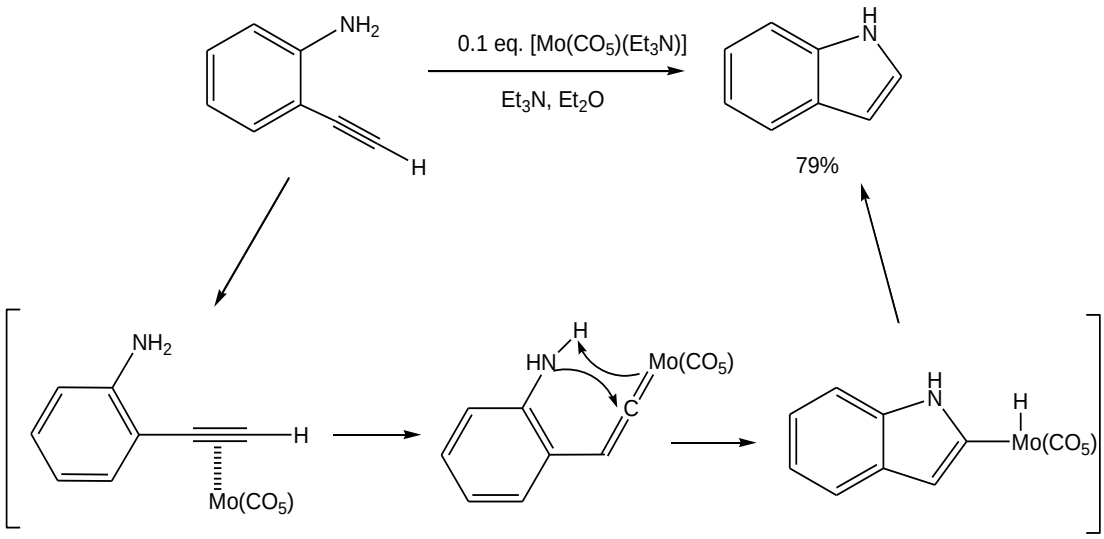

Scheme 1-27 Indole Formation via Vinylidene Intermediates

The use of rhodium, however, has proven to have numerous advantages. A system developed more recently by Trost et al.[118] has been shown to catalyse similar reactions with much improved catalyst turnover, functional group tolerance and selectivity, all without the impracticalities associated with a photochemical reaction (Scheme 1-28).

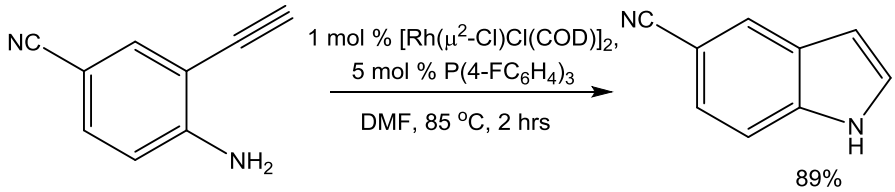

Scheme 1-28 Improved Indole Formation (Excess Ligand was Found to Suppress Alkyne Dimerisation)

1.7 Allenylidenes

1.7.1 Bonding in Allenylidenes

Like vinylidenes, allenylidenes have been implicated as intermediates in many important reactions such as alkene metathesis. As a result much work towards understanding their formation and bonding interactions has been carried out.[119, 120] 'Free' allenylidenes are considerably more stable than 'free' vinylidenes, and have been observed in interstellar clouds.[121-123] Species of the formula C_3H_2 have been experimentally observed in three tautomeric forms (Figure 1-15).[119] Various theoretical studies have been carried out on these systems and it has been consistently found that cyclopropenylidene is the most stable of the three.[124-126] The W-shaped propynylidene species is then found to be the next lowest in energy[124] with linear allenylidene the least stable.

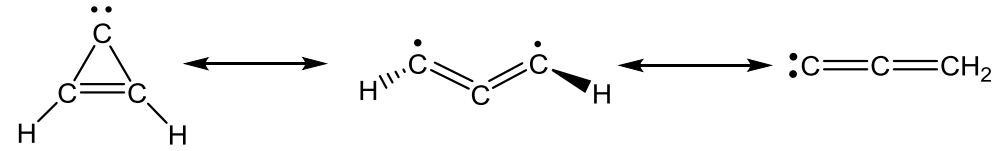

Figure 1-15 Tautomers of the C_3H_2 Fragment

As with vinylidenes (Section 1.6.1), it is found that coordination to a metal centre reverses this trend in stability. C_3H_2 is a σ-donor, π-acceptor ligand[127] and is found as linear allenylidene bound through the lone pair. Three resonance forms are generally used to describe the bonding in allenylidene ligands (Figure 1-16). Comparison with crystallographic bond lengths leads to the conclusion that structure **B** is the dominant form, though **C** becomes more important in systems with heteroatom substituents, R_1.[119]

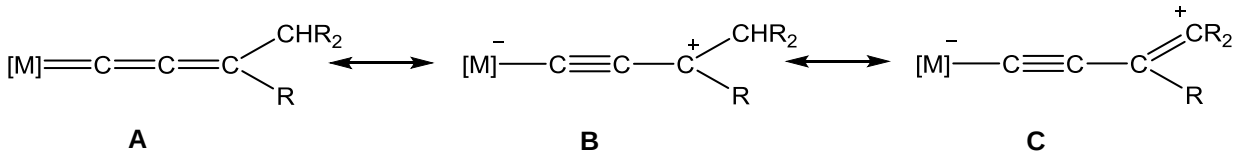

Figure 1-16 Three Resonance forms of Allenylidene Ligands

A more detailed look at the bonding can be achieved using the simplified π-orbital interaction diagram below (Figure 1-17). The LUMO is mainly localised on the Cα and Cγ atoms and as a result nucleophilic attack is favoured on these positions.[62, 119] The contributions of Cα and Cγ to the LUMO are similar[127, 128] and therefore the preference for nucleophilic attack at either of these site is determined by the substituents on the allenylidene, ancillary ligands on the metal centre or the nature of the nucleophile.[119]

The HOMO is localised on Cβ and the metal centre, and therefore electrophilic attack occurs at these atoms.

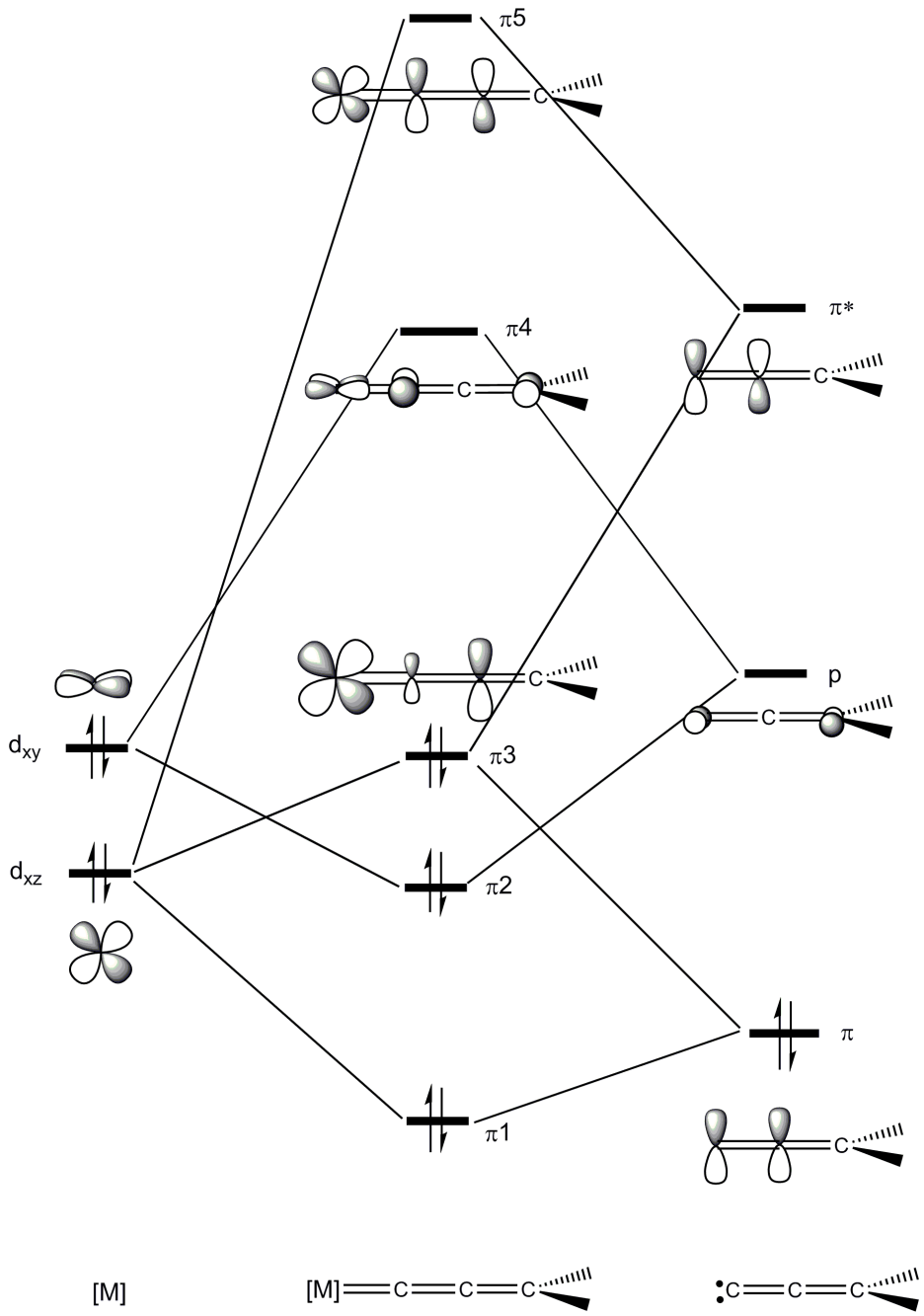

Figure 1-17 Simplified π-orbital Diagram for Transition-Metal Allenylidene Complexes

The first experimental evidence for the nucleophilic nature of Cβ was obtained in 1984 by Kolobova's group who synthesised alkenylcarbyne complexes $[MnCp\{\equiv CC(H)=CR_2\}(CO)_2][X]$ (R = ^{t}Bu or Ph; X^- = Cl^-, BF_4^- or $CF_3CO_2^-$) by reaction of neutral manganese (I) allenylidenes $[MnCp(=C=C=CR_2)(CO)_2]$ with Brønsted acids (HX).[129]

However, the allenylidene literature is dominated by nucleophilic attack on to the Cα and Cγ atoms. One example, showing the importance of ancillary ligands in

determining the preference for attack on either Cα or Cγ, is the reaction of a series of ruthenium allenylidene complexes with phosphine nucleophiles. The complexes $[RuCp(=C=C=CPh_2)(CO)(P^iPr_3)][BF_4]$[130] and $[RuCp^*(=C=C=CPh_2)(CO)(PMe^iPr_2)][B(Ar_F)_4]$[131] were found to add phosphines at the C_α carbon to yield phosphino-allenyl derivatives of the type $Ru(C(PR_3)=C=CPh_2$. If, however, bulkier ligand systems ($[Ru(\eta^5\text{-}C_9H_7)(=C=C=CR_1R_2)(PPh_3)_2][PF_6]$)[132-134] were used then addition was found to occur at the C_γ position to give phosphino-alkynyl complexes $[Ru(\eta^5\text{-}C_9H_7)\{C{\equiv}CCR_1R_2\text{-}(PR_3)\}(PPh_3)_2][PF_6]$ (R_1, R_2 = alkyl, aryl or H; PR_3 = PPh_3, $PMePh_2$, PMe_2Ph, PMe_3). Interestingly, if R_1 or R_2 = H then deprotonation of these complexes affords ylide-alkynyl species that have proven to be useful precursors for the formation of a wide variety of enynyl ligands (Scheme 1-29) via Wittig-type reactions.[135-137]

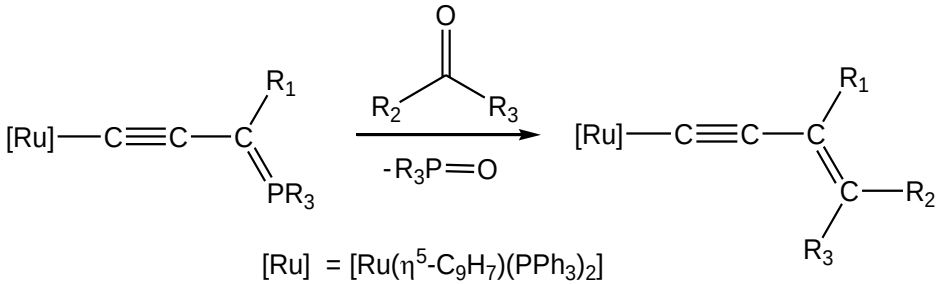

Scheme 1-29 Use of a Metal Coordinated Phosphorus Ylide in Wittig-Type Chemistry

The lengthening of the carbon chain also introduces structural changes in the orientation of the ligand substituents. The empty p-orbital of the carbene ligand is aligned so as to optimise overlap with the metal orbital. With additional π-bonds, the preferred orientation is changed by a series of 90° twists (Figure 1-18).[138]

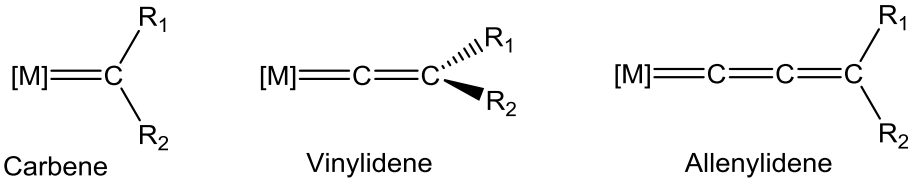

Figure 1-18 Orientation of Carbene Substituents

1.7.2 Allenylidene Formation

Since it was first demonstrated in 1982 by Selegue's group[139], the method of choice for the synthesis of allenylidenes has been the dehydration of hydroxy-vinylidenes (Scheme 1-30). For Group 8 systems it is commonly found that this loss of water is spontaneous and the intermediate hydroxyl-vinylidene is not observed. However in some cases it is necessary to promote dehydration by addition of acid[120] or by passing the complex through acidic alumina.[140]

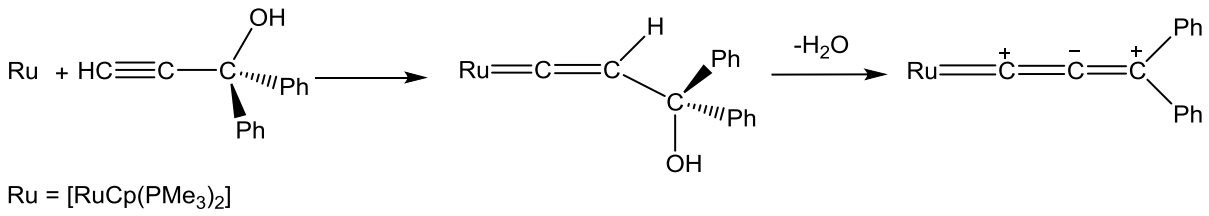

Scheme 1-30 Formation of Allenylidenes via Dehydration of Hydroxy-Vinylidenes

One of the draw-backs of this method is the competitive formation of vinyl vinylidene species which can occur when a proton is present in the β position to the OH group (Scheme 1-31).

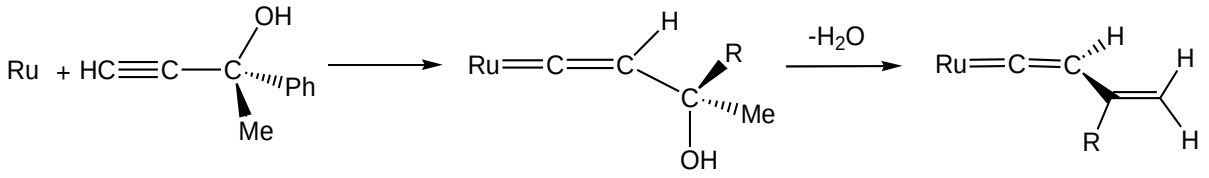

Scheme 1-31 Formation of Vinyl Vinylidene via Dehydration of Hydroxy-Vinylidenes

Theoretical studies (carried out at the MP2/DZV(d,p)+*G* level) on $[Ru(\eta^5\text{-}C_5H_5)\{=C=C=C(H)CH_3\}(PH_3)_2]^+$ and $[Ru(\eta^5\text{-}C_5H_5)\{=C=C(H)CH=CH_2\}(PH_3)_2]^+$ showed that the vinyl vinylidene tautomer is 8.8 kJ mol^{-1} more stable than the allenylidene, explaining its competitive formation.[134]

Another competing reaction that has been observed is the formation of indenylidene ligands from di-phenyl substituted allenylidenes. The first synthesis of a ruthenium phenylindenylidene complex was reported in 1999 by Hill's group (Scheme 1-32),[141] but they were unaware of their breakthrough and instead believed their product to be an allenylidene.

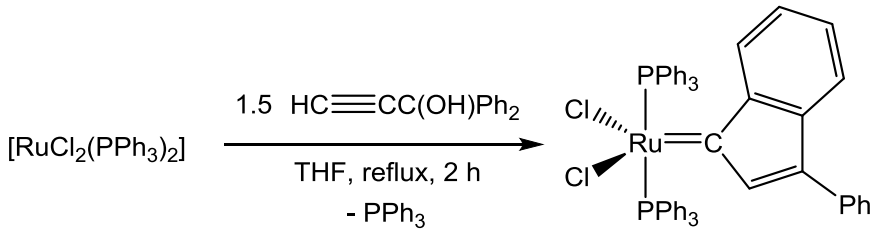

Scheme 1-32 Formation of the First Ruthenium Indenylidene Complex

The true nature of the complex was first postulated later that year by Fürstner[142] when inconsistencies were spotted in the spectroscopic data.[143] In particular, peaks for the β and γ carbon atoms were not observed in the ^{13}C-NMR spectrum and the aromatic region of the ^{1}H-NMR was far too complicated for the product to contain the allenylidene ligand. Use of 2D-NMR techniques showed the presence of the

indenylidene ligand[143] and a crystal structure was obtained by Nolan's group to complete the characterisation.[144]

Dixneuf and Castarlenas have used low temperature studies to show that the allenylidene complex, $[RuCl(=C=C=CPh_2)(PCy_3)(\eta^6\text{-p-cymene})][CF_3SO_3]$, when treated with triflic acid at -40 °C, is transformed into the vinyl carbyne complex $[RuCl(\equiv C\text{-}CH=CPh_2)(PCy_3)(\eta^6\text{-p-cymene})][CF_3SO_3]$. When the reaction is warmed to -20 °C resonances associated with the indenylidene complex $[RuCl(\eta^6\text{-p-cymene})\{=C\text{-}CH=C(Ph)C_6H_4\}(PCy_3)][CF_3SO_3]$ were observed, thus suggesting a likely route of formation for the indenylidene complexes (Scheme 1-33).[99, 145] There has been much recent interest in ruthenium indenylidene complexes as they have proved to have considerable potential as alkene metathesis catalysts.[143, 145, 146]

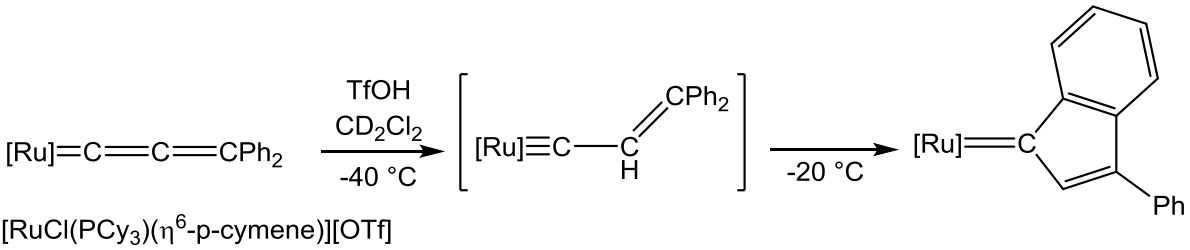

Scheme 1-33 Mechanism of Formation of Ruthenium Indenylidene Complexes

Another major draw-back is that the propargylic alcohol method is not applicable to all systems and alternative routes to allenylidene ligands must be found. For example, allenylidene complexes of Group 6 metal carbonyl fragments ($[M(CO)_5]$ where M = Cr or W) require electron-donating substituents on the allenylidene chain to aid their thermal stability. In response to this, Fischer developed an alternative route in which the metal carbonyl is reacted with a deprotonated propynoic acid amide to form a metal acetylide complex (Scheme 1-34). On treatment with $[R_3O]BF_4$ the allenylidene (now with two different electron-donating substituents) can be isolated.[147]

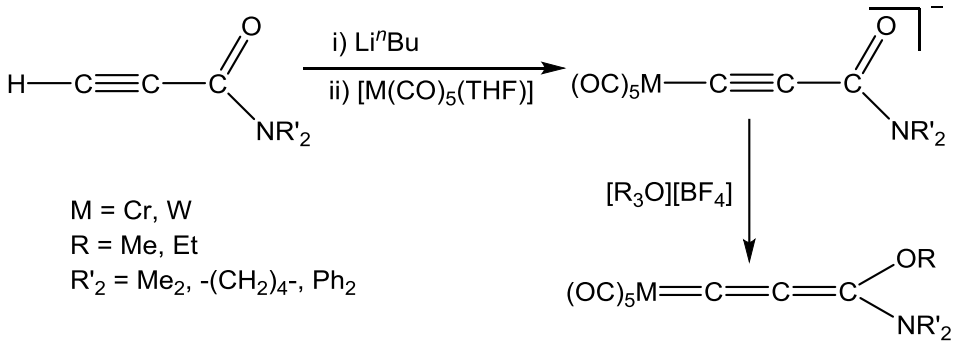

Scheme 1-34 Fischer's Alternative Synthetic Route to Allenylidene Complexes of Cr and W

This method is a good example of the main alternative synthetic route. Terminal alkynes are used to form intermediate acetylide complexes and the isomerisation to allenylidenes effected using a variety of reagents.[148]

1.7.3 Allenylidenes as Catalytic Intermediates

Allenylidene complexes are increasingly proving to be of interest in catalysis. There are two main types: those examples where the allenylidene is implicated as an intermediate, and those where the allenylidene complex is the catalyst precursor.

There are a wide range of catalytic reactions where allenylidenes are observed or implicated as intermediates.[9, 119] Not all of these can be discussed here; however, one of the most important is propargylic substitution (Scheme 1-35).

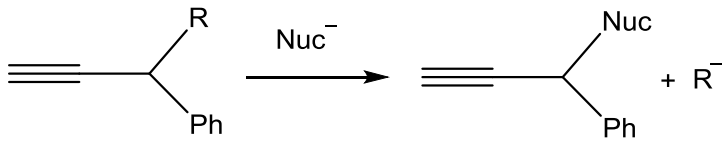

Scheme 1-35 A General Scheme for Propargylic Substitution

This susceptibility of Cγ towards nucleophilic attack has led to the development catalytic methods for the direct substitution of the hydroxyl group in propargylic alcohols. This offers an alternative to the Nicholas reaction which uses stoichiometric $Co_2(CO)_8$ to stabilise intermediate carbocations (Scheme 1-36). [149]

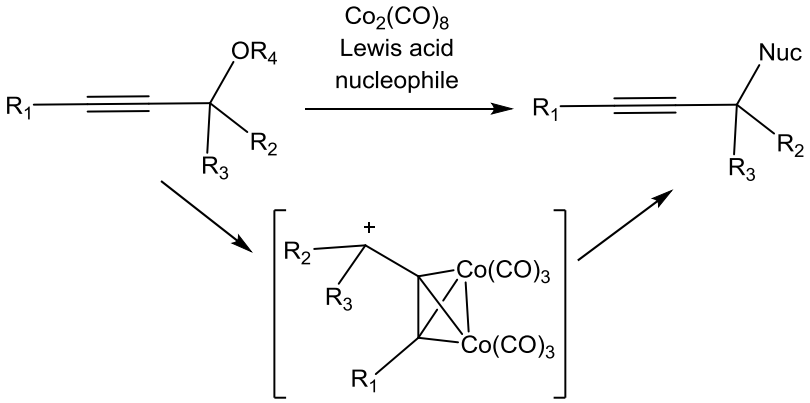

Scheme 1-36 The Nicholas Reaction

Work in this area was first undertaken in 2000 by the collaborative work of Nishibayashi, Hidai, and Uemura, using the thiolate-bridged diruthenium(III) complexes $[\{Cp^*RuCl(\mu\text{-}SR)\}_2]$ (R = Me, Et, ^{n}Pr or ^{i}Pr) as catalyst precursors (Figure 1-19).[51, 150]

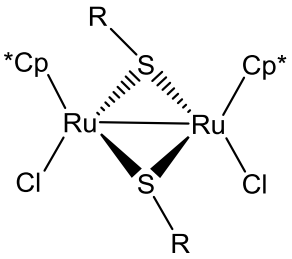

R = Me, Et, ^{n}Pr, or ^{i}Pr

Figure 1-19 A Catalyst for Propargylic Substitution

This was the first example of a general route for catalytic propargylic substitution, which can be used for O, S, N, P centred nucleophiles and a few C centred nucleophiles (Scheme 1-37).[151] Previous examples had found that the range of substrates had depended heavily on the metal used.

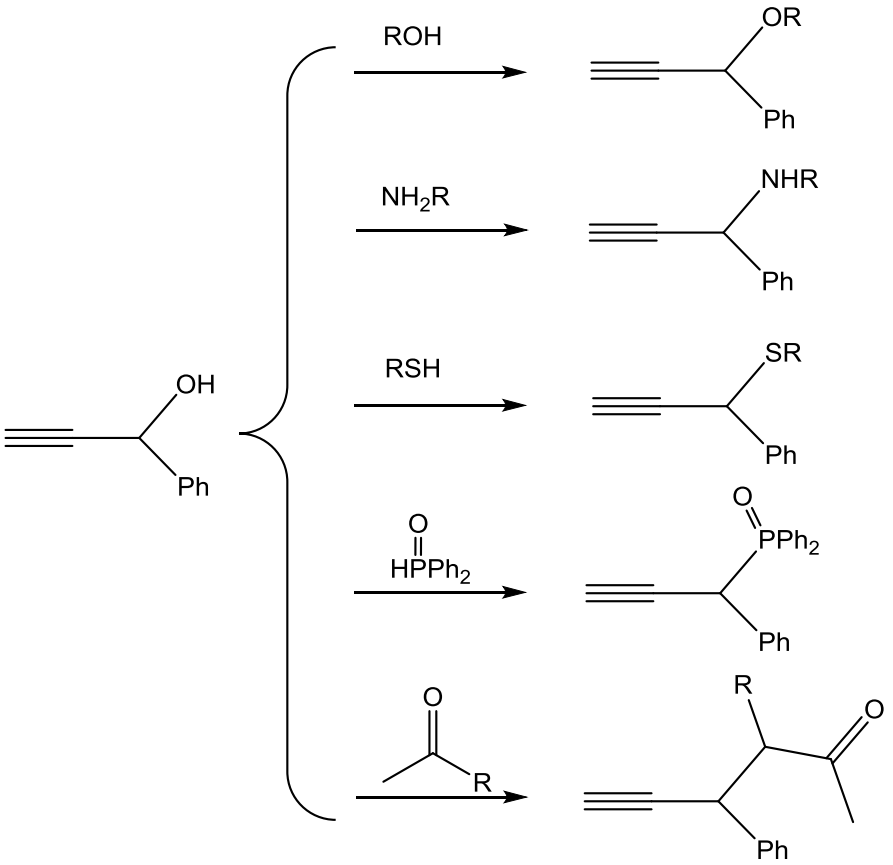

Scheme 1-37 Propargylic Substitution Reactions: In the presence of Catalyst (5 mol%, Figure 1-19) and NH_4BF_4 (10 mol%)

By using chiral sulfur ligands, it is possible for enantioselective transformations to be effected.[152, 153] More recently this work has been extended with the use of transition metal co-catalysts to activate carbon-based nucleophiles. Copper has been used to form enolates from β-ketoesters, and it is these that then attack the allenylidene intermediate formed by the ruthenium catalyst (Scheme 1-38).[154, 155]

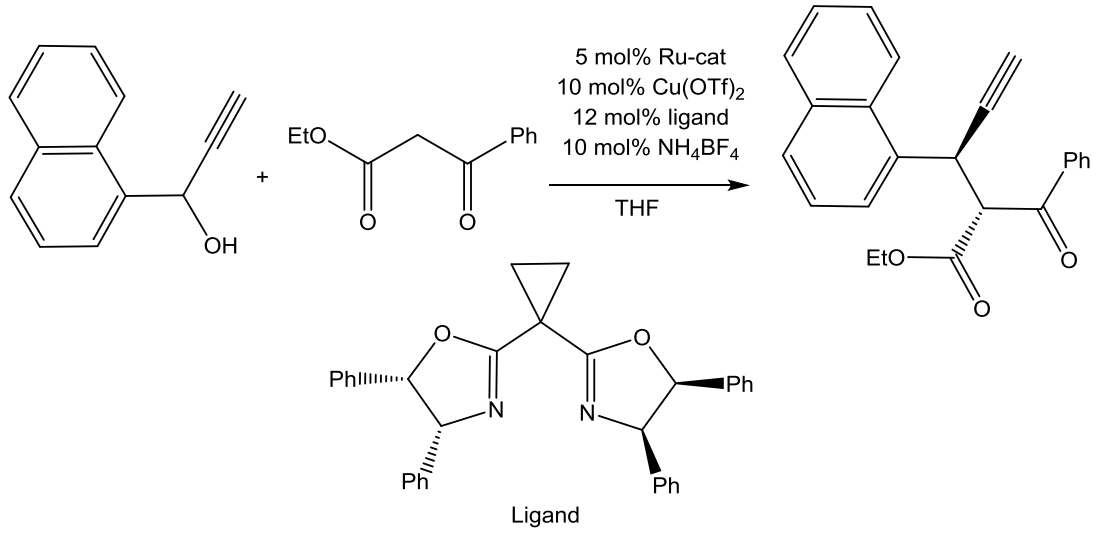

Scheme 1-38 Use of a Copper Co-Catalyst to Enable Enantioselective Propargylic Substitution

1.7.4 Allenylidenes as Catalytic Precursors

Over the last few decades, alkene metathesis has proved to be an important reaction class in synthetic chemistry. Much work has been invested in improving the efficiency and functional group tolerance of the catalysts used in these reactions. Some of the most recent additions to the family of metathesis catalyst precursors have been ruthenium allenylidene complexes. These species have proved to be accessible and easy to handle alternatives with excellent catalytic properties and numerous reviews have been published.[8, 119, 156, 157]

Dixneuf and Fürstner were the first to employ ruthenium allenylidene complexes in alkene metathesis, RCM in this case though they have been shown to promote ROMP.[158-160] Several cationic half sandwich complexes of the type $[RuCl(=C=C=CR_2)(\eta^6\text{-}p\text{-cymene})(PR_3)][X]$ were screened for catalytic activity. A bulky phosphine ligand was required to prevent solvent attack at C_α which resulted in the formation of inactive vinyl carbene ligands. Electron-rich phosphines increased the catalytic activity and the following trend was observed: $PCy_3 > P^iPr_3 >> PPh_3$. Changing the substituents on the allenylidene ligand was also had an effect on the catalytic activity, However, the most efficient was the simplest di-phenyl substituted. The largest effect was found when the weakly-coordinating anion was changed with the catalytic activity increasing with the following trend: $[X]^- = TfO^- >> PF_6^- \approx BPh_4^- >> BF_4^-$. Use of triflate enabled room temperature catalysis, whereas tetrafluoroborate inhibited the reaction. The observation that acidic conditions promoted the catalysis led to investigations that showed that the active species was the indenylidene. This led to the first detailed study of the rearrangement mechanism (see Section 1.7.2 on allenylidene formation, Scheme 1-33).[99, 145] The isolated indenylidene complex was found to be a more active species than the allenylidene, able to catalyse ring closing methathesis

(RCM), ring opening metathesis polymerisation (ROMP), acyclic diene metathesis (ADMET) and enyne metathesis (Scheme 1-39).

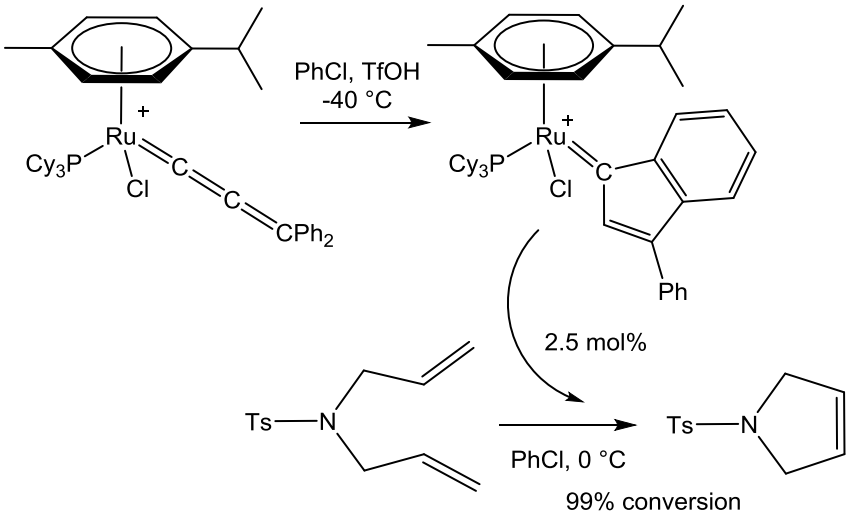

Scheme 1-39 An Indenylidene Complex Catalysing Ring-Closing Metathesis

1.8 Carbyne complexes

Carbyne ligands have a formal metal-carbon triple bond which results in short M-C bond distances and approximately linear geometry in the M≡C-R fragment. The bonding can be viewed in a similar manner to that observed in carbene complexes (Section 1.5.1), with carbyne ligands also having an sp-hybrid orbital which allows for a σ-interaction with the metal orbitals. There are however two p-orbitals available for bonding, leading to the formation of two π-interactions (Figure 1-20).[11]

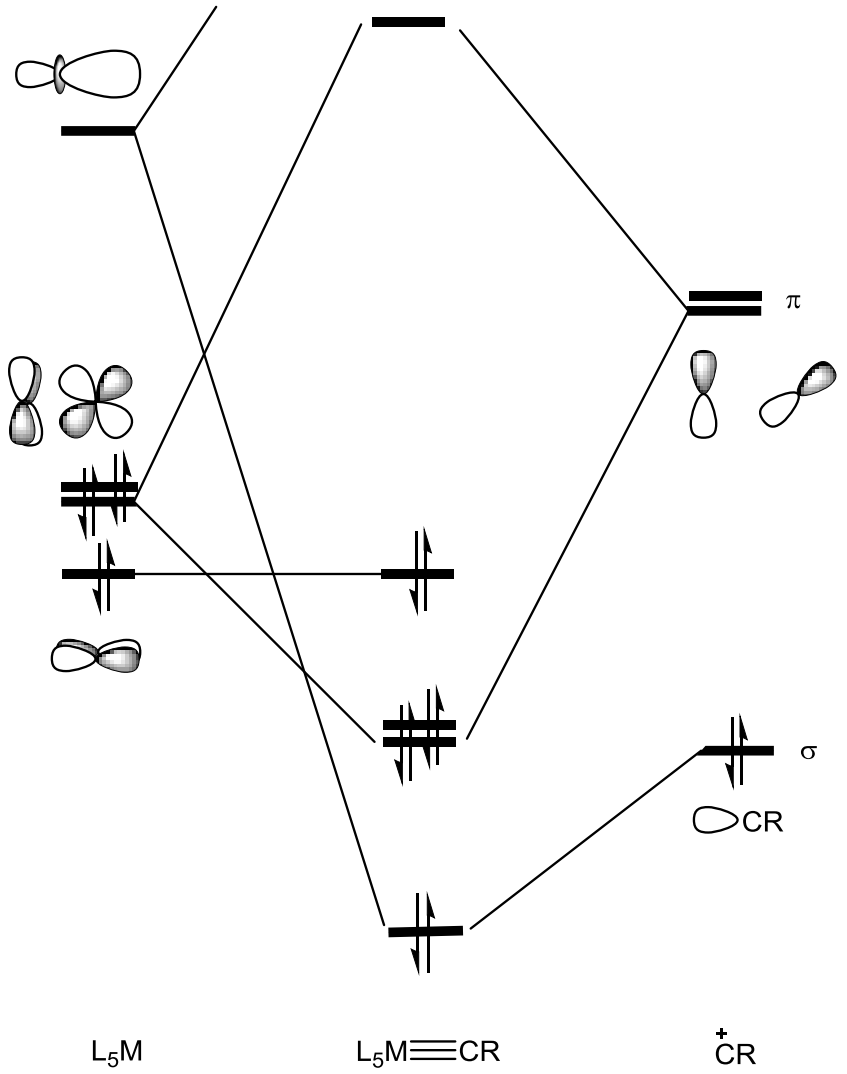

Figure 1-20 Molecular Orbital Diagram for a Metal Carbyne Complex that is Assigned as Cationic

They can also be classed as Fischer-type or Schrock-type with similar reactivity trends to the corresponding carbenes expected. This is shown in the above molecular orbital diagram (Figure 1-20) where the HOMO of the Fischer carbyne is mostly centred on the metal and therefore the LUMO is predominantly ligand based. This then explains the tendency for nucleophillic attack at the carbon of Fischer carbynes.

Carbyne complexes are most commonly found for metals in Groups 5-7. Schrock carbynes of molybdenum and tungsten have been found to be highly active alkyne metathesis catalysts (carbynes are also intermediates in these transformations).[161-163] Schrock was the first to develop structurally defined carbyne complexes which were the first to find widespread use as alkyne metathesis catalysts (Figure 1-21).[36, 164] However, traditionally these have been highly air and moisture, sensitive making them difficult to use and restricting their applications. In 2009 Fürstner et al.[165] developed a complex (Figure 1-20) that proved stable enough to weigh out and use in air, and tolerant to the presence of a range of functional groups.

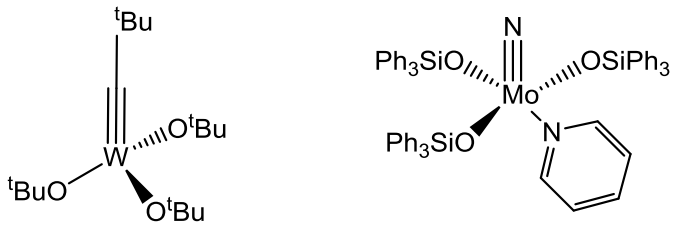

An Early, Highly Active Catalyst

Air Moisture and Functional Group Tolerant

Figure 1-21 Alkyne Metathesis Catalysts

The field of alkyne metathesis is relatively new and underdeveloped, particularly in comparison to the vast, and increasingly useful, field of alkene metathesis.[166] Alkyne metathesis is already being applied however, in particular in the synthesis of conjugated polymers for electronic applications and in the stereoselective (*E*- or *Z*-geometry) synthesis of alkene containing macrocycles.[161, 163, 166] For example, below is shown the synthesis of the valuable fragrance molecule civertone via alkyne metathesis followed by selective hydrogenation (Scheme 1-40).[167]

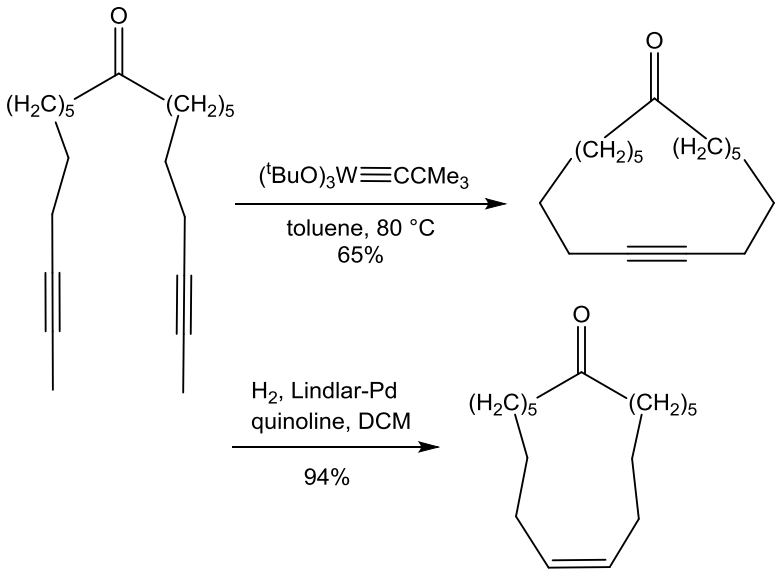

Scheme 1-40 Stereoselective Synthesis of Civetone via Alkyne Metathesis

1.9 Project Background

1.9.1 Previous Work in the Group

The easily prepared ruthenium acetate complex *cis*-[Ru(κ^2-OAc)$_2$(PPh$_3$)$_2$] **1a** was first described by Wilkinson in 1973,[168] but its reactivity has been little explored. Acetate ligands are known to exhibit fluxional behaviour, and with the aim of exploiting this property, a study into the reactivity of **1a** was carried out by Dr Christine Welby.[169] The hemilabile nature of the acetate ligand provides a simple route for the generation of a free coordination site at the metal without loss of a ligand. The common ruthenium

precursor $[RuCl_2(PPh_3)_3]$ exhibits similar chemistry to **1a**, but the necessary loss of a phosphine ligand in order to generate a free coordination site slows reaction rates and causes purification difficulties.

Complex **1a** was reacted with a range of ligands (L) to form complexes of the type $[Ru(\kappa^2\text{-OAc})(\kappa^1\text{-OAc})(PPh_3)_2(L)]$, with the phosphine ligands now in a *trans*-orientation and containing κ^1 and κ^2 acetate ligands. The acetate ligands were found to be fluxional and exchanged rapidly on the NMR timescale with only one resonance for the acetate methyl groups observed in the ^1H and ^{13}C- NMR spectra. However, the exchange is slow on the IR timescale and so it was possible to observe both coordination modes via IR spectroscopy.[170] An acetate ligand has two IR active stretching modes, the symmetric and the asymmetric stretches. The difference between the two (Δv) is characteristic of the binding modes and can be used for assignment, with the chelating κ^2-acetate ligands displaying a small difference (Δv ca. 40 – 130 cm^{-1}) and the mono-dentate κ^1-acetates exhibiting a much larger difference (Δv ca. 210 – 270 cm^{-1}).[171, 172]

The $[Ru(\kappa^2\text{-OAc})_2(PPh_3)_2]$ scaffold was found to be particularly suited to the stabilisation of π-accepting ligands such as carbon monoxide, isocyanides and carbenes.[173] The reaction of **1a** with alkynes to form vinylidene complexes was found to be particularly fast, with complete clean conversion observed within minutes (Scheme 1-41). This is in comparison to the reaction with the chloride analogue $[RuCl_2(PPh_3)_3]$ which takes approximately 24 hours to reach full conversion to the vinylidene complex.[71]

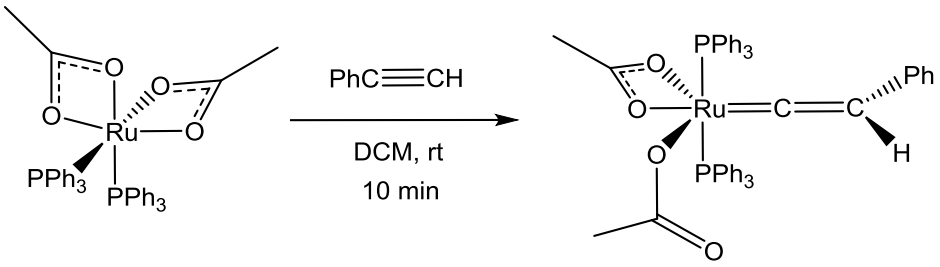

Scheme 1-41 Reaction of **1a** with Phenylacetylene to form a Vinylidene

An investigation into the mechanism was then instigated in order to understand the origins of this remarkable enhancement in reaction rate. Through a combination of experimental and theoretical work it was found that the acetate ligands play a key role in the isomerisation from alkyne to vinylidene. Like the mechanisms discussed in Section 1.6.2, the alkyne initially binds in an η^2-fashion. The κ^1-acetate ligand then deprotonates the alkyne ligand to form an acetylide complex, which is then reprotonated by the acetic acid at the β-carbon to form the vinylidene product (Scheme 1-42). This has been termed a Ligand-Assisted Proton Shuttle (LAPS) mechanism and

the acetate ligands have provided a low energy route for the alkyne to vinylidene isomerisation.[174]

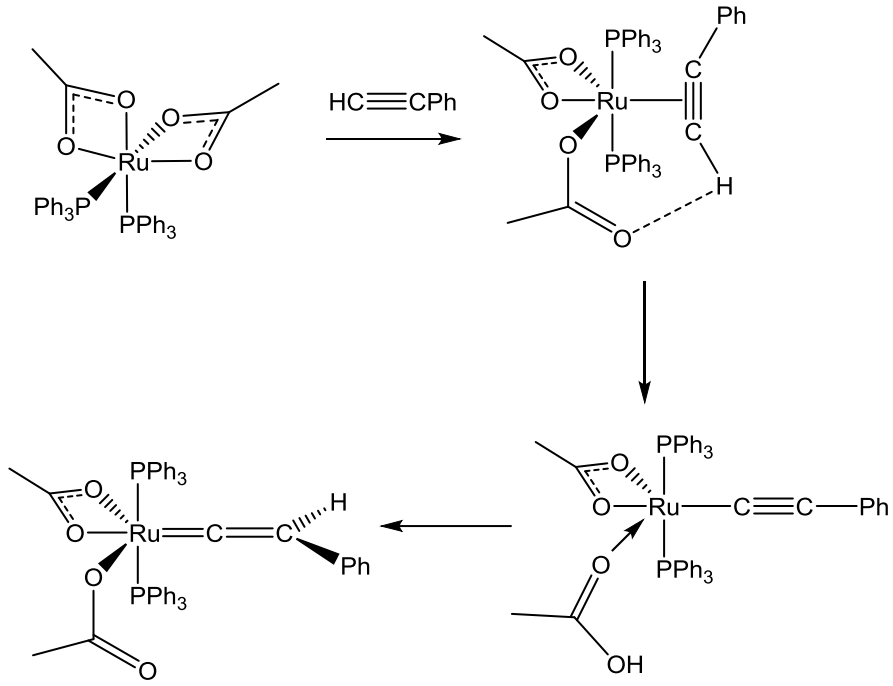

Scheme 1-42 LAPS Mechanism for the Formation of Vinylidene Complexes

When **1a** was reacted with propargylic alcohols the corresponding hydroxy-vinylidene complexes were isolated. As discussed in Section 1.7.2, compounds of this type frequently undergo dehydration to form allenylidene complexes.[120] However, here it was found the hydroxy-vinylidene converted through to 1,1-disubstituted (geminal) alkene and a carbonyl complex over time (Scheme 1-43).[170]

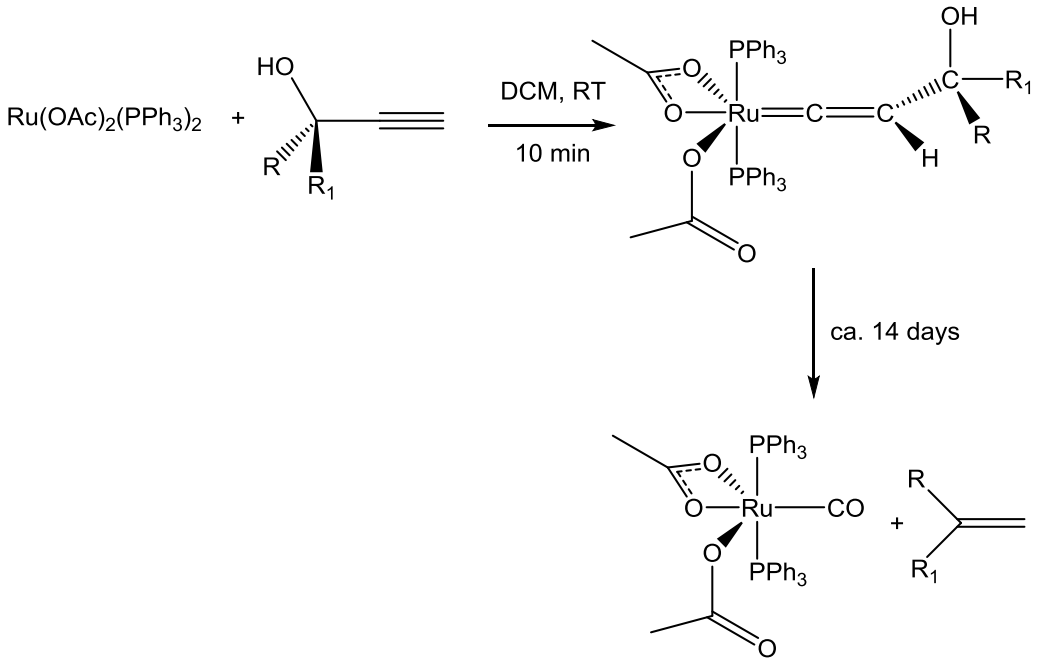

Scheme 1-43 Transformation of Propargylic Alcohols via a Vinylidene Intermediate

In an effort to understand the mechanism by which this decarbonylation occurs, an isotopic labelling study was carried out. ^{18}O labelled acetic acid was used to synthesise **1a** and the reaction followed by IR spectroscopy. It was observed that ^{18}O atoms from the acetate groups were incorporated into the carbonyl ligand of the product. Even with the use of DFT calculations it has not been possible to establish the exact mechanism of this transformation, though it is clear that the acetate ligands play a key role.

1.10 Conclusion

The field of organometallic chemistry is vast, but growing faster than ever courtesy of its potential for delivering new synthetic methodologies. It has been found that alkynes are excellent ligands for transition metals and as a result the chemistry of alkynes has been dramatically expanded. The synthesis and reactivity of a wide range of compounds has been discussed in this chapter, focussing on C_3 moieties and their relation to alkynes. Previous work in the Lynam group has shown that this chemistry can be expanded further through the use of acetate ligands. Their hemilabile nature, and their ability to act as an internal base, opens up scope for much future work which will be the subject of this thesis.

1.11 Overview and Aims of this Project

The overarching theme of this thesis is to understand the mechanisms by which alkyne isomerisation occurs and extend the knowledge of what structures can be formed. Another important aspect of the work is to build upon the project carried out by Dr Christine Welby, outlined in Section1.9, and to expand the chemistry of the $[Ru(\kappa^2\text{-}OAc)_2(PPh_3)_2]$ system. This fragment is known to form complexes with π-accepting ligands, the work outlined in Chapters 3 and 4 has the aim of expanding the chemistry to new ligand classes such as allenylidenes or alkenes.

The initial work presented in Chapter 2 will involve further investigation into the decarbonylation of propargylic alcohols. The ultimate aim here is to develop a novel catalytic route for the synthesis of geminal alkenes. Discussion will focus around the reactivity and kinetic effects caused by changing the phosphorus ligands, effects due to the carboxylate ligands have previously been investigated by Oliver Pickup.[175] It is anticipated that by making the metal centre less electron-rich the levels of back-bonding to the CO ligand in the final CO-complex will be reduced. This will weaken the M-CO bond and encourage CO loss, leading to regeneration of the starting *cis*-$[Ru(\kappa^2\text{-}OAc)_2(PPh_3)_2]$ **1a** complex (Scheme 1-43) and thereby allowing for a catalytic cycle to occur. Development of a new route to complexes $[Ru(\kappa^2\text{-}OAc)_2(PR_3)_2]$ is required since the synthetic route to complex **1a** has been found to work only in the

case of triphenylphosphine.[176] A few analogues of **1** containing different phosphine ligands are present in the literature, however they are all produced via different methods.[177-181] The development of a general route will allow easy preparation of a range of analogues of **1** and allow for an investigation into the steric and electronic parameters of the system.

It is hoped that mechanistic insight into the decarbonylation will further aid development of a catalytic system. The ReactIR instrument will be used to obtain kinetic data from the reaction and potential intermediate complexes from the resulting proposed mechanism will be synthesised.

In later chapters this work will move on to investigating the synthesis and reactivity of novel organometallic complexes formed from alkynes. In Chapter 3 novel vinyl carbene complexes are presented which were synthesised as potential intermediates in the decarbonylation. Their reactivity towards nucelophiles and bases is discussed and followed with experimental results showing the selective synthesis and charaterisation of new allenylidene or vinylvinylidene complexes, depending on the substituents present (Scheme 1-44). Theoretical calculations (DFT) are then used to probe the mechanism of the reaction and to explore the origin of the selectivity.

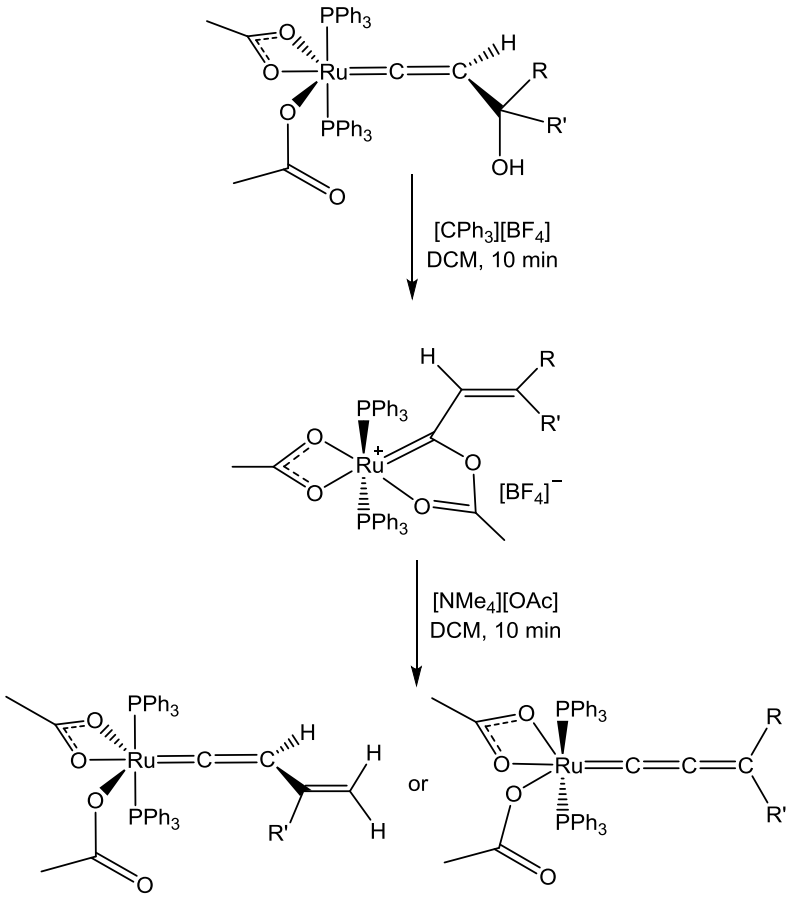

Scheme 1-44 Route for the Stepwise Formation of Allenylidene and Vinylvinylidene Complexes

In Chapter 4 the aim is to synthesise a new class of organometallic complexes, phosphine-substituted vinylidenes. The chemistry of the [Ru(κ^2-OAc)$_2$(PPh$_3$)$_2$] system is expanded to include allene complexes, which are found to form alongside the targeted vinylidenes (Scheme 1-45). Again DFT will be used to probe the alkyne to allene isomerisation that leads to the formation of these two products.

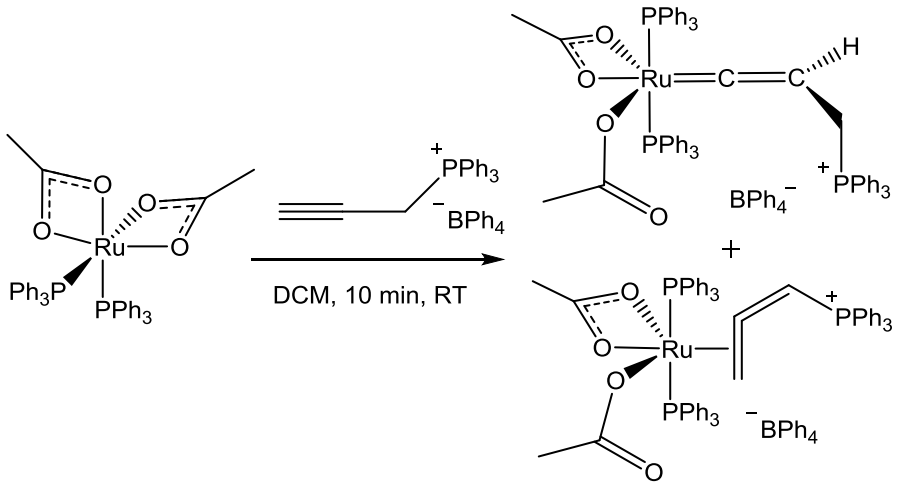

Scheme 1-45 Reaction of *cis*-[Ru(κ^2-OAc)$_2$(PPh$_3$)$_2$] **1a** with Triphenylpropargylphosphonium Tetraphenylborate **39c**

2. Phosphorus Ligand effects in $[Ru(\kappa^2OAc)_2(PR_3)_2]$

2.1 Introduction

Previous work in the Lynam group has led to the development of the system shown in Scheme 2-1. It would normally be expected that such a reaction with a propargylic alcohol would lead to the formation of an allenylidene (as discussed in Section 1.7.2 of the introduction).[139] However, due to the presence of the acetate ligands, an alternative mechanism is followed, which leads to the formation of a 1,1-disubstituted (geminal) alkene **5** and a carbonyl complex **4**.[170]

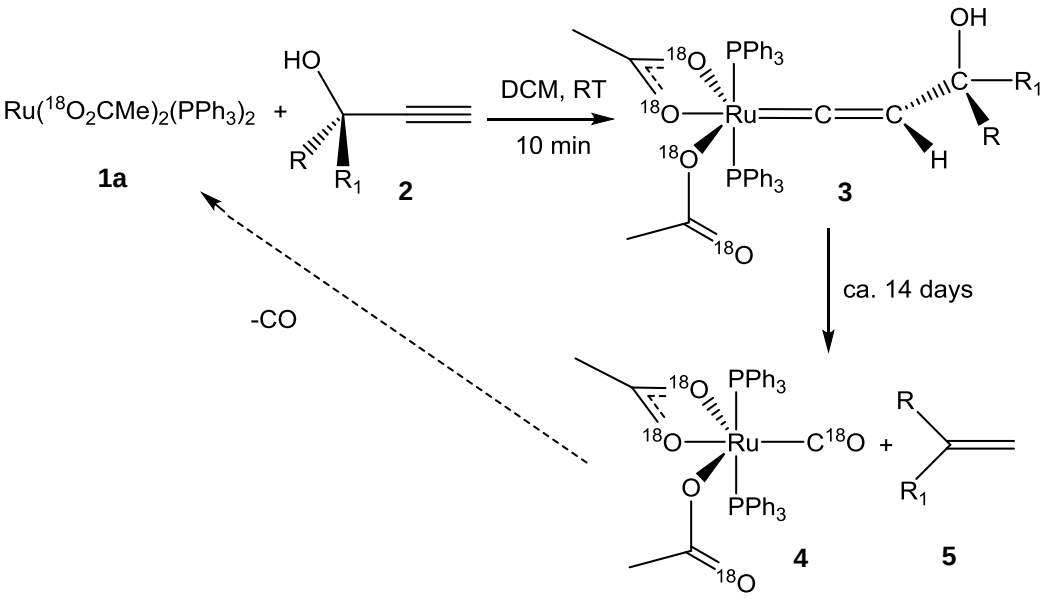

Scheme 2-1 Transformation of Propargylic Alcohols via a Vinylidene Intermediate

A similar reaction was observed by Dixneuf and Bustelo, and it is postulated that the transformation of $[RuCl(p\text{-cymene})(PCy_3)]$ and HC≡CCH(OH)Ph into $[RuCl(CO)(p\text{-cymene})(PCy_3)]$ $[B(Ar_F)_4]$ and styrene proceeds via allenylidene and hydroxycarbene intermediates.[182, 183]

The initial aim of this project was to gain mechanistic insight into the reaction and if possible identify any intermediates. It is hoped that this information will then be able to aid development of a catalytic system. Once catalytic, this reaction would provide a new route to geminal alkenes.

One of the most reliable and general routes to geminal alkenes is the Wittig reaction.[184] However this reaction has many disadvantages, the main one being the involvement of

phosphines which results in the formation of a stoichiometric amount of phosphine oxide as a by-product. Not only does this lower the atom economy of the reaction,[185] the oxide can also be difficult to remove from the desired product, even by column chromatography.[186]

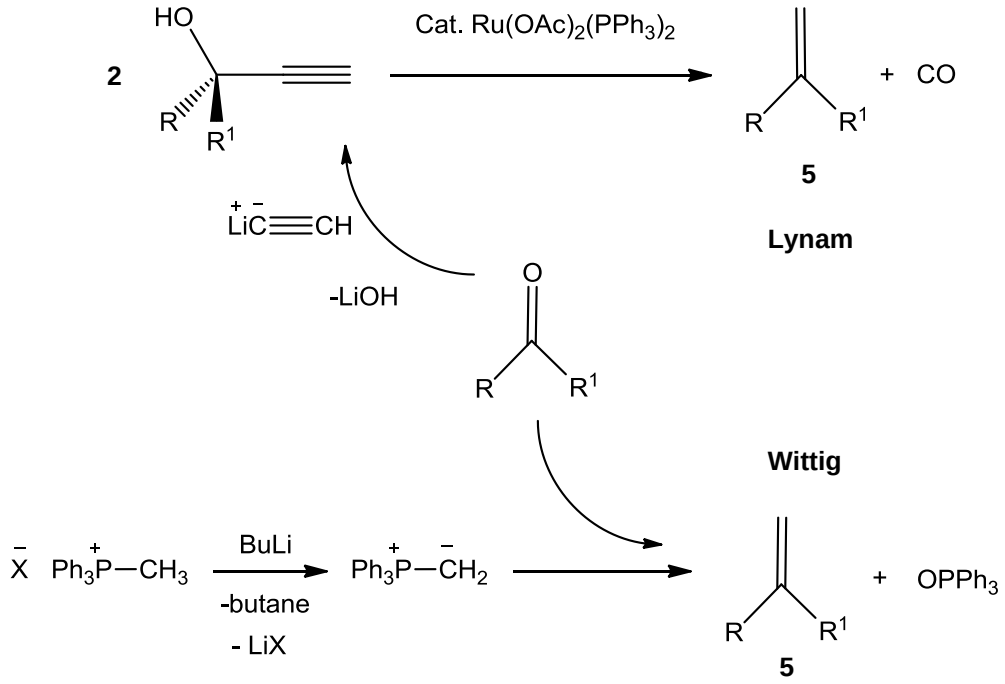

Figure 2-1 A Comparison to the Wittig Reaction

Our proposed route (Figure 2-1) uses propargylic alcohols as the starting point. Many simple examples of these are available commercially, however, more complex structures can be synthesised from lithium acetylide and the appropriate ketone.[187]

However, in order for our route to improve upon the Wittig reaction, the final step must use catalytic amounts of ruthenium. For the catalytic cycle to be completed, the CO ligand from complex **4** needs to be lost, so that the catalyst precursor **1a** can be regenerated.

2.2 Photolysis of Complex 1a

Carbonyl ligands are often found to be photochemically labile[11] and so it was decided to attempt photochemical regeneration of the catalyst (Scheme 2-2). A sample of complex **4** (δ 39.1 in the ^{31}P-NMR) was irradiated with broad-spectrum UV radiation to see if the carbonyl ligand could be removed and complex **1a** (δ 63.6) formed.

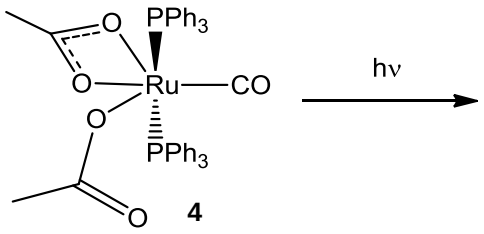

4

Scheme 2-2 Attempted Photo-decarbonylation

The reaction was monitored by ^{1}H and ^{31}P-NMR spectroscopy (Figure 2-2). Whilst only the ^{31}P-NMR data are presented, the ^{1}H-NMR of the acetate region (δ 0.2-0.8) displayed the same trends. It was found that two new species were formed, an unknown complex at δ 35.7 and a resonance at δ 42.3 which, by comparison with data in the literature, was assigned as the *cis*-isomer of complex $\mathbf{4}_{\mathbf{cis}}$.[188] Once irradiation was halted this *cis*-isomer was no-longer observed. Over time, a small amount of **1a** was formed, but conversion halted at ~15% of the total material.

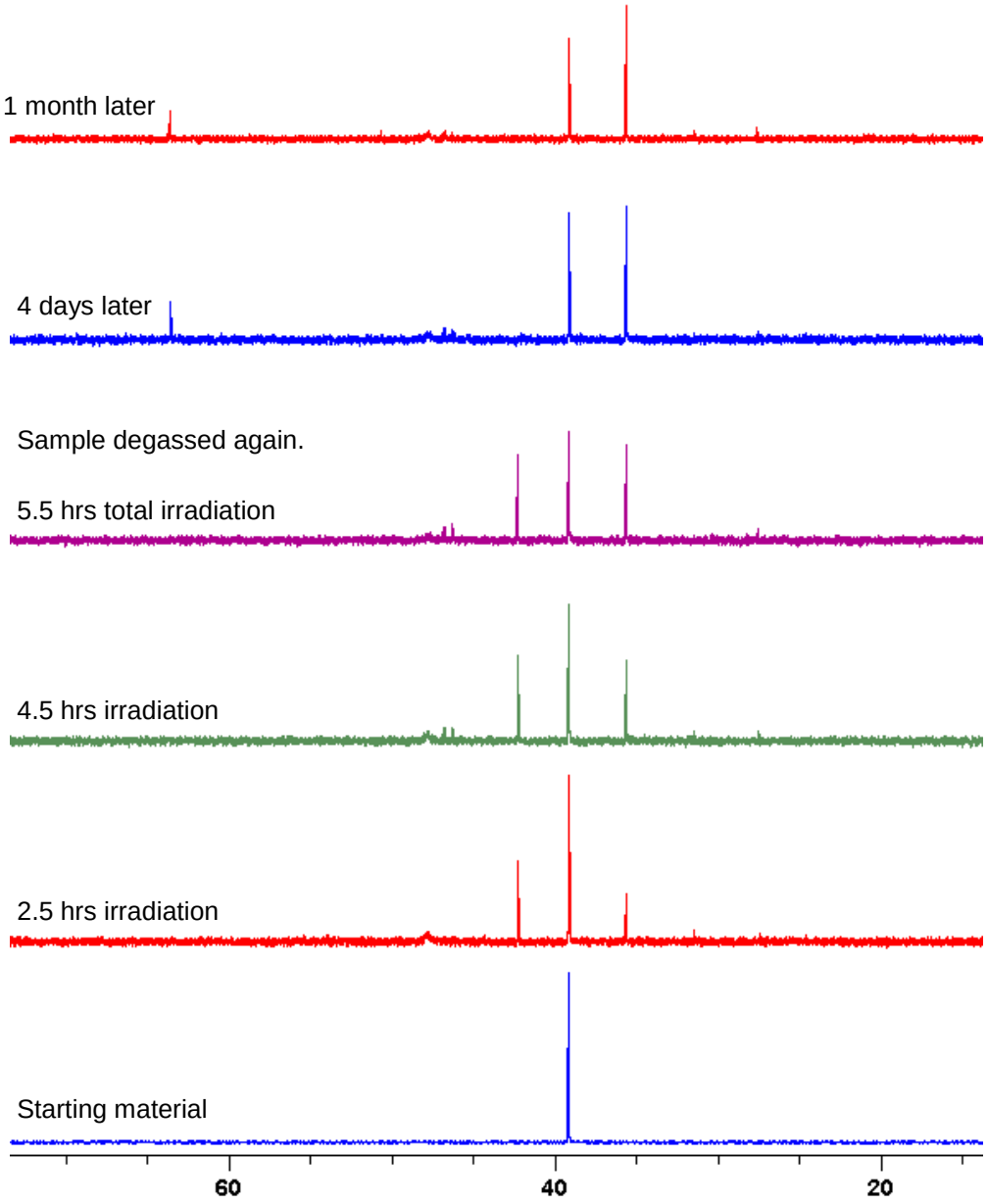

Figure 2-2 Results of Attempted Photo-Decarbonylation

As regeneration of the starting complex by photochemical activation proved unsuitable, it was decided to investigate ligand effects in the system instead. By altering the properties of the phosphine ligands the coordination environment may be fine-tuned (effects due to the carboxylate ligands have previously been investigated by Oliver Pickup[175]). For example, if the metal centre in complex **4** can be made less electron-rich, levels of back-bonding to the CO ligand will be reduced therefore weakening the M-CO bond and encouraging CO loss.

The synthetic route to complex **1a** has been found to work only in the case of triphenylphosphine.[176] A few analogues of **1** containing different phosphine ligands are present in the literature, however they are all produced via different methods.[177-181] Therefore the development of a general route to complexes of the general formula

$[Ru(\kappa^2\text{-}OAc)_2(PR_3)_2]$ (where $(PR_3)_2$ could also be chelating phosphines ($PC_x(R)_xP$)) was sought. Once these complexes were synthesised, their catalytic properties were explored and these will be discussed in Section 2.5. This alteration of the electronic and steric properties of the complex is expected to also provide some important mechanistic information.

2.3 Development of a General Route for Phosphine Addition

2.3.1 Preamble

Extensive experimental and theoretical investigations have been carried out into the mechanism of vinylidene formation in the $[Ru(\kappa^2\text{-}OAc)_2(PR_3)_2]$ **1** system (Scheme 2-3).[174] Whilst it is assumed that the phosphorus ligands isomerise to the *trans* configuration as soon as the complex reacts with an alkyne, DFT calculations do suggest that the *cis* pathway is feasible. Therefore it was decided to synthesise a complex with a chelating diphosphine. This would force any resulting vinylidene complexes to have a *cis* configuration of phosphorus ligands and would enable investigation of the '*cis*' route experimentally.

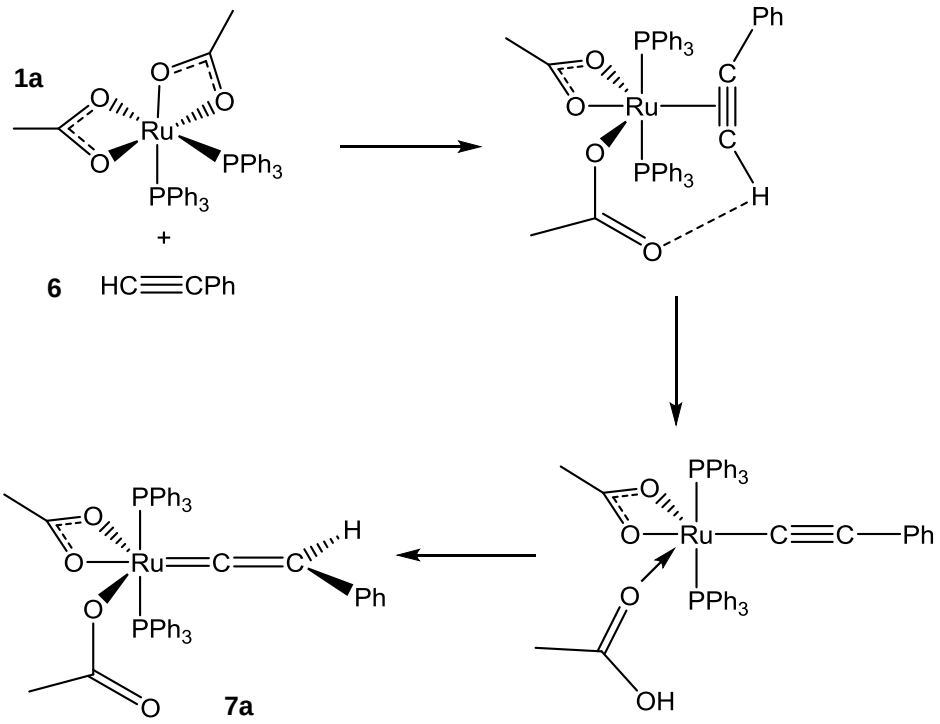

Scheme 2-3 Ligand Assisted Proton Shuttle Mechanism

It has also been found that chelating phosphines can have advantages over mono-dentate ligands. They increase the basicity at the metal centre and can slow down exchange processes.[180] More importantly they have also been found to exert control over the coordination number and stereochemistry of complexes which can

have a significant effect on the outcome of catalytic reactions.[180] As a result, initial work was carried out with 1,2-bis(diphenylphosphino)ethane (dppe) **8**.

2.3.2 Use of the Chelate Effect

It was thought that simple use of the chelate effect could lead to the formation of [Ru(κ^2-OAc)$_2$(dppe)] **9** by reaction of complex **1a** with dppe (Scheme 2-4). Wong et al. have already shown that this reaction is dependent on the size of the chelating phosphine ligand.[180] When the ligand 1,4-bis(diphenylphosphino)butane (dppb) is used [Ru(κ^2-OAc)$_2$(dppb)] is formed and the 1,1'-bis(diphenylphosphino)ferrocene (dppf) analogue [Ru(κ^2-OAc)$_2$(dppf)] has also been synthesised via this method by Lu et al.[178] However, when the smaller 1,1-bis(diphenylphosphino)methane (dppm), dppe and 1,3-bis(diphenylphosphino)propane (dppp) are used, only one of the PPh_3 ligands is displaced and complexes of type **10** are produced (Scheme 2-4). This route is therefore not applicable for general use.

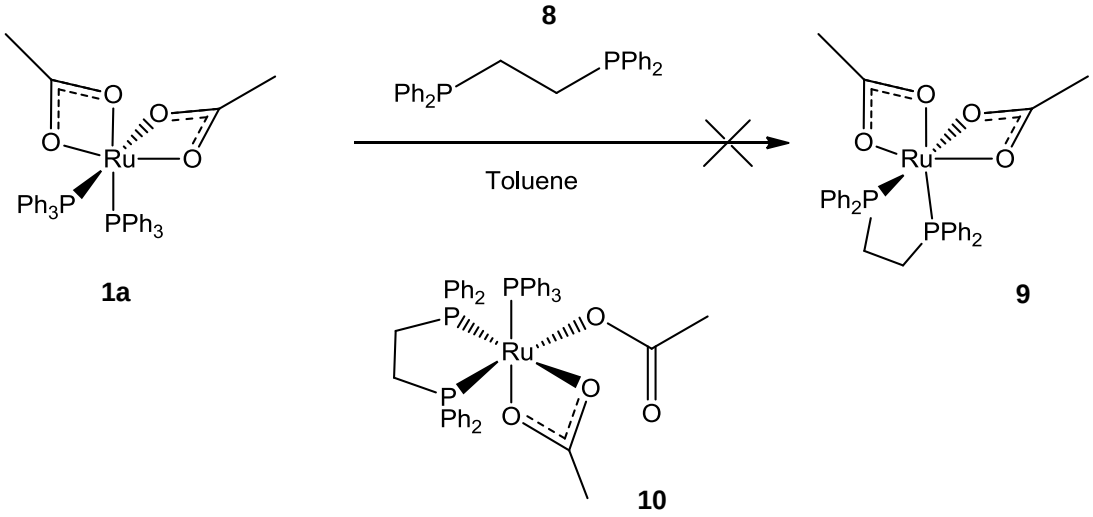

Scheme 2-4 Reaction of **1a** with dppe.

2.3.3 Adaption of Noyori's BINAP Synthetic Route

Noyori and co-workers[189] have reported the synthesis of BINAP-Ru^{II} dicarboxylate (BINAP = 2,2'-Bis(diphenylphosphino)-1,1'-binaphthyl) complexes from [Ru(η^6-C_6H_6)Cl_2]$_2$ and it was reasoned that a similar procedure could be used to form the desired chelating phosphine complex **9** . An improved synthesis published later[190] was modified to incorporate the change in phosphine, and a switch from the benzene precursor to the *p*-cymene analogue [Ru(*p*-cymene)Cl_2]$_2$ **11**.

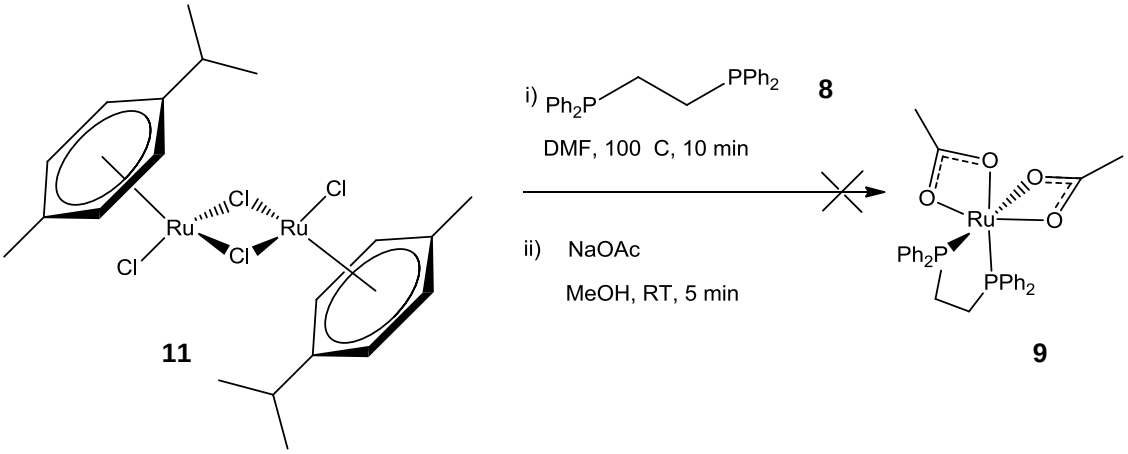

Scheme 2-5 Proposed Synthetic Route Based on Noyori's BINAP Method

A DMF solution of dppe **8** and [Ru(*p*-cymene)Cl_2]$_2$ **11** was heated at 100 ˚C for 10 minutes. The solution was then cooled to room temperature and a methanolic solution of NaOAc added. NMR samples taken from the reaction mixture after work up showed evidence for three products and free dppe (singlet at δ -12.4) (Figure 2-3). The ^{31}P-NMR spectrum showed evidence for all three species, a singlet at δ 44.8 assigned to *trans*-[$RuCl_2$(dppe)$_2$] **14** (a known complex),[191] another singlet at δ 24.7 thought to be due to [($RuCl_2$(*p*-cymene))$_2$(μ^2-dppe)] **12** and doublets at δ 25.9 ($^3J_{PP}$ = 35.3 Hz) and δ -12.6 ($^3J_{PP}$ = 35.3 Hz) due to [$RuCl_2$(*p*-cymene)η^1-dppe] **13**. The ratio of species **12**:**13**:**14**:**8** was found to be 3:6:1:1 therefore the major product was complex **13**. Electrospray ionisation (ESI) MS analysis also showed evidence for **13** (*m/z* 705). Crystallisation lead to the formation of crystals of **14** (structure confirmed by comparison of the unit cell to the literature)[191] and an amorphous solid. On removal of the mother liquor the ^{31}P-NMR spectrum now only showed the resonances for **12** and **14.** A LIFDI MS only exhibited a peak for **14** (*m/z* 968). Recrystallisation afforded crystals of both **12** (Figure 2-4) and **14** (structures confirmed by X-ray diffraction).

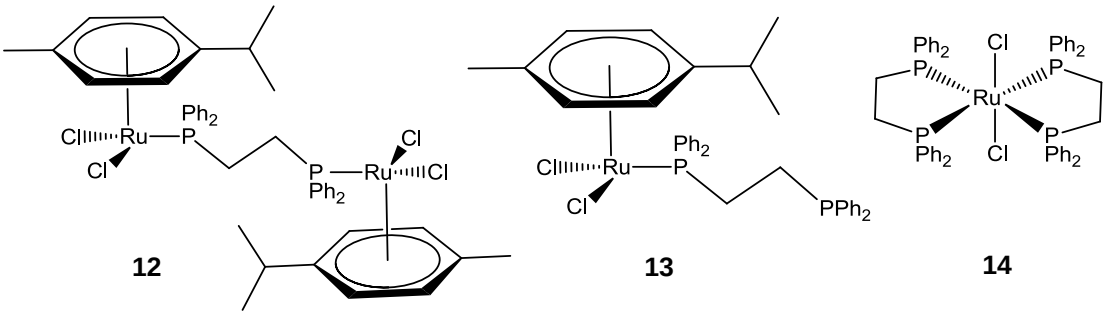

Figure 2-3 Observed Products of the One-Pot Route

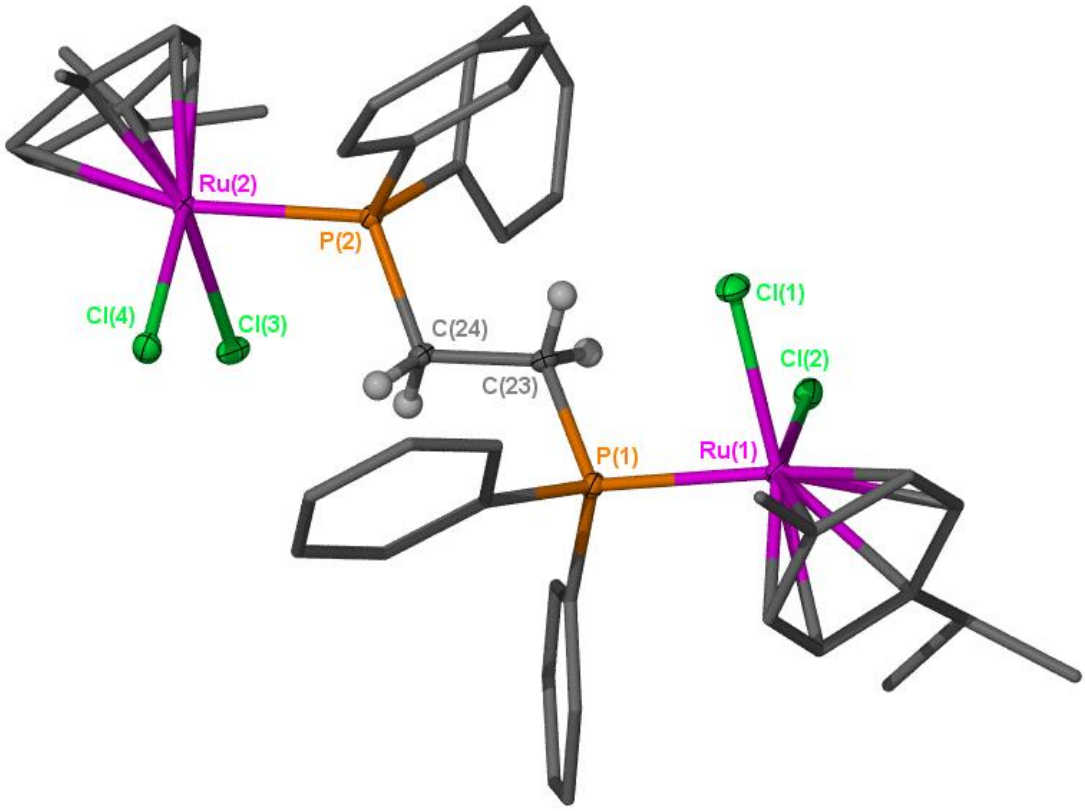

Figure 2-4 ORTEP Representation of Complex **12**; Thermal Ellipsoids, Where Shown, are at 50% Probability, Hydrogen Atoms and Solvent Molecules have been Omitted for Clarity (Except Those on the dppe Backbone).

Table 2-1 Selected Bond Lengths and Angles for Complex **12**

Bond	Bond Length (Å)	Angle	Bond Angle (°)
P(1) – Ru(1)	2.3480(7)	P(1) – Ru(1) – Cl(1)	87.09(3)
P(2) – Ru(2)	2.3372(7)	P(3) – Ru(1) – Cl(2)	83.82(2)
P(1) – C(23)	1.829(3)	Cl(1) – Ru(1) – Cl(2)	88.16(2)
P(2) – C(24)	1.821(3)	P(2) – Ru(2) – Cl(3)	83.20(2)
C(23) – C(24)	1.531(4)	P(2) – Ru(2) – Cl(4)	88.18(2)
Cl(1) – Ru(1)	2.4128(7)	Cl(3) – Ru(2) – Cl(4)	87.80(2)
Cl(2) – Ru(1)	2.4162(7)	Ru(1) – P(1) – C(23)	112.99(9)
Cl(3) – Ru(2)	2.4001(7)	P(1) – C(23) – C(24)	116.79(18)
Cl(4) – Ru(2)	2.4132(7)	Ru(2) – P(2) – C(24)	115.24(9)
		P(2) – C(24) – C(23)	114.10(18)

2.3.5 Utilising the Labile COD Ligand

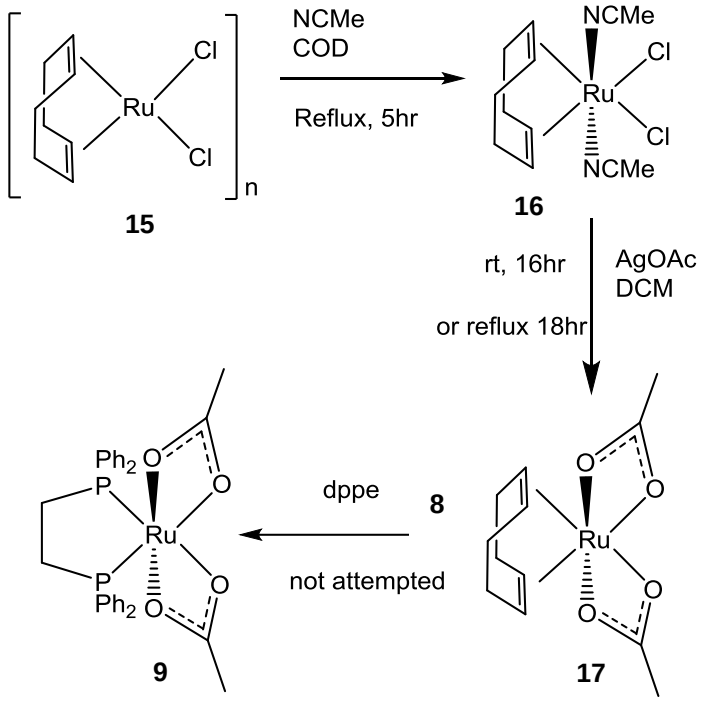

Scheme 2-6 Use of a Labile COD Ligand

Another general route was investigated which was designed to exploit the labile nature of 1,5-cyclooctadiene (COD) ligands (Scheme 2-6). The commercially available dichloro(COD)ruthenium(II) oligomer **15** was reacted with acetonitrile to form the commonly used, air stable precursor $[RuCl_2(NCMe)_2(COD)]$ **16**.[192] Reaction of **16** with silver acetate yielded $[Ru(\kappa^2\text{-}OAc)_2(COD)]$ **17** which, it was hoped, could be used to form the desired $[Ru(\kappa^2\text{-}OAc)_2(PR_3)_2]$ complexes by substitution of the COD ligand. However, complex **17** proved difficult to separate from residual silver impurities making this synthetic route impractical.

2.3.6 A Successful Route

A return to use of the dichloro(*p*-cymene)ruthenium(II) dimer **11** as a precursor lead to more success.[193] Again silver acetate was used to introduce acetate ligands to the system,[194] but the purification proved to be more effective. The resulting complex $[Ru(\kappa^1\text{-}OAc)(\kappa^2\text{-}OAc)(p\text{-cymene})]$ **18** was then reacted with dppe **8** (Scheme 2-7) and the reaction followed by NMR spectroscopy.

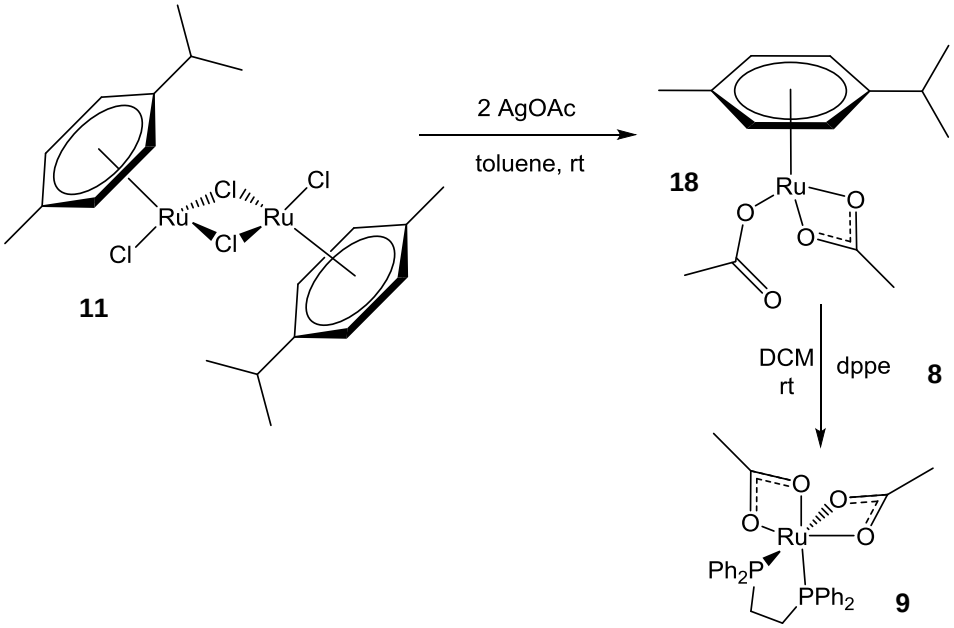

Scheme 2-7 Successful Route to [Ru(κ^2-OAc)$_2$(dppe)] **9**

It was found that the dppe **8** added in a stepwise fashion, with an intermediate observed containing a κ^1 bound dppe ligand, two κ^1 bound acetate ligands and a *p*-cymene ligand (complex **19**). It took ~4 hours for complete conversion to the desired product to occur, the following ^{31}P-NMR spectrum was observed directly after addition (Figure 2-5).

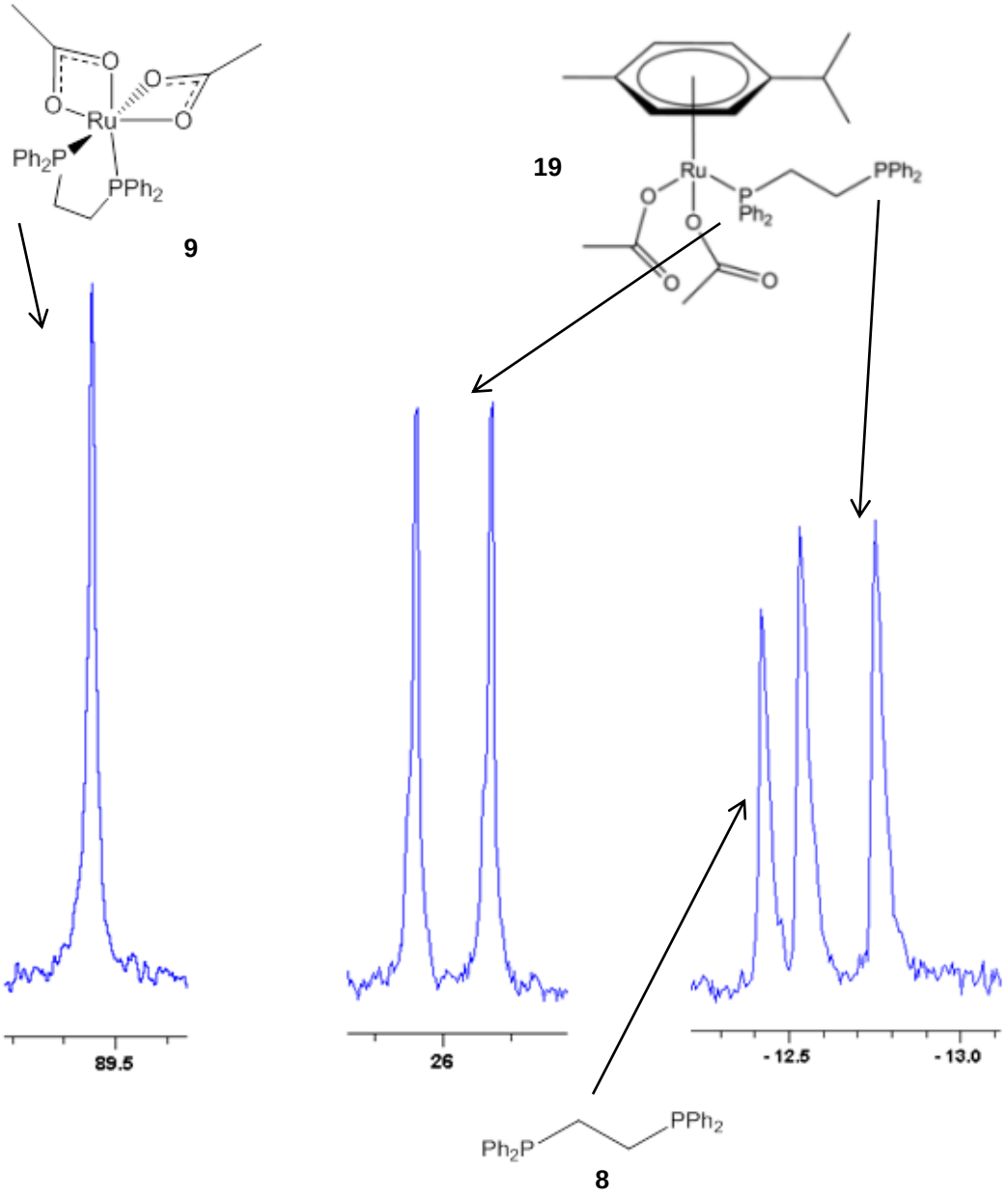

Figure 2-5 ^{31}P-NMR Showing the Stepwise Formation of dppe Complex **9** via Monodentate Complex **19**

To ensure the reaction had gone to completion, complex **9** was formed by stirring complex **18** with dppe in DCM for 18 hours. Subsequent removal of the solvent followed by pentane washing gave a yellow powder. LIFDI mass spectrometry confirmed the identity of the product (*m/z* 618), and a peak was observed in the ^{31}P-NMR spectrum at δ 89.5. The ^{1}H-NMR spectrum was found to contain residual *p*-cymene making the aromatic region very complicated. One resonance was observed for the acetate ligands, however' and IR spectroscopy was able to confirm that only κ^2 acetate ligands were present ($\Delta\nu$ 53 cm^{-1}).[171] Slow diffusion of pentane into a DCM solution of **9** yielded crystals suitable for X-ray diffraction. The resulting structural analysis confirmed the presence of one chelating dppe ligand with two κ^2 acetate ligands (Figure 2-6). The complex displays a distorted octahedral geometry with the

small bite-angle (~60˚) of the acetate ligands the source of the greatest distortion. The dppe ligand also displays a relatively small bite-angle (84.23(2)˚) forcing the geometry further from ideality. In structures of other complexes of the type [Ru(κ^2-OAc)$_2$(Ph_2P(R)PPh_2)] larger metallocycles are formed, allowing for more flexibility and for angles closer to the ideal of 90˚. For example, use of the 6,6'-dimethoxybiphenyl-2,2'-diyl)bis(diphenylphosphine (MeO-Biphep)[195] and N,N'-bis(diphenylphosphino) 1,2-diamine[196] ligands both give 7-membered metallocycles and so give approximately 90˚ P-Ru-P angles. Use of dppf however leads to a very large angle of ~100˚ caused by the inflexible nature of the 6-membered ring.[178]

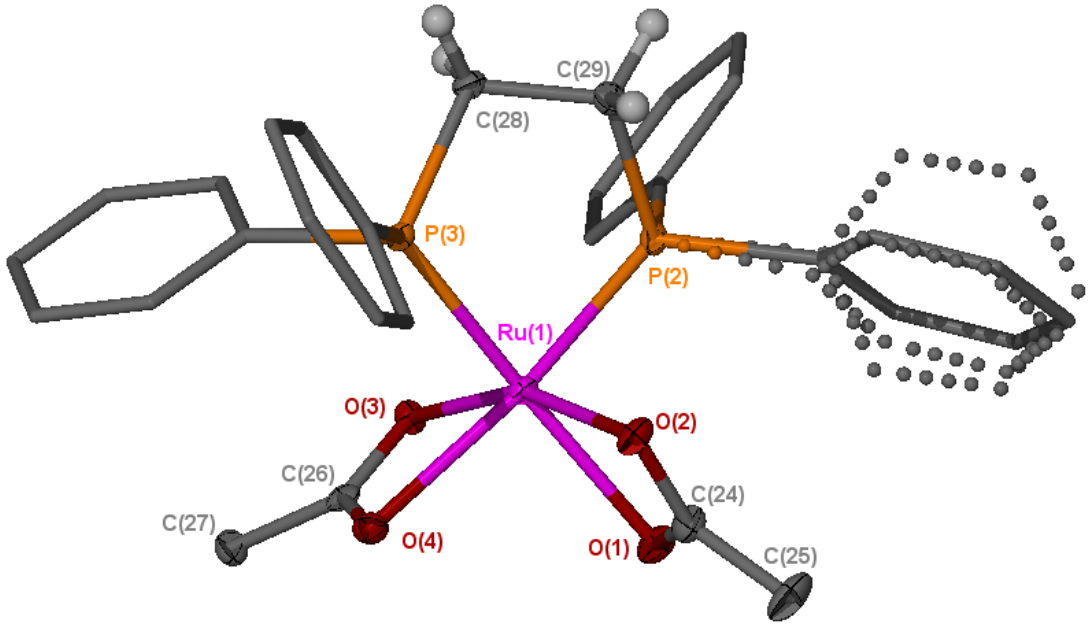

Figure 2-6 ORTEP Representation of Complex **9**; Thermal Ellipsoids, Where Shown, are at 50% Probability. Hydrogen Atoms have been Omitted for Clarity (Except Those on the dppe Backbone). The Disordered Phenyl Ring on the dppe Ligand is Shown with Dotted Lines.

Table 2-2 Selected Bond Lengths and Angles for Complex **9**

Bond	Bond Length (Å)	Angle	Bond Angle (°)
P(2) – Ru(1)	2.2156(6)	P(2) – Ru(1) – P(3)	84.23(2)
P(3) – Ru(1)	2.2262(6)	P(2) – Ru(1) – O(1)	97.12(5)
O(1) – Ru(1)	2.2123(16)	P(2) – Ru(1) – O(2)	88.97(5)
O(2) – Ru(1)	2.1208(15)	P(2) – Ru(1) – O(3)	107.12(4)
O(3) – Ru(1)	2.1098(15)	P(2) – Ru(1) – O(4)	167.37(4)
O(4) – Ru(1)	2.2212(15)	P(3) – Ru(1) – O(1)	165.81(5)
		P(3) – Ru(1) – O(2)	105.53(4)
		P(3) – Ru(1) – O(3)	90.72(4)
		P(3) – Ru(1) – O(4)	92.76(4)
		O(1) – Ru(1) – O(2)	60.46(6)
		O(1) – Ru(1) – O(3)	102.29(6)
		O(1) – Ru(1) – O(4)	88.81(6)
		O(2) – Ru(1) – O(3)	158.36(6)
		O(2) – Ru(1) – O(4)	103.65(6)
		O(3) – Ru(1) – O(4)	60.56(6)

If any excess of dppe **8** was added, addition of two dppe ligands was observed to give complex **20** which gave rise to a singlet at δ 44.2 in the ^{31}P-NMR spectra. This species was then observed to lose an acetate ligand to yield cationic **21** which was observed as two triplets at δ 57.5 and δ 58.5 (Figure 2-7). The loss of an acetate ligand was supported by IR spectroscopy as bands due to the κ^1 acetate ligand were no longer observed. Both **20** and **21** are known species.[180]

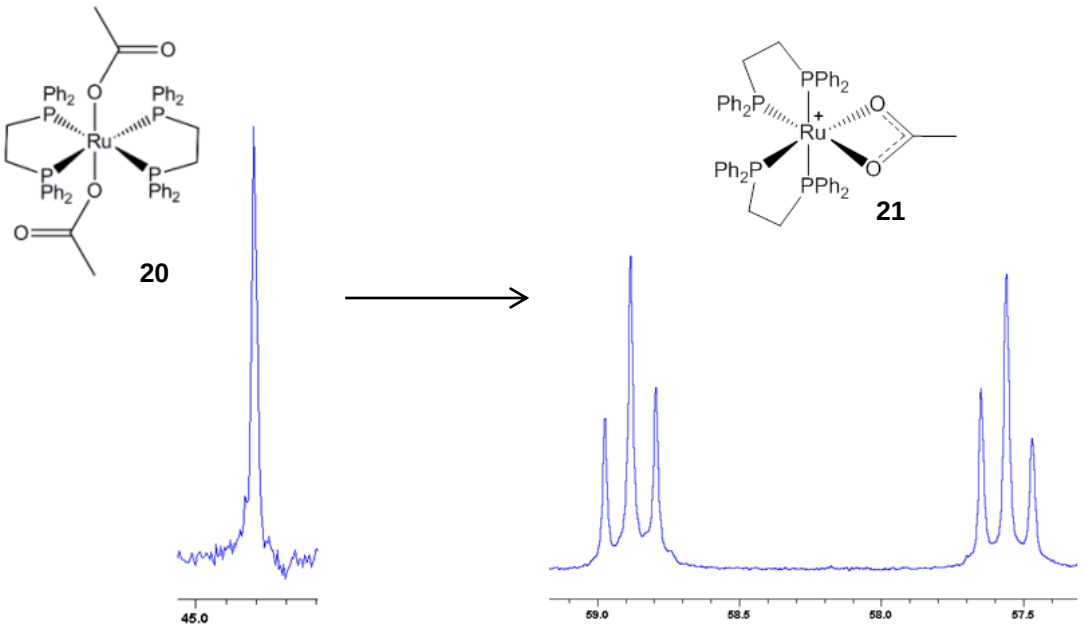

Figure 2-7 Addition of More than One Equivalent of dppe

This synthetic route has been extended to a variety of phosphorus-containing ligands. Reaction of **18** with dppb gave the known complex [Ru(κ^2-OAc)$_2$(dppb)] **22** (Scheme 2-8).[180] This was observed as a singlet at δ 63.5 in the ^{31}P-NMR spectrum, and again just one resonance was observed (δ 1.54) for the equivalent acetate ligands in the ^{1}H-NMR spectrum. Broad resonances at δ 1.70 and δ 2.53 were assigned to the dppb backbone, and these compare favourably with those reported in the literature.[180]

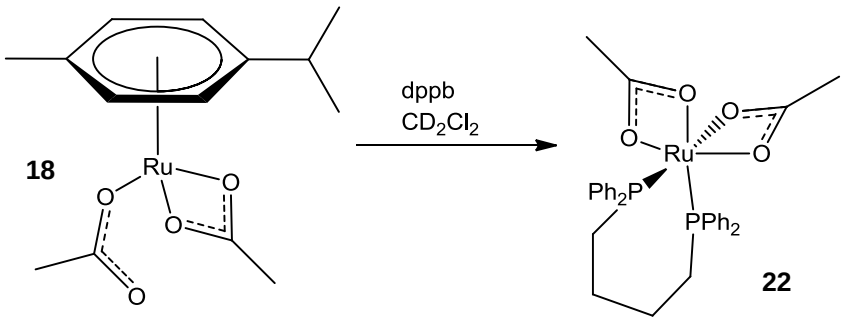

Scheme 2-8 Formation of [Ru(κ^2-OAc)$_2$(dppb)] **22**

This synthetic procedure was extended to give complexes of the type [Ru(κ^2-OAc)$_2$(PR$_3$)$_2$] **1** by using monodentate phosphorus ligands. Reaction of **18** with PPh$_3$ gave complex **1a**, all data matched that in the literature.[170] P^{i}Pr$_3$ was then used for comparison as it is bulkier and more electron-rich than PPh$_3$. The complex formed, *cis*-[Ru(κ^2-OAc)$_2$(P^{i}Pr$_3$)$_2$] **1b,** is also known,[177] however, it has not previously been isolated. The ^{31}P-NMR resonance at δ 60.6 compares well with that reported. The ^{13}C and ^{1}H-NMR spectra both show a single acetate environment, and the IR spectrum suggests that this ligand is bound κ^2 ($\Delta\nu$ 109 cm^{-1}).

Crystals suitable for X-ray diffraction and elemental analysis were obtained by cooling a pentane solution of **1b** to -15 ˚C. The resulting structure determination confirmed the *cis*-configuration of the phosphine ligands, which forms despite the increase in steric bulk over the triphenylphosphine analogue. Like all complexes of this type **1b** adopts a distorted octahedral geometry with the distortion caused by the small bite-angle of the acetate ligands.[170, 179, 197] The main differences observed between complexes of the type $[Ru(\kappa^2\text{-}OAc)_2(PR_3)_2]$ **1** are the changes in the C-P bond lengths induced by the change in phosphine. PPh_3 gives bond lengths of Ru-P(1) = 2.2467(5) Å, Ru-P(2) = 2.2463(5) Å[170] whereas use of the larger phosphines t-butyl-bis(2-thienyl)phosphine (bbtp) (Ru-P(1) = 2.281(3) Å, Ru-P(2) = 2.270(3) Å)[179] and P^iPr_3 (Ru-P(1) = 2.2904(4) Å, Ru-P(2) = 2.2879(4) Å) give significantly longer C-P bond lengths.

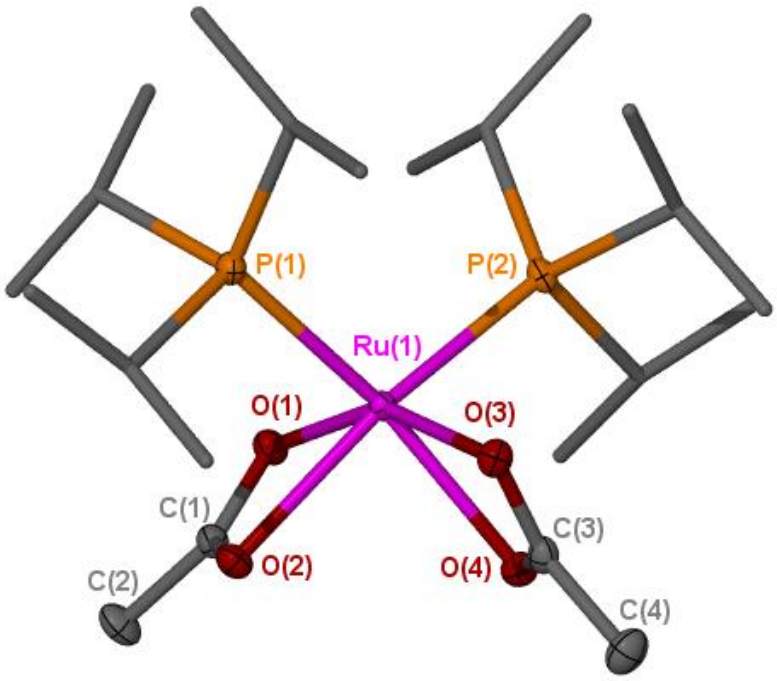

Figure 2-8 ORTEP Representation of Complex **1b**; Thermal Ellipsoids, Where Shown, are at 50% Probability. Hydrogen Atoms have been Omitted for Clarity.

Table 2-3 Selected Bond Lengths and Angles for Complex **1b**

Bond	Bond Length (Å)	Angle	Bond Angle (°)
P(1) – Ru(1)	2.2904(4)	P(1) – Ru(1) – P(2)	105.803(14)
P(2) – Ru(1)	2.2879(4)	P(1) – Ru(1) – O(1)	94.06(3)
O(1) – Ru(1)	2.1252(10)	P(1) – Ru(1) – O(2)	87.94(3)
O(2) – Ru(1)	2.2134(10)	P(1) – Ru(1) – O(3)	102.11(3)
O(3) – Ru(1)	2.1385(10)	P(1) – Ru(1) – O(4)	158.79(3)
O(4) – Ru(1)	2.1966(10)	P(2) – Ru(1) – O(1)	101.74(3)
		P(2) – Ru(1) – O(2)	158.74(3)
		P(2) – Ru(1) – O(3)	93.53(3)
		P(2) – Ru(1) – O(4)	88.28(3)
		O(1) – Ru(1) – O(2)	60.39(4)
		O(1) – Ru(1) – O(3)	153.85(4)
		O(1) – Ru(1) – O(4)	98.56(4)
		O(2) – Ru(1) – O(3)	99.43(4)
		O(2) – Ru(1) – O(4)	83.62(4)
		O(3) – Ru(1) – O(4)	60.46(4)

In order to investigate the electronic properties of these systems, the analogous triisopropylphosphite complex, *cis*-[Ru(κ^2-OAc)$_2$(P(O^{i}Pr)$_3$)$_2$] **1c**, was synthesised. As a ligand it should have very similar steric properties to the phosphine, but is significantly less electron-rich allowing comparison of the electronic effects of the phosphine ligand.[198] In this case the reaction with **18** was much slower, taking five days to go to completion. This reaction was only performed on an NMR scale and therefore the product not isolated. The ^{1}H-NMR spectrum compared well with other complexes in this series, and only one resonance was observed in the ^{31}P-NMR spectrum at δ 147.2.

2.3.7 Conclusion

This work has been able to show that [Ru(κ^1-OAc)(κ^2-OAc)(*p*-cymene)] **18** is a suitable precursor for the formation of complexes of the type [Ru(κ^2-OAc)$_2$(PR$_3$)$_2$] **1**, and can be used with a range of phosphorus ligands, including a phosphite ligand and chelating diphosphine ligands (Scheme 2-9, Table 2-4). Whilst many of these complexes were previously known in the literature, to the best of our knowledge this is the first general route to complexes of this type.

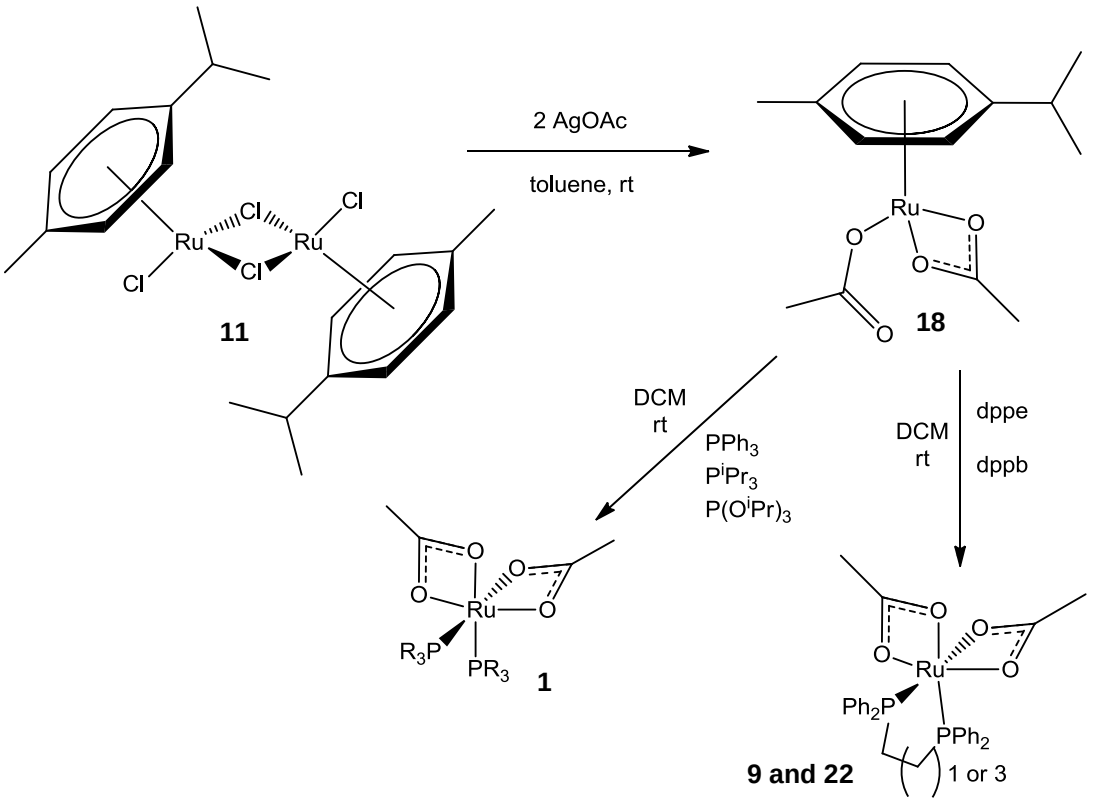

Scheme 2-9 Successful Two-Step Method for the Synthesis of [Ru(κ^2-OAc)$_2$(PR$_3$)$_2$] Complexes.

Table 2-4 ^{31}P-NMR data for [Ru(κ^2-OAc)$_2$(PR$_3$)$_2$]

Complex	^{31}P-NMR Chemical Shift (ppm)
cis-[Ru(κ^2-OAc)$_2$(PPh$_3$)$_2$]	63.6
cis-[Ru(κ^2-OAc)$_2$(P^{i}Pr$_3$)$_2$]	59.5
cis-[Ru(κ^2-OAc)$_2$(P(O^{i}Pr)$_3$)$_2$]	147.2
[Ru(κ^2-OAc)$_2$(dppe)]	89.6
[Ru(κ^2-OAc)$_2$(dppb)]	63.5

2.4 Reaction of [Ru(κ^2-OAc)$_2$(PR$_3$)$_2$] 1 with Alkynes

With the development of this general route to [Ru(κ^2-OAc)$_2$(PR$_3$)$_2$] **1** it was now possible to investigate ligand effects on their reaction with terminal alkynes. The phosphine-containing complexes discussed in the previous section were therefore reacted with phenyl acetylene. Reactions were carried out on 20 mg of ruthenium complex in CD_2Cl_2, and followed by ^{1}H and ^{31}P-NMR.

Unfortunately the complexes of the chelating phosphines (dppe **9** and dppb **22**) failed to form vinylidene complexes and were instead found to unselectively dimerise both phenyl acetylene and 4-ethynyl-*α,α,α*-trifluorotoluene to give a mixture of products.

The use of triisopropylphosphine (P^{i}Pr$_3$) proved far more successful than the chelating system. Complex **1b** has been found to react in an analogous fashion to the triphenylphosphine-containing complex. Reaction of **1b**, in pentane and at room temperature, with phenyl acetylene **6** leads to the formation of vinylidene complex **7b** over the course of three hours (Scheme 2-10). A crystal structure of this complex has been acquired (Figure 2-9) and further confirmation of the structure obtained from LIFDI MS (*m/z* 642.26 [M]$^+$), IR (C=C stretch at 1643 cm^{-1}, $\Delta\nu_{(uni)}$ 235 cm^{-1}and $\Delta\nu_{(chelate)}$ 99 cm^{-1}) and ^{13}C-NMR (triplets at δ 352.8 ($^2J_{PC}$ = 15.14 Hz) due to the α-carbon, and δ 112.4 ($^3J_{PC}$ = 3.81 Hz) due to the β-carbon).

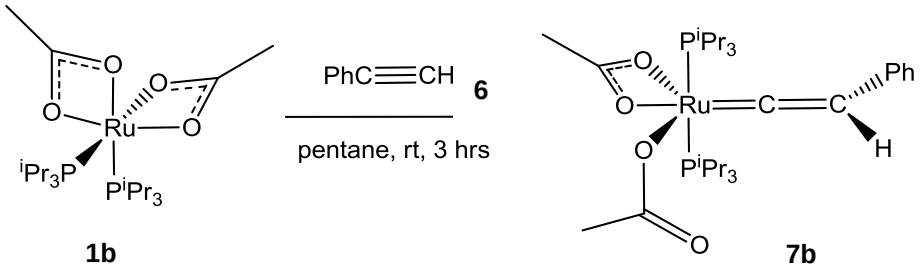

1b **7b**

Scheme 2-10 Vinylidene formation from cis-[Ru(κ^2-OAc)$_2$(P^{i}Pr$_3$)$_2$] **1b** and Phenyl Acetylene **6**

The structure of **7b** is typical of its type.[170, 173, 199] The small bite-angle of the κ^2-acetate ligand causes a distortion from the ideal octahedral geometry, although the P-Ru-P angle is close to linear (176.57(13)˚). The vinylidene residue is also essentially linear (Ru(1)-C(5)-C(6) = 176.6(7)˚) as would be expected.[57]

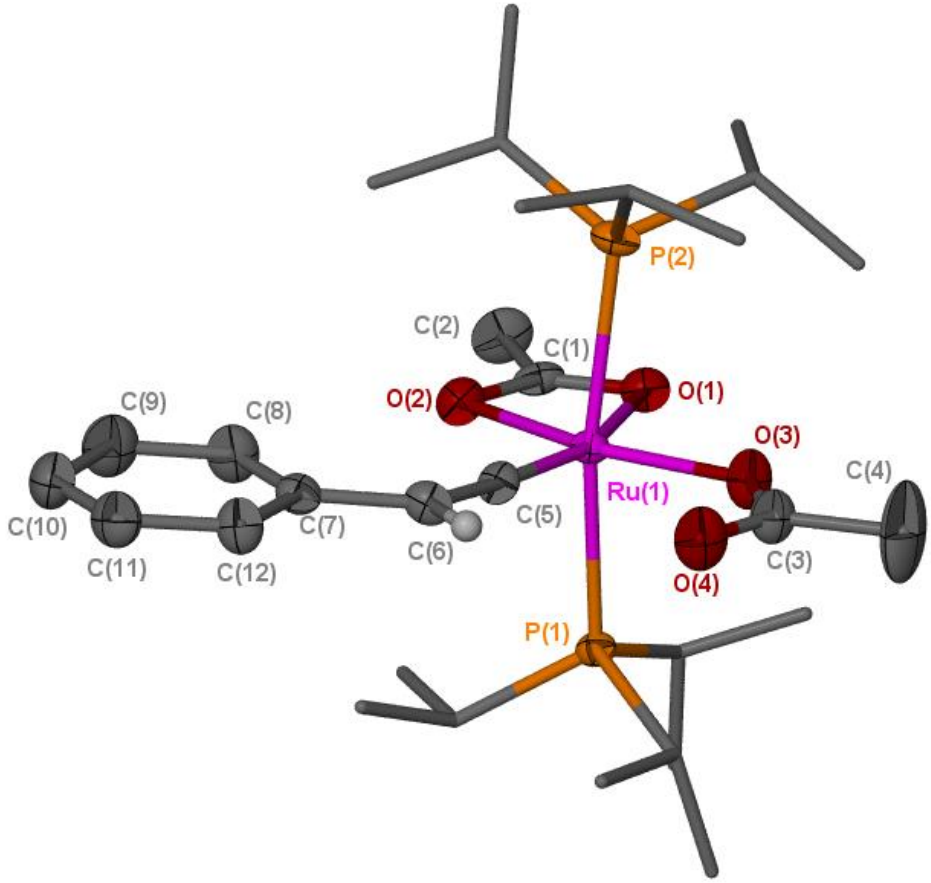

Figure 2-9 ORTEP Representation of Complex **7b**; Thermal Ellipsoids, Where Shown, are at 50% Probability. The Structure was Disordered, Therefore Only One Set of Ligands is Shown and Most of the Hydrogen Atoms have been Omitted for Clarity.

Table 2-5 Selected Bond Lengths and Angles for Complex **7b**

Bond	Bond Length (Å)	Angle	Bond Angle (°)
P(1) – Ru(1)	2.4307(15)	P(1) – Ru(1) – P(2)	169.90(7)
P(2) – Ru(1)	2.453(2)	P(1) – Ru(1) – O(1)	87.65(9)
O(1) – Ru(1)	2.255(3)	P(1) – Ru(1) – O(2)	90.92(9)
O(2) – Ru(1)	2.158(3)	P(1) – Ru(1) – O(3)	86.9(3)
O(3) – Ru(1)	2.032(5)	P(1) – Ru(1) – C(5)	93.5(3)
C(5) – Ru(1)	1.777(6)	Ru(1) – C(5) – C(6)	176.6(7)
C(5) – C(6)	1.342(8)	O(1) – Ru(1) – O(2)	59.14(12)
		O(1) – Ru(1) – O(3)	100.8(3)

O(2) – Ru(1) – O(3)	159.9(3)
O(1) – Ru(1) – C(5)	160.8(3)
O(2) – Ru(1) – C(5)	101.6(3)
O(3) – Ru(1) – C(5)	98.5(3)

In order to probe the electronic properties of this system, $P(O^iPr)_3$ was also used. It has similar steric bulk to P^iPr_3 but the additional oxygen atoms make it much less electron-rich. It was found that *cis*-[Ru(κ^2-OAc)$_2$($P(O^iPr)_3$)$_2$] **1c** did not react with phenyl acetylene to form vinylidene **7c**, and instead formed a complex mixture of unknown products (Scheme 2-11). This is not entirely surprising as the metal centre must be electron-rich in order for the back-bonding required to stabilise the vinylidene to occur.[199]

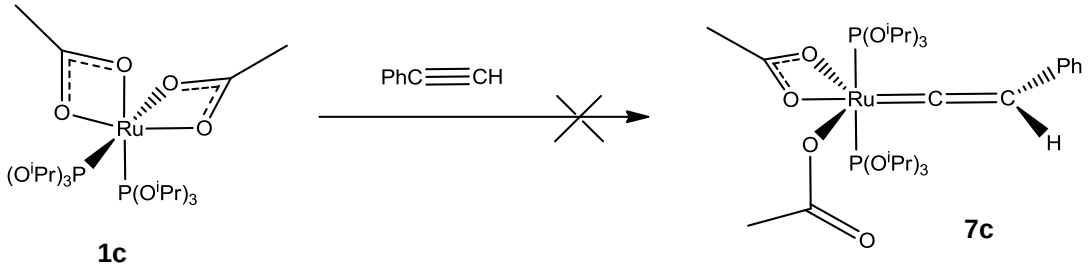

Scheme 2-11 Reaction of *cis*-[Ru(κ^2-OAc)$_2$($P(O^iPr)_3$)$_2$] **1c** with Phenyl Acetylene

2.5 Reaction of Complex 1 with Propargylic Alcohols and Ethers

Following the successful synthesis of [Ru(κ^2-OAc)(κ^1-OAc)(P^iPr_3)$_2$(=C=CHPh)] **7b** it was decided to investigate the reactivity of complex **1** towards propargylic compounds. None of the reactions proved to be catalytic, however, much useful information was obtained from these studies.

Reaction of complex **1b** with 1,1-diphenylprop-2-yn-1-ol **2a** lead to the formation of 1,1-diphenylethylene **5a** and carbonyl complex **4b** (Scheme 2-12) as in the triphenylphosphine system.[169, 170] It was not possibly to purify complex **4b** as its non-polar nature led to similar solubility to the impurities, however, evidence for its formation in the crude reaction mixture was obtained by IR (CO stretch at 1927 cm^{-1}, $\Delta\nu_{(uni)}$ 295 cm^{-1} and $\Delta\nu_{(chelate)}$ 94 cm^{-1}) and LIFDI MS (*m/z* 568.20 $[M]^+$). Complex **4b** has also been synthesised from the direct reaction of **1b** with CO gas. The ^{31}P-NMR of both crude reaction mixtures contains a peak at δ 37.8 which has been assigned to the carbonyl complex **4b**.

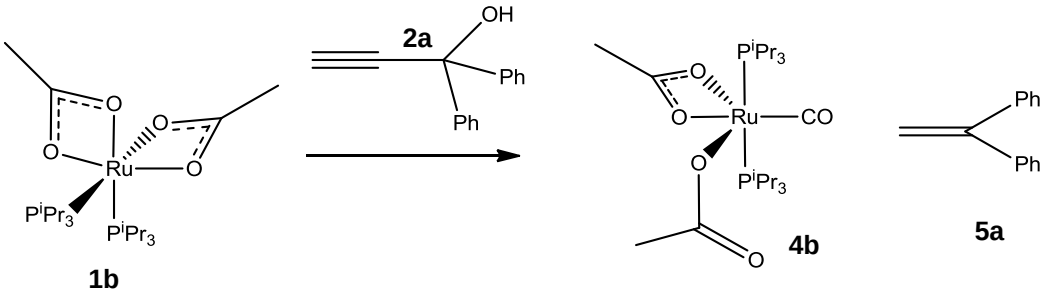

Scheme 2-12 Reaction of *cis*-[Ru(κ^2-OAc)$_2$(P^{i}Pr$_3$)$_2$] **1b** with Propargylic Alcohols

Reaction of complex **1b** with propargylic ether **24** leads to the formation of vinyl carbonyl complex **23b** and phenyl acetate (Scheme 2-13). Purification again proved difficult, but evidence for the formation of **23b** has been obtained from LIFDI MS (*m/z* 536.20 [M]$^+$), and IR (CO stretch at 1908 cm^{-1}and C=C stretch at 1772 cm^{-1}). The vinyl protons were observed as multiplet resonances at δ 4.91, 5.42 and 7.92 in the ^{1}H-NMR spectrum.

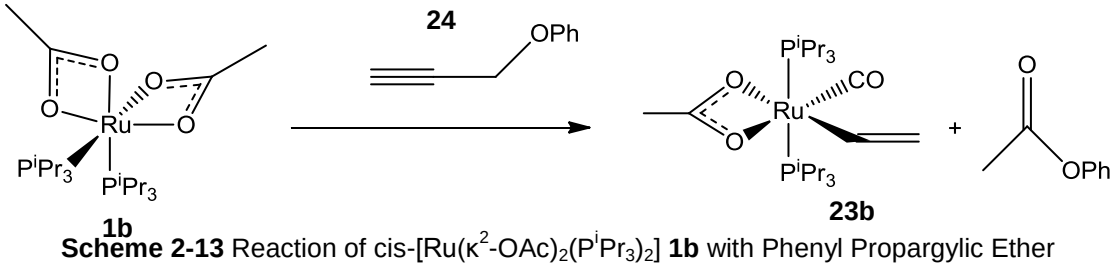

Scheme 2-13 Reaction of cis-[Ru(κ^2-OAc)$_2$(P^{i}Pr$_3$)$_2$] **1b** with Phenyl Propargylic Ether

2.6 Kinetic Studies

2.6.1 Experimental Details

It was decided to carry out kinetic investigations in order to gain some further mechanistic insight into the decarbonylation of propargyl alcohols and esters. These studies were performed on the reaction of *cis*-[Ru(κ^2-OAc)$_2$(PR$_3$)$_2$] **1** with phenyl propargyl ether **24** (Scheme 2-13) as this reaction was found to be cleaner than the reaction with propargylic alcohols. The reaction of **1b** was found to be too fast for kinetic measurements to be collected by NMR spectroscopy. It was therefore decided to use the ReactIR instrument to collect kinetic data. It has an attenuated total reflectance (ATR) probe with a silicon crystal which allows for *in situ* measurement of the IR spectrum. In this way the growth of the CO stretching band for **4b** at 1904 cm^{-1} was followed. In order to allow comparison with previous NMR measurements, the first experiment using the ReactIR was carried out using complex **1a** (the PPh$_3$ system, Scheme 2-14). Here the carbonyl stretching frequency was observed at 1919 cm^{-1}.

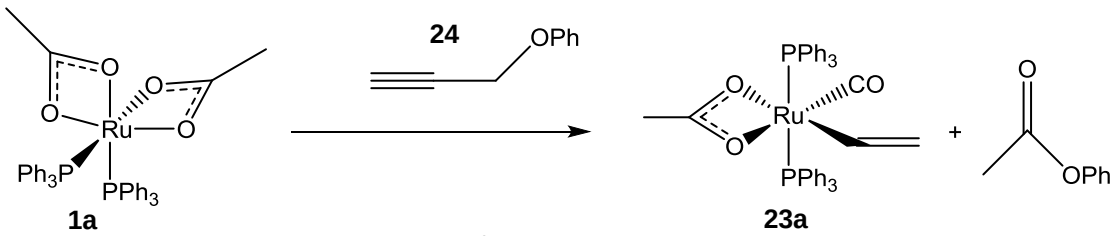

Scheme 2-14 Reaction of *cis*-[Ru(κ^2-OAc)$_2$(PPh$_3$)$_2$] **1a** with Phenyl Propargylic Ether

Phenyl propargyl ether **24** was added to a solution of *cis*-[Ru(κ^2-OAc)$_2$(PPh$_3$)$_2$] **1a** and after an initial induction period of ca. 10 minutes the intensity of the CO peak was found to grow in accordance with approximate 1st order kinetics. For the reaction of complex **1a** it was found that the reaction was complete in approximately 11 hours (Figure 2-10).

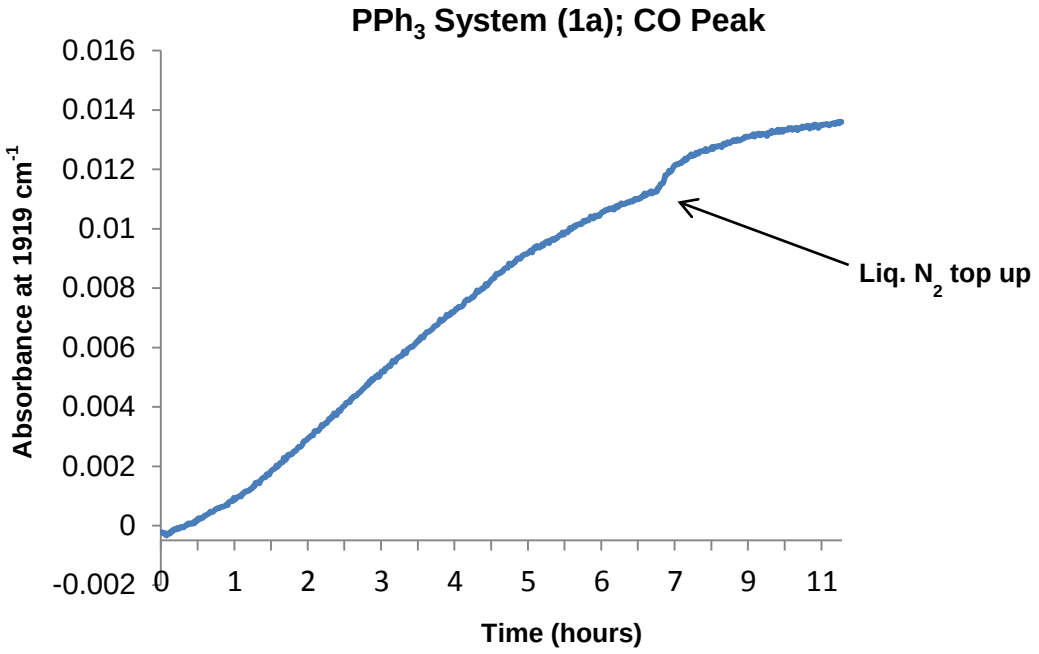

Figure 2-10 Reaction of **1a** with Phenyl Propargyl Ether **24**, Growth of the Carbonyl Containing Product Followed by ReactIR

2.6.2 Fitting the Data to a First Order Rate Constant

A kinetic study into this reaction has been carried out before by Dr Christine Welby, but as that data was collected by NMR, some comparison should be made between the two sets of data to assess the suitability of the ReactIR experiment.[169] In the previous work an approximate overall rate constant was calculated by fitting the data to a first order rate constant. Only the data points in the central section after the induction period and before completion were used. Using the equations shown below, the data collected by NMR at 300K gave a first order rate constant of 8.6 ± 0.02 x 10^{-5} s^{-1}.

$$rate = -\frac{d[SM]}{dt} = \frac{d[product]}{dt} = k_{obs}[SM] \qquad \text{Equation 2.1}$$

[91]

This can then be rearranged:

$$-\frac{d[SM]}{[SM]} = k_{obs}dt \qquad \text{Equation 2.2}$$

Integration of this over the limits [SM] = $[SM]_0$ to [SM] and t = 0 to t gives:

$$\ln[SM] - \ln[SM]_0 = -k_{obs}t \qquad \text{Equation 2.3}$$

Therefore, if the overall reaction is first order, then a plot of ln[SM] versus time should be a straight line.

Treating the ReactIR data shown in Figure 2-10 (those data points before the liquid nitrogen top-up and after the induction period) in this same manor lead to an overall first order rate constant of 6 x 10^{-5} ± 0.02 s^{-1} (Figure 2-11). These rate constants give a good indication that the two methods of data collection are compatible.

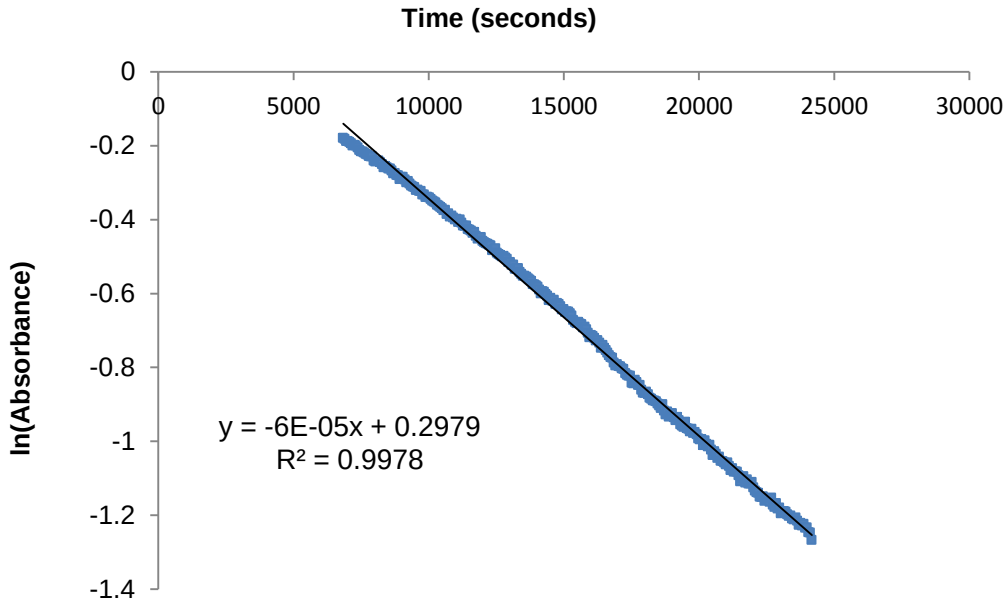

Figure 2-11 Reaction of **1a** with Phenyl Propargyl Ether **24**, Fitted to a First Order Rate Law

There was also an induction period of about 10 minutes for the reaction of *cis*-[Ru(κ^2-OAc)$_2$(P^iPr_3)$_2$] **1b** with **24**, however, the CO peak was found to reach maximum intensity after just 4 hours (Figure 2-12).

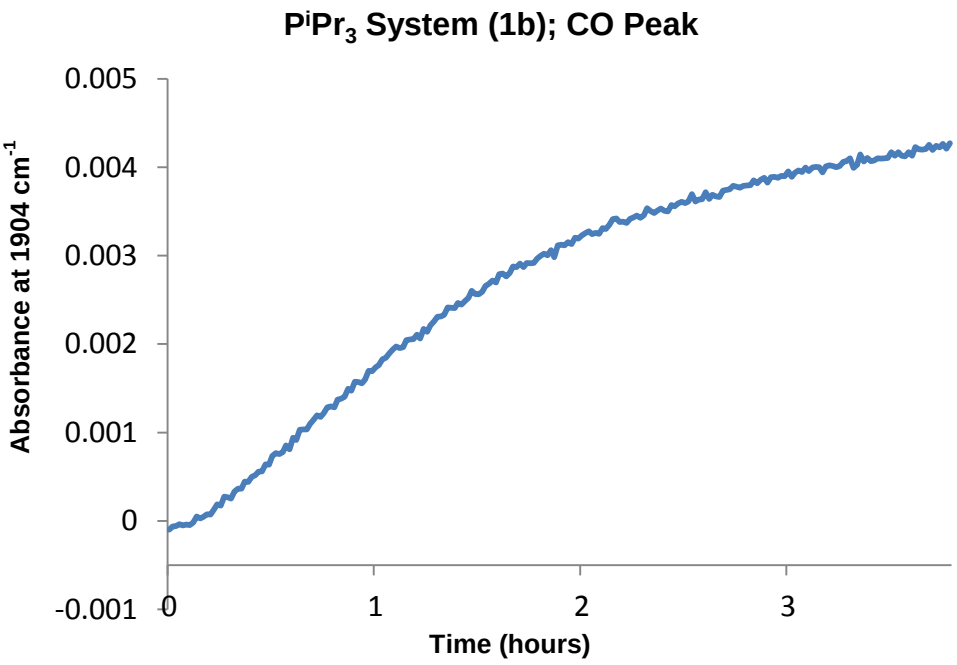

Figure 2-12 Reaction of **1b** with Phenyl Propargyl Ether **24**, Growth of the Carbonyl Containing Product Followed by ReactIR

2.6.3 Modelling the Data as an Autocatalytic Process

Attempts to fit this data to a first order rate law failed, a straight line could not be obtained, however small a selection of data was used. It was therefore suggested that the whole data set could be used to fit the data to a sigmoidal curve, characteristic of an autocatalytic process.

$$[B] = \frac{[A]_0 - [B]_0}{1 + \frac{[B]_0}{[A]_0}\, e^{-([A]_0+[B]_0)kt}}$$

Application of this equation to the reaction of **1b** (triisopropylphosphine) give an overall rate constant of (1.31 ± 0.3) x 10^{-1} s^{-1} (Figure 2-13). Whilst it would be expected that this reaction would have a larger rate constant than the triphenylphosphine system as it is faster, this rate constant appears to be far too large. It is also clear that the fit is not good, suggesting that this is not the correct equation for modelling this data.

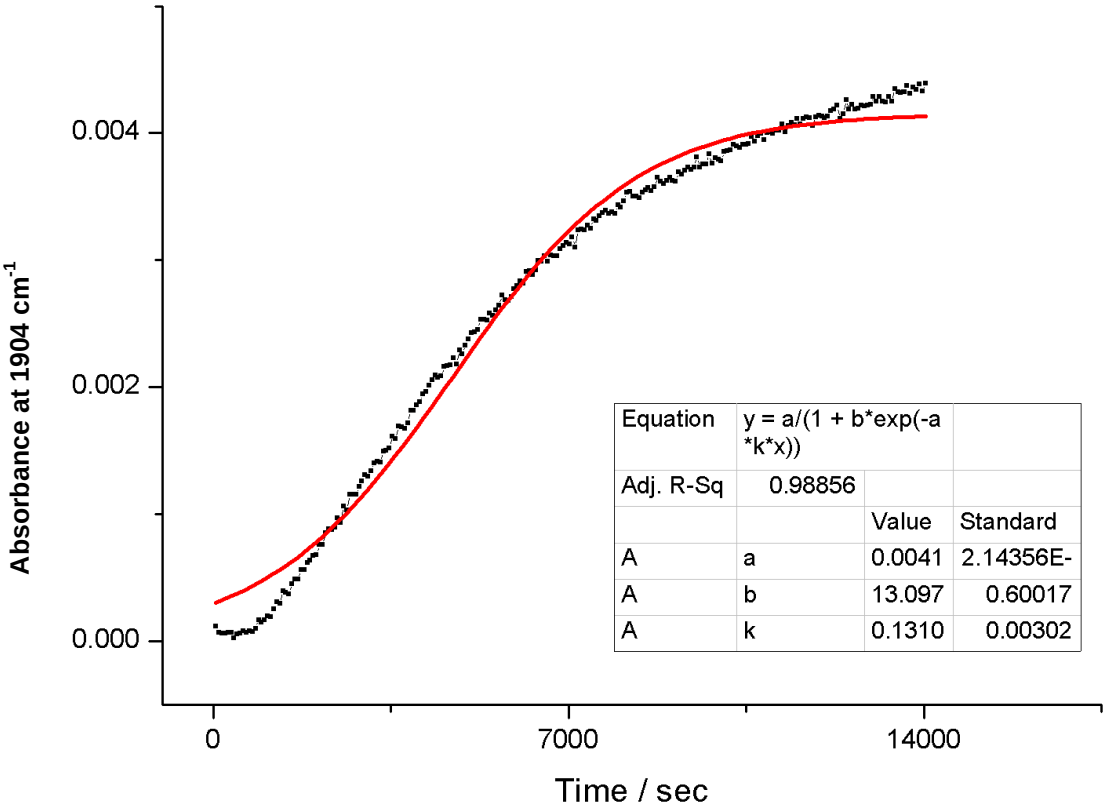

Figure 2-13 Reaction of **1b** with Phenyl Propargyl Ether **24**, Fitting of the Data to a Sigmoidal Curve. a = $[A]_0 + [B]_0$, b = $[A]_0 / [B]_0$

It was therefore decided to treat the data (before the liquid nitrogen top-up) collected for the reaction of **1a** (triphenylphosphine) in the same way to enable comparison of the two data analysis methods. A rate constant of (2.09 ± 0.03) x 10^{-2} s^{-1} was calculated (Figure 2-14), far larger than that estimated using first order kinetics.

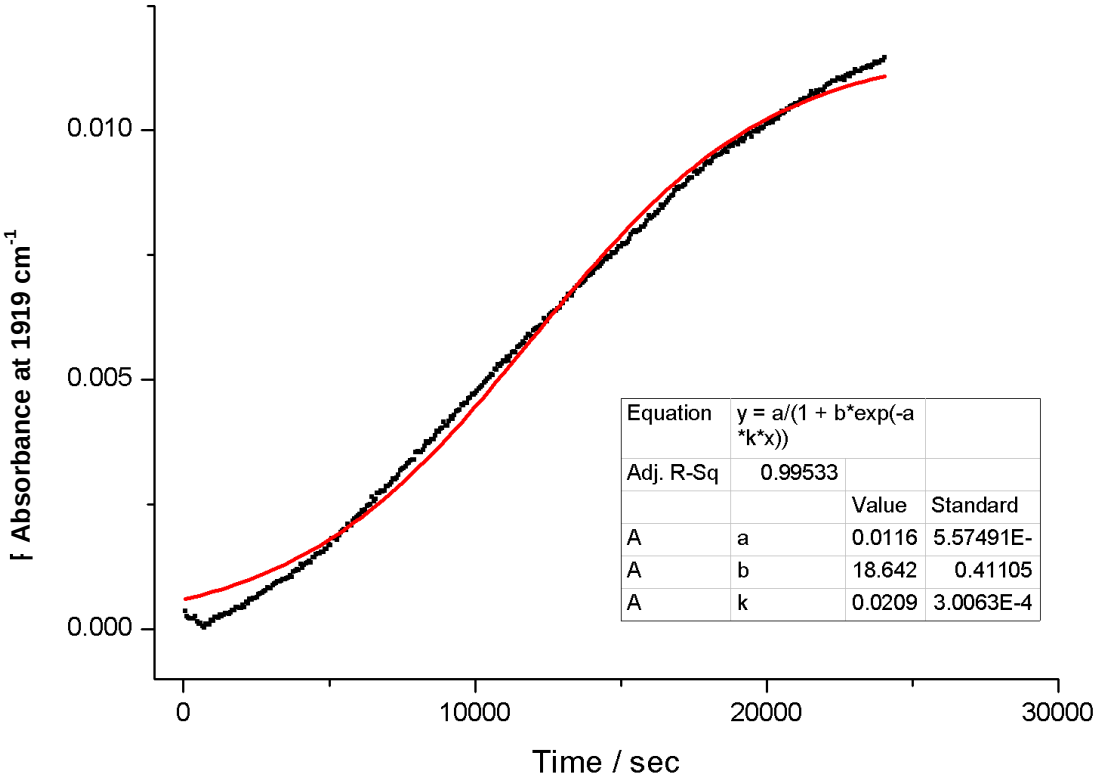

Figure 2-14 Reaction of **1a** with Phenyl Propargyl Ether **24**, Fitting of the Data to a Sigmoidal Curve. $a = [A]_0 + [B]_0$, $b = [A]_0 / [B]_0$

This suggests that one or both of these ways of viewing these reactions is not correct and that an alternative mechanism or data analysis method should be sought.

The plots shown in Figures 2-13 and 2-14 were re-plotted using absolute concentrations (using the initial reaction concentrations of 1.35×10^{-2} mol dm^{-3} for the PPh_3 system and 3.35×10^{-3} mol dm^{-3} for the P^iPr_3 system and assuming complete conversion) rather than peak intensity, but again the rate constant obtained from the PPh_3 system did not match that determined by Welby. It was therefore concluded that this was an unsatisfactory method to model the kinetics of these processes.

Therefore it was decided to analyse the data using percentage conversion, thus enabling a qualitative comparison to be made between the two systems (Figure 2-15). The percentage conversion was calculated by assuming that when there was no further change to the absorbance in the IR spectrum then complete conversion to the product had occurred.

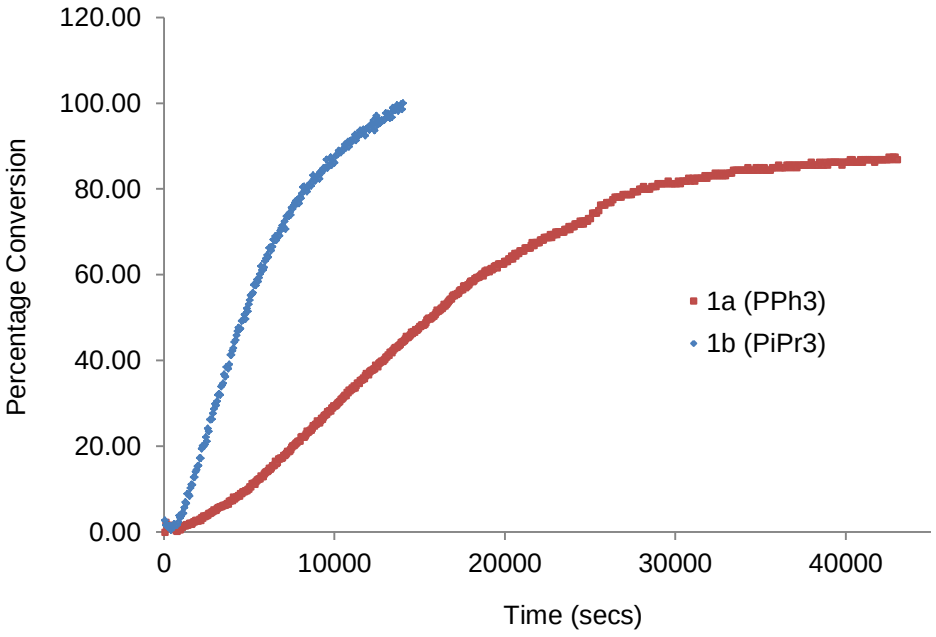

Figure 2-15 Using Percentage Conversion to Compare the Rate of Reaction of **1a** and **1b** with Phenyl Propargyl Ether **24**

From this plot and inspection of the raw data, the half-lives of the reactions can be estimated to give $t_{1/2}$ = 15593 s for the PPh_3 system, and $t_{1/2}$ = 4.67 x 103 s in the P^iPr_3 case. If the reactions are assumed to be first order, then the equation

$$t_{1/2} = {ln2}/{k}$$

can be used to estimate the rate constants. Although the two experiments were conducted at different concentrations, as so this analysis is only valid if the reactions obey first order kinetics, the resulting values of 4.44 x 10^{-5} s^{-1} for the PPh_3 system and 1.48 x 10^{-4} s^{-1} for the P^iPr_3 system suggest that the use of triisopropylphosphine increases the rate of the reaction over the use of triphenylphosphine. Furthermore, the first order rate constant obtained by this method for the PPh_3 system was comparable to that determined by Welby using NMR spectroscopy, giving confidence in this method of analysis.

2.6.4 Mechanistic Implications

The increase in reaction rate observed when PPh_3 was replaced by the more electron-rich P^iPr_3 suggested that an electron-poor intermediate may be involved. It is known that the reaction initially forms vinylidene **25b** and so any further intermediates involved must lead to a three step mechanism (Scheme 2-15). DFT calculations carried out by Dr David Johnson failed to find any neutral intermediates that were at a low enough energy to match experimental findings,[200] and these two occurrences led to the proposal that the mechanism went through cationic intermediate. Vinyl carbene **26**

(Scheme 2-15) was postulated as a possible structure for this intermediate and its synthesis and reactivity will be discussed in Chapter 3.

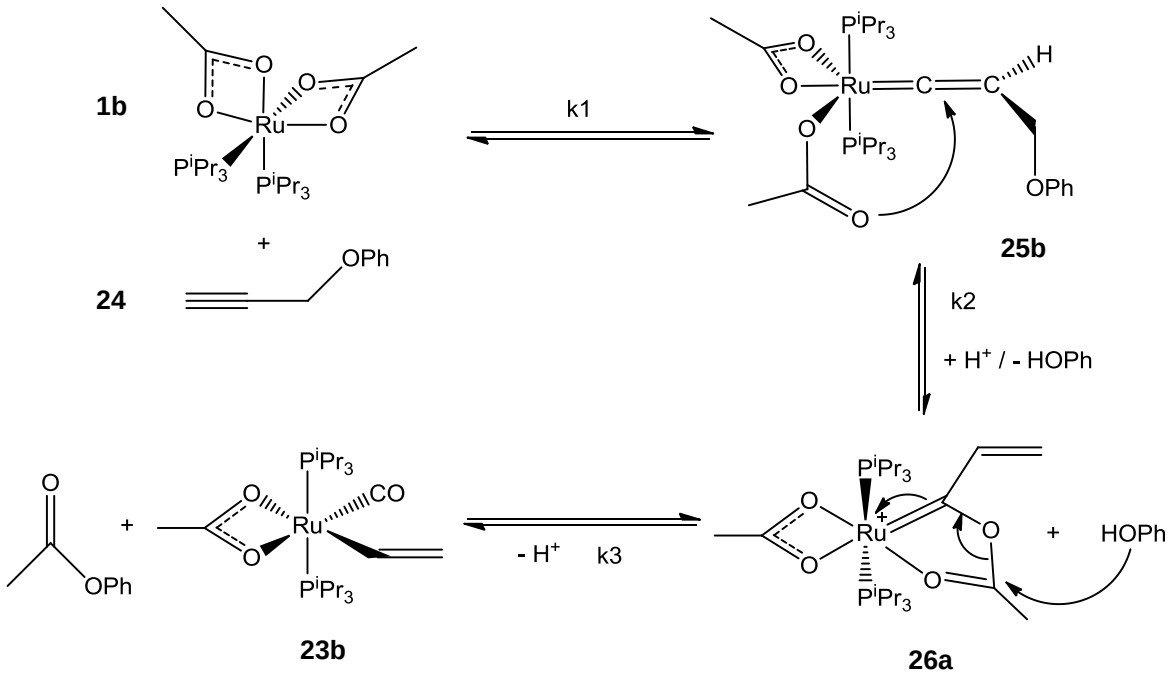

Scheme 2-15 Proposed Mechanism

2.7 Conclusion

This chapter has described the development of a general route to complexes of the type *cis*-[Ru(κ^2-OAc)$_2$(PR_3)$_2$] **1**. The commercially available ruthenium precursor [Ru(*p*-cymene)Cl_2]$_2$ **11** was used. It was initially found that sodium acetate did not displace the chloride ligands, however use of silver acetate resulted in the ready formation of [Ru(κ^1-OAc)(κ^2-OAc)(*p*-cymene)] **18**. This was found to react with a range of phosphorus ligands (including chelating diphosphines and phosphites) to give complexes of the type *cis*-[Ru(κ^2-OAc)$_2$(PR_3)$_2$] **1**. To the best of our knowledge this is the only general route to these complexes.

These complexes were then reacted with terminal alkynes. It was found that the chelating systems [Ru(κ^2-OAc)$_2$(dppe)] **9** and [Ru(κ^2-OAc)$_2$(dppb)] **22**, did not react, presumably the enforced *cis*-geometry prevents any reaction occurring. *Cis*-[Ru(κ^2-OAc)$_2$(P(O^{i}Pr)$_3$)$_2$] **1c** also did not react, here it is assumed that the ruthenium centre is too electron-poor to support a vinylidene ligand. In contrast the more electron-rich *cis*-[Ru(κ^2-OAc)$_2$(P^iPr_3)$_2$] **1b** did react with phenyl acetylene **6** to give [Ru(κ^2-OAc)(κ^1-OAc)(P^iPr_3)$_2$(=C=CHPh)] **7b**. Compound **1b** was found to have analogous reactivity to complex **1a**, reacting with propargyl alcohols **2** to form geminal alkenes **5** and carbonyl complex **4b**. Triisopropylphosphine complex **1b** was found to

undergo this reaction significantly faster than triphenylphosphine complex **1a** and a ReactIR instrument was used to measure the kinetic data. This kinetic study was inconclusive in determining detailed information about the reaction mechanism, but it was able to confirm that use of triisopropylphosphine over triphenylphosphine was able to increase the reaction rate. It is has been suggested that this is evidence for a cationic intermediate and a mechanism has been proposed based on this. This mechanism was investigated experimentally and the results will be discussed in Chapter 3.

3. Synthesis and Reactivity of Substituted Vinyl Carbenes

3.1 Introduction

In Chapter 2 the reaction of *cis*-[Ru(κ^2-OAc)$_2$(PPh$_3$)$_2$] **1a** with propargylic alcohols **2** was investigated. The initial product was found to be a hydroxy vinylidene **3**[170] but this was subsequently found to degrade to [Ru(κ^2-OAc)(κ^1-OAc)(CO)(PPh$_3$)$_2$] **4a** and a geminal alkene **5**. A mechanism was proposed, based on the findings of DFT calculations carried out by Dr David Johnson, and the kinetics studies discussed in Chapter 2 (Scheme 3-1). It was decided to independently synthesise postulated intermediate **26** and investigate its reactivity towards nucleophiles, in order to determine whether the proposed mechanism is in any way plausible.

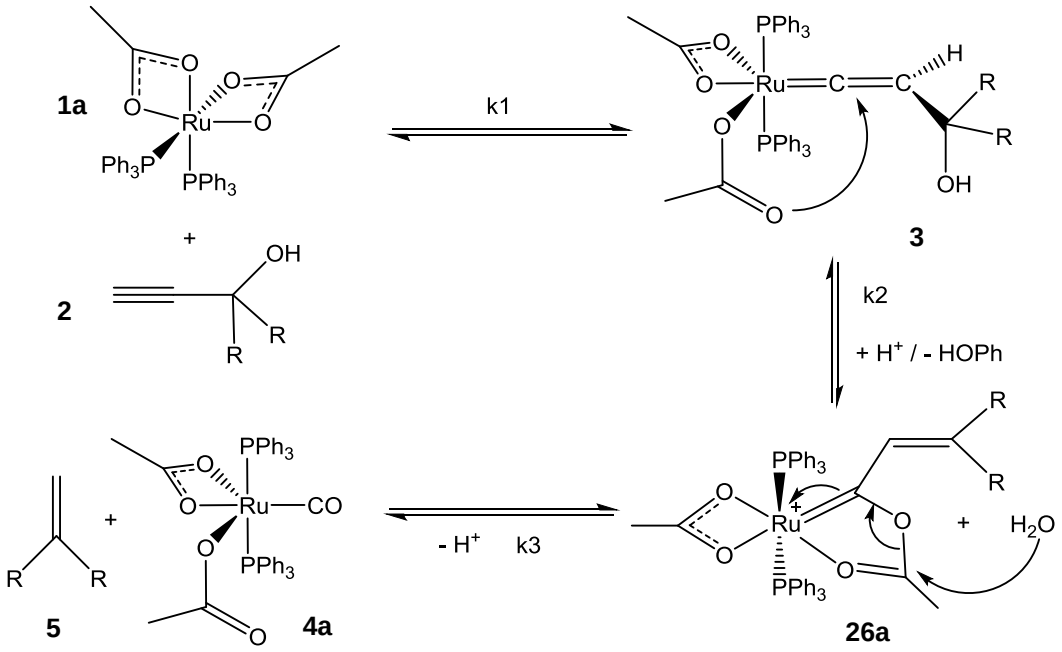

Scheme 3-1 Proposed Mechanism

We planned to synthesise vinyl carbenes **26** by treating hydroxy vinylidenes **3** with a Lewis acid to remove the hydroxy group. Due to their role as intermediates in enyne metathesis there are a number of synthetic routes to vinyl carbene complexes in the literature.[45] A related method is the addition of nucleophiles to the α-carbon of allenylidenes which have been formed from propargylic alcohols (via hydroxy vinylidenes) (Scheme 3-2).

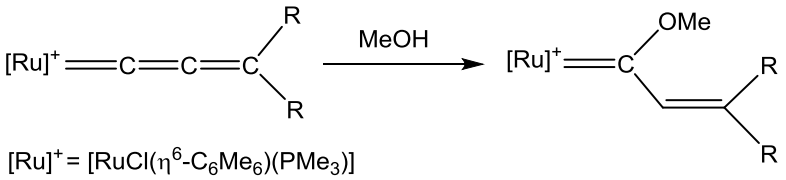

Scheme 3-2 Nucleophilic addition to Allenylidenes to form Vinyl Carbenes

It is also possible to insert a propargylic halide into a metal hydride bond and then eliminate the halide to give the vinyl carbene (Scheme 3-3). They can also be formed via metathesis. Alkene metathesis using conjugated dienes can be used to yield a vinyl carbene. It is also possible to isolate the vinyl carbene intermediate of enyne metathesis half way by use of chelated carbenes or silylacetylenes.[201]

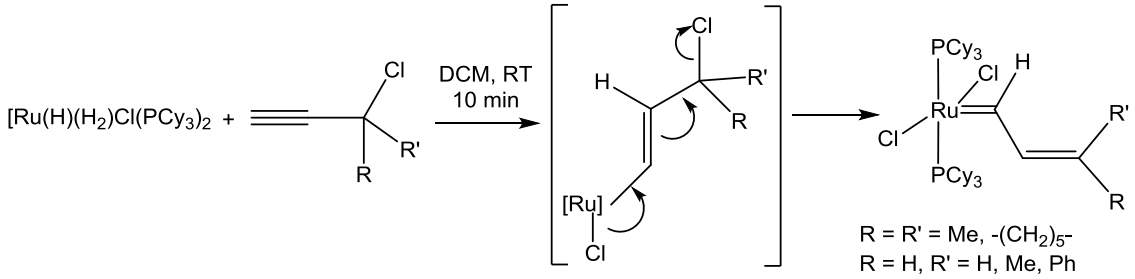

Scheme 3-3 Use of Metal Hydride Precursors to Form Vinyl Carbenes

3.2 Synthesis of Substituted Vinyl Carbenes

3.2.1 Synthesis

In order to investigate its reactivity, it was decided to synthesise some analogues of the cationic intermediate **26** postulated in Chapter 2. Reacting a DCM solution of *cis*-[Ru(κ^2-OAc)$_2$(PPh$_3$)$_2$] **1a** with substituted propargylic alcohol resulted in the formation of orange hydroxy vinylidene complexes **3**.[173] These orange hydroxy vinylidenes were then treated *in situ* with tritylcarbenium tetrafluoroborate (chosen because it was anticipated that the resultant trityl alcohol would be too large to react with **26**) to generate complexes **26** which were either green (in the case of **26b** and **26c**) or purple (example **26d**) (Scheme 3-4). The unsubstituted analogue **26a** will be discussed in Chapter 4.

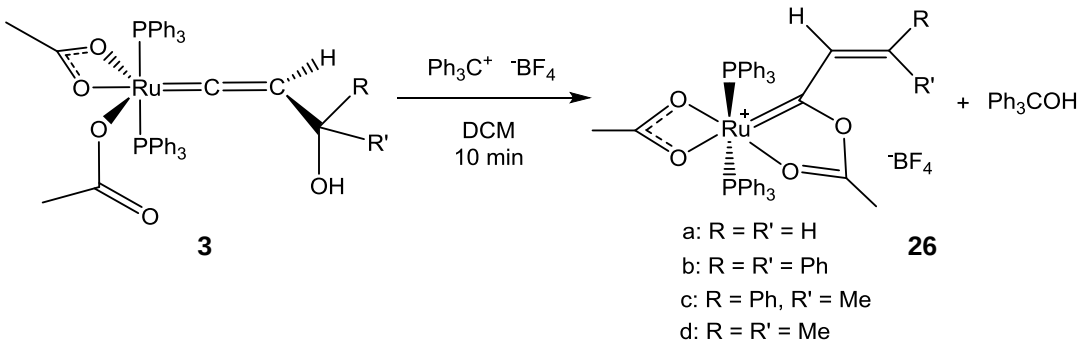

Scheme 3-4 Synthesis of [Ru(κ^2-OAc)(OC{Me}OCC{H}=CRR')(PPh$_3$)$_2$][BF$_4$] **26**

The spectroscopic data for **26b** showed characteristic peaks in the ^{13}C-NMR spectrum for the organic ligand (a singlet at δ 127.7 for the β-carbon, a singlet δ 146.9 for the γ-carbon and a triplet at δ 279.8 for the α-carbon ($^2J_{PC}$ = 9.3 Hz)) and one peak observed in the ^{31}P-NMR spectrum at δ 32.4. Two sets of acetate resonances were observed in the ^{1}H (δ 0.79 and 1.31) and ^{13}C-NMR (methyl resonances at δ 17.7 and 21.9, carbonyl resonances at δ 183.2 and 186.6) spectra, showing that these ligands are not equivalent on the NMR timescale. The IR spectrum also shows the different coordination modes of the acetate groups. The κ^2-OAc exhibits a symmetric stretch at 1434 cm^{-1} and the asymmetric at 1530 cm^{-1} (therefore a characteristically small Δv of 96 cm^{-1} showing that it is coordinated through both oxygen atoms[171, 172]). The acetate group in the metallocycle, however, has only one band at 1630 cm^{-1} which indicated a higher degree of ester character. ESI-MS showed an intense molecular ion peak at *m/z* 935.1998 providing further evidence for the formation of **26b**.

The data for **26c** and **26d** were similar with α-carbon resonances observed at δ 284.3 and 284.9 respectively in the ^{13}C-NMR spectra. Additionally the Nuclear Overhauser effect spectroscopy (NOESY) spectrum for complex **26c** showed NOE cross-peaks between the vinyl-proton and the aromatic region, not the methyl group. This suggests that the complex adopts the structure shown in Scheme 3-4 with the proton *cis* to the phenyl group. This NOESY spectrum also exhibited exchange spectroscopy (EXSY) peaks between the two acetate resonances which suggests that they are exchanging, but that this exchange must be slow on the NMR time-scale.

3.2.2 Structural Data

Obtaining good structural data of these compounds proved challenging. Although they crystallised very easily, the resulting crystals were often twinned and highly disordered. Many attempts were made to change the crystallisation in order to reduce these effects. A variety of solvent systems (DCM:pentane, DCM:diethyl ether, acetone:diethyl ether) were used for both layering and jar-in-jar crystallisation methods. The counter

ions were also changed to PF_6 (using $Ph_3C^+[PF_6]$) and triflate (using TMS-OTf), also to no effect.

The best data sets for **26b** and **26d** (Figure 3-1and Figure 3-2) are presented and confirm the formation of the metallocyclic structure. However, due to the poor resolution no discussion of bond lengths and angles will be attempted.

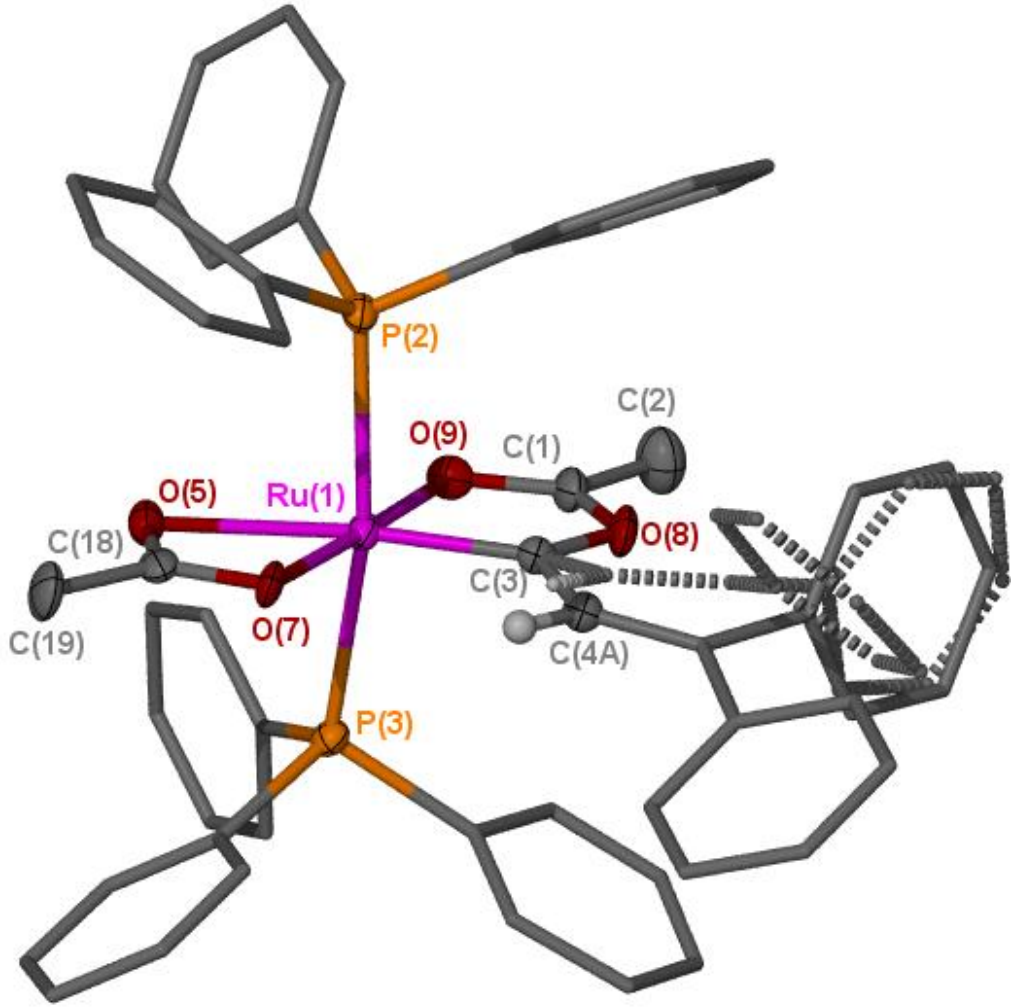

Figure 3-1 ORTEP Representation of Complex **26b**; Thermal Ellipsoids, where shown, are at 50% Probability, Hydrogen Atoms, the BF_4 Counter Ion and Solvent Molecules have been Omitted for Clarity. The disordered alkene moiety on the organic ligand is shown with dotted lines.

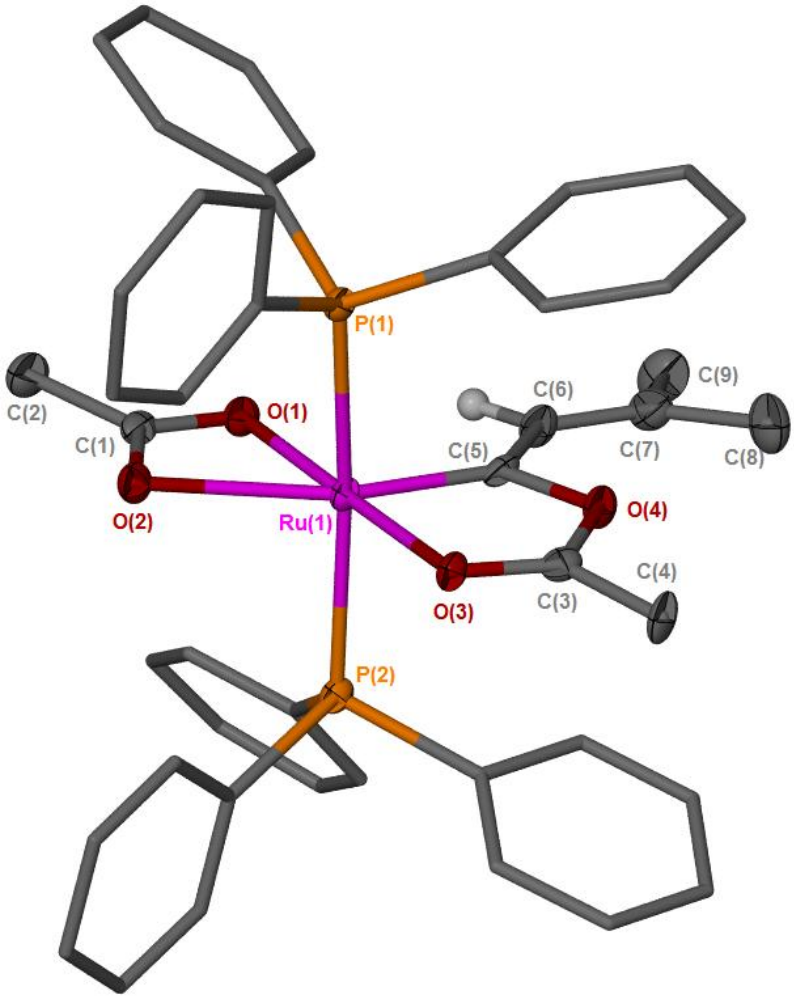

Figure 3-2 ORTEP Representation of Complex **26d**; Thermal Ellipsoids, where shown, are at 50% Probability, Hydrogen Atoms, the BF_4 Counter Ion and Solvent Molecules have been Omitted for Clarity.

3.2.3 Synthesis of Benzoate Analogue 27

In order to obtain a structure of suitably high resolution the benzoate analogue of compound **26** was synthesised. [Ru(κ^2-O_2CPh)(OC{Ph}OCC{H}=CPh_2)(PPh_3)$_2$][BF_4] **27** was synthesised from *cis*-[Ru(κ^2-O_2CPh)$_2$(PPh_3)$_2$] **28** and 1,1-diphenylprop-2-yn-1-ol **2a**, and dark green crystals were grown by slow diffusion of diethyl ether into a saturated DCM solution of **27** (Scheme 3-5 and Figure 3-3). The complex was fully characterised, with the data closely matching that for complexes **26**.

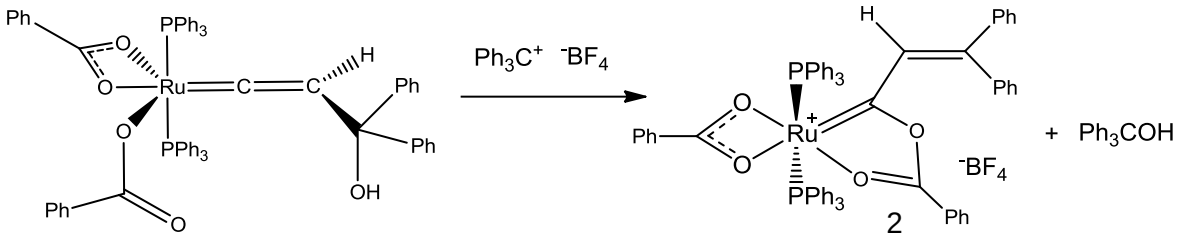

Scheme 3-5 Synthesis of [Ru(κ^2-O_2CPh)(OC{Ph}OCC{H}=CPh_2)(PPh_3)$_2$][BF_4] **27**

Complex **27** adopts a distorted octahedral geometry, with much of the distortion being caused by the small bite angle of the κ^2-OBz ligand (O(1)-Ru-O(2) = 60.12(7)°). This has led to the angles between κ^2-OBz and the chelating carbene being over 90˚ (Table 3-1). A more uncommon distortion is the greater than usual deviation of the angle between the phosphine ligands from 180˚ (P(1)-Ru-P(2) = 166.03(2)˚). This is presumably caused by steric clashes between the phenyl rings of phosphine ligand based on P(2) (at the top of Figure 3-3) and the vinyl phenyl rings.

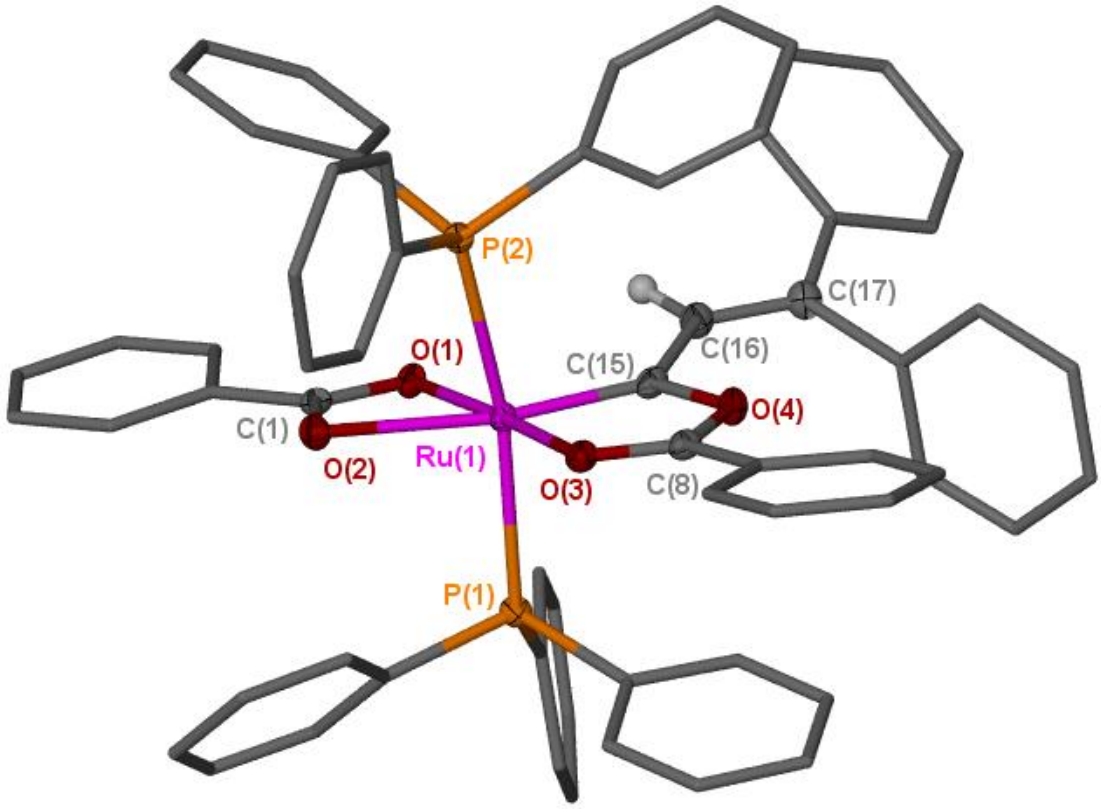

Figure 3-3 ORTEP Representation of Complex **27**; Thermal Ellipsoids, where shown, are at 50% Probability, Hydrogen Atoms, the BF_4 Counter Ion and Solvent Molecules have been Omitted for Clarity.

Table 3-1 Selected Bond Lengths and Angles for Complex **27**

Bond	Bond Length (Å)	Angle	Bond Angle (°)
C(15) – Ru	1.862(3)	C(15) – Ru – O(1)	106.24(10)
C(15) – C(16)	1.440(4)	C(15) – Ru – O(2)	165.66(9)
C(16) – C(17)	1.356(4)	C(15) – Ru – O(3)	78.39(10)
O(1) – Ru	2.1018(18)	C(15) – Ru – P(1)	96.12(9)
O(2) – Ru	2.2521(17)	C(15) – Ru – P(2)	95.42(9)
O(3) – Ru	2.0720(18)	O(1) – Ru – O(2)	60.12(7)
P(1) – Ru	2.3836(8)	O(3) – Ru – O(1)	175.37(7)
P(2) – Ru	2.3931(8)	O(3) – Ru – O(2)	115.25(7)
O(3) – C(8)	1.238(3)	O(1) – Ru – P(1)	92.88(5)
C(8) – O(4)	1.341(3)	O(2) – Ru – P(1)	89.33(5)
O(4) – C(15)	1.417(3)	O(3) – Ru – P(1)	86.84(5)
		P(1) – Ru – P(2)	166.03(2)
		C(16) – C(15) – Ru	129.2(2)
		C(15) – C(16) – C(17)	130.1(3)
		O(3) – C(8) – C(4)	119.8(2)
		C(8) – O(3) – Ru	112.75(17)
		C(8) – O(4) – C(15)	111.7(2)
		O(4) – C(15) – C(16)	113.1(2)

Only one previous example of a ligand of this type has been crystallised before, $[RuCl_2(OC\{Me\}OCC\{H\}=CPh_2)(PPh_3)_2]$.[202] This example from Schanz's group was synthesised by the addition of acetic acid to the carbyne complex $[RuCl_3(CCH_2CPh_2)(PPh_3)_2]$. A comparison of the bond lengths and angles shows that the two complexes are very similar (Table 3-2). The bond between Cα-Cβ (1.440(4) Å) is longer than Cβ-Cγ (1.356(4) Å) showing the single and double bond characters of the bonds.

Table 3-2 Comparison of **27** with Literature Data

	Complex **27**	$[RuCl_2(OC\{Me\}OCC\{H\}=CPh_2)(PPh_3)_2]$
Ru-Cα (Å)	1.862(3)	1.862(5)
Cα-Cβ (Å)	1.440(4)	1.434(7)
Cβ-Cγ (Å)	1.356(4)	1.347(7)
Ru-Cα-Cβ (°)	129.2(2)	1.341(3)
Cα -Cβ-Cγ (°)	130.1(3)	1.300(5)

The ruthenium-carbon bond length (1.862(3) Å) is very similar to that observed in the related octahedral Fischer carbenes $[Ru(\kappa^1\text{-}OAc)(\kappa^2\text{-}OAc)(=CO\{CH_2\}_n)(PPh_3)_2]$ where n = 3 (1.878(6) Å) or 5 (1.902(3) Å).[173] These neutral complexes all display shorter bond lengths than those observed in cationic systems such as $[Ru(\eta^5\text{-}C_5H_5)(=C\{OMe\}Et)(PPh_3)_2][PF_6]$ (1.959(6) Å)[203] and $[Ru(\eta^5\text{-}C_5H_5)(=C\{OMe\}CH_2Ur)(PPh_3)_2][X]$ (Ur = uracil) (X = PF_6,[204] 1.946(3) Å; X = OTf,[205] 1.9541(17)); this can be attributed to lower levels of back-bonding in the cationic species.

3.2.4 Vinyl Carbonyl By-Product

Whilst compounds **26** could be isolated in moderate yields (ca. 50-70%), it should be noted that a major by-product, vinyl carbonyl species **29**, was sometimes observed during the synthesis of **26b** (up to ca. 15% in the ^{31}P-NMR spectra of reaction mixtures). In the ^{31}P-NMR spectra, the resonance for **29** was apparent at δ 38.1 and was observed to convert through to carbonyl complex **4** (δ 39.1) and geminal alkene **5a** over time (Scheme 3-6). These by-products could easily be removed by washing **26** with diethyl ether.

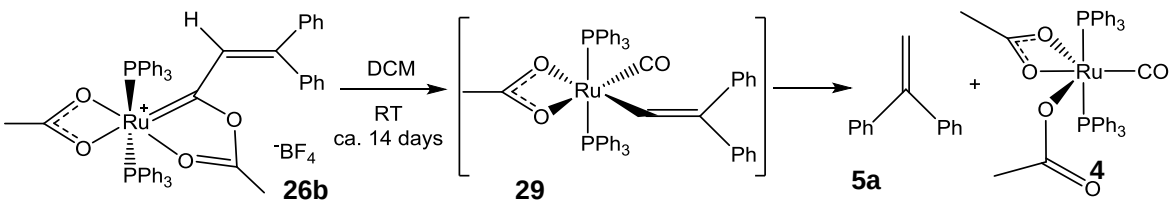

Scheme 3-6 Decomposition of **26b** to **29**, then to **4** and **5a**

The related species $[Ru(\kappa^2\text{-}OAc)(CH=CH_2)(CO)(PPh_3)_2]$ **23a** has been isolated previously.[169] The majority of this by-product was removed during purification (it was

only observed when the reactions were monitored by NMR), however crystals of **29** (Figure 3-4) were obtained during crystallisation of **26b**.

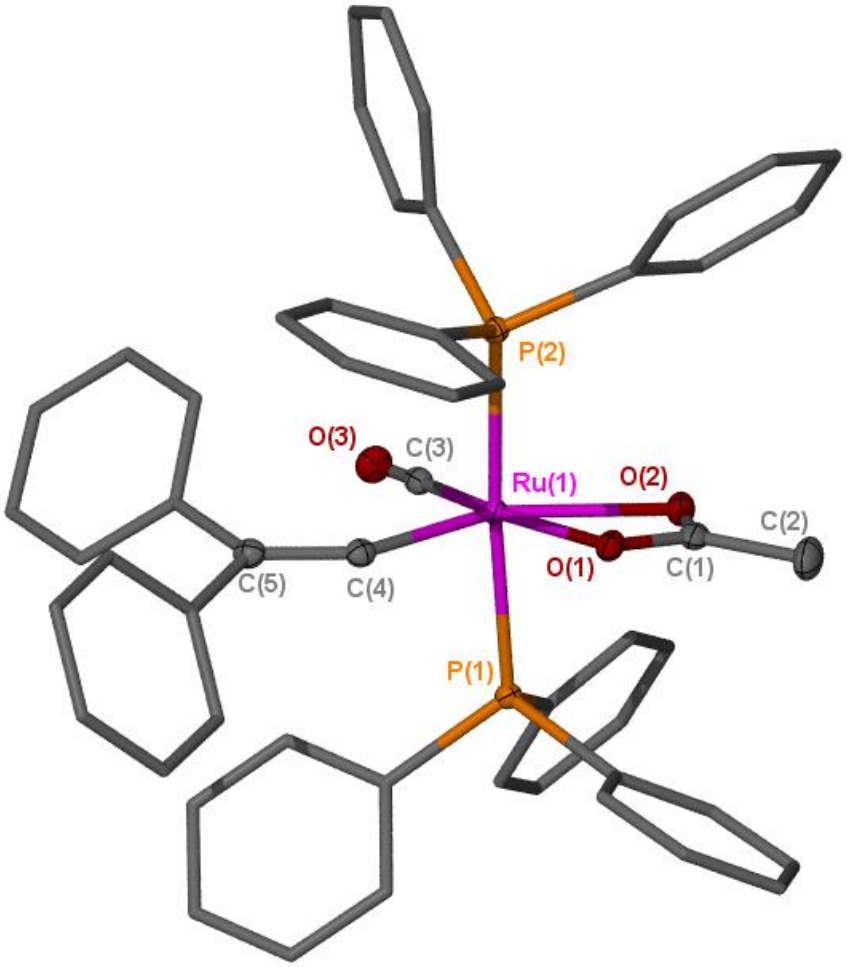

Figure 3-4 ORTEP Representation of Complex **29**; Thermal Ellipsoids, where shown, are at 50% Probability, Hydrogen Atoms have been Omitted for Clarity.

Table 3-3 Selected Bond Lengths and Angles for Complex **29**

Bond	Bond Length (Å)	Angle	Bond Angle (°)
C(3) – O(3)	1.154(3)	C(3) – Ru(1) – C(4)	95.94(11)
C(3) – Ru(1)	1.817(3)	C(3) – Ru(1) – O(1)	171.00(9)
C(4) – C(5)	1.343(4)	C(3) – Ru(1) – O(2)	112.13(9)
C(4) – Ru(1)	2.036(3)	C(3) – Ru(1) – P(1)	87.17(8)
O(1) – Ru(1)	2.1809(17)	C(3) – Ru(1) – P(2)	98.18(8)
O(2) – Ru(1)	2.2732(18)	C(4) – Ru(1) – O(1)	92.99(9)
P(1) – Ru(1)	2.3721(7)	C(4) – Ru(1) – O(2)	151.02(9)
P(2) – Ru(1)	2.3913(7)	C(4) – Ru(1) – P(1)	90.55(7)
		C(4) – Ru(1) – P(2)	90.46(7)
		O(1) – Ru(1) – O(2)	58.87(7)
		O(1) – Ru(1) – P(1)	91.62(5)
		O(1) – Ru(1) – P(2)	82.84(5)
		O(2) – Ru(1) – P(1)	84.03(5)
		O(2) – Ru(1) – P(2)	92.44(5)
		P(1) – Ru(1) – P(2)	174.42(2)
		C(5) – C(4) – Ru(1)	144.3(2)
		O(3) – C(3) – Ru(1)	176.2(2)

The single crystal X-ray diffraction study confirms the presence of both vinyl and carbonyl ligands. Overall **29** adopts a distorted octahedral geometry, with the distortion arising from the κ^2-OAc ligand (O(1)-Ru(1)-O(2) = 58.87(7)°). This has led to the other bond angles in this plane being significantly larger than 90°. The C≡O (1.154(3) Å) and Ru-C (1.817(3) Å) bond lengths of the carbonyl ligand are within the expected ranges,[206] as are the vinyl bond lengths of C=C (1.343(4) Å) and Ru-C (2.036(3) Å).[207] These ligands are found to be coplanar, an orientation which allows for the optimisation of π-back-bonding interactions for both ligands.[208] Comparison of the structure of **29** with the analogous species $[Ru(\kappa^2\text{-OAc})(CO)(CH{=}CH_2)(PPh_3)_2]$[169] and $[Ru(\kappa^2\text{-OAc})(CO)(CH{=}CPhH)(PPh_3)_2]$[209] shows that alteration of the vinyl substituents makes little difference to the vinyl bond lengths (C=C bond lengths 1.343(4), 1.227(5) and 1.294(14) Å respectively).

3.3 Vinyl Carbene Reactivity

Compounds **26** were treated with various nucleophiles to test the hypothesis that they are key intermediates in the formation of carbonyl complexes **4** from **1** and propargyl

alcohols (Chapter 2). These reactions were carried out in Young's tap NMR tubes, 0.027 mmol of vinyl carbene **26** and either one or five equivalents of the nucleophile were dissolved in 0.5 ml of CD_2Cl_2 and the reactions followed by ^{1}H and ^{31}P-NMR spectroscopy.

3.3.1 Reaction of 26 with Neutral Nucleophiles

The study began with the investigation of neutral nucleophiles as these species are proposed to be the types of nucleophiles involved in the formation of carbonyl complex **4** (Scheme 2-15). When the di-methyl analogue **26d** was treated with acetic acid (AcOH) or phenol (PhOH), no reaction was observed and solutions were unaltered even after several months. However, reaction of **26b** with one equivalent of ethanol or acetic acid lead to complex mixtures of unidentified products after 1-2 weeks. It should be noted that **26b** alone in CD_2Cl_2 solution also forms a complex mixture of products, on approximately the same timescale. However more products are seen when ethanol or acetic acid are present.

These reactions were also carried out with an excess of organic reactant. Both were found to produce carbonyl complex **4** and 1,1-diphenylethene **5a** over the course of a week. Reaction with ethanol also produced ethyl acetate (seen in the ^{1}H-NMR spectrum) and an unknown phosphorus-containing species (Scheme 3-7). In the NMR spectra of the acetic acid reaction there was also evidence for a range of other unidentified products (Scheme 3-8) and this reaction was far less selective than that with ethanol.

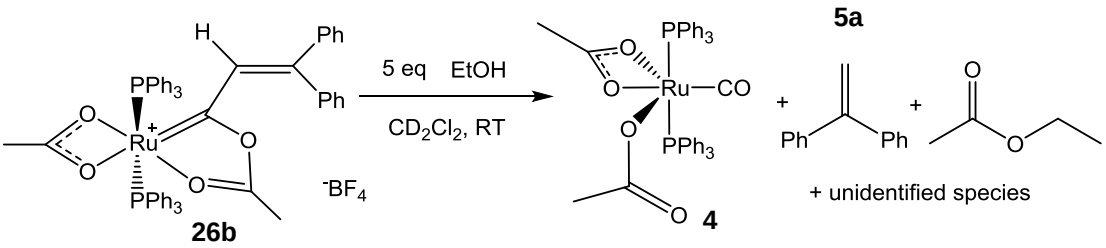

Scheme 3-7 Reaction of Complex **26b** with an Excess of Ethanol

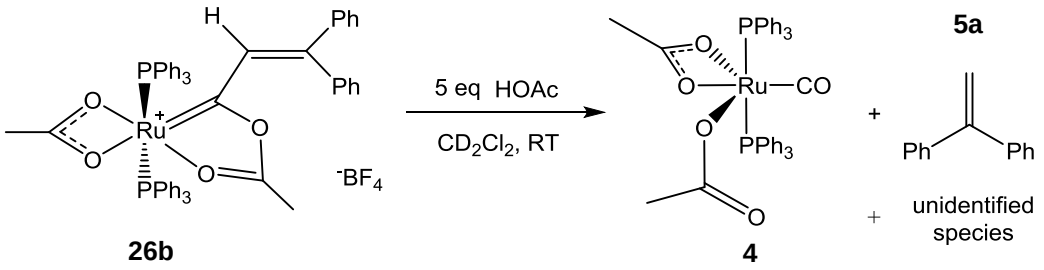

Scheme 3-8 Reaction of Complex **26b** with an Excess of Acetic Acid

3.3.2 Reaction of 26 with Anionic Nucleophiles

One possible explanation for these observations is that an excess of ethanol allows the formation of ethoxide/acetate species and it is these species that react with complex **26**. The cationic complexes were therefore treated directly with anionic nucleophiles.

DABCO (1,4-diazabicyclo[2.2.2]octane), tetrabutylammonium phenoxide and sodium methoxide were found to react with complex **26**, but highly unselectively with a large number of resonances observed in the NMR spectra.

Selective reactivity was observed with the use of sodium hexamethyldisilazane (NaHMDS), potassium/sodium *tert*-butoxide, tetrabutylammonium acetate and tetramethylammonium acetate. The reactivity observed was deprotonation, none of the expected nucleophillic addition products were observed. The site of deprotonation, and therefore the product formed, was dependent on the nature of the vinyl substituents and discussion of these reactions will form the remainder of Chapter 3.

3.3.3 Deprotonation of 26b, Synthesis of an Allenylidene Complex 30

In the case of the deprotonation of compound **26b** the optimal reaction conditions were found to be addition of one equivalent of sodium *tert*-butoxide to a DCM solution of **26b**. The resulting solution was then stirred for 15 minutes at room temperature before the solvent was removed and the residue extracted with diethyl ether. Cooling of this ether solution produced allenylidene complex **30** as a red powder (Scheme 3-9).

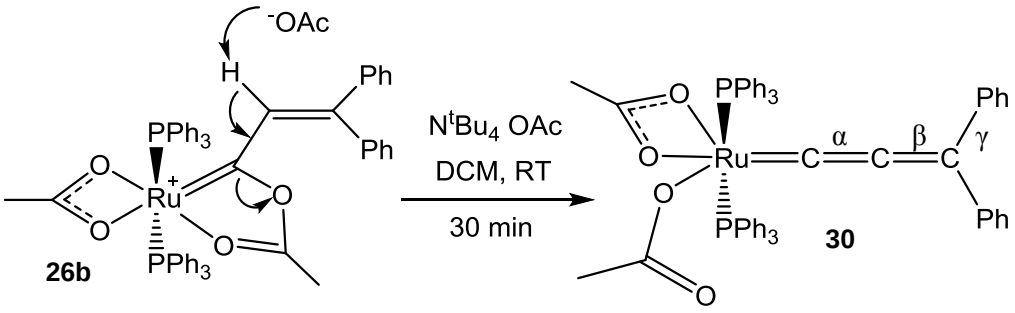

Scheme 3-9 Reaction of Complex **26b** with Sodium *tert*-Butoxide

The ^{1}H-NMR spectrum showed only one non-aromatic peak, at δ 0.91, which was assigned to the methyl groups of the acetate ligands. The presence of a single resonance suggests that the metallocyclic acetate has been lost, and that only κ^1/κ^2 acetate groups (which are exchanging on the NMR timescale) are present. The ^{13}C-NMR spectrum was far more diagnostic with a triplet due to the α-carbon observed at δ 305.0 ($^{2}J_{PC}$ = 17.3 Hz), the β-carbon triplet at δ 232.8 ($^{3}J_{PC}$ = 5.5 Hz) and a singlet at δ 147.3 assigned to the γ-carbon (Figure 3-5). A single peak in the ^{13}P-NMR spectrum was observed at δ 32.6.

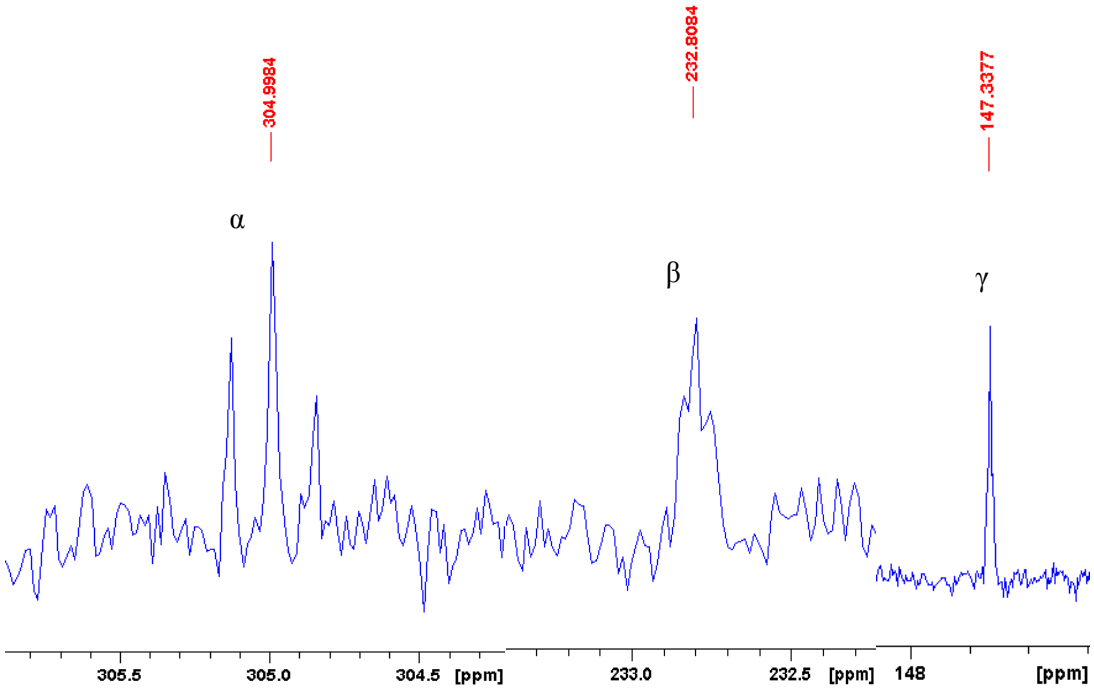

Figure 3-5 Low Field Region of the ^{13}C-NMR Spectrum of Allenylidene **30**

Mass spectra were recorded using both ESI and LIFDI as ionisation techniques. Use of LIFDI was able to show an $[M]^+$ peak (*m/z* 934.13). When the spectrum was recorded using ESI peaks at *m/z* 935.1993 [M+H] and *m/z* 957.1781 [M+Na] were observed. Importantly, the latter was not observed in the corresponding spectrum of the precursor complex **26b** giving confidence in the proposed formula.

Crystals were obtained by cooling of a concentrated ether solution of **30** to -15 °C (Figure 3-7). The resulting structure shows that the complex adopts a distorted octahedral geometry. This distortion is attributed to the small bite-angle of the κ^2-OAc ligand (O(1)-Ru-O(2) = 59.06(4)°) and leads to the angle between the two acetate ligands (O(2)-Ru-O(3) = 112.87(4)°) being significantly larger than the ideal 90°. The allenylidene bond lengths were found to be within the expected ranges given by Bruce.[120] The Ru-C(5) bond length is short (1.8468(13) Å) and within the reported range of 1.84-2.00 Å. As expected the C(5)-C(6) (1.2635(19) Å, expected range 1.18-1.27 Å) bond length is shorter than the C(6)-C(7) (1.3569(19) Å, expected range 1.35-1.41 Å) length, which is consistent with the presence of the alkynyl resonance structure **B** discussed in Chapter 1 (Figure 3-6 below).

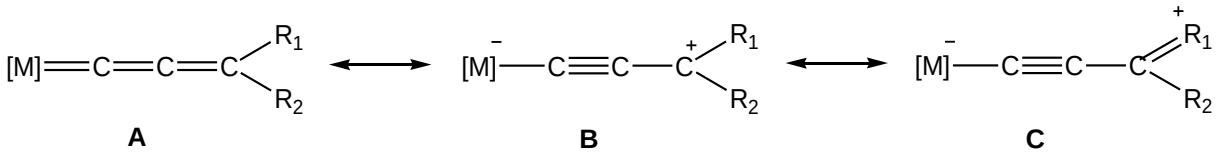

Figure 3-6 Three Resonance forms of Allenylidene Ligands

Allenylidene ligands typically exhibit almost linear geometry, with the bond angles at Cα and Cβ expected in the range 165-180°.[120] In this case it has been found that the angle Ru-C(5)-C(6) (169.03(12)°) deviates more than the C(5)-C(6)-C(7) (178.80(16)°) angle. Again this is consistent with the presence of a resonance form with a single bond between the ruthenium and carbon, leading to weaker conjugation between these atoms and therefore deviation from linearity.

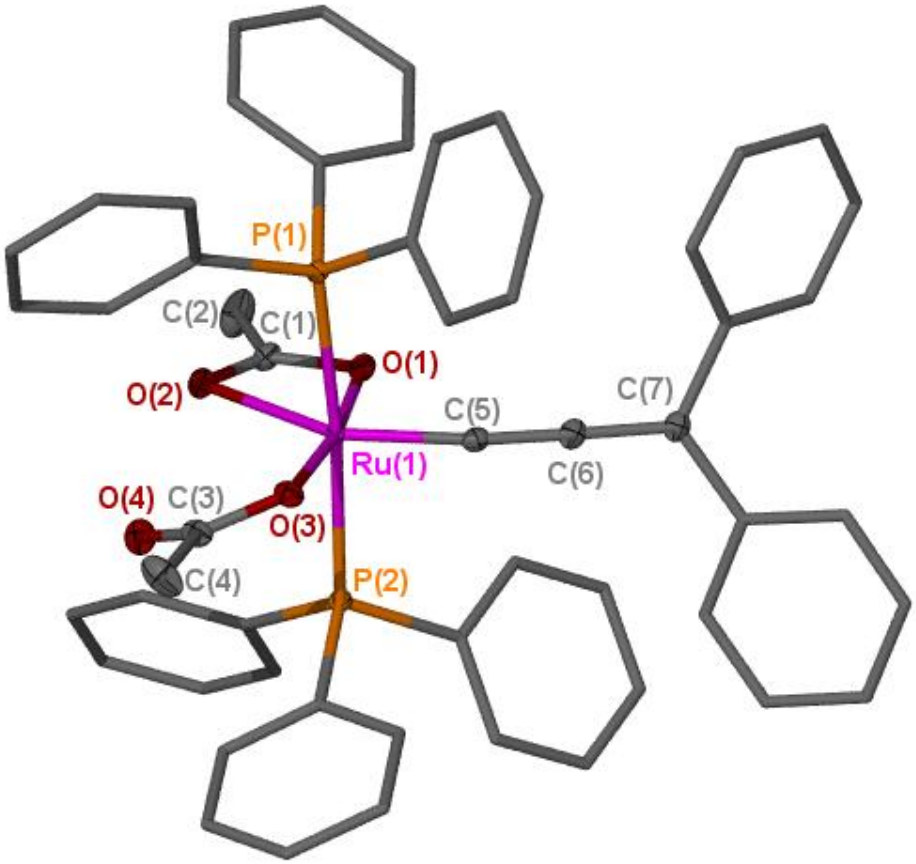

Figure 3-7 ORTEP Representation of Complex **30**; Thermal Ellipsoids, where shown, are at 50% Probability, Hydrogen Atoms and Solvent Molecules have been Omitted for Clarity.

Table 3-4 Selected Bond Lengths and Angles for Complex **30**

Bond	Bond Length (Å)	Angle	Bond Angle (°)
C(5) – Ru	1.8468(13)	C(5) – Ru – O(1)	92.16(5)
C(5) – C(6)	1.2635(19)	C(5) – Ru – O(2)	150.96(5)
C(6) – C(7)	1.3569(19)	C(5) – Ru – O(3)	95.83(5)
O(1) – Ru	2.1110(10)	C(5) – Ru – P(1)	92.54(4)
O(2) – Ru	2.2914(10)	C(5) – Ru – P(2)	91.31(4)
O(3) – Ru	2.0675(10)	O(1) – Ru – O(2)	59.06(4)
P(1) – Ru	2.3844(3)	O(3) – Ru – O(1)	171.89(4)
P(2) – Ru	2.3787(3)	O(3) – Ru – O(2)	112.87(4)
		O(1) – Ru – P(1)	93.90(3)
		O(2) – Ru – P(1)	86.19(3)
		O(3) – Ru – P(1)	84.41(3)
		P(1) – Ru – P(2)	174.454(12)
		C(6) – C(5) – Ru	169.03(12)
		C(5) – C(6) – C(7)	178.80(16)

A search of the Cambridge Structural Database for di-phenyl substituted ruthenium allenylidene complexes resulted in 27 hits.[210] However, of these over half were piano-stool complexes and only four were octahedral species with *trans*-phosphine ligands. These were reported in 2007 by Schanz et al. in which $[RuCl_2(PPh_3)_2(=C=C=CPh_2)]$ was trapped with a different alcohols and an amine.[202] Under acidic conditions this complex has been found to be unstable with respect to the indenylidene complex (see Chapter 1),[144] whereas at higher pH it has been found to complex nucleophiles to form the octahedral complexes $[RuCl_2L(PPh_3)_2(=C=C=CPh_2)]$ (where L = EtOH, MeOH, H_2O or DMAP).

Table 3-5 Comparison of **30** with Literature Data

	O-Donor Nucleophiles	Complex **30**
Ru-Cα (Å)	1.833(6) – 1.848(9)	1.8468(13)
Cα-Cβ (Å)	1.236(7) – 1.250(4)	1.2635(19)
Cβ-Cγ (Å)	1.345(11) – 1.384(8)	1.3569(19)
Ru-Cα-Cβ (°)	177.1(5) – 179.1(8)	169.03(12)
Cα -Cβ-Cγ (°)	176.5(4) – 178.9(6)	178.80(16)

As can be seen from Table 3-5, the bond lengths are found to be very much the same; however the data highlights the deviation from linearity at the Cα observed in complex **30**. Previous work in the Lynam group has shown that the π-acceptor/donor properties of various ligands can be determined by comparison of their structural metrics. The ligands were placed in their relative order of π-acceptor ability through analysis of the Ru-O bond lengths of π-donor ligands (κ^2-OAc) *trans* to the ligand of interest and the bite angle of the κ^2-OAc (carbene < vinylidene ≈ CN^tBu < CO < NO^+).[173] Comparison with this data places the π-accepting ability of this allenylidene ligand between the carbene and vinylidene ligands (Table 3-6). This is also consistent with the trend discussed by Bruce in which the chemical shift of ancillary Cp ligands was used to conclude that allenylidene ligands have less π-accepting ability than vinylidene or CO ligands.[120]

Table 3-6 Summary of the Pertinent Bond Angles and Lengths for Estimating the π-Accepting Ability of Allenylidene **30**

	Ru-O(2) (Å)	O(1)-Ru-O(2) (°)
Carbene	2.355(4) – 2.325(2)	56.40(15) – 58.92(8)
Allenylidene	2.2914(10)	59.06(4)
Vinylidene	2.2465(12) – 2.2863(18)	59.08(6) - 59.86(4)
CN^tBu	2.2465(16)	60.42(4)
CO	2.1897(11)	61.55(8)
NO	2.0744(19)	59.80(6)

3.3.4 Deprotonation of 29

The deprotonation of the benzoate analogue of **26**, complex **29** was also investigated. Whilst the expected allenylidene complex **31** was formed, the reaction with sodium *tert*-butoxide was found to be slow and full conversion to allenylidene complex **31** was not obtained (Scheme 3-10). Residual starting material could be removed by extraction

with diethyl-ether and the resulting dark red powder analysed. Resonances due to allenylidene complex **31** were observed as triplets in the ^{13}C-NMR spectrum at δ 304.0 (J_{PC} = 18.6 Hz), δ 232.0 (J_{PC} = 5.1 Hz), δ 147.4 (J_{PC} = 2.7 Hz) and a characteristic IR band was observed at 1918 cm^{-1} in addition to those due to the impurities. A significant by-product was observed (and free PPh_3) at δ 55.6 in the ^{31}P-NMR. A series of high field doublets in the ^{13}C-NMR were assigned to this by-product (δ 281.9 (d, J_{PC} = 14.8 Hz), δ 209.7 (d, J_{PC} = 4.5 Hz), δ 175.8 (d, J_{PC} = 2.7 Hz)). These coupling constants are consistent with a *cis*-arrangement of the organometallic ligand to the phosphine ligands.

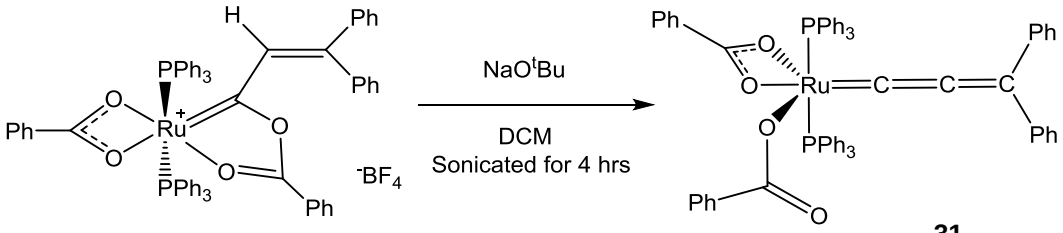

29 **31**

Scheme 3-10 Formation of Allenylidene **31**

Reaction of complex **29** with tetramethylammonium acetate was almost instantaneous, requiring only ~1 minute sonication (no residual starting material was observed). However, extensive exchange was observed between the benzoate ligands and the acetate leading to acetate/benzoate mixtures of the product and the by-product at ~ δ 55 in the ^{31}P-NMR spectrum. It was also found that allenylidene **31** produced in this way decomposed too fast for meaningful ^{13}C-NMR data of the allenylidene species to be observed. However, MS evidence was obtained for acetate/benzoate exchange.

3.3.5 Deprotonation of 26c and 26d, Synthesis of Vinylvinylidenes

The optimal reaction conditions were found to involve the use of acetate as the base for the deprotonation of **26c** (with a phenyl and a methyl substituent) and **26d** (the di-methyl analogue). Initially tetrabutylammonium acetate was utilised as it is soluble in DCM, however the use of tetramethylammonium acetate allowed the reactions to be followed by NMR spectroscopy more readily. For both reactions, one equivalent of acetate was added to a DCM solution of **26** and the resulting suspension sonicated for 2 minutes. The DCM was then removed and the residue extracted with diethyl ether; removal of the ether gave the product as an orange powder. For both of these complexes deprotonation occured at the methyl group of the vinyl moiety and therefore vinylvinylidene complexes **32** were formed (Scheme 3-11 and Scheme 3-12).

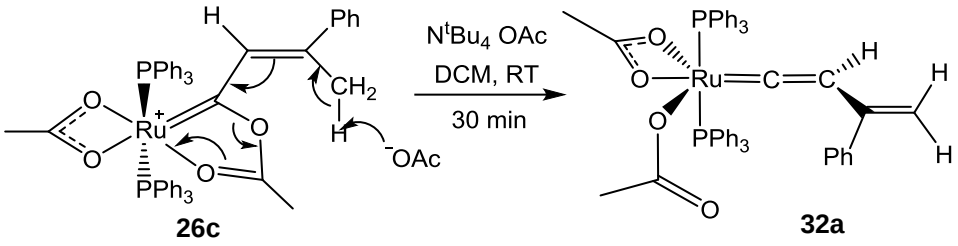

Scheme 3-11 Reaction of Complex **26c** with [NMe_4][OAc]

Evidence for the structure of **32a** comes from the ^{1}H-NMR spectrum where a triplet (δ 5.17) and two singlet resonances (δ 4.87 and 4.70, HSQC shows these to be bound to the same carbon), all of which integrate to one proton, were observed (Figure 3-8). Only one acetate resonance was observed (δ 0.84) and so it was assumed that only κ^1/κ^2 acetate groups are present. A singlet in the ^{31}P-NMR spectrum at δ 34.5 was also observed. Complex **32a** was found to be unstable in solution and so a ^{13}C-NMR spectrum could not be recorded.

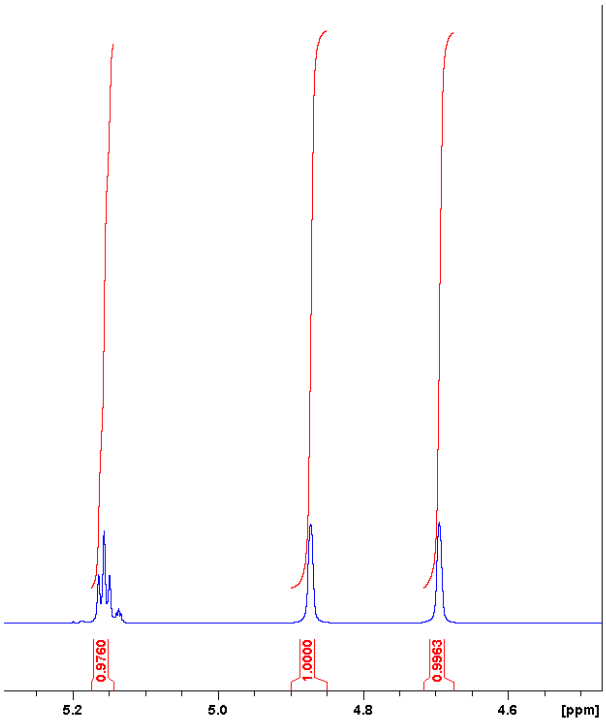

Figure 3-8 Detail of the ^{1}H-NMR of Complex **32a**

Formation of vinylvinylidene ligands instead of allenylidenes when a suitable proton is present is well documented.[119] Theoretical studies (carried out at the MP2/DZV(d,p)+*G* level) on the complexes $[Ru(\eta^5\text{-}C_5H_5)\{=C=C=C(H)CH_3\}(PH_3)_2]^+$ and $[Ru(\eta^5\text{-}C_5H_5)\{=C=C(H)CH=CH_2\}(PH_3)_2]^+$ showed that the vinylvinylidene tautomer is 8.8 kJ mol^{-1} more stable than the allenylidene form, giving some explanation for its competitive formation.[134]

The di-methyl substituted vinyl carbene **26d** also forms a vinylvinylidene complex (**32b**) when deprotonated. Analogous resonances were observed in the ^{1}H-NMR spectrum as

those seen for **32a**, however in this case a ^{13}C-NMR spectrum could be recorded. The characteristic triplet resonance for the α-carbon was observed at δ 360.4 with the β-carbon at δ 117.4.

If the reaction is not halted and **32b** isolated then subsequent transformations occur to form an unknown species (Scheme 3-12).

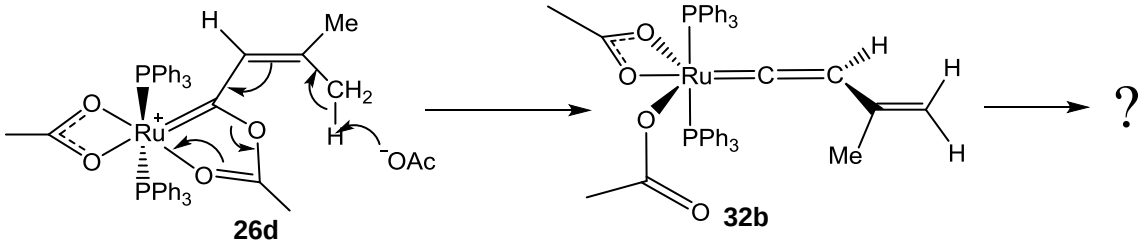

Scheme 3-12 Reaction of Complex **26d** with [NMe_4][OAc]

Vinyl vinylidene **32b** (resonance at δ 33.4 in the ^{31}P-NMR) is formed upon addition of tetramethylammonium acetate to complex **26d** (Figure 3-9 and Figure 3-10); however after two hours two more species were observed. An AB doublet of doublets (J_{pp} = 161.8 and 58.5 Hz) was observed at δ 33.1 in the ^{31}P-NMR (♦), presumably due to a short lived complex in which the two phosphine ligands are now inequivalent.

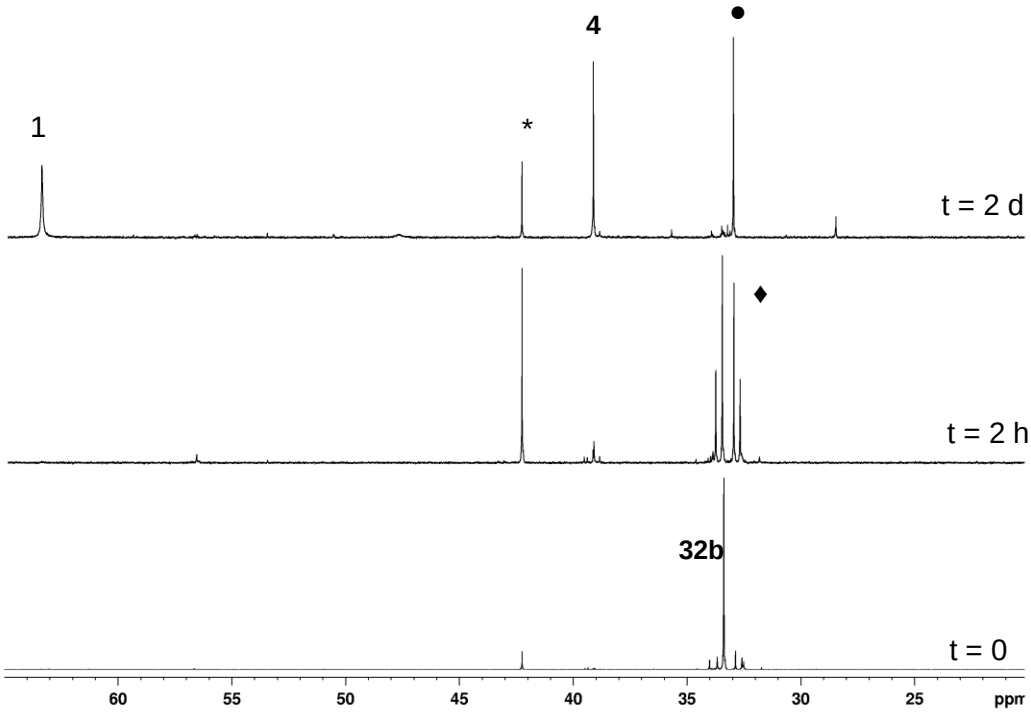

Figure 3-9 ^{31}P-NMR of the Reaction of Complex **26d** with [NMe_4][OAc] Over Time. Spectra Recorded After Addition (Bottom), After 2 Hours (Middle) and After 2 Days (Top).

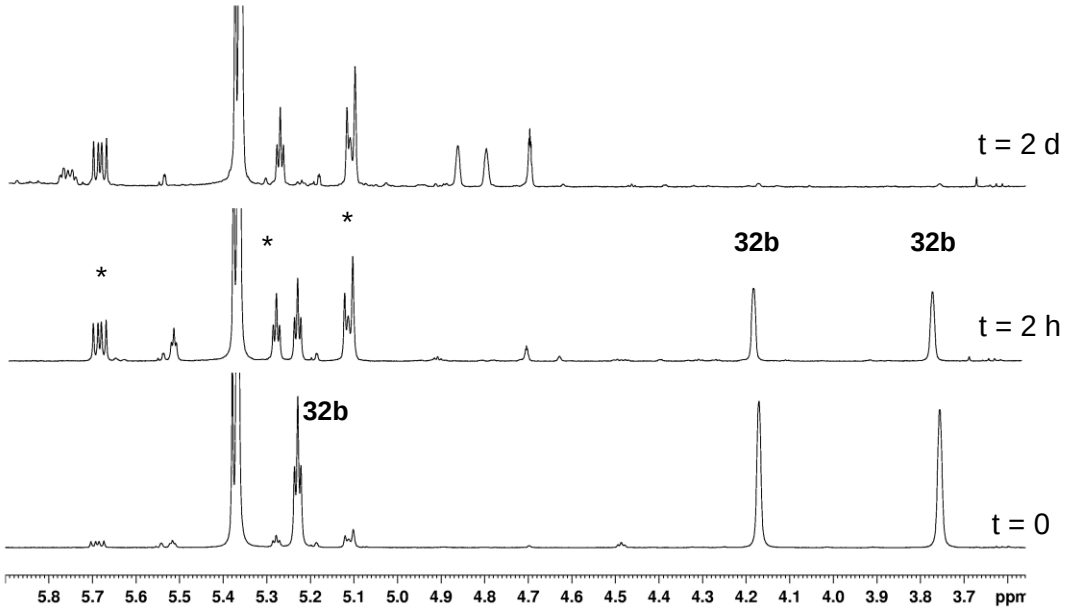

Figure 3-10 ^{1}H-NMR of the Reaction of Complex **26d** with [NMe_4][OAc] Over Time. Spectra Recorded After Addition (Bottom), After 2 Hours (Middle) and After 2 Days (Top).

Another unidentified species gave a singlet at δ 42.3 (indicated by a * in Figure 3-9 and Figure 3-10), a resonance that suggests the complex still possesses trans-phosphine ligands. This species also gave rise to proton resonances; a doublet of doublets at δ 5.69 (J_{HH} = 9.32, J_{HH} = 3.8) which integrates to one, a triplet at δ 5.28 (J_{PH} = 3.8 Hz, indicative coupling to *trans*-phosphine ligands) which also integrates to one proton, and a multiplet at δ 5.11 which integrates as two with the two protons being shown by HSQC to be bound to different carbon atoms (Figure 3-11 and Figure 3-12).

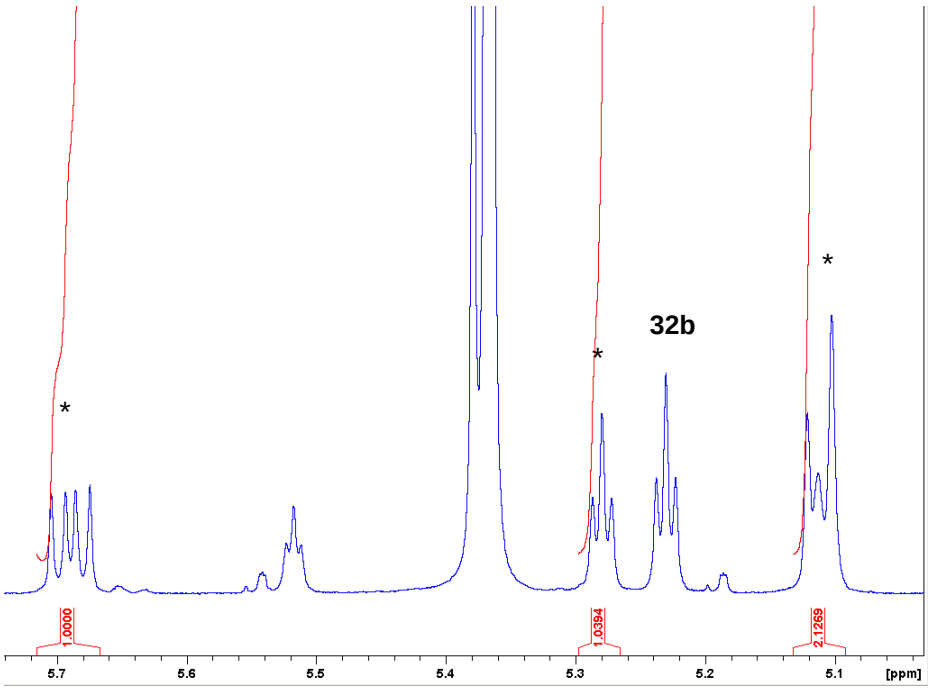

Figure 3-11 Detail of the ^{1}H-NMR Spectrum of the Reaction of **26d** with [NMe_4][OAc] (Scheme **3-12**) after 2 hours

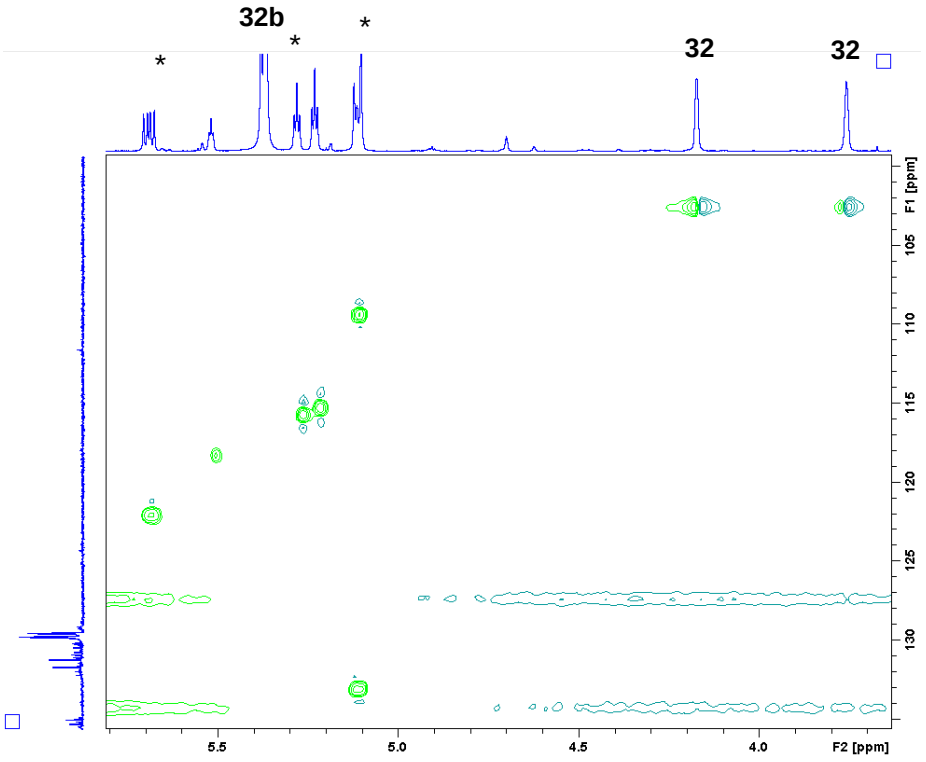

Figure 3-12 Detail of the HSQC Spectrum of Figure 3-8 after 2 hours

The resonances at δ 5.1 and 5.7 both show coupling to a resonance at δ 1.6 (which integrates to 2H) in the COSY spectrum. This resonance at δ 1.6 also displays cross-peaks in the HSQC to a resonance at δ 41.1 in the ^{13}C-NMR spectrum. This suggests that the complex has three alkene protons and two alkyl protons. If we assume that the unknown complex * has arisen from a rearrangement of the

vinylvinylidene ligand of **32b**, then the new organometallic ligand in * could reasonably consist of a C_5H_6 unit. An example would be an η^2-bound cyclopentadiene (CpH) ligand (Figure 3-13), however this structure does not match the data observed as it would be expected that both of the protons on the coordinated alkene would display phosphorus coupling.

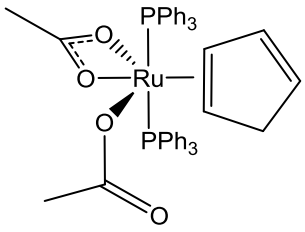

Figure 3-13 A Possible, but Unlikely Structure for Unknown Complex *

The ^{31}P-NMR spectrum of the final reaction mixture contains four species, bis-acetate complex **1a** (δ 63.5), the previously mentioned unknown species * (δ 42.3), carbonyl complex **4** (δ 39.1) and another unknown species at δ 32.9 (● in Figure 3-9). ESI-MS of this final reaction mixture was taken in which four ruthenium-containing peaks were observed. Only one could be identified and this was for complex **1a**.

3.4 Mechanistic Implications

3.4.1 Preamble

These deprotonation reactions to form allenylidene complex **30** and vinylvinylidene complexes **32** can also be viewed in terms of the Selegue mechanism.[139] Hydroxy vinylidenes are known to be intermediates in the formation of allenylidene complexes from propargylic alcohols.[139] The unusually stable hydroxy vinylidenes synthesised here have allowed the stepwise formation of an allenylidene (or vinylvinylidene) complex from *cis*-[Ru(κ^2-OAc)$_2$(PPh$_3$)$_2$] **1a** (Scheme 3-13). This has allowed an investigation into the mechanism of water elimination from hydroxy vinylidenes to form allenylidenes to be undertaken.

The first step in the potential mechanism is the abstraction of the hydroxy-substituent of the vinylidene using [CPh$_3$][BF$_4$] (Scheme 3-13). Ordinarily the unsaturated vinyl carbene ligand formed by this reaction would be highly unstable and would not be observed. However in this system the versatility of the acetate ligands allows the formation of a metallocyclic vinyl carbene ligand, therefore stabilising this reaction intermediate.

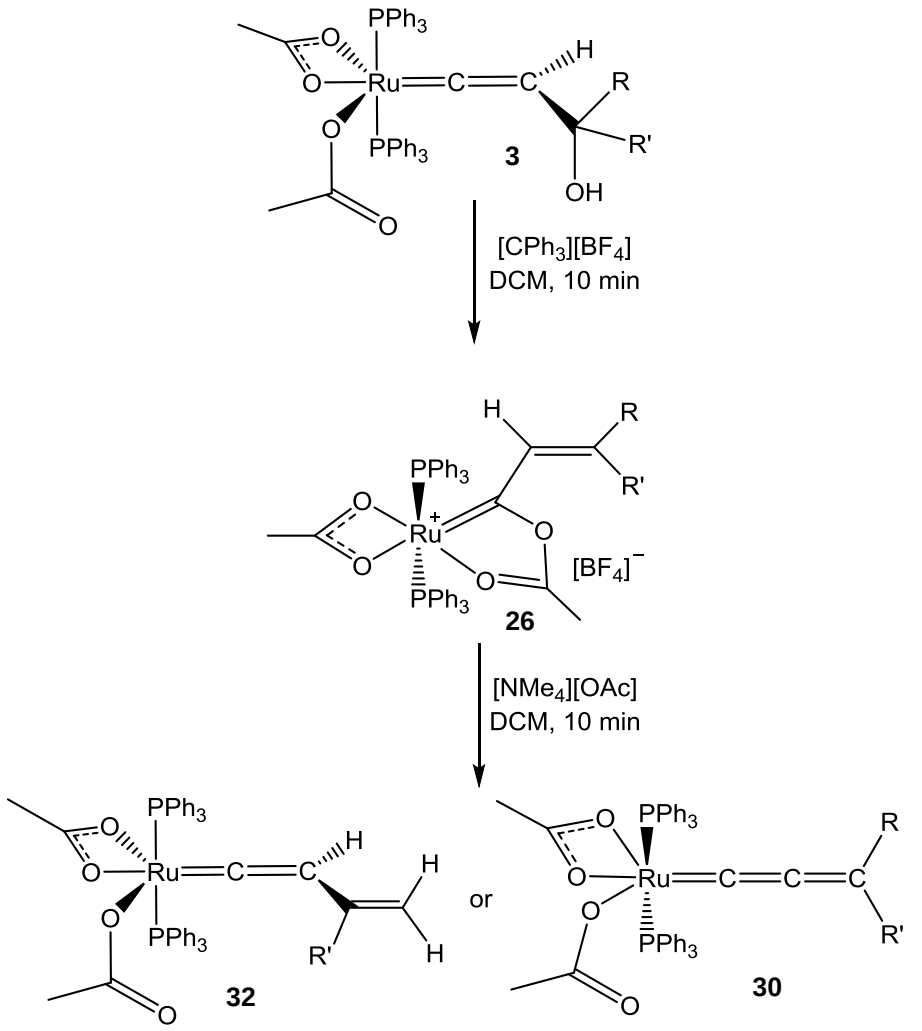

Scheme 3-13 Route for the Stepwise Formation of Allenylidene and Vinylvinylidene Complexes

This vinyl carbene must then be deprotonated to complete the elimination of water. The product formed by reaction with base is dependent on the nature of the substituents on the vinyl group (Scheme 3-13). If R and/or R' = methyl, deprotonation occurs at this position to form a vinylvinylidene complex. If no β-proton is present relative to the vinyl group then deprotonation occurs on the ligand backbone to form the allenylidene isomer.

3.4.2 Hydrogen Migration Pathway

This highly selective reactivity contrasts with the behaviour observed for many half-sandwich complexes where the allenylidene and vinylvinylidene isomers are often in equilibrium. For example, vinylidene and allenylidene complexes supported by the $[Ru(\eta^5\text{-}C_7H_9)(PPh_3)_2]^+$ fragment have been found to be in equilibrium and theoretical studies (carried out at the MP2/DZV(d,p)+*G* level) by Cadierno et al. have shown that a hydrogen migration pathway (Scheme 3-14) is accessible for the interconversion (though it is relatively high in energy).[134] It was decided to carry out a theoretical

investigation, using density functional theory (DFT), into the selectivity in order to elucidate the reasons for the lack of interconversion.

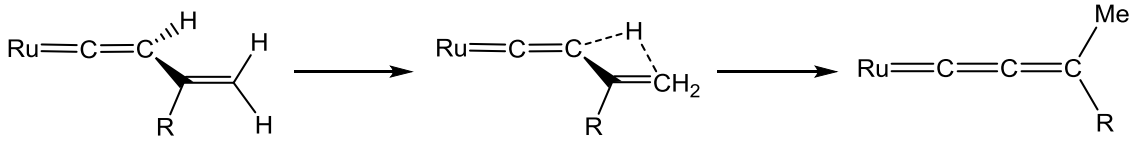

Scheme 3-14 Hydrogen Migration Pathway for the Interconversion of Vinylvinylidene and Allenylidene Ligands

Calculations were carried out by Dr Jason Lynam to investigate the relative energies of the vinylvinylidene **32b**, allenylidene **30b** and metalloenol ester **33** isomers (

Figure 3-14). Calculations were performed with the Turbomole program; initial geometry optimisations and frequency calculations were performed at the BP86/SV(P) level and subsequent single point energies at pbe0/def2-TZVPP.[211-220]

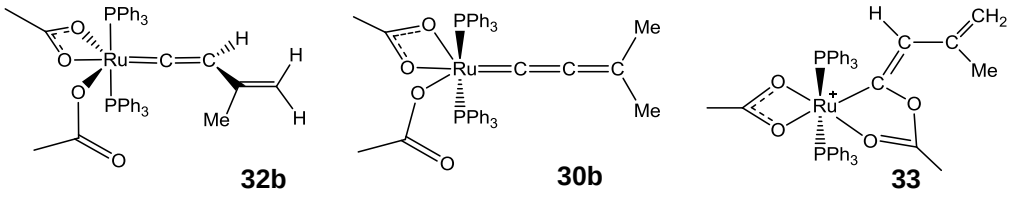

32b **30b** **33**

ΔG_{298K} (bp86/SVP)	+0 kJ mol^{-1}	+7 kJ mol^{-1}	+14 kJ mol^{-1}
ΔE (pbe0/def2-TZVPP)	+0 kJ mol^{-1}	+20 kJ mol^{-1}	+1 kJ mol^{-1}
	+0 kJ mol^{-1}		

Figure 3-14 Isomers of **32b** Investigated by DFT. The Energies are Shown Relative to Complex **32b** which is Set to Zero

Various isomers of the three structures were examined and the isomer of **32b** shown in

Figure 3-14 was found to be global minimum at all levels of theory used. Notably the relative energies of **30b** and **33** were found to vary depending on the level of theory used. The isomers of allenylidene **30b** were found to be lower in energy at the BP86/SV(P) level whereas the metalloenol ester **33** was found to be the lower in energy at the pbe0/def2-TZVPP level. The fact that these isomers all have similar energies suggests that the formation of vinylvinylidene complexes over allenylidene

ligands is kinetically driven. It is therefore surprising that no exchange is observed between the two species experimentally.

The hydrogen migration pathway mentioned previously in relation to the $[Ru(\eta^5\text{-}C_7H_9)(PPh_3)_2]^+$ fragment was then investigated for this *cis*-$[Ru(\kappa^2\text{-}OAc)_2(PPh_3)_2]$ system. When the crucial transition state was located it was found to have a relative free energy at 298 K of 264 kJ mol^{-1} (at the pbe0/def2-TZVPP level), which is far too high an energy barrier for the migration to occur at ambient conditions (Figure 3-15).[134]

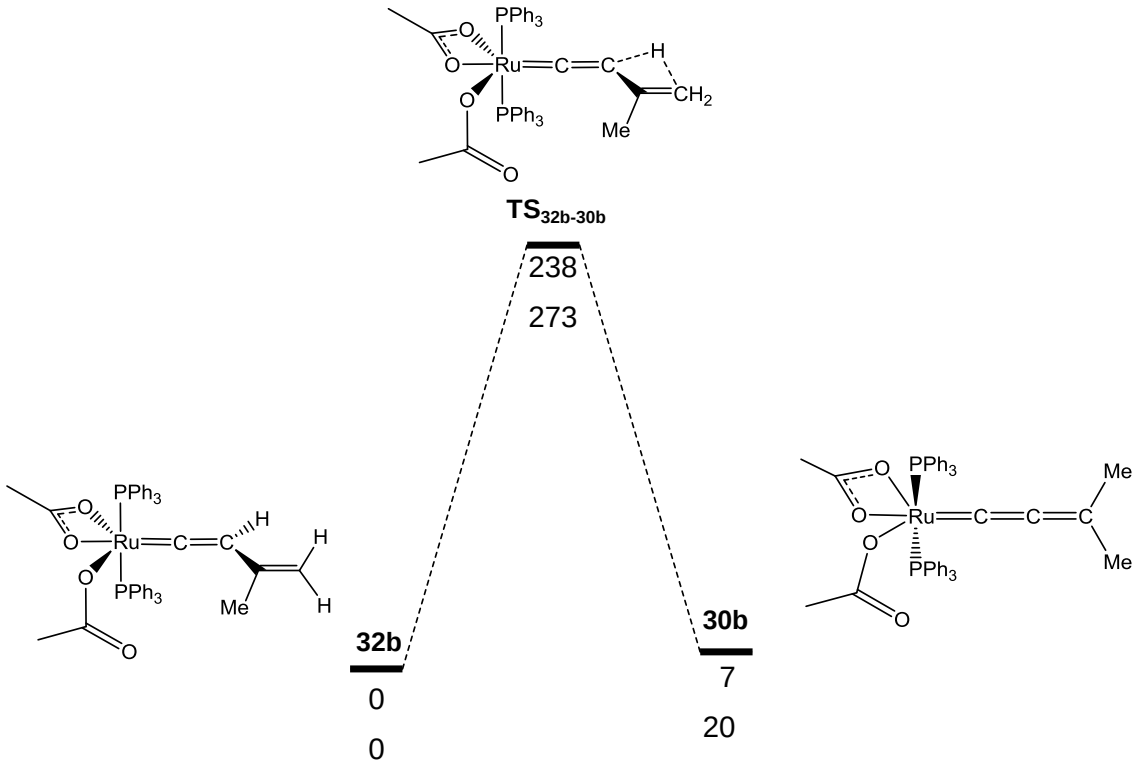

Figure 3-15 Potential Energy Surface for the Interconversion of **32b** and **30b** via **TS$_{32b\text{-}30b}$**. Energies relative to **32b** are given in kJ mol^{-1} for ΔG_{298K} at the bp86/SVP level (top), ΔE at the pbe0/def2-TZVPP level (middle) and ΔG_{298K} at the pbe0/def2-TZVPP level (bottom).

This is similar to the +288 kJ mol^{-1} barrier reported by Gimeno, who noted that this barrier was high for rapid room temperature conversion.[134] Therefore, the energy of this transition state cannot explain the difference in reactivity observed between the two systems, with rapid equilibrium between the allenylidene and vinylvinylidene isomers observed in the $[Ru(\eta^5\text{-}C_7H_9)(PPh_3)_2]^+$ system, but not in the case of $[Ru(\kappa^2\text{-}OAc)_2(PPh_3)_2]$ **1a**.

3.4.3 Via an Intermediate Alkynyl Species

As a result of this, an alternative mechanistic explanation for the difference in behaviour was sought. Deprotonation of either the allenylidene or the vinylvinylidene

would lead to a common alkynyl intermediate **34** which could then be re-protonated to form either complex (Scheme 3-15). This alkynyl species has already been observed by treatment of equilibrium mixtures of the cationic half sandwich allenylidene **37** and vinylvinylidene **35** with base. Addition of acid then reforms the equilibrium mixture showing that this process is reversible.[134] It is possible to probe this pathway by calculating the energy barriers involved in the deprotonation. Therefore a difference in pK_a values between the two systems could explain their observed reactivity differences.

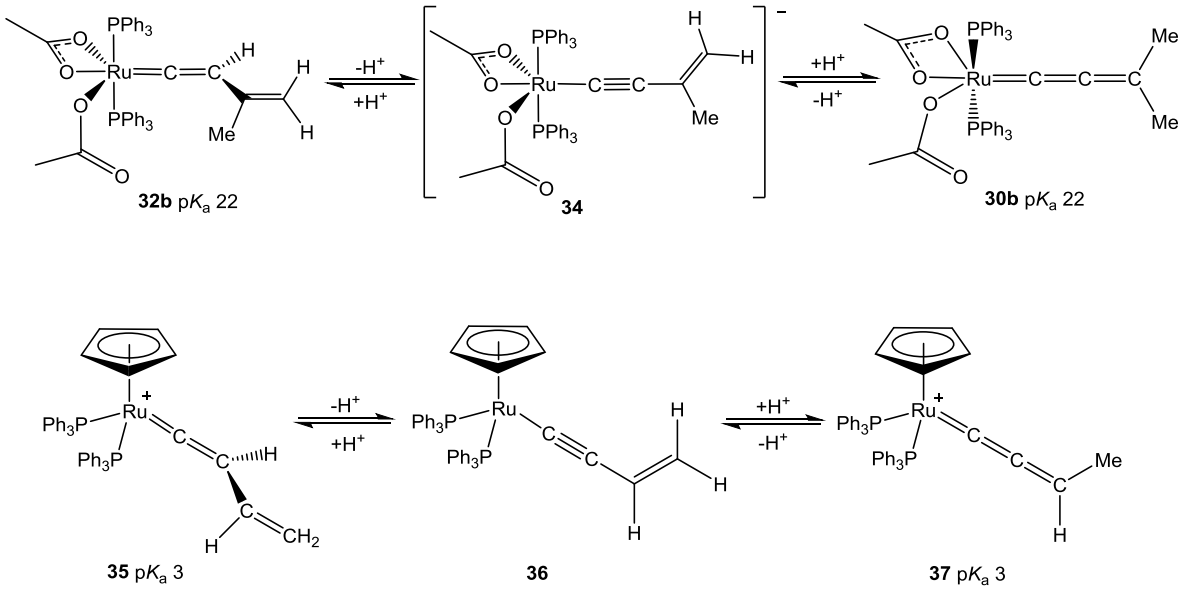

Scheme 3-15 Interconversion of Vinylvinylidene and Allenylidene Complexes via an Alkynyl Species. Relevant pK_a Values are Shown

The pK_a values for the allenylidene and vinylvinylidene isomers of the two systems in methanol were calculated using the alkynyl complex as the conjugate base in all cases.[221-224] These showed that the cationic species **35** and **37** are far more acidic (pK_a 3) than the neutral species **30b** and **32b** (pK_a 22) (Scheme 3-15). Whilst this does not give any information on the rate of proton transfer, it does give an indication that the process would be more favourable for the cationic system. This mechanism therefore does discriminate between the two systems and can be considered as a viable alternative to the proton migration pathway discussed earlier.

3.5 Conclusion

In this chapter is has been demonstrated that vinyl carbene complexes **26** can be synthesised from hydroxy-vinylidene complexes and tritylcarbenium tetrafluoroborate. Their relevance to the mechanism shown in Scheme 2-15 for the decarbonylation of hydroxy vinylidene complexes to form geminal alkenes and carbonyl complex **4** was investigated. No reaction was observed with one equivalent of a selection of nucleophiles. A stoichiometric amount of nucleophile is considerably more than would

be present in the decarbonylation reaction mixture, therefore suggesting that this complex is not a relevant intermediate in this mechanism.

However, reaction did occur with bases and deprotonation of vinyl carbene **26** leads to the formation of either allenylidene or vinylvinylidene complexes. The product obtained depends on the substituents on the vinyl moiety, with vinylvinylidene complexes being formed when protons are present on the δ-carbon of the ligand chain. These products suggest that vinyl carbenes such as **26** could be relevant reaction intermediates in the dehydration of hydroxy vinylidenes to form allenylidenes. The presence of acetate ligands has allowed the stabilisation of these intermediates in metallocyclic form.

A theoretical investigation into this mechanism was carried out using DFT. It was found that all of the isomers studied had very similar Gibbs free energies. As a result it is suggested that the formation of vinylvinylidene complexes rather than allenylidenes in the case of methyl substituted vinyl carbenes (**26c** and **26d**) is a kinetic effect. Despite these low energy differences no interconversion was observed experimentally between the two forms. The hydrogen migration pathway proposed by Gimeno[134] was investigated for this system and the transition state was found to provide a very high barrier (ΔG_{298K} = 264 kJ mol^{-1}) to interconversion. An alternative deprotonation mechanism to interconversion, via an alkynyl intermediate **34** was investigated. The pK_a of complex **26** was calculated to be 22 (compared to a pK_a of 3 for Gimeno's cationic species) which could explain the lack of interconversion between the allenylidene **30** and vinylvinylidene **32** isomers in this system.

4. Phosphine-Substituted C_3 Organometallic Species

4.1 Introduction

In Chapter 3, the synthesis and reactivity of substituted vinyl carbene complexes **26** was outlined. These could be isolated in high yield from the reaction of hydroxy vinylidene **3** with a Lewis acid such as trityl carbenium tetrafluoroborate, followed by crystallisation via the diffusion of diethyl ether into a DCM solution containing the complex (Scheme 4-1).[225]

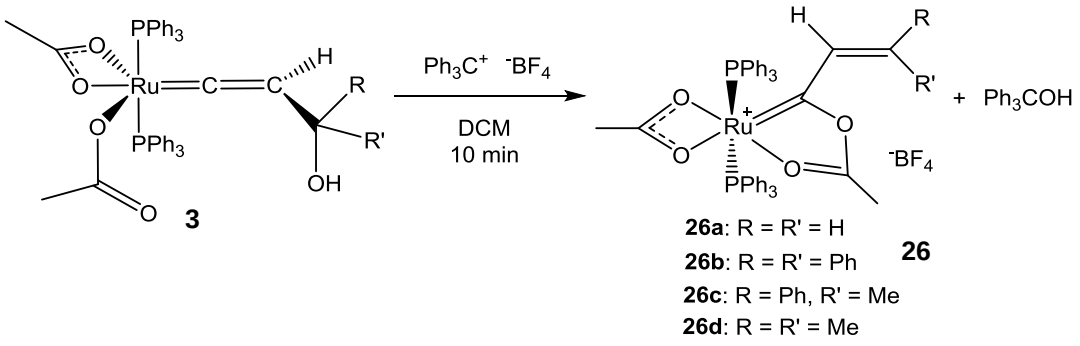

Scheme 4-1 Synthesis of [Ru(κ^2-OAc)(OC{Me}OCC{H}=CRR')(PPh_3)$_2$][BF_4] **26**

In this chapter the synthesis of the unsubstituted analogue **26a** will be discussed. Although this complex proved too reactive to isolate, some interesting products were observed in the reaction mixtures which prompted a study into a number of phosphine-substituted species.

4.2 Synthesis of Unsubstituted Vinyl Carbene 26a

4.2.1 Synthesis of Complex 26a

Following the successful synthesis of methyl- and phenyl-substituted carbene complexes **26b-d** attempts were made to isolate the unsubstituted analogue **26a** (Scheme 4-2).

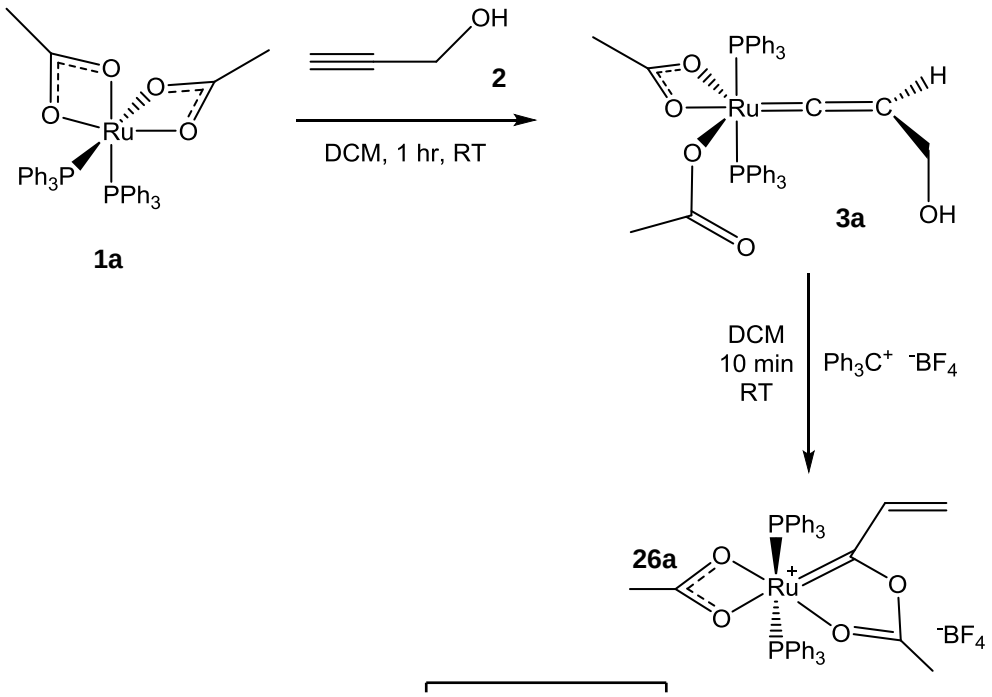

Scheme 4-2 Attempted Synthesis of [Ru(κ^2-OAc)(OC{Me}OCC{H}=CMe_2)(PPh_3)$_2$][BF_4] **26a**

Formation of vinylidene **3a** via the literature method[170] proved simple, however the subsequent dehydroxylation with tritylcarbenium tetrafluoroborate to form **26a** failed to produce one isolable product and evidence for many products were observed in the NMR spectra (some examples are shown below). Some of these products have been characterised, though the ratios (and sometimes the identity) of products varied with the length of time between addition of the tritylcarbenium tetrafluoroborate and obtaining NMR spectra.

As these synthetic studies indicated that the final product was too reactive to isolate at room temperature, the tritylcarbenium salt was added to a thawing DCM solution of **3a**. The sample was then warmed to room temperature and placed directly into a NMR spectrometer. This allowed resonances for the desired product **26a** to be observed as the major product. For example, in the ^{1}H-NMR spectrum (designated by × in the NMR spectra shown in Figure 4-1), doublets for the geminal protons on the vinyl group were observed at δ 6.32 (d, $^3J_{HH}$ = 11.0 Hz) and δ 6.50 (d, $^3J_{HH}$ = 17.3 Hz) with both displaying a cross-peak in the COSY spectrum to another proton in the aromatic region. The methyl resonances for the two acetate groups were observed at δ 0.82 and δ 1.86 and the PPh_3 groups as one singlet in the ^{31}P-NMR at δ 31.1 (× in Figure 4-2).

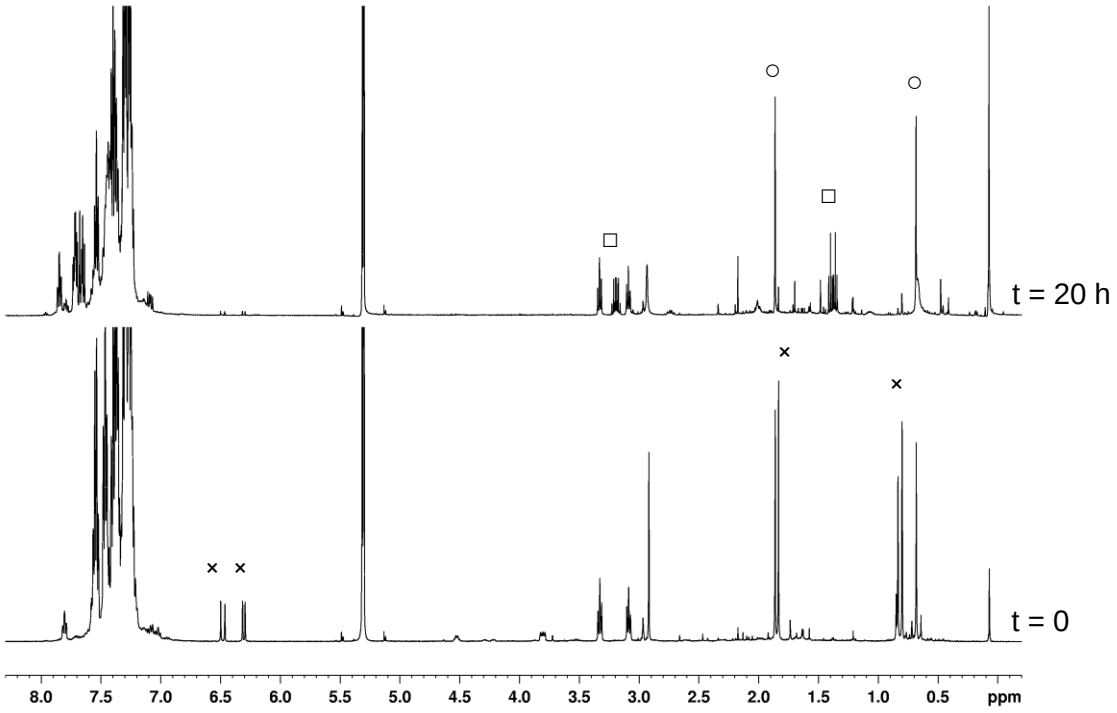

Figure 4-1 ^{1}H-NMR Showing Formation of **26a** (×), **41** (○) and **43** (□), Showing the Short Lived Nature of **26a**. Bottom Spectrum is of the Initial Sample, the Top Spectrum the Same Sample 20 Hours Later

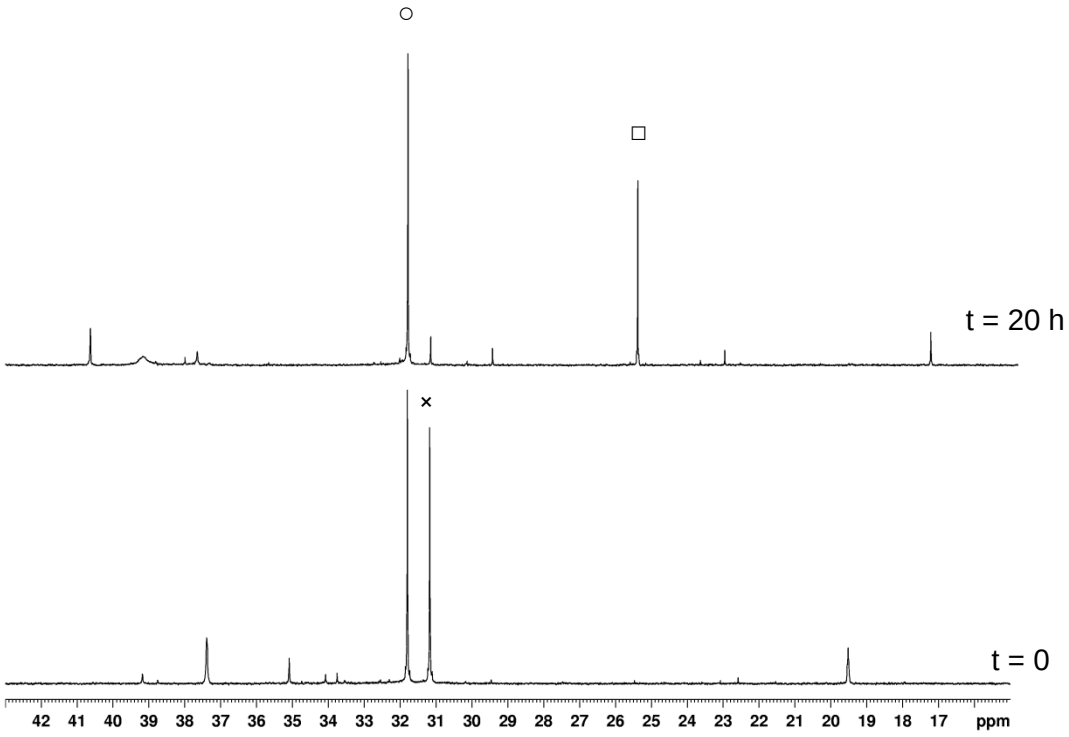

Figure 4-2 ^{31}P-NMR Showing Formation of **26a** (×), **41** (○) and **43** (□). Bottom Spectrum is of the Initial Sample, the Top Spectrum the Same Sample 20 Hours Later

4.2.2 Discussion of the Products

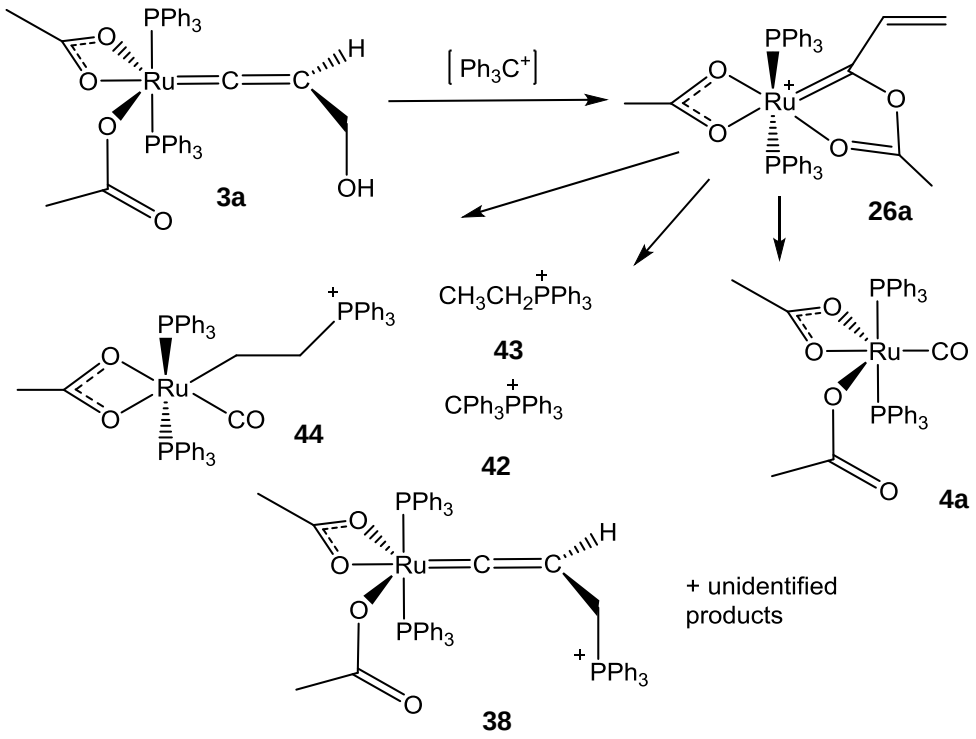

Scheme 4-3 Formation of Vinyl Carbene **26a** and the Products Formed via its Decomposition

In the reactions to form **26a** cooled by liquid nitrogen other species were observed (Scheme 4-3) and **26a** was not long lived (Figure 4-1 and Figure 4-2). One of the major products **41** (^{31}P-NMR = δ 31.8, ^{1}H-NMR = δ 0.69 and 1.86, ○ in Figure 4-2) has yet to be identified, however carbonyl complex **4a** (^{31}P-NMR = δ 39.1) was often observed (particularly when no cooling was used).

It was postulated that the resonance observed at δ 24.4 (ǂ in Figure 4-5) in the ^{31}P-NMR spectrum could be due to [Ph_3C-PPh_3][BF_4] **42** formed by reaction of the trityl salt with free phosphine. Whilst this compound is present in the literature[226] it has not been fully characterised and so it was decided to synthesise it independently in order to confirm its presence. Tritylcarbenium tetrafluoroborate was added to a DCM solution of triphenylphosphine After 5 minutes stirring at room temperature the product was precipitated with pentane and the solvent removed by filtration to give [Ph_3C-PPh_3][BF_4] **42** as a white solid. Formation of **42** was confirmed by observation of phosphorus couplings throughout the ^{1}H and ^{13}C-NMR spectra and crucially the ^{31}P-NMR resonance was observed at δ 24.4. Crystals suitable for X-ray diffraction were grown by the slow diffusion of pentane into a DCM solution of **42** (Figure 4-3). The structure was of low quality due to disordered solvent molecules, but does show the successful synthesis of **42**.

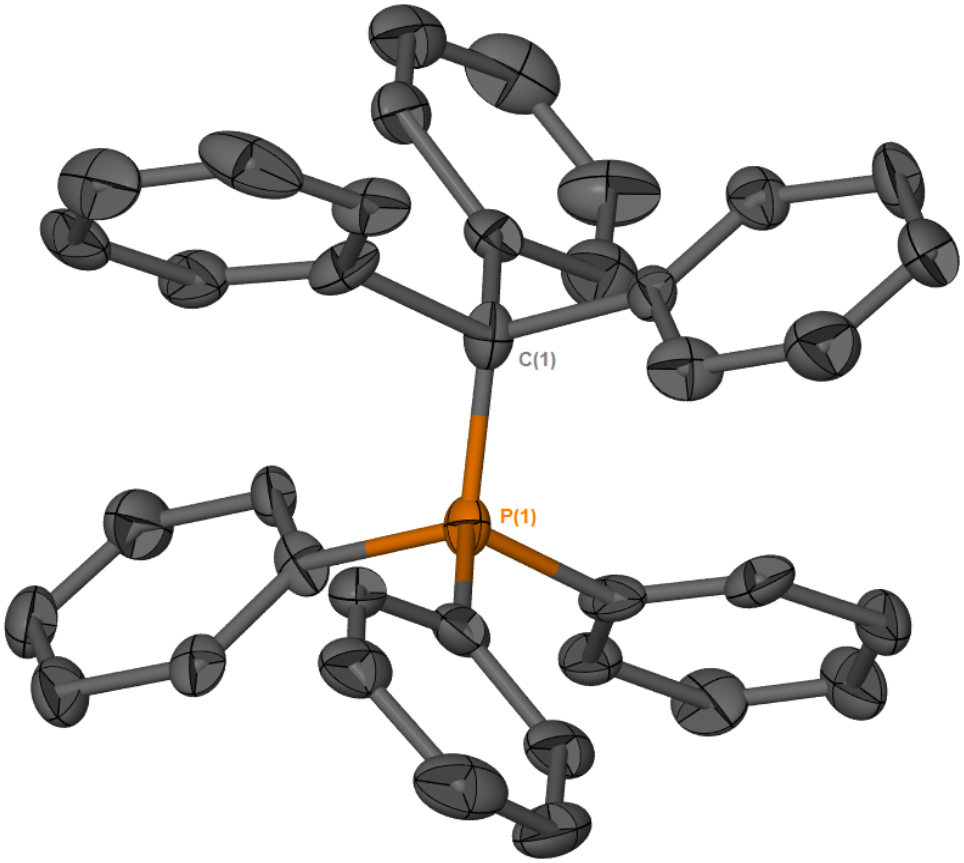

Figure 4-3 ORTEP Representation of Complex **42**; Thermal Ellipsoids are at 50% Probability, Hydrogen Atoms, $[BF_4]^-$ Counter Ions and Solvent Molecules have been Omitted for Clarity. C(1) and P(1) were Found to have ca. 50% Occupancy in Each Position, Only one Orientation is Shown.

Another of the products observed in the ^{31}P-NMR spectra (singlet at δ 25.5, □ in Figure 4-2), ^{1}H-NMR (multiplets at δ 3.20 and 1.38 due to the ethyl group (□ in Figure 4-1), was the triphenylethylphosphonium ion **43** (Scheme 4-3). The assignment was confirmed by comparison with an authentic sample and MS data (peak at *m/z* = 291 in ESI).

Whilst the exact mechanism of formation of **43** is unknown, evidence for the vinylidene $[Ru(\kappa^2\text{-}OAc)(\kappa^1\text{-}OAc)(PPh_3)_2(=C=CH\text{-}CH_2\text{-}PPh_3)]^+$ **38** (Scheme 4-3) was obtained in the by NMR and MS. In the ^{31}P-NMR spectra a triplet at δ 19.5 and doublet at δ 37.3 (J_{PP} = 3.9 Hz) were observed, (shown by ▲ in Figure 4-5), and in the ^{1}H-NMR spectrum a 2H multiplet at δ 3.86 and a 1H multiplet at δ 4.61 (shown by▲ in Figure 4-4). ESI MS of the reaction mixture showed a peak at *m/z* 1045.227 corresponding to the molecular ion.

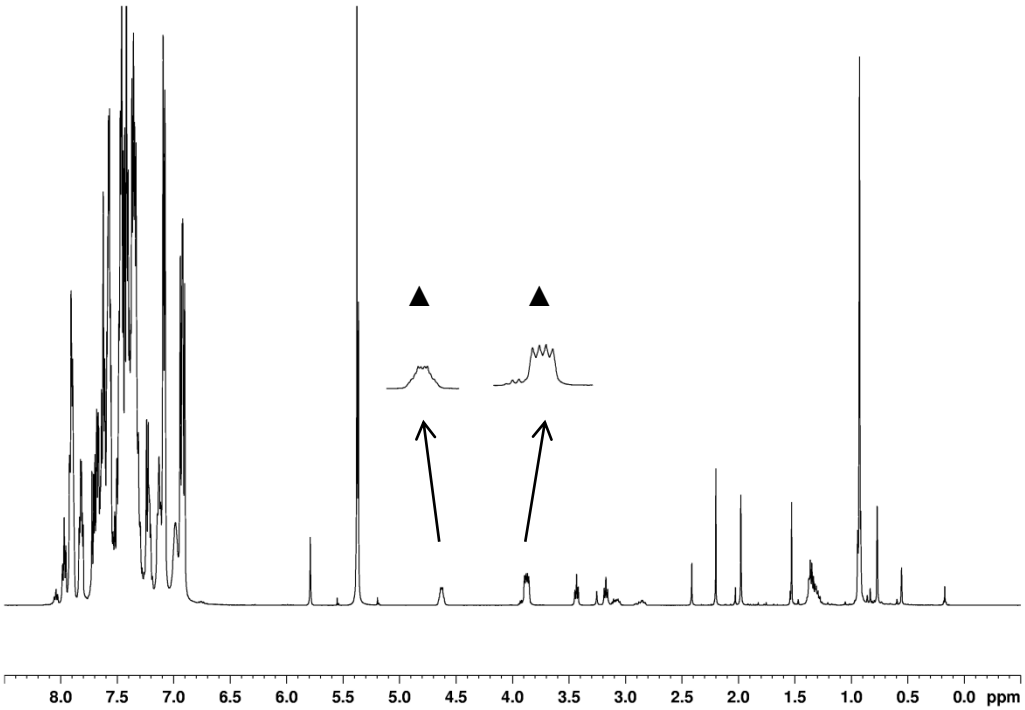

Figure 4-4 ^{1}H-NMR Showing Formation of Vinylidene **38** (▲)

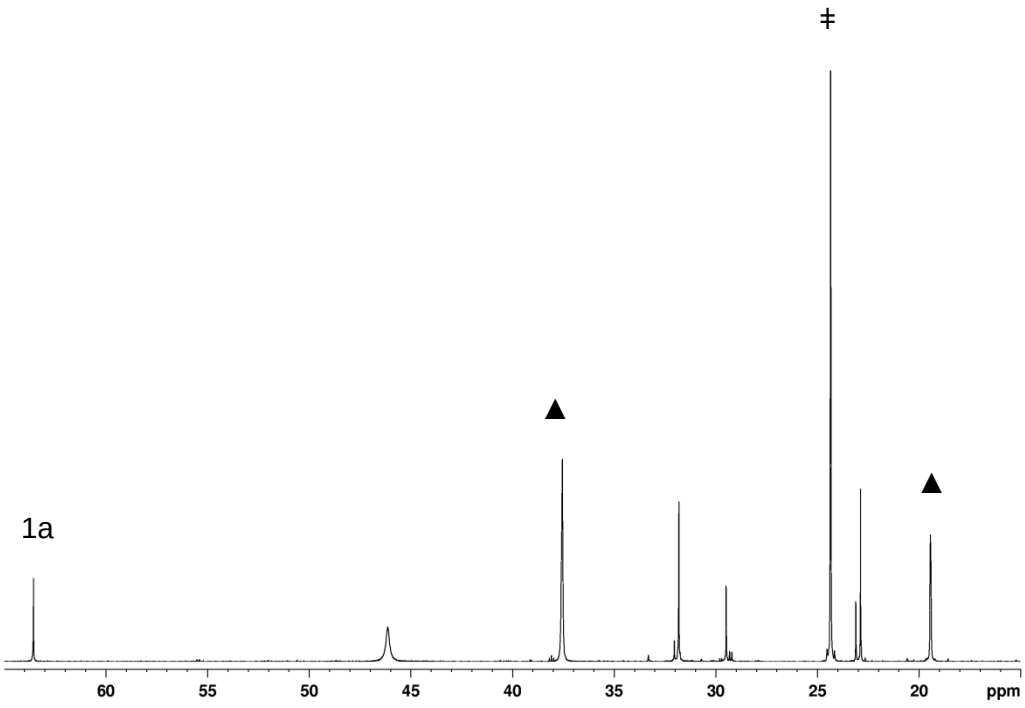

Figure 4-5 ^{31}P-NMR Showing Formation of **38** (▲) and **42** (‡)

On one occasion crystals of the phosphino-ethyl complex **44** were isolated and a crystal structure obtained (Figure 4-6). Further evidence for the formation of **44** was obtained in the ESI-MS spectrum I which a small peak was observed at *m/z* 1003.2166

corresponding to the molecular mass, but no evidence for **44** was observed in the NMR spectra. The crystal structure showed the presence of a carbonyl ligand alongside κ^2-OAc ligand and two *trans*-orientated PPh_3 ligands. Interestingly, it also shows a phosphino-ethyl ligand with the single bond character shown by the long Ru-C and C-C bonds (Ru-C(1) = 2.112(4) Å, C(1)-C(2) = 1.517(6) Å)).

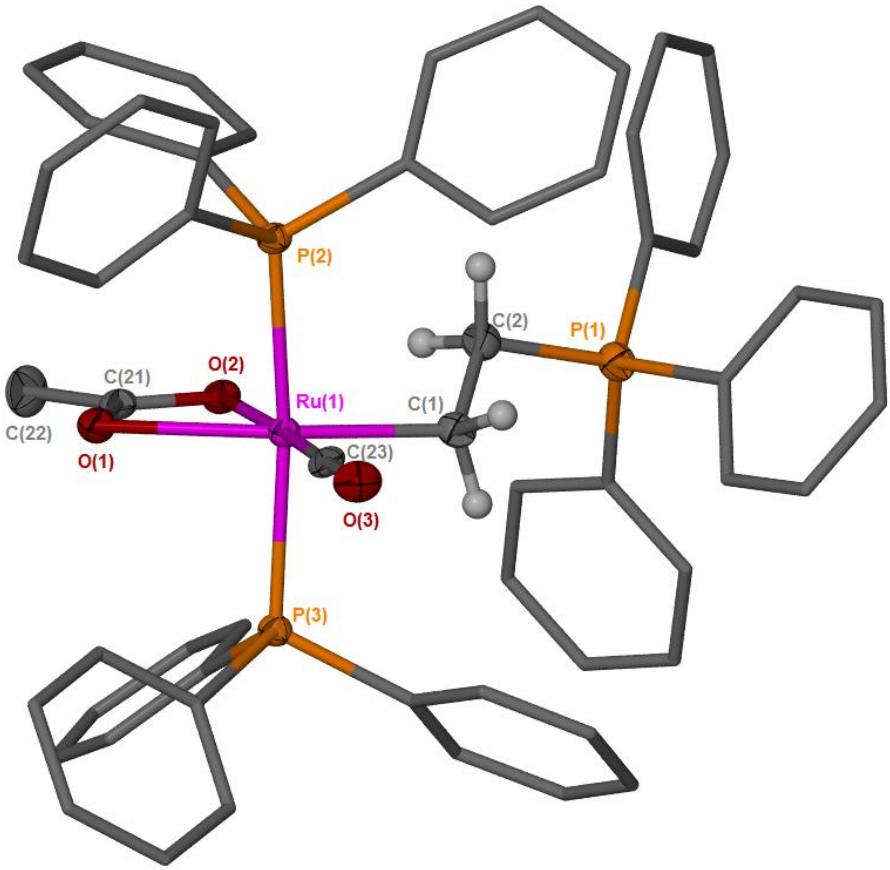

Figure 4-6 ORTEP Representation of Complex **44**; Thermal Ellipsoids, where shown, are at 50% Probability, Hydrogen Atoms and BF_4 Counter Ion have been Omitted for Clarity.

Table 4-1 Selected Bond Lengths and Angles for Complex **44**

Bond	Bond Length (Å)	Angle	Bond Angle (°)
C(1) – Ru	2.112(4)	C(1) – Ru – O(1)	154.14(14)
C(1) – C(2)	1.517(6)	C(1) – Ru – O(2)	95.10(14)
C(2) – P(1)	1.813(4)	C(1) – Ru – C(23)	89.08(17)
O(1) – Ru	2.267(3)	C(1) – Ru – P(3)	90.90(12)
O(2) – Ru	2.166(3)	C(1) – Ru – P(2)	95.68(12)
C(23) – Ru	1.814(4)	O(1) – Ru – O(2)	59.16(11)
C(23) – O(3)	1.167(5)	C(23) – Ru – O(1)	116.67(15)
P(3) – Ru	2.3724(11)	C(23) – Ru – O(2)	175.82(15)
P(2) – Ru	2.3608(11)	O(1) – Ru – P(2)	87.74(7)
		O(2) – Ru – P(2)	90.74(8)
		C(23) – Ru – P(2)	88.75(13)
		P(3) – Ru – P(2)	172.64(4)
		C(2) – C(1) – Ru	112.4(3)
		P(1) – C(2) – C(1)	113.0(3)
		Ru – C(23) – O(3)	177.7(4)

Esteruelas has observed a similar reaction with the addition of P^iPr_3 to an ethene ligand to form a phosphino-ethyl ligand (Scheme 4-4). This complex was found to be unstable over time and formation of triisopropylethylphosphonium was observed.[227]

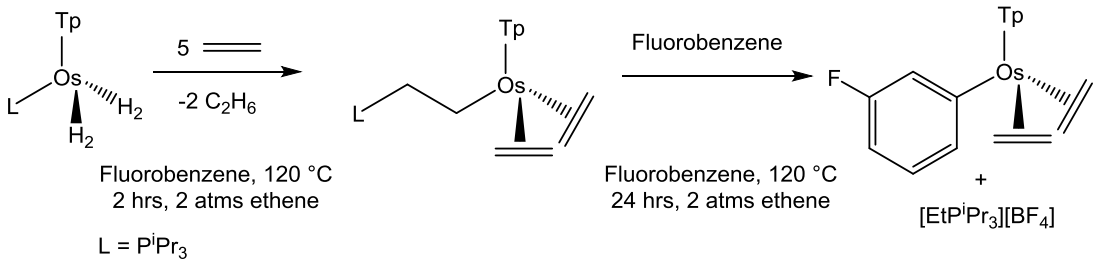

Scheme 4-4 Observation of the Formation of Ethyl Phosphonium Species from Phosphino-Ethyl a Complex

The observation of complex **44** offers some explanation towards the formation of triphenylethylphosphonium **43**. The formation of these two species and vinylidene **38,** suggests that any free triphenylphosphine being formed in the reaction mixture is being scavenged by complex **26a**. That these product types are not observed in reactions involving the substituted analogues of **26** suggests that the phenyl and methyl substituents are providing steric protection which prevents attack of PPh_3 at the vinyl moiety.

In order to test this theory and to observe any potential reaction selectively, an extra equivalent of triphenylphosphine was added to the reaction of **3a** with tritylcarbenium tetrafluoroborate whilst it was still cold. The major product was found to be *cis*-[Ru(κ^2-OAc)$_2$(PPh_3)$_2$] **1a**, and whilst evidence for [Ru(κ^2-OAc)(κ^1-OAc)(PPh_3)$_2$(=C=CH-CH_2-PPh_3)]$^+$ **38** was observed in the NMR spectra, numerous other products were also formed.

It was therefore decided to synthesise the PPh_3-substituted vinylidene **38** independently as this would enable confirmation of the assignment, and as far as we are aware that no phosphorus-substituted vinylidenes have previously been reported.

4.3 Reaction of 1a with Triphenylpropargylphosphonium

4.3.1 Background

In order to ascertain whether [Ru(κ^2-OAc)(κ^1-OAc)(PPh_3)$_2$(=C=CH-CH_2-PPh_3)]$^+$ **38** is being formed in the reaction of hydroxy-vinylidene **3a** with trityl carbenium tetrafluoroborate (Section 4.2.2) it was decided to synthesise **38** independently. A synthetic route involving the reaction of **1a** with the commercially available alkyne [HC≡CCH_2PPh_3][Br] **39a** was envisaged (Scheme 4-5).

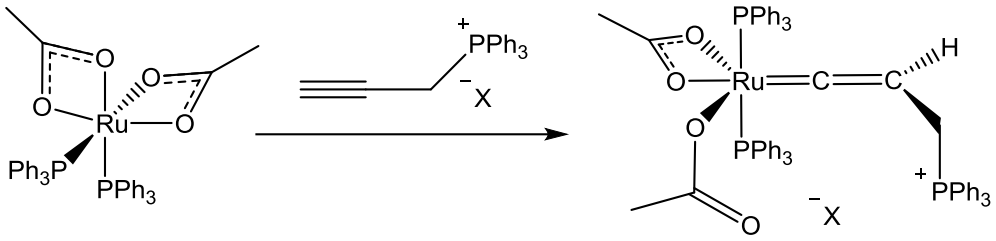

Scheme 4-5 Proposed Synthesis of Phosphino-Vinylidene **38**

There have been a number of other examples where **39a** has been used as a precursor for organometallic complexes. In the reactions documented it has been found that a propargylic rearrangement readily occurs to give the allene complexes and Hill's group have reported ruthenium[31] and platinum[32] allene complexes synthesised directly from **39a** (Scheme 4-6).

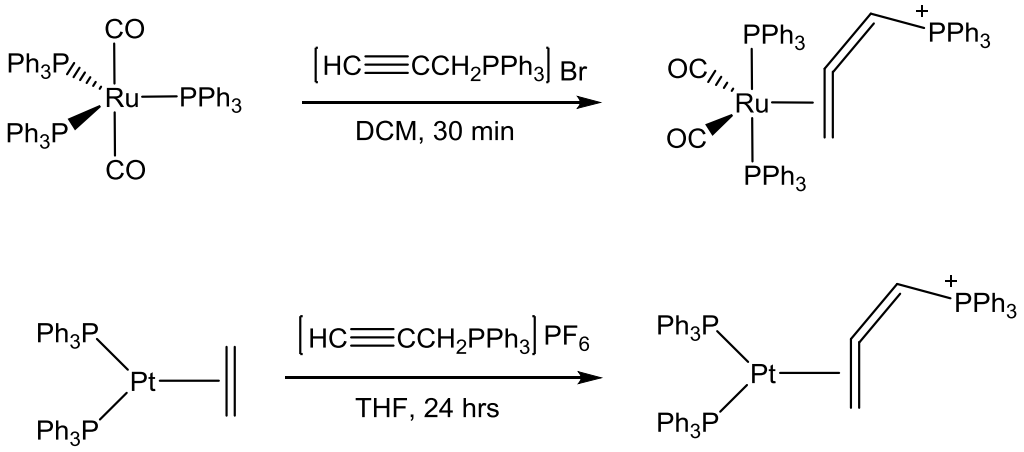

Scheme 4-6 Phosphino-Allenes from the Literature

4.3.2 Synthesis of an Allene Complex

As it was anticipated that the bromide anion in **39a** might exchange with the acetate ligands of *cis*-[Ru(κ^2-OAc)$_2$(PPh$_3$)$_2$] **1a**, a counter-ion exchange was carried out in order to introduce a more weakly coordinating anion. [HC≡CCH$_2$PPh$_3$][Br] **39a** and silver tetrafluoroborate were stirred in DCM for 5 minutes before filtration into a DCM solution of **1a** (it was found that the sodium salt did not give rise to metathesis). After **1a** and **39a** at stirring at room temperature for 15 minutes, and washing with pentane, one product was obtained. As in Hill's case it was found to be the allene complex **45a** that had been formed, presumably by isomerisation of the alkyne to the allene form (Scheme 4-7).

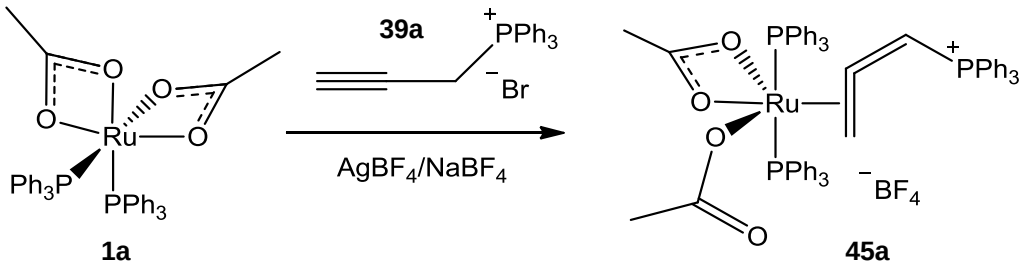

1a **45a**

Scheme 4-7 Reaction of *cis*-[Ru(κ^2-OAc)$_2$(PPh$_3$)$_2$] **1a** with Triphenylpropargylphosphonium Tetrafluoroborate **39b**

The ^{1}H-NMR spectrum of **45a** was found to be diagnostic with resonances at δ 2.81 (m, 2H, CH$_2$) and 6.46 (ad, J_{PH} = 23.6 Hz, 1H, CH) for the protons of the allene ligand. This large phosphorus coupling shows that in fact it is the CH group that is closest to the single PPh$_3$, not the CH$_2$ as it would be in vinylidene isomer **38**.The most downfield resonance observed in the ^{13}C-NMR spectrum was the quaternary allene carbon at δ 218.7 with the CH$_2$ at δ 27.3 and the CH observed as a doublet at δ 86.5 ($^2J_{PC}$ = 88.5 Hz). In the ^{31}P-NMR spectrum the ligand-based PPh$_3$ was observed as a triplet at δ 13.8 ($^4J_{PP}$ = 3.0 Hz), and the metal-based PPh$_3$ ligands as a doublet at δ 29.1 ($^4J_{PP}$ =

3.0 Hz). A peak was also observed at *m/z* 1045.2290 in the ESI-MS corresponding to the molecular ion.

Crystals were grown by the slow diffusion of pentane into a DCM solution of complex **45a**. If the crystals were analysed less than 24 hours after the crystallisation was set up then allene complex **45a** was observed with a small amount (~8%) of exchange between the κ^1-acetate ligand and bromide to give complex **45a'** (Figure 4-7). Further evidence for this bromide exchange was observed in the CHN elemental analysis results which suggested that 0.7% of the sample consisted of the Br containing complex ($C_{61}H_{54}BF_4O_4P_3Ru$ • 0.7 $C_{59}H_{51}BBrF_4O_2P_3Ru$, (calc) C 63.37, H 4.66; (found) C 63.36, H 4.69).

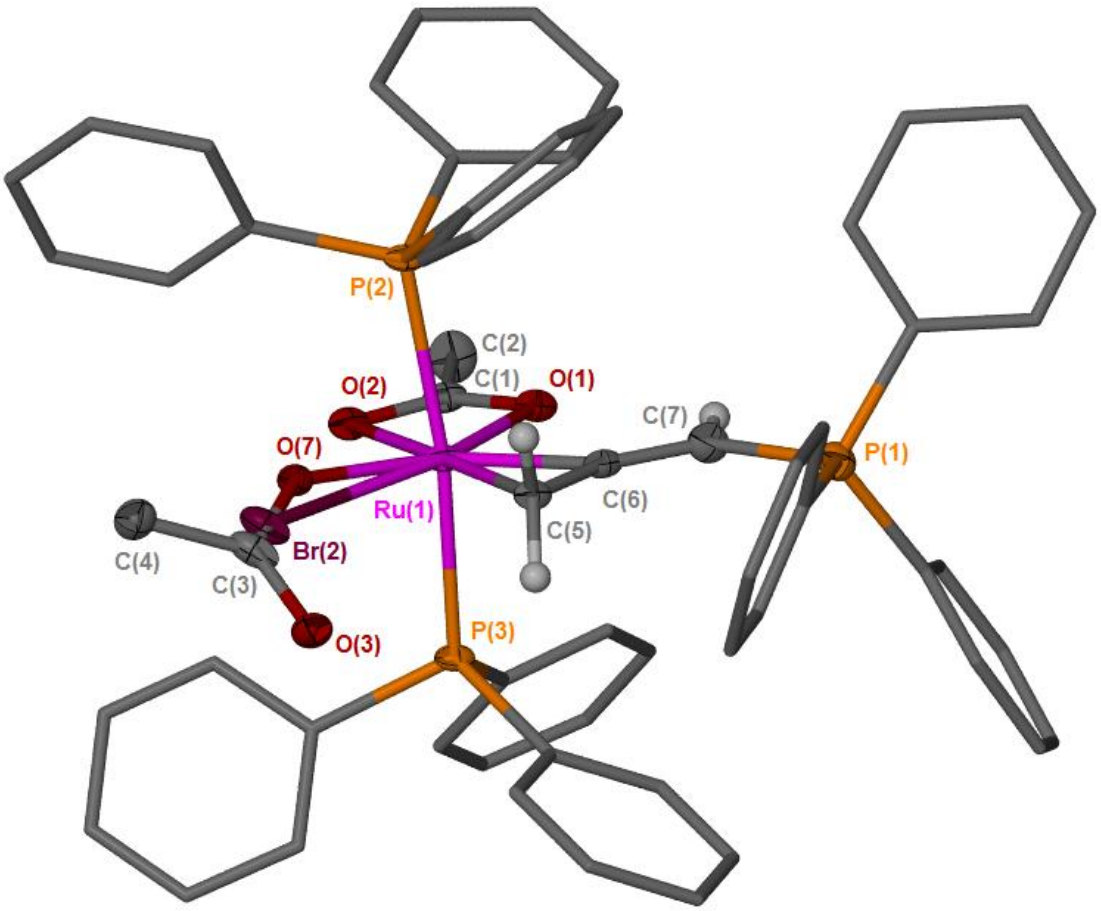

Figure 4-7 ORTEP Representation of Compounds **45a** and **45a'**; Thermal Ellipsoids, where shown, are at 50% Probability, Hydrogen Atoms (except those on the allene moiety), Solvent Molecules and the Counter Ion have been Omitted for Clarity.

Table 4-2 Selected Bond Lengths and Angles for Complex **45a** (with Partial Br Exchange)

Bond	Bond Length (Å)	Angle	Bond Angle (°)
C(5) – Ru	2.149(4)	C(5) – Ru – O(1)	120.58(14)
C(6) – Ru	1.999(4)	C(6) – Ru – O(1)	82.29(15)
C(5) – C(6)	1.368(6)	C(5) – Ru – O(2)	178.64(13)
C(6) – C(7)	1.329(6)	C(6) – Ru – O(2)	142.90(15)
C(7) – P(1)	1.769(5)	C(5) – Ru – O(7)	86.18(14)
O(1) – Ru	2.096(3)	C(6) – Ru – O(7)	124.32(15)
O(2) – Ru	2.200(3)	C(5) – Ru – Br(2)	76.8(3)
O(7) – Ru	2.015(3)	C(6) – Ru – Br(2)	115.1(3)
Br(2) – Ru	2.775(11)	C(5) – Ru – P(2)	93.97(11)
P(3) – Ru	2.3899(10)	C(6) – Ru – P(2)	96.02(12)
P(2) – Ru	2.4113(11)	O(1) – Ru – O(2)	60.64(12)
		O(1) – Ru – O(7)	152.56(13)
		O(2) – Ru – O(7)	92.67(12)
		Br(2) – Ru – O(1)	162.6(3)
		Br(2) – Ru – O(2)	102.0(3)
		O(1) – Ru – P(2)	90.71(9)
		O(2) – Ru – P(2)	86.55(8)
		O(7) – Ru – P(2)	80.72(9)
		Br(2) – Ru – P(2)	89.0(3)
		P(3) – Ru – P(2)	172.22(4)
		C(5) – Ru – C(6)	38.30(17)
		C(5) – C(6) – C(7)	150.1(4)
		C(6) – C(7) – P(1)	122.7(3)

The structural data confirmed the formation of the η^2-allene complex and was seen to adopt a distorted octahedral geometry in the solid state. As in many of the previous crystal structures described, much of the distortion is generated by the small bite-angle of the κ^2-OAc ligand. There was also a small distortion of the P(3)–Ru–P(2) angle away from 180° (172.22(4)°) which was presumably caused by steric clashes with the ligand-based triphenylphosphine. For the allene ligand the three carbon atoms all lie in one plane, which was perpendicular to the P(3)–Ru–P(2) plane.

The central carbon of the allene ligand was observed to be closer to the ruthenium atom than the bound carbon atom (C(6)–Ru = 1.999(4) Å versus C(5)–Ru = 2.149(4) Å). This is a commonly observed phenomenon and is thought to be due to an additional interaction between the metal and the π-electrons of the non-coordinated double bond of the allene.[34] Another commonly observed feature of allene complexes also observed in complex **45a** was the coordinated double bond being longer than the non-coordinating bond (C(5)-C(6) = 1.368(6) Å versus C(6)–C(7) = 1.329(6) Å). As discussed in Chapter 1, this can be explained through the Dewar-Chatt-Duncanson model of alkene coordination. In this model the alkene π-electrons of the double bond form a σ-interaction with empty d-orbitals on the metal centre and in turn the metal donates electron density from full d-orbitals into the π*-orbital of the double bond. This interaction weakens the C-C bond at the expense of the M-C bonds and can be observed through lengthening of the alkene double bond. The bending of the allene fragment away from the metal centre provides further evidence for these interactions.

One other ruthenium phosphino-allene complex has been reported; $[Ru(\eta^2\text{-}H_2C{=}C{=}CHPPh_3)(CO)_2(PPh_3)_2]^+$ was synthesised by Hill's group in a similar fashion to **45a,** using triphenylpropargylphosphonium bromide **39a** as the precursor (Scheme 1-8).[31] Hill's complex features ruthenium in the zero oxidation state, as a result there is much more electron density at the metal centre than in complex **45a**. This has led to higher levels of back-bonding into the π*-orbital of the allene ligand and so the coordinated double bond is much longer (C=C = 1.421(4) Å), whereas in the ruthenium (II) complex **45a** a C(5)-C(6) of 1.368(6) Å was observed. This also means that difference in bond length observed between the coordinated and non-coordinated double bonds was more pronounced in Hill's complex (C=C of 1.342(4) Å for the non-coordinating bond) and therefore **45a** can be viewed as having significant metallocyclopropane character (Figure 4-8).

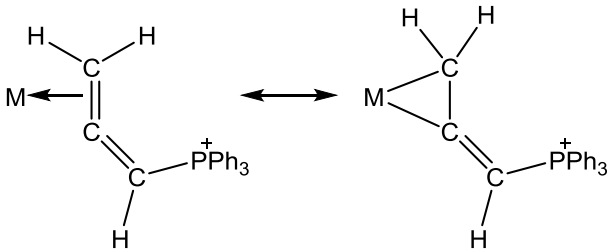

Figure 4-8 Resonance forms to Describe the Bonding in Allene Complex **45**

If the crystals of **45** were grown for longer than a day before analysis, the κ^1-acetate ligand of **45a** was found to have completely exchanged with a chloride atom (Figure 4-9) to give complex **45a''**. The crystals were found to have a minor component (31.5%) consisting of complex **44** (Figure 4-10). Crystals of **44** have also been isolated

during the reaction of hydroxy-vinylidene **3a** with tritylcarbenium tetrafluoroborate to form unsubstituted vinyl carbene **26a** (Section 4.2.2), suggesting that there is a link between these reactions with triphenylpropargylphosphonium salts **39** and the reaction of vinyl carbene **26a** with PPh_3.

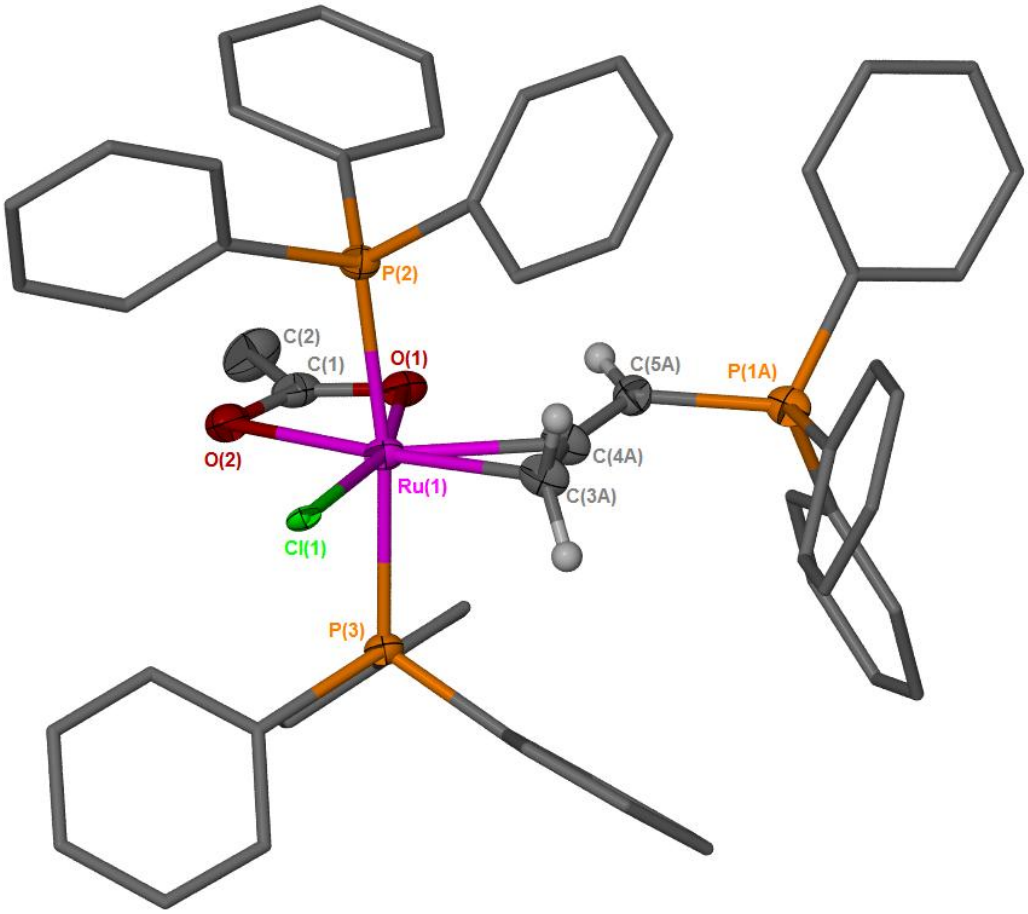

Figure 4-9 ORTEP Representation of Compound **45a''**; Thermal Ellipsoids, where shown are at 50% Probability, Hydrogen Atoms (except those on the allene moiety), Solvent Molecules and the Counter Ion have been Omitted for Clarity. This is the Major Component (68.5%) of this Co-Crystal, Figure 4-10 shows the Minor Component.

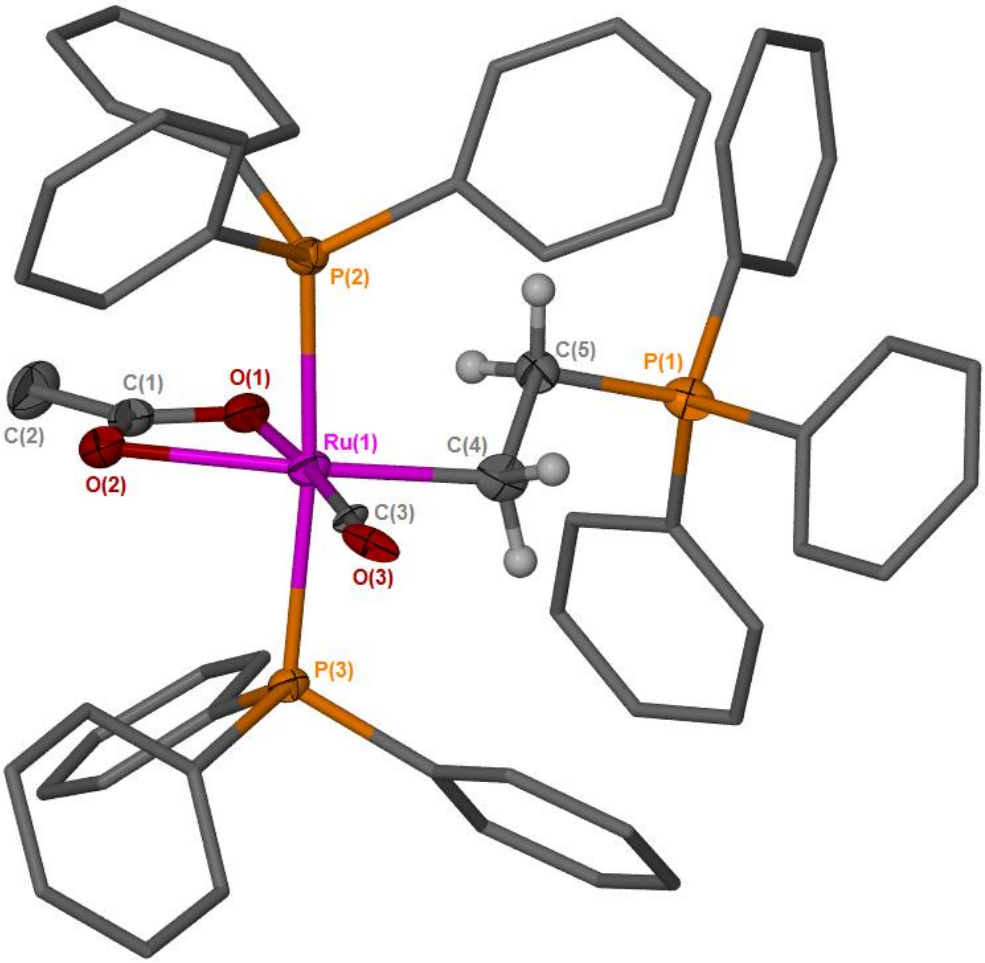

Figure 4-10 ORTEP Representation of Compound **44**; Thermal Ellipsoids, where shown, are at 50% Probability, Hydrogen Atoms (except those on the allene moiety), Solvent Molecules and the Counter Ion have been Omitted for Clarity. This is the Minor Component (31.5%) of this Co-Crystal, Figure 4-9 shows the Major Component.

4.3.3 Counter Ion Effects in the Propargylic Isomerisation

The formation of allene complex **45a** has shown that the reactions conditions used lead to isomerisation of alkyne **39b** to the allene **40b**. Hill has suggested that this isomerisation is metal-mediated,[32] in which case formation of the vinylidene complex **38** will not be possible. However, Hill has also reported that the isomerisation of alkyne **39** to allene **40** occurs spontaneously in solution and that the solvent affects the rate of conversion, with the isomerisation occurring slowest in $CDCl_3$ (no reaction was observed in CD_3CN). It was therefore decided to investigate whether a similar counter ion effect could be observed, therefore reducing the rate of the isomerisation and allowing formation of vinylidene complex **38** from alkyne **39**.

The isomerisation of **39** to **40** is thermodynamically favourable[32] and simply stirring **39** in DCM generated the isomerised species, **40** (therefore the reaction is not metal-mediated). However, counter-ion metathesis can be carried out in methanol[228]

without isomerisation occurring and so it was possible to investigate the effects of different counter-ions.

CD_2Cl_2 solutions of various triphenylpropargylphosphonium salts were monitored by NMR spectroscopy over time. It was found **39a** (Br) took ca. 3 days to isomerise fully to the allene, whilst **39b** (BF_4) isomerisation was complete in just an hour. Isomerisation of the BPh_4 salt **39c** took ca. 24 hours and so it was hoped that this might offer a route to vinylidene formation (Scheme 4-8). Additional evidence for this counter ion effect was observed in the ^{1}H-NMR chemical shifts, the coupling constants and multiplicity remained consistent. For the alkyne isomer **39** it was found that the CH_2 resonance shifted downfield with increasingly coordinating anions; **39a** (Br) = δ 5.20, **39b** (BF_4) = δ 4.32, **39c** (BPh_4) = δ 3.08. The CH resonance was independent of the counter ion. For the allene however it was found that the CH_2 resonance was unaffected whilst the CH resonance exhibited a similar counter ion dependent shift; **40a** (Br) = δ 7.68, **40b** (BF_4) = δ 6.52, **40c** (BPh_4) = δ 6.05. From this it can be seen that only the protons close to the phosphorus atom are affected in both isomers, suggesting that in solution there is an appreciable cation/anion interaction

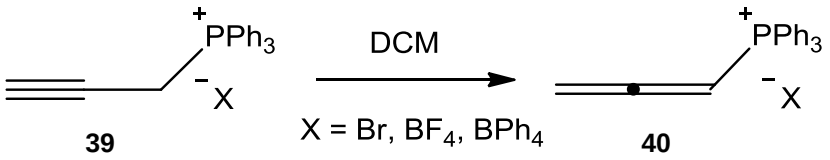

Scheme 4-8 Isomerisation of Triphenylpropargylphosphonium **39**

Crystals of the BPh_4 salt of free allene **40c** were obtained by slow diffusion of pentane into a CD_2Cl_2 solution containing the product (Figure 4-11). The structure displayed the linear nature of the allene with a C(1)-C(2)-C(3) angle of 178.25(16)° and the two double bonds were seen to be approximately of the same length (C(1)–C(2) = 1.3025(18) Å, C(2)–C(3) = 1.294(2) Å). These bonds were both shorter than those observed in allene complex **45a**, showing the effect that back-bonding has on coordinated allenes. Hill published a crystal structure of the PF_6 salt of **40**, where the C-C bond lengths were observed to be slightly shorter (C(1)-C(2) = 1.297(3) Å, C(2)-C(3) = 1.286(4) Å) than for the BPh_4 case (C(1)-C(2) = 1.3025(18) Å, C(2)-C(3) = 1.294(2) Å).[32] With no more examples for comparison it is difficult to draw firm conclusions, but it is possible that this is another effect due to the change in counter ion.

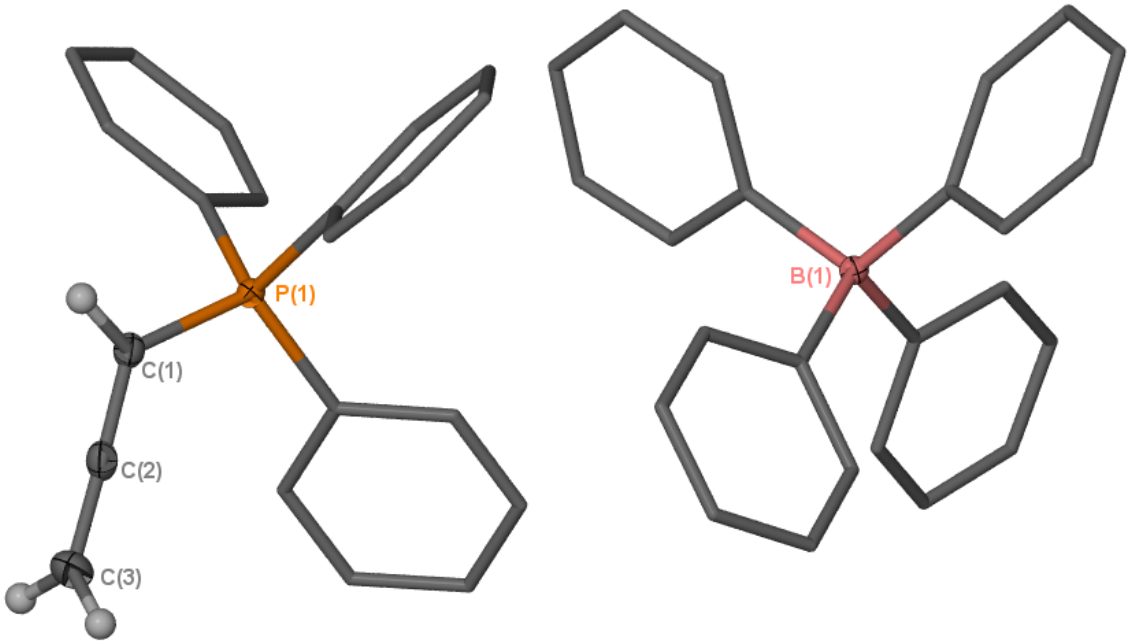

Figure 4-11 ORTEP Representation of Compound **40c**; Thermal Ellipsoids, where shown, are at 50% Probability, Hydrogen Atoms (except those on the allene moiety) have been Omitted for Clarity.

Table 4-3 Selected Bond Lengths and Angles for Complex **40c**

Bond	Bond Length (Å)	Angle	Bond Angle (°)
C(1) – P	1.7719(13)	P – C(1) – C(2)	122.91(10)
C(1) – C(2)	1.3025(18)	C(1) – C(2) – C(3)	178.25(16)
C(2) – C(3)	1.294(2)		

4.3.4 Formation of a Vinylidene Complex

Having established that the slowest isomerisation was **39c** to **40c** (the BPh_4 salt) *cis*-[Ru(κ^2-OAc)$_2$(PPh_3)$_2$] **1a** was reacted with triphenylpropargylphosphonium tetraphenylborate **39c** and a mixture of allene **45b** and the vinylidene **38** was produced (Scheme 4-9). The ratio of products was found to change with order of addition and reaction conditions. The greatest percentage of vinylidene **38** was obtained (3:1 vinylidene:allene) when both solids were added to the reaction vessel before the addition of solvent (Scheme 4-9). This ratio was determined by ^{31}P-NMR with the vinylidene resonances occurring at δ 19.63 (t) and 37.53 (d) ($^4J_{PP}$ = 3.4 Hz). The ^{1}H-NMR data (2H multiplet at δ 3.94 and a 1H multiplet at δ 4.74, ▲ in Figure 4-12) matched that of species **38** observed when unsubstituted vinyl carbene **26a** was synthesised (Section 4.2.2).

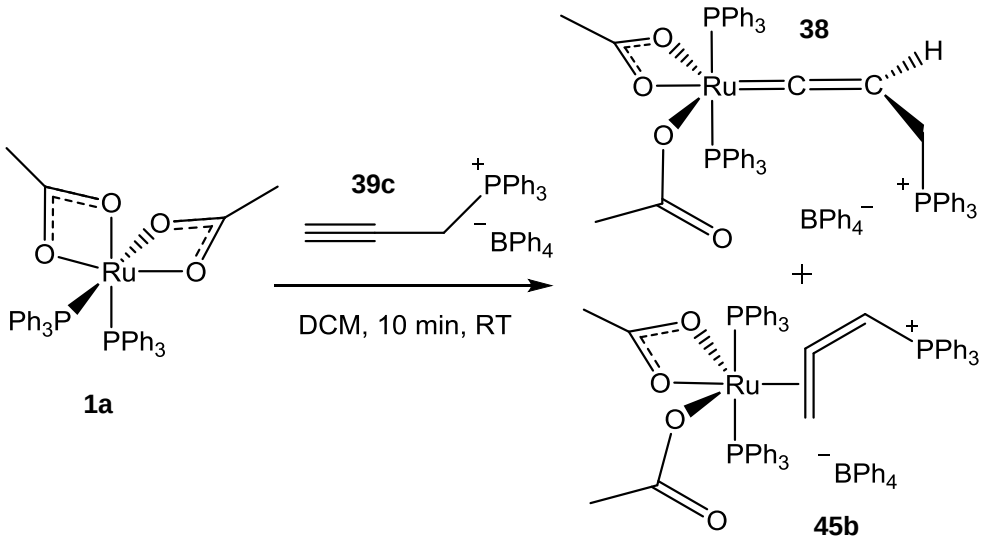

Scheme 4-9 Reaction of *cis*-[Ru(κ^2-OAc)$_2$(PPh$_3$)$_2$] **1a** with Triphenylpropargylphosphonium Tetraphenylborate **39c**

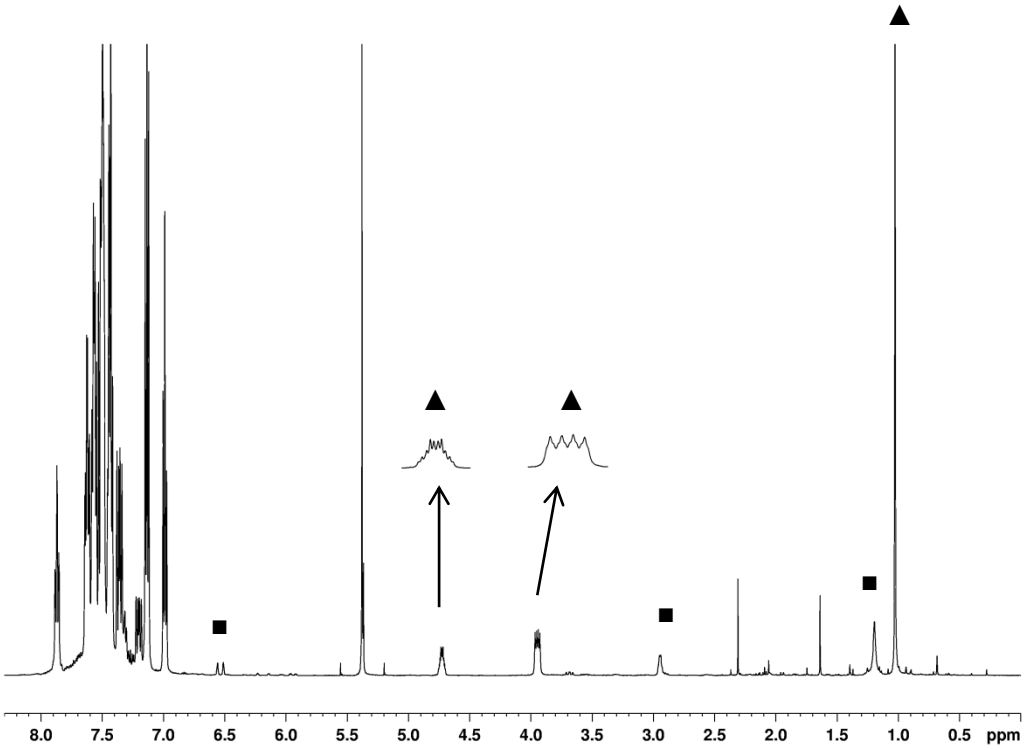

Figure 4-12 ^{1}H-NMR of Phosphino-Vinylidene **38** (▲) and Allene **45b** (■). The Expanded Peaks Correspond to the Protons of Vinylidene **38** and Exhibit an Integral Ratio of 1:2.

The ^{13}C-NMR data for **38** are less consistent with the vinylidene structure with the β- and γ-carbons being observed at lower chemical shift than would be expected (22.8 (d, $^1J_{PC}$ = 51.5 Hz) and 96.5 (m) respectively). The α-carbon resonance is even more unusual, observed at δ 254.0 rather than the expected ca. δ 350. One possible explanation for this could be the involvement of the enol ester isomer **46** in which the κ^1-acetate attacks the vinylidene α-carbon to form a metallocycle (Scheme 4-10). The enol ester complex [Ru(κ^2-OAc)(CO)(OC{Me}OC=CHPh)(PPh$_3$)$_2$] has been previously

reported and was found to have an α-carbon shift of δ 193.3.[174] The intermediate nature of the data collected for **38** suggests that an equilibrium between the two structures may be present in solution. This possibility was assessed using NMR and theoretical methods in Section 4.3.5.

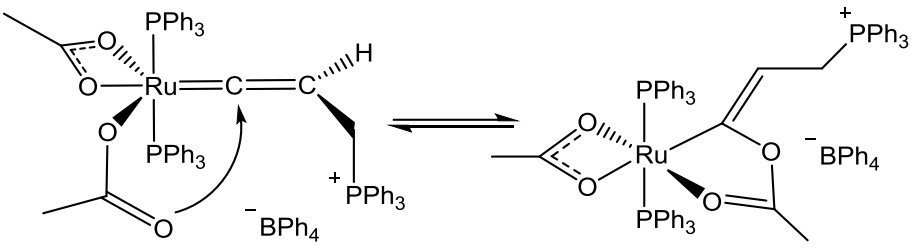

Scheme 4-10 Formation of the Enol Ester Isomer **46**

4.3.5 NMR and Theoretical Studies into the Enol Ester 46

If vinylidene **38** is in equilibrium with enol ester **46**, then it may be possible to probe the isomerisation through exchange of the acetate ligands. Only one resonance was observed in the ^{1}H-NMR at room temperature; however the exchange can be slowed enough through low temperature NMR for two resonances to be observed. These experiments also allow the calculation of rate constants and free energies for the exchange.

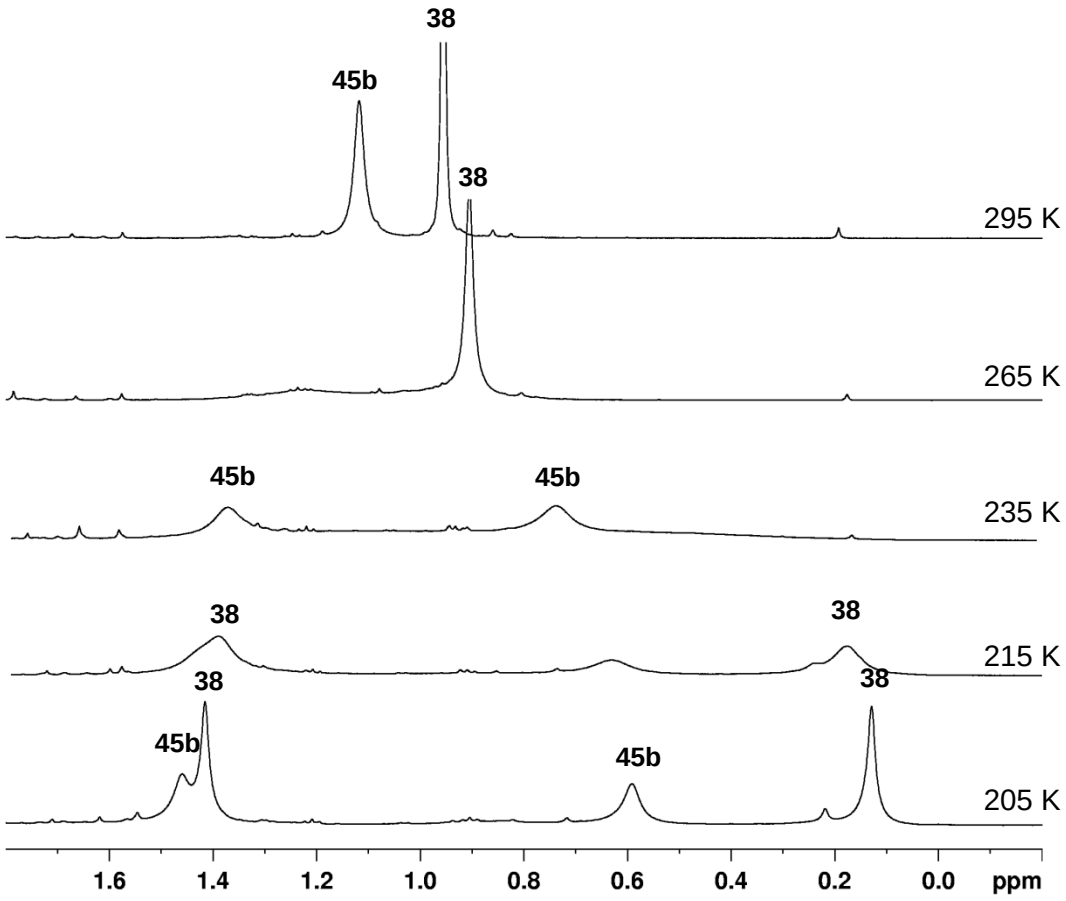

Figure 4-13 Variable temperature ^{1}H-NMR of the mixture of **38** and **45b** Showing Coalescence of the Acetate Ligands

Variable temperature ^{1}H-NMR of the mixture of **38** and **45b** was carried out between the temperatures of 295 - 205 K (Figure 4-13). It was found that the acetate resonances (δν = 433.5 Hz) of allene complex **45b** coalesced at 270 K and those of vinylidene **38** at 235 K (δν = 643.2 Hz). These data can be used to find the rate constant at coalescence (k_{coal}) by using the equation:

$$k_{coal} = \frac{\pi\delta\nu}{\sqrt{2}} = 2.22\delta\nu \qquad \text{Equation 4.1}$$

This can then be combined with the Eyring equation to give an expression for the free energy of the process:

$$k = \kappa \frac{k_B T}{h}(-\Delta G^{\ddagger}/RT) \qquad \text{Equation 4.2}$$

$$\Delta G^{\ddagger} = RT[23.76 - \ln(k/T)] \qquad \text{Equation 4.3}$$

$$\Delta G^{\ddagger} = RT_C[22.96 + \ln(T_C/\delta\nu)]\, Jmol^{-1} \qquad \text{Equation 4.4}$$

Using these equations it was found that the rate constant (k_{coal}) for acetate exchange in allene complex **45b** is fairly large at 962.4 s^{-1} with the barrier also relatively high ($\Delta G^{\ddagger}_{270K}$ = 50.5 kJ mol^{-1}). This is in comparison to the related complexes [Ru(κ^1-OAc)(κ^2-OAc)L(PPh_3)$_2$] (where L = CO ($\Delta G^{\ddagger}_{195K}$ = 37.4 kJ mol^{-1}), NO ($\Delta G^{\ddagger}_{235K}$ = 45.3 kJ mol^{-1}), =C=CC{H}C(OH)Ph_2 ($\Delta G^{\ddagger}_{215K}$ = 40.5 kJ mol^{-1}), =CO{CH_2}$_3$ ($\Delta G^{\ddagger}_{185K}$ = 35.2 kJ mol^{-1})), although a true comparison cannot be made as the ΔG values are for different temperatures (due to different coalescence temperatures).[173] However, for vinylidene complex **38** k_{coal} is even faster at 1427.9 s^{-1}, though the barrier to exchange is fairly typical ($\Delta G^{\ddagger}_{235K}$ = 42.9 kJ mol^{-1}) when compared to those observed for similar complexes.[173]

The use of DFT has provided further insight into this system, with the relative energies of the allene **45**, vinylidene **38** and enol ester **46** isomers being investigated. Calculations were performed by Dr Jason Lynam with the Turbomole program; initial geometry optimisations and frequency calculations were performed at the BP86/SV(P) level and subsequent single point energies at pbe0/def2-TZVPP(with COSMO DCM solvent correction).[211-220]

In order to validate the method used, the initial calculations investigated the propargylic rearrangement of alkyne **39** to allene **40**. We have demonstrated experimentally that formation of allene **40** is thermodynamically favoured, and Hill has also reported theoretical calculations (using M06/6-31+G(d,p) that give the same conclusion .[32] The methods used here were also able to demonstrate that the allene isomer **40** is thermodynamically favoured over the alkyne isomer **39** with a difference in free energy (ΔG_{298K}) of 29 kJ mol^{-1}.

For the ruthenium complexes **45**, **38**, and **46**, the energies of a number of different conformations of the acetate ligands were calculated and only the lowest energy conformers will be discussed here. These calculations were run at the pbe0/def2-tzvpp level of theory and a solvent correction was applied using a dielectric continuum model. It was found that the enol ester isomer **46** was the lowest energy structure, with vinylidene **38** having a relative energy of +5 kJ mol^{-1} and allene **45** +10 kJ mol^{-1} (Figure 4-14). The interconversion between **38** and **46** was then probed, and a low energy transition state found (**$TS_{38\text{-}46}$**, ΔG_{298K} = +31 kJ mol^{-1}) which would enable room temperature interconversion of **38** and **46**. This supports the theory that the vinylidene and enol ester isomers are in rapid equilibrium in solution and is consistent with the observed ^{13}C-NMR chemical shift of δ 254.0 lying between the typical values expected for vinylidene complexes (*ca.* δ 350) and enol ester complexes (*ca.* δ 180).

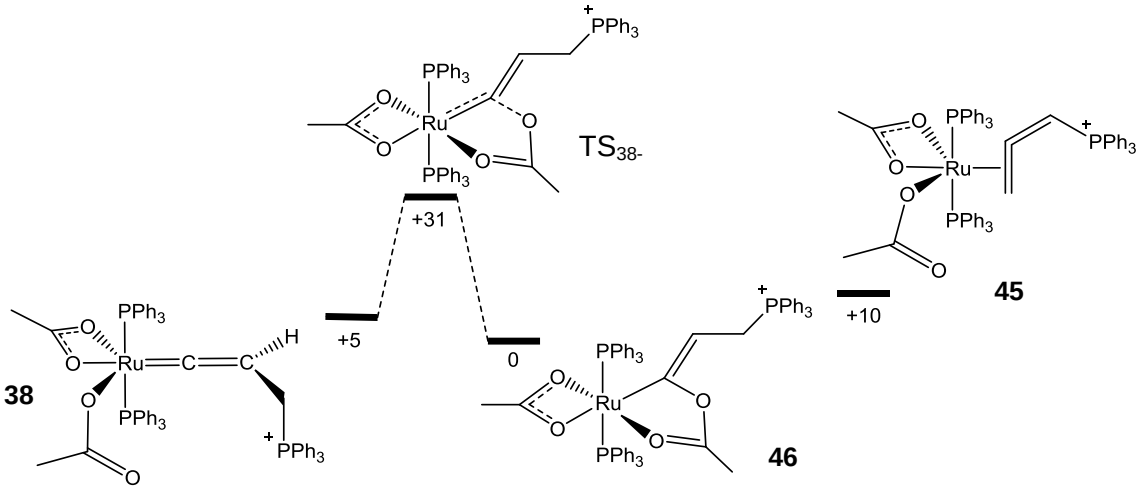

Figure 4-14 Interconversion of Vinylidene **38** and Enol Ester **46**, with the Relative Energies in kJ mol^{-1}. Allene Complex **45** is shown for comparison.

4.3.6 Isolation of a Phosphino-Vinylidene Complex

As the formation of **38** could not be unequivocally determined it was decided to synthesise the benzoate analogue $[Ru(\kappa^2\text{-}O_2CPh)(\kappa^1\text{-}O_2CPh)(C{=}C{=}CHCH_2PPh_3)(PPh_3)_2][BPh_4]$ **47** for comparison. It was also hoped that this would aid crystallisation attempts. *cis*-$[Ru(\kappa^2\text{-}O_2CPh)_2(PPh_3)_2]$ **34** was reacted with **39c** in DCM for 2 minutes before being washed with pentane. This yielded an orange solid identified as complex **47** with very little contamination from allene complex **50** (~ 7% by ^{31}P-NMR) (Scheme 4-11).

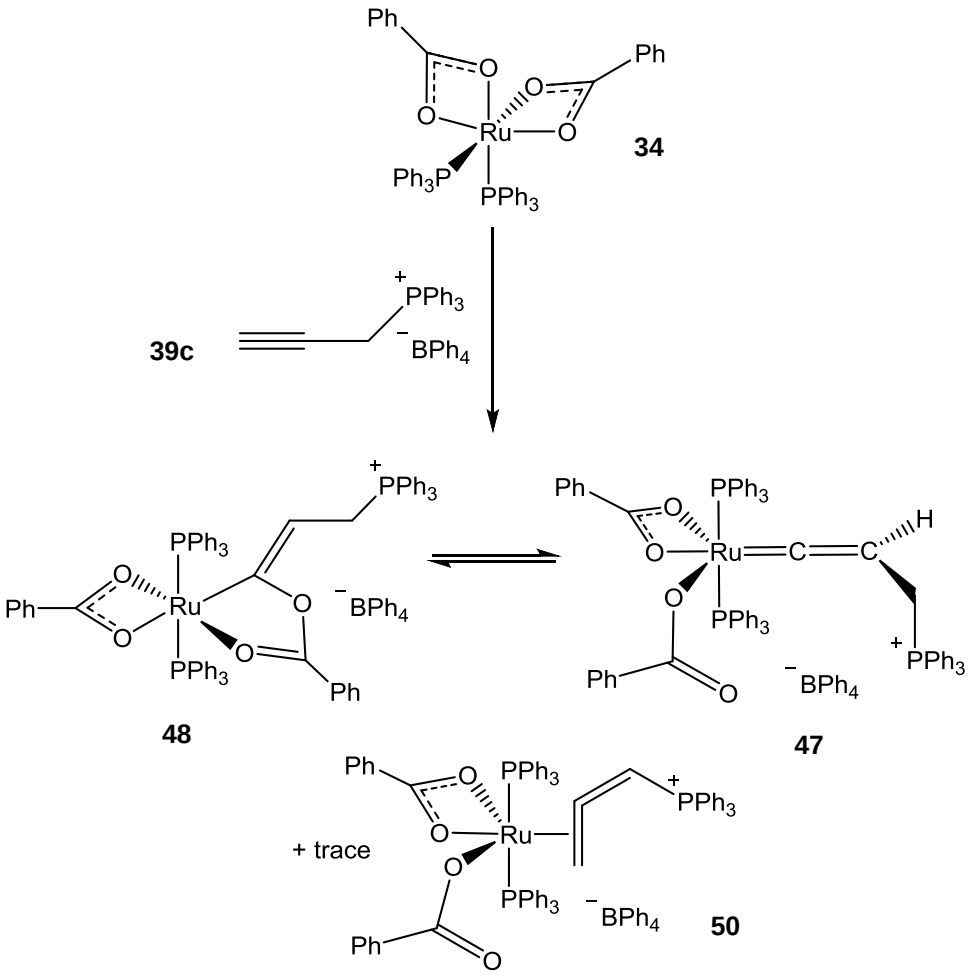

Scheme 4-11 Reaction of *cis*-[Ru(κ^2-$O_2CPh)_2(PPh_3)_2$] **34** with [$HC{\equiv}CCH_2PPh_3$][BPh_4] **39c**

Characterisation data for **47** are essentially the same as those for the acetate analogue **38**. The ^{31}P-NMR resonances occur at δ 20.00 (t) and 35.85 (d) with a coupling of $^4J_{PP}$ = 3.0 Hz. There is also the expected doublet of doublets (δ 4.06) and triplet of doublets (δ 4.84) observed in the ^{1}H-NMR spectrum assigned to the CH_2 and CH protons of the allene ligand respectively. It was not possible to directly observe the α-carbon of the organic ligand in the ^{13}C-NMR spectrum, however a cross-peak from the CH proton was observed in the HMBC spectrum at δ 259.4. This confirms that the composition of the benzoate and acetate analogues are similar (they are an exchanging mixture of isomers).

Crystals were grown by the slow diffusion of diethyl ether into a DCM solution of **47** and were found to be the vinylidene isomer (Figure 4-15). This suggests that there may be a dynamic equilibrium in solution between the enol ester and vinylidene isomers and that in the solid state the vinylidene is the prevalent species. Solid-state cross-polarisation magic angle spinning (CP-MAS) NMR experiments were carried to probe this, but insufficient signal was obtained for the α-carbon resonance to be observed.

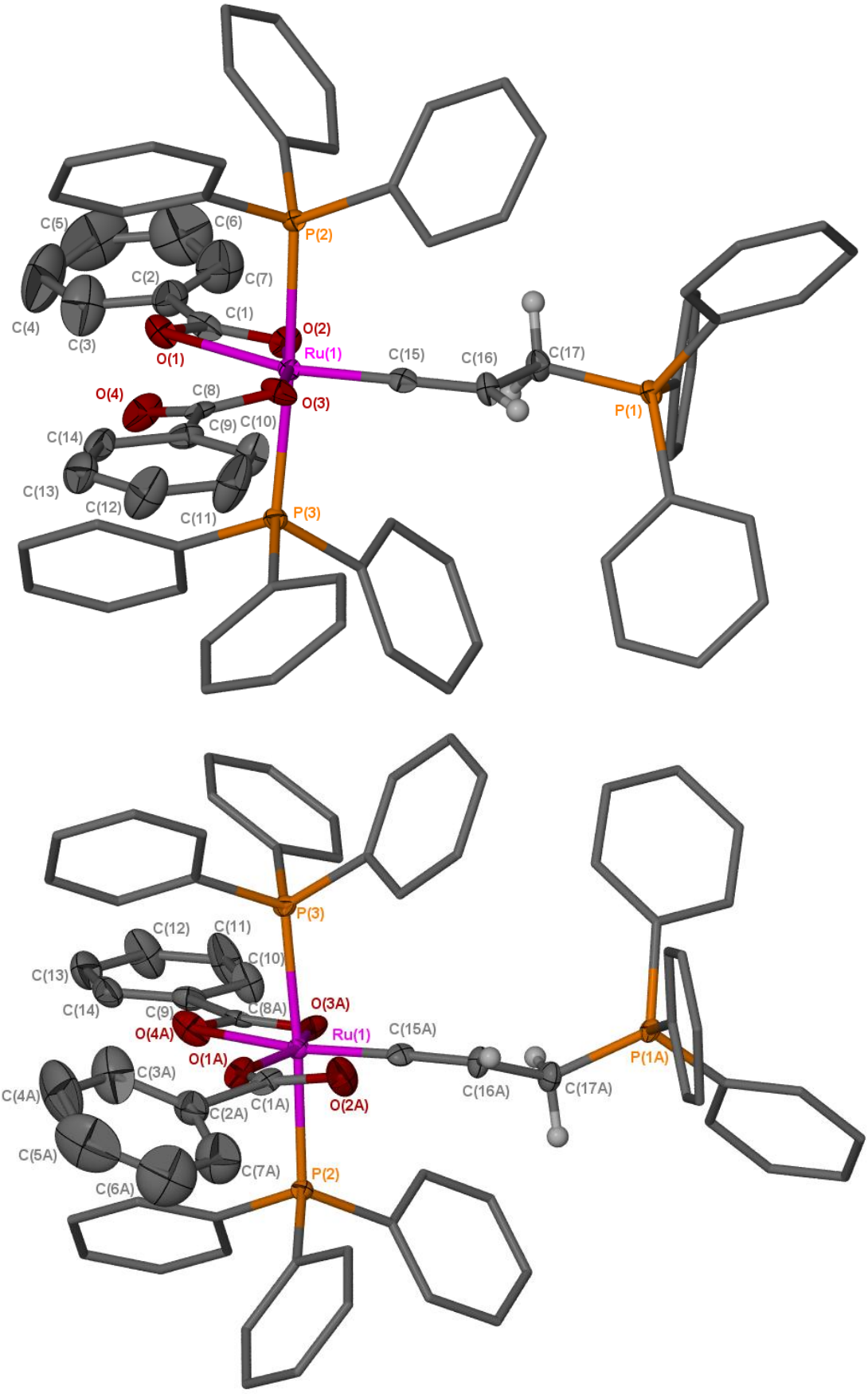

Figure 4-15 ORTEP Representation of Complex **47a** (top) **47b** (bottom); Thermal Ellipsoids, where shown, are at 50% Probability, Hydrogen Atoms, Solvent and the BPh_4 Counter Ion have been Omitted for Clarity.

Table 4-4 Selected Bond Lengths and Angles for Complex **47a**

Bond	Bond Length (Å)	Angle	Bond Angle (°)
C(15) – Ru	1.762(4)	C(15) – Ru – O(1)	152.55(15)
C(15) – C(16)	1.323(5)	C(15) – Ru – O(2)	95.32(15)
C(16) – C(17)	1.510(5)	C(15) – Ru – O(3)	90.96(17)
C(17) – P(1)	1.797(4)	C(15) – Ru – P(2)	92.95(12)
O(1) – Ru	2.342(3)	O(1) – Ru – O(2)	57.66(10)
O(2) – Ru	2.112(3)	O(1) – Ru – P(2)	85.12(7)
O(3) – Ru	2.095(5)	O(2) – Ru – P(2)	94.33(8)
P(3) – Ru	2.3848(8)	O(3) – Ru – P(2)	83.91(14)
P(2) – Ru	2.3841(8)	P(3) – Ru – P(2)	175.38(3)
		C(16) – C(15) – Ru	176.3(3)
		C(17) – C(16) – C(15)	120.5(4)
		P(1) – C(17) – C(16)	118.6(11)

Table 4-5 Selected Bond Lengths and Angles for Complex **47b**

Bond	Bond Length (Å)	Angle	Bond Angle (°)
C(15a) – Ru	1.789(16)	C(15a) – Ru – O(1a)	99.1(8)
C(15a) – C(16a)	1.33(2)	C(15a) – Ru – O(3a)	103.2(7)
C(16a) – C(17a)	1.48(2)	C(15a) – Ru – O(4a)	164.0(7)
C(17a) – P(1a)	1.868(17)	C(15a) – Ru – P(2)	89.5(5)
O(1a) – Ru	2.024(14)	O(4a) – Ru – O(3a)	61.2(7)
O(3a) – Ru	2.02(3)	O(1a) – Ru – P(2)	90.9(5)
O(4a) – Ru	2.140(15)	O(3a) – Ru – P(2)	86.2(7)
P(3) – Ru	2.3848(8)	O(4a) – Ru – P(2)	92.7(5)
P(2) – Ru	2.3841(8)	P(3) – Ru – P(2)	175.38(3)
		C(16a) – C(15a) – Ru	176.6(13)
		C(17a) – C(16a) – C(15a)	127.1(14)
		P(1a) – C(17a) – C(16a)	118.6(11)

The crystal structure confirmed the synthesis of vinylidene **47** and the asymmetric unit was found to contain two forms of the complex (**47a** and **47b**), both of which are shown

in (Figure 4-15). The two forms differ in the relative orientation of the benzoate ligands. In **47a** the κ^1-OBz is pointing away from the vinylidene ligand, however in **47b** the non-coordinating oxygen atom is relatively close to the α-carbon of the vinylidene (O(2A)-C(15A) = 2.791(2) Å). This is reminiscent of the enol ester isomer **48** and provides some evidence for its involvement.

In other respects the two forms are similar, with the P-Ru-P moiety being essentially identical. The vinylidene bond lengths are statistically indistinguishable (when the ESD values are taken into account) with form **47a** having bond lengths of Ru-C(15) = 1.762(4), C(15)-C(16) = 1.323(5) and C(16)-C(17) = 1.510(5) Å and form **47b** Ru-C(15A) = 1.789(16), C(15A)-C(16A) = 1.33(2) and C(16A)-C(17A) = 1.482(1) Å. These bond lengths fall within the range observed for the closely related complexes $[Ru(\kappa^1\text{-}OAc)(\kappa^2\text{-}OAc)(=C=CHR)(PPh_3)_2]$ where Ru-Cα = 1.766(6) - 1.805(3) Å and Cα-Cβ = 1.296(8) – 1.325(2) Å.[173]

4.3.7 Synthesis of $[Ru(\kappa^2\text{-}O_2CPh)(\kappa^1\text{-}O_2CPh)(\eta^2\text{-}H_2C=C=CHPPh_3)(PPh_3)_2][BF_4]$ 49 and Evidence for Ligand Exchange

The benzoate analogue of the allene complex **49** was also synthesised using the same synthetic method as for acetate complex **45** (Scheme 4-12). It was found that significant bromide exchange for the benzoate ligands occurred on standing in solution (a small amount was also observed in the acetate case Figure 4-7) and therefore only crystals of this exchange product **50** could be obtained. However, the material obtained directly from the reaction mixture was mostly the desired allene complex with two benzoate ligands. Both compounds were fully characterised, with the data matching well to that acquired for the acetate allene complex **45**. For example, the protons on the allene ligand were observed at δ 3.04 (m, 2H, CH_2) and δ 6.73 (ad, $^2J_{PH}$ = 23.8 Hz, 1H, C*H*) in the ^{1}H-NMR spectrum. In the ^{31}P-NMR spectrum the ligand-based PPh_3 was observed as a triplet at δ 14.2 ($^4J_{PP}$ = 3.3 Hz), and the metal-based PPh_3 ligands as a doublet at δ 27.9 ($^4J_{PP}$ = 3.3 Hz).

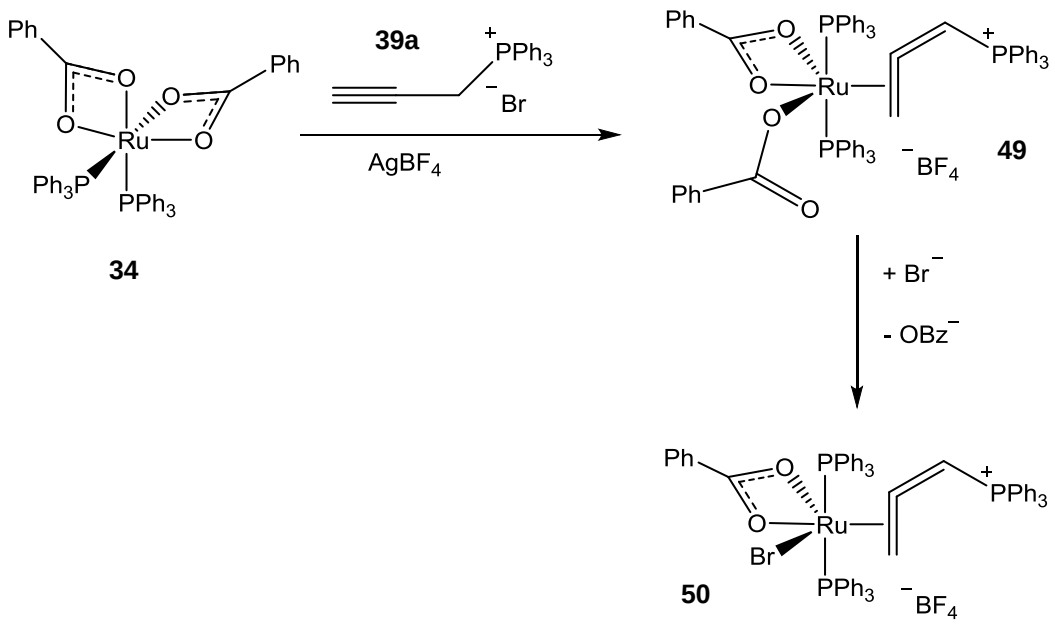

Scheme 4-12 Synthesis of the Benzoate Analogue of the Allene Complex, **49**

The structural data for **50** display similar metrics to those observed for the acetate analogue **45**, and again the bond lengths are lengthened in comparison to the non-coordinated allene **40c**.

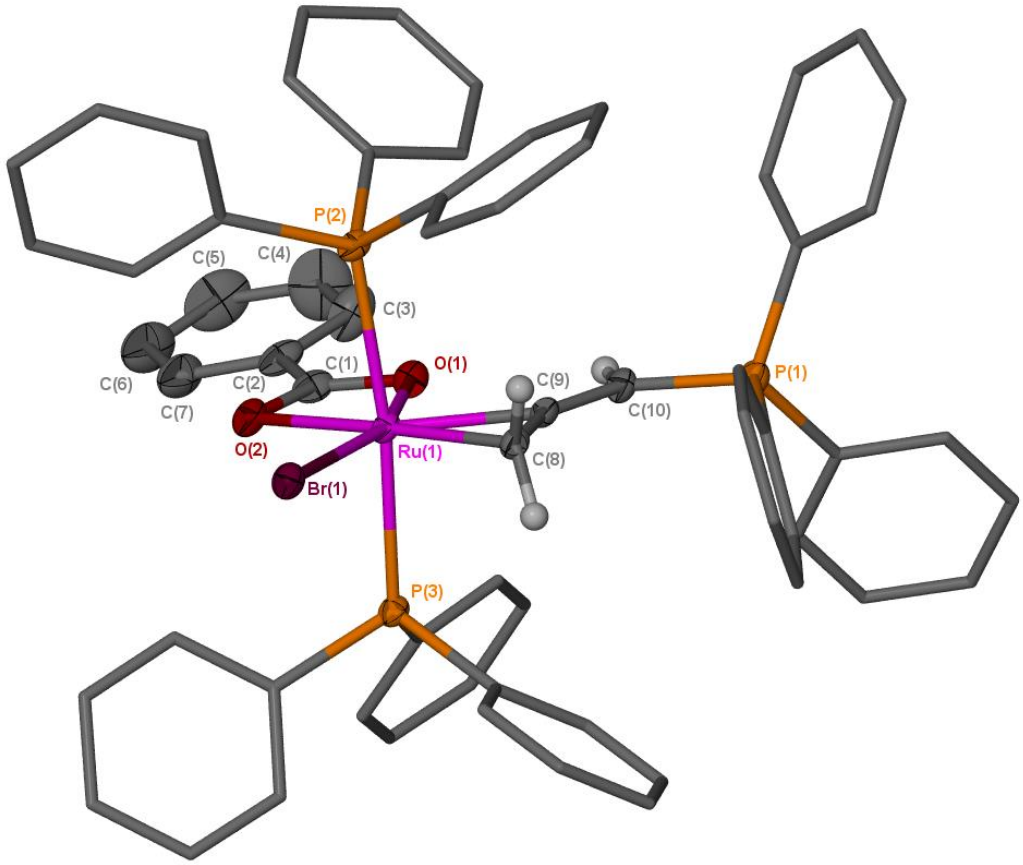

Figure 4-16 ORTEP Representation of Compound **50**; Thermal Ellipsoids, where shown, are at 50% Probability, Hydrogen Atoms (except those on the allene moiety), the Counter Ion and Solvent Molecules have been Omitted for Clarity.

Table 4-6 Selected Bond Lengths and Angles for Complex **50**

Bond	Bond Length (Å)	Angle	Bond Angle (°)
C(8) – Ru	2.157(3)	C(8) – Ru – O(1)	121.73(10)
C(9) – Ru	2.010(3)	C(9) – Ru – O(1)	83.18(11)
C(8) – C(9)	1.383(4)	C(8) – Ru – O(2)	177.37(10)
C(9) – C(10)	1.333(4)	C(9) – Ru – O(2)	143.74(11)
C(10) – P(1)	1.768(3)	C(8) – Ru – Br	78.53(8)
O(1) – Ru	2.093(2)	C(9) – Ru – Br	117.09(9)
O(2) – Ru	2.207(2)	C(8) – Ru – P(2)	92.18(8)
Br – Ru	2.5138(4)	C(9) – Ru – P(2)	93.23(9)
P(3) – Ru	2.3918(8)	Br – Ru – O(1)	159.64(7)
P(2) – Ru	2.4099(8)	Br – Ru – O(2)	99.16(6)
		O(1) – Ru – O(2)	60.62(9)
		O(1) – Ru – P(2)	89.72(7)
		O(2) – Ru – P(2)	88.96(6)
		Br – Ru – P(2)	87.37(2)
		P(3) – Ru – P(2)	173.04(3)
		C(10) – C(9) – C(8)	148.1(3)
		P(1) – C(10) – C(9)	120.1(2)

4.4 Reaction of Triphenylpropargylphosphonium Salts with Other Organometallic Precursors

4.4.1 Preamble

In Section 4.3.4, phosphino-vinylidene complexes **38** and **47** were shown to have unusual ^{13}C-NMR spectra in which the chemical shift of the α-carbons were observed at δ 254.0 and 259.4 respectively. This is in contrast to the expected region of ca. δ 350 usually expected for ruthenium vinylidene α-carbon chemical shifts. In order to investigate this further it was decided to synthesise some further examples of phosphino-vinylidene ccomplexes. Complexes without ancillary acetate ligands would not be able to isomerise to an enol ester and so it was hoped that a ‘normal’ phosphino-vinylidene could be synthesised. It was an opportunity to further investigate the different outcomes in the formation of allene and vinylidene complexes. Therefore

[HC≡CCH$_2$PPh$_3$][BPh$_4$] **39c** was reacted with a range of complexes that are known to react with terminal alkynes to form vinylidene complexes.

4.4.2 Use of Ruthenium Precursors

[HC≡CCH$_2$PPh$_3$][BPh$_4$] **39c** was heated at reflux in methanolic solutions of the ruthenium complexes [RuCpCl(PPh$_3$)$_2$] **51** and [RuCp(MeCN)(dppe)] **52**.[229] Compound **39c** was also added to a CD_2Cl_2 solution of [RuCl(dppe)$_2$][X] (where X = OTf, BPh$_4$) **53**.[230, 231] However, in all cases no evidence for a reaction at the ruthenium centre was obtained, only conversion of the alkyne **39c** to free allene **40c** was observed in the NMR spectra. (Scheme 4-13).

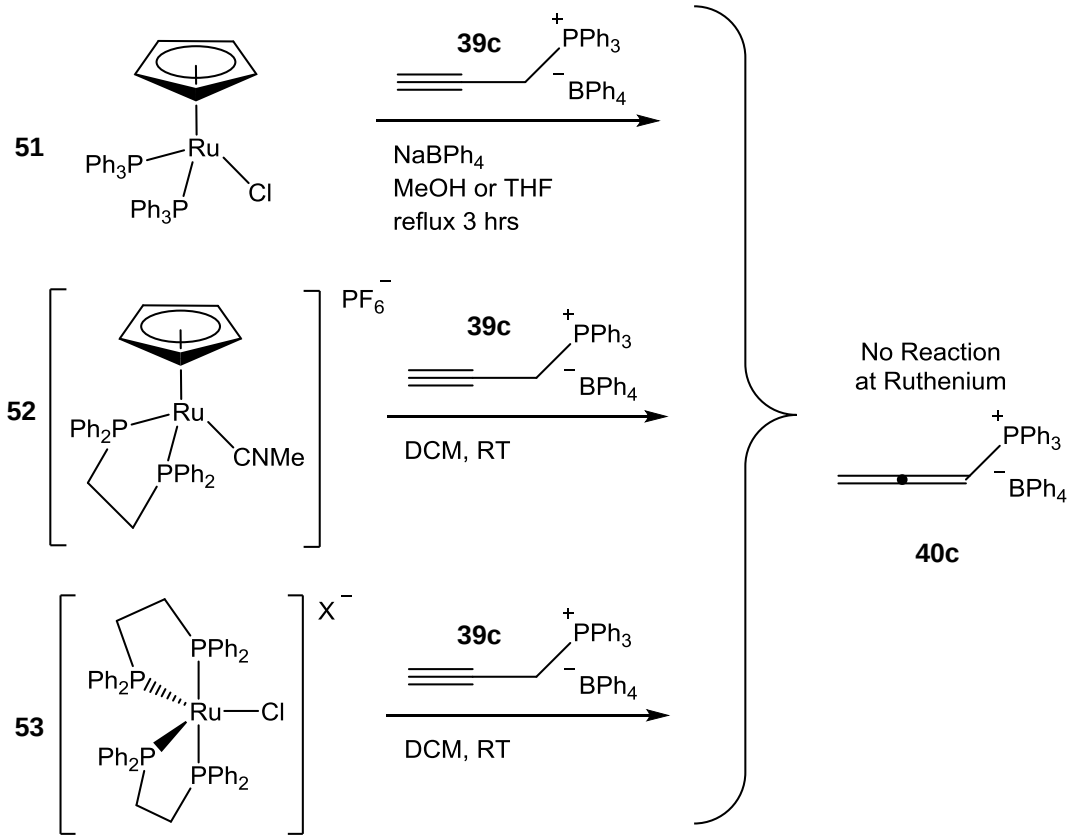

Scheme 4-13 Reaction of **39c** with Common Ruthenium Precursors

On addition of alkyne **39c** to a THF solution of the precursor [RuCl$_2$(PPh$_3$)$_3$] **54** at reflux,[176] many ruthenium-containing products were formed. The major product observed resulted from addition of PPh$_3$ to the free allene **40c** (the ^{31}P-NMR spectrum exhibited two doublets at δ 23.3 and 28.76 with a mutual coupling of 19.8 Hz) to form [H$_2$C=C(PPh$_3$)CH$_2$PPh$_3$]$^{2+}$ **55** (Scheme 4-14). A second equivalent of alkyne **39c** was added in the hope it would scavenge any free phosphine and allow clean reaction. However this reaction was unselective with **55** being the only identifiable product.

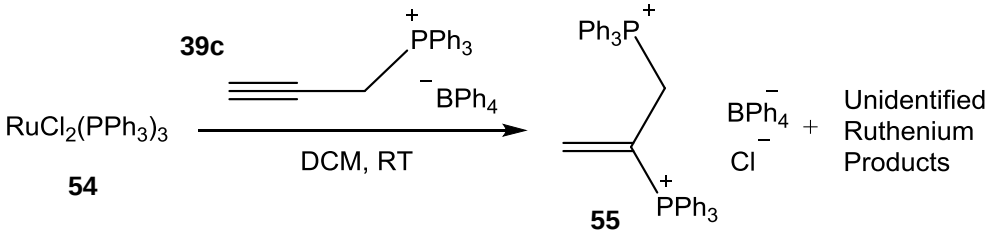

Scheme 4-14 Reaction of **39c** with $RuCl_2(PPh_3)_3$ **54**

As an allene with an electron-withdrawing substituent, the central carbon of **40** is susceptible to nucleophilic attack[232] and it is therefore unsurprising that by-products like **55** have been observed. The addition of nucleophiles such as PPh_3 and methanol to the central carbon of **40** has been observed as unwanted side reactions in a number of cases.[233] [32] Phosphine addition product **55** was independently synthesised and isolated to confirm the assignment.

Triphenylphosphine was added to a DCM solution $[H_2C=C=CHPPh_3][BF_4]$ **40b** and when the reaction was followed by NMR it was found that the initial product was a short lived ylide **56** (Scheme 4-15). The ylide was found to have a lifetime of ~ 8 hours, allowing characterisation by ^1H and ^{31}P-NMR. A pair of doublets in the ^{31}P-NMR spectrum at δ 11.3 and 26.0 with a $^3J_{PP}$ =67.1 Hz were assigned to this species. In the ^1H-NMR spectrum three resonances were assigned to compound **56** (a triplet of doublets at δ 2.24 (CH), a doublet of triplets at δ 4.01 and a doublet of doublets at δ 4.74 (the inequivalent alkene protons), all of which integrated to one proton and exhibited phosphorus coupling.

Ylide **56** could then be protonated to yield the di-cation **55** which is the species observed in the reaction between $RuCl_2(PPh_3)_3$ **54** and alkyne **39c**. The di-cation **55** was formed from a DCM solution of **56** left to stand at room temperature, but could also be synthesised more reliably by addition of HBF_4 to ylide **56**. Compound **55** gave rise to doublets in the ^{31}P-NMR spectrum at δ 23.0 and 28.0 which had a $^3J_{PP}$ of 20.1 Hz. In the ^1H-NMR spectrum resonances were observed at δ 4.87 (2H), 6.47 (1H) and 6.78 (1H), all of which displayed coupling to phosphorus (Scheme 4-15).

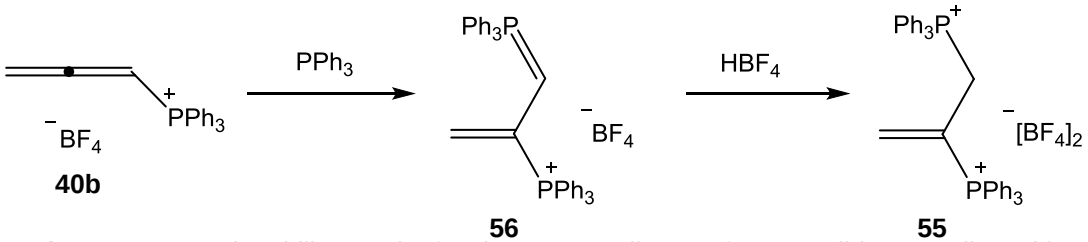

Scheme 4-15 Nucleophilic Attack of PPh_3 onto an Allene to form an Ylide **56**, Followed by Protonation to form a Stable Geminal Alkene **55**

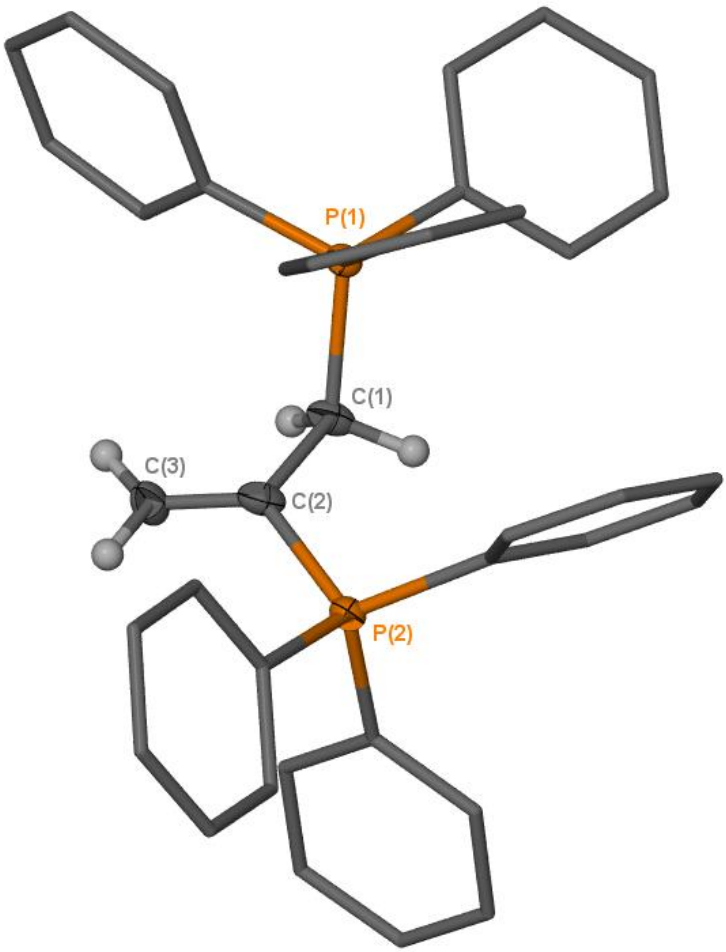

Figure 4-17 ORTEP Representation of Compound **55**; Thermal Ellipsoids, where shown, are at 50% Probability, Hydrogen Atoms, and BF_4 Counter Ions have been Omitted for Clarity. The Minor Component of the Disorder has also been Omitted.

Table 4-7 Selected Bond Lengths and Angles for **55**

Bond	Bond Length (Å)	Angle	Bond Angle (°)
P(1) – C(1)	1.818(3)	P(1) – C(1) – C(2)	115.8(3)
C(1) – C(2)	1.517(5)	C(1) – C(2) – C(3)	121.1(4)
C(2) – C(3)	1.239(7)	C(1) – C(2) – P(2)	116.8(3)
C(2) – P(2)	1.816(4)	C(3) – C(2) – P(2)	120.5(4)

Crystals of **55** suitable for elemental analysis and X-ray diffraction could be grown by the slow diffusion of pentane into a DCM solution of the compound. The structural data exhibited the presence of the two phosphonium groups. The hydrogen atoms shown in Figure 4-17 (those on C(3) and C(1)) were found by difference map and they, alongside the short bond length (C(2) – C(3) = 1.239(7) Å), confirm the location of the alkene (Table 4-7).

Addition of alkyne **39c** to a $CDCl_3$ solution of $[RuCl_2(MeCN)_2(PiPr_3)_2]$ **57** (synthesised by Ozawa's route[176]) led to unselective reactions at the ruthenium centre and phosphine addition to the alkyne to form the ylide $[CH_2C(P^iPr_3)CHPPh_3]$ **58** (Scheme 4-16). Mutually coupled doublets for **58** were observed in the ^{31}P-NMR spectrum at δ 40.7 and 12.1 ($^3J_{PP}$ = 55.5 Hz) (comparable to that observed for ylide **56**). In the ^{1}H-NMR spectrum the geminal alkene protons are found at δ 4.10 (J_{PH} = 18.6 Hz) and 4.49 (J_{PH} = 43.6 Hz) which again supports formation of the ylide species **58**. The ylide proton is obscured by the isopropyl resonances, but 2D experiments have suggested it appears at δ 2.15, as expected through comparison to compound **55**. The ESI-MS of this reaction mixture exhibited a large peak at *m/z* 461.2515, the mass expected for **58**. This rapid addition of P^iPr_3 to **39c** means that the desired vinylidene complex could not be synthesised.

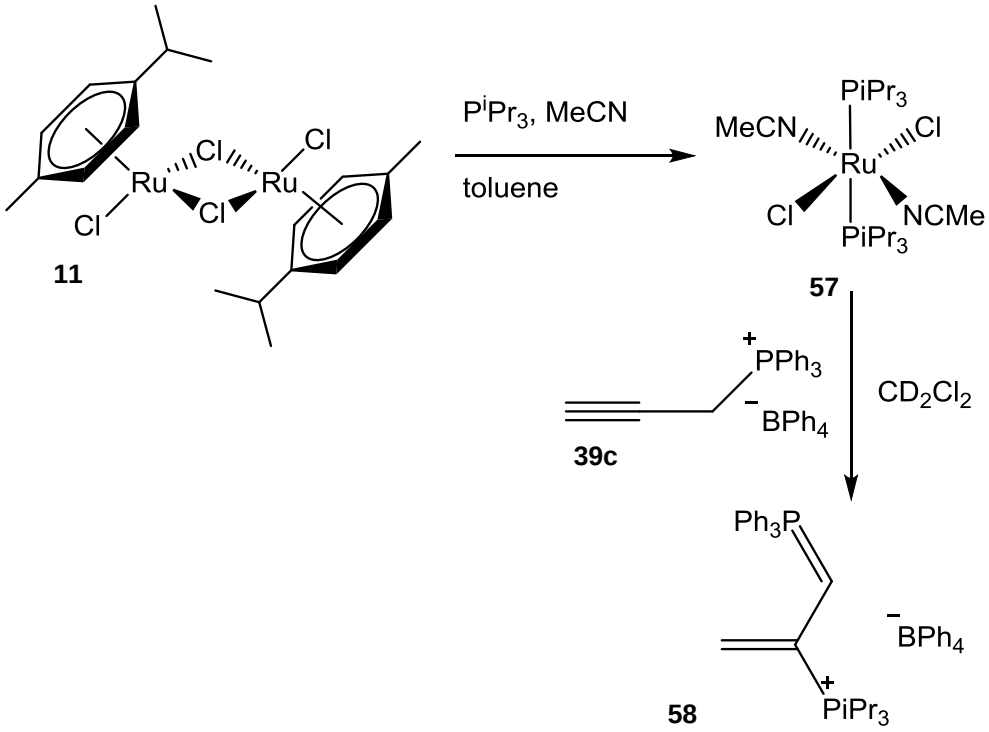

Scheme 4-16 Reaction of Alkyne **39c** with Complex **57**

Compound **58** was independently synthesised in order to confirm the assignment (Scheme 4-17). Unfortunately no crystals suitable for X-Ray diffraction could be grown, but full NMR, IR and MS data were obtained. The data matched that observed during reaction of alkyne **39c** with complex **57**, and the ylide proton could be clearly observed as a doublet of doublets of doublets (ddd) at δ 2.13 (J_{PH} = 15.0 Hz, J_{PH} = 12.0 Hz, $^3J_{HH}$ = 2.3 Hz).

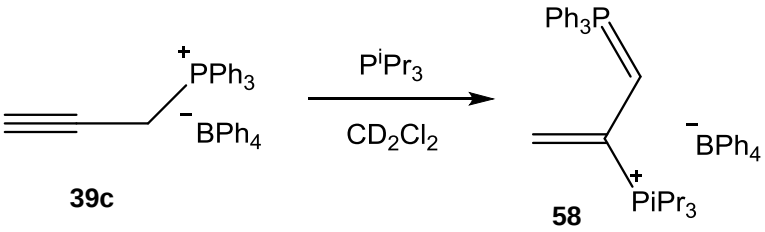

Scheme 4-17 Formation of Ylide **58**

4.4.3 Synthesis of a Rhodium Allene 60 and Vinylidene 63

The rhodium dimer $[Rh(\mu^2\text{-}Cl)(P^iPr_3)_2]_2$ **59** is known to be highly reactive towards alkynes and the mechanism of vinylidene formation is well-understood.[76, 77, 85-87] Reactions generally take several hours to reach completion at room temperature and are known to begin with the binding of the alkyne to the metal centre in an η^2-fashion (**A** in Scheme 4-18). The terminal proton then migrates to the metal leading to the formation of an alkynyl hydride species **B**, a further hydrogen migration then completes the isomerisation to the vinylidene complex **C**. In the example shown below Werner et al. were able to isolate the alkynyl hydride complex and show that it was then converted through to the vinylidene complex (Scheme 4-18).[76, 77]

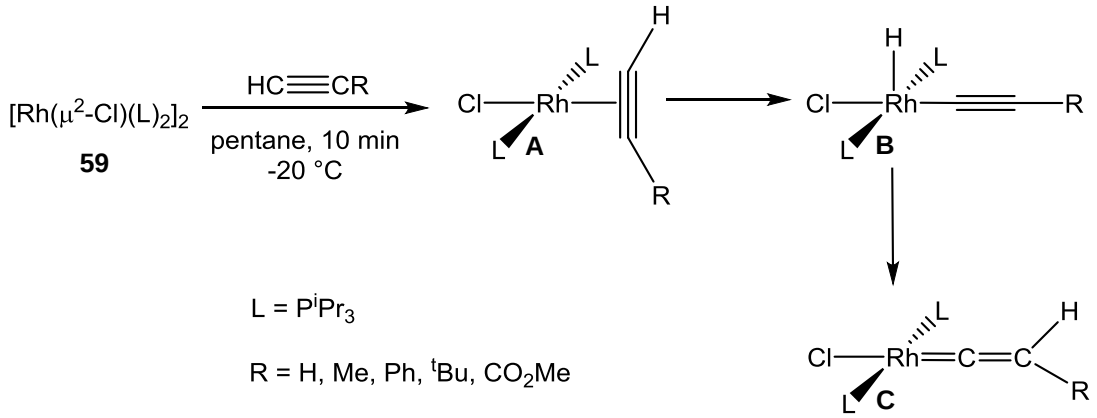

Scheme 4-18 Isolation of an Alkynyl Hydride Species and Subsequent Conversion to a Vinylidene Complex

With the reaction of $[HC{\equiv}CCH_2PPh_3][BPh_4]$ **39c** and $[Rh(\mu^2\text{-}Cl)(P^iPr_3)_2]_2$ **59** the order of addition was found to be very important, greatly affecting the product distribution. Addition of $[HC{\equiv}CCH_2PPh_3][BPh_4]$ **39c** to a THF solution of $[Rh(\mu^2\text{-}Cl)(P^iPr_3)_2]_2$ **59**, or addition of $[Rh(\mu^2\text{-}Cl)(P^iPr_3)_2]_2$ **59** to a THF solution of $[HC{\equiv}CCH_2PPh_3][BPh_4]$ **39c** lead to clean formation of allene complex **60** (Scheme 4-19). This was observed in the ^{31}P-NMR spectrum as a doublet of triplets at δ 8.24 ($^3J_{PRh}$ = 12.2 Hz, $^4J_{PP}$ = 2.1 Hz, PPh_3), and a doublet of doublets at δ 34.75 ($^1J_{PRh}$ = 111.9 Hz, $^4J_{PP}$ = 2.1 Hz, P^iPr_3). The quaternary allene carbon resonance was observed at δ 210.7 in the ^{13}C-NMR spectrum which displayed a characteristic rhodium-carbon coupling of 26.5 Hz).[234, 235] A band was also observed in the IR spectrum for the allene group at 1653 cm^{-1}.

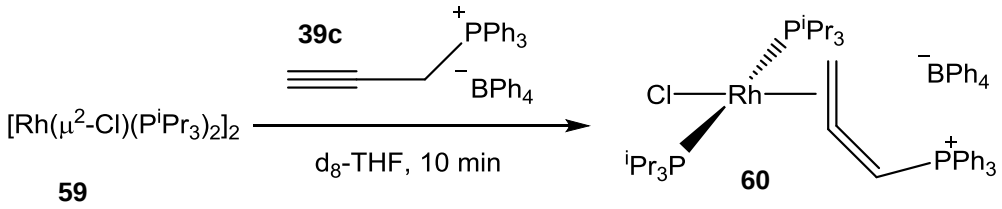

Scheme 4-19 Synthesis of Rhodium Allene **60**

However, if **59** and **39c** were mixed before being dissolved in THF then the initial reaction mixture was found to be a mixture of allene complex **60** and alkyne complex **61** (Scheme 4-20). The reaction was followed by ^{1}H and ^{31}P-NMR spectroscopy and the resonances assigned by comparison to data reported by Dr Michael Cowley for the [RhCl(C=C=C{H}Ur)(P^{i}Pr$_3$)$_2$] (Ur = uracil).[236] Alkyne complex **61** was observed as two doublets in the ^{31}P-NMR spectrum displaying coupling to rhodium at δ 12.4 (J = 9.83 Hz, PPh$_3$) and at δ 34.4 (J = 114.6 Hz, P^{i}Pr$_3$). Whilst the allene complex then remains unchanged, resonances for the alkyne **61** are found to bleach in favour of resonances assigned to alkynyl hydride complex **62** observed as a hydride resonance at δ -29.83 (br d, J_{RhH} = 48.4 Hz) in the ^{1}H-NMR spectrum. At this point a further hydride resonance was observed at δ -20.34 (dt, J_{RhH} = 22.2 Hz, J_{PH} = 12.0 Hz) along with a corresponding P^{i}Pr$_3$ resonance in the ^{31}P-NMR spectrum at δ 42.38 (d, J_{RhP} = 121.7 Hz). Comparison with data reported by Werner et al*.* suggests that this corresponds to an octahedral species with a solvent molecule coordinated *trans* to the hydride ligand such as [RhCl(C≡CC{H}CH$_2$PPh$_3$)H(Sol)(P^{i}Pr$_3$)$_2$].[237, 238]

These resonances reduced in intensity in favour of those for the vinylidene complex **63** (Scheme 4-20), which in the ^{31}P-NMR spectrum were seen as a triplet at δ 20.9 ($^{4}J_{PP}$ = 3.4 Hz, PPh$_3$) and a doublet of doublets at δ 43.2 ($^{1}J_{PRh}$ = 132.1 Hz, $^{4}J_{PP}$ = 3.4 Hz, P^{i}Pr$_3$). The ratio of allene to vinylidene complex observed varied enormously, from a maximum of ca. 37% vinylidene (by ^{31}P-NMR) to just 2% in other repeats. The ~7 hours required for vinylidene formation in these rhodium systems is in contrast to the instantaneous reactivity observed in the reaction of **1** with alkynes. This is due to a difference in mechanism, with LAPS being accessible to the acetate-containing ruthenium system.[174]

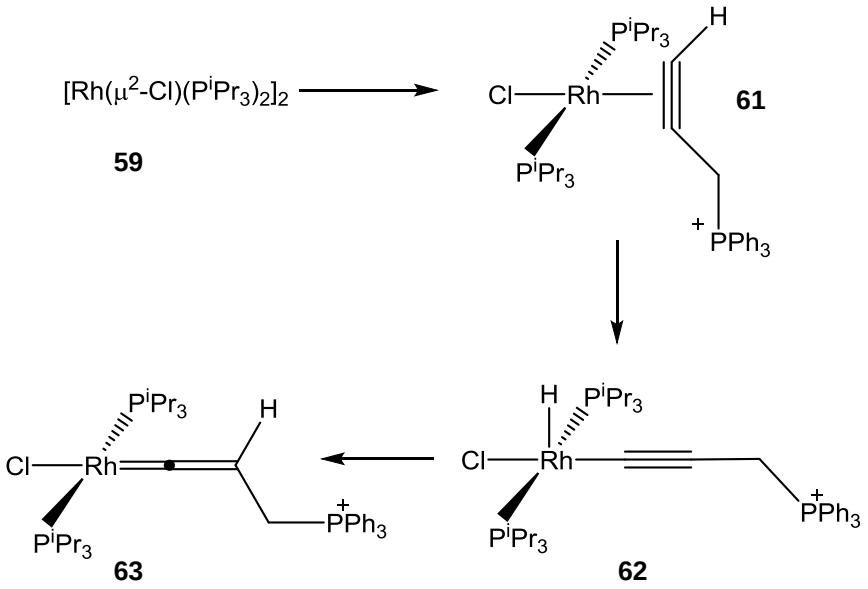

Scheme 4-20 Rhodium Vinylidene Formation Mechanism

The mechanism of this system has been probed via DFT and the calculations carried out by Dr Jason Lynam. Calculations were performed with the Turbomole program; initial geometry optimisations and frequency calculations were performed at the BP86/SV(P) level and subsequent single point energies at pbe0/def2-TZVPP(with COSMO THF solvent correction).[211-220] It was found that formation of the allene complex **60** is thermodynamically favoured over formation of the alkyne complex **61**, with the difference in free energy at 298 K (ΔG_{298K}) being 75 kJ mol^{-1} in favour of allene **60**. Therefore experimental observation of the formation of the alkyne complex **61** suggests that this reaction is under kinetic control. If the reaction was under thermodynamic control, ΔG_{298K} could be used to calculate the equilibrium constant for the interconversion of **60** and **61**. The result of this (K =1.4 x 10^{13}) shows that the reaction would produce essentially only allene complex **60** and therefore no alkyne **61** would be observed.

Once alkyne complex **61** has been formed, the subsequent formation of vinylidene complex **63** is thermodynamically favourable (ΔG_{298K} = -49 kJ mol^{-1})(Figure 4-18). At the time of writing, the transition state between the alkyne complex **61** and alkynyl hydride **62** (**TS_{61-62}**) had not been located. However, a high-energy transition state was found for the subsequent transformation of **62** into the vinylidene **63** (**TS_{62-63}** = +136 kJ mol^{-1}) and therefore it is assumed that this is the rate determining step. This view is supported by comparison with the literature; Lynam has compared the potential energy surfaces in the formation of 18 Rh-vinylidene systems and in all cases the alkynyl hydride to vinylidene transformation is found to have the highest barrier.[58] The highest reported barrier is 130 kJ mol^{-1}(for the formation of [RhCl(PMe_3)(=C=CH_2][87]) and highlights just how high the barrier calculated for **TS_{62-63}** is.

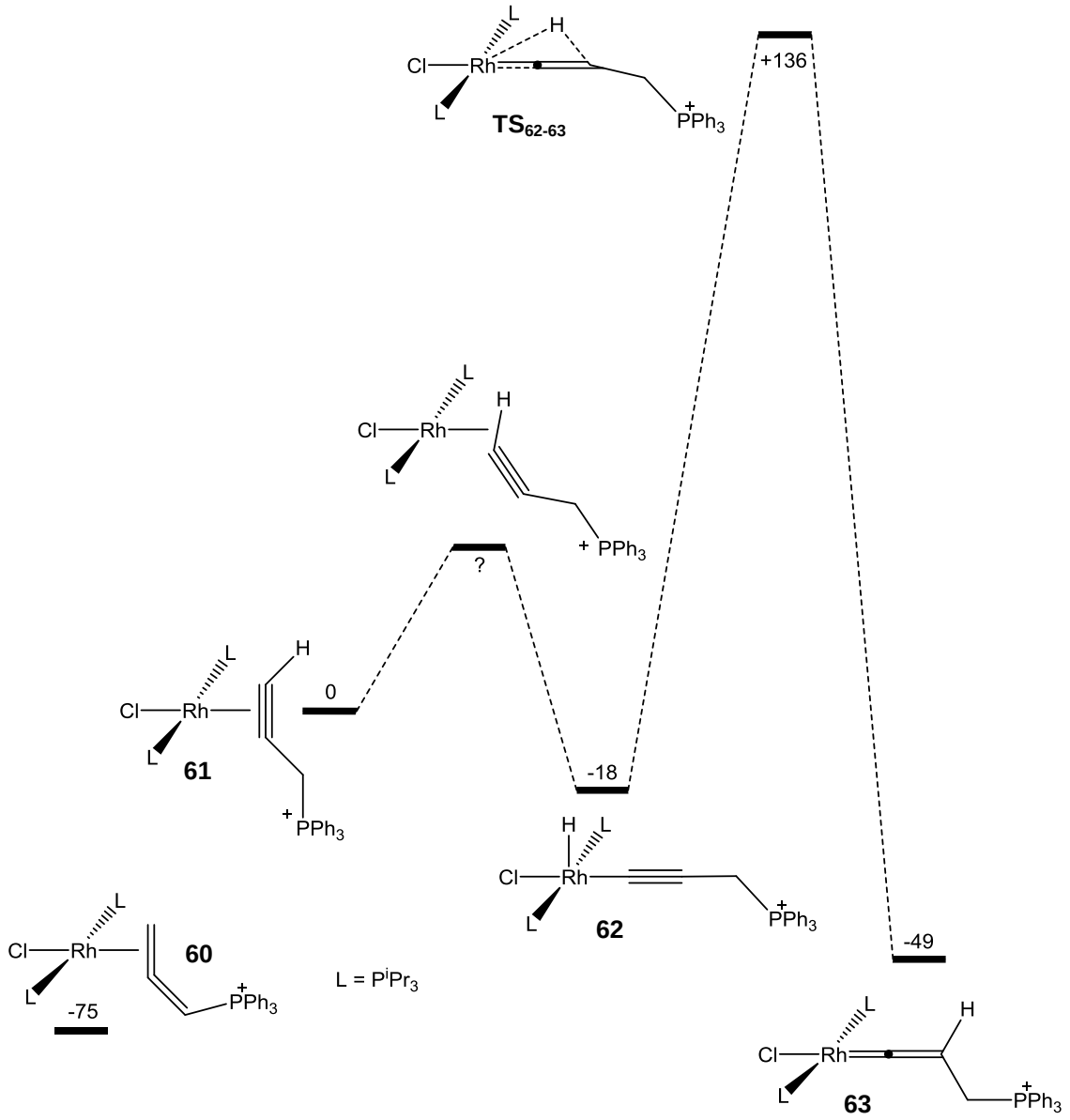

Figure 4-18 Potential Energy Surface Showing the Formation of Vinylidene **63** via Alkyne Complex **61** and Alkynyl Hydride **62**, Free Energies are Shown in kJ mol^{-1}. Allene Complex **60** is Shown for Reference.

Whilst vinylidene complex **63** could not be isolated, it was possible to observe the important resonances in the NMR spectra. The vinylidene proton was observed at δ 0.39 in the ^{1}H-NMR spectrum which is characteristic for a rhodium vinylidene.[238] The CH_2 resonance at δ 4.46 displayed coupling to both phosphorus environments and to the CH proton (ddt, $^{2}J_{PH}$ = 13.1 Hz, $^{3}J_{HH}$ = 6.3 Hz, $^{5}J_{PH}$ = 2.0 Hz). There were also characteristic resonances observed in the ^{13}C-NMR spectrum with the vinylidene α-carbon at δ 283.1, the β-carbon as a doublet due to rhodium coupling at δ 94.0 ($^{2}J_{RhC}$ = 15.5 Hz) and the γ-carbon at δ 8.3 which was split by the triphenylphosphine ($^{1}J_{PC}$ = 52.6 Hz). The slow diffusion of pentane into a THF solution of this reaction mixture lead to the growth of three types of crystals. Large yellow plates were found to be either just the allene isomer **60** (Figure 4-19), or a co-crystal containing both the allene and

vinylidene isomers (Figure 4-20 and Figure 4-21). Small blue crystals (which are presumably the vinylidene **63**) were found to be too small to diffract, despite being sent to the synchrotron at Diamond. The data presented in Figure 4-19 were collected at the National Crystallography Service in Southampton.

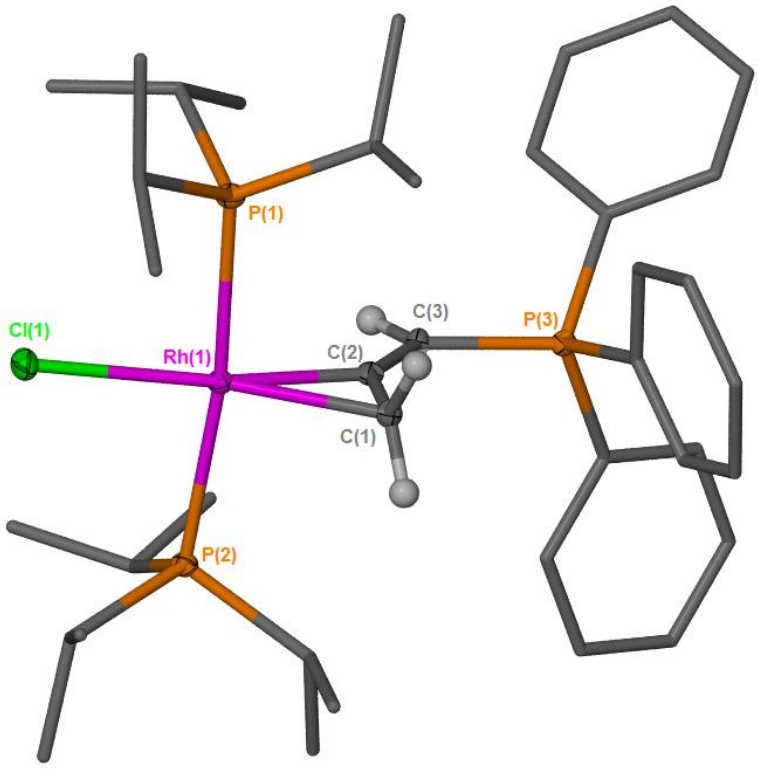

Figure 4-19 ORTEP Representation of Complex **60**; Thermal Ellipsoids, where shown, are at 50% Probability, Hydrogen Atoms, Solvent Molecules and the Counter Ion have been Omitted for Clarity.

Table 4-8 Selected Bond Lengths and Angles for Complex **60**

Bond	Bond Length (Å)	Angle	Bond Angle (°)
C(1) – Rh(1)	2.102(2)	C(1) – Rh(1) – Cl(1)	160.53(6)
C(2) – Rh(1)	1.972(2)	C(2) – Rh(1) – Cl(1)	159.59(6)
C(1) – C(2)	1.394(3)	C(1) – Rh(1) – P(2)	94.69(6)
C(2) – C(3)	1.341(3)	C(2) – Rh(1) – P(2)	93.78(6)
C(3) – P(3)	1.767(2)	C(1) – Rh(1) – C(2)	39.85(8)
Cl(1) – Rh(1)	2.3536(6)	Cl(1) – Rh(1) – P(2)	86.37(2)
P(1) – Rh(1)	2.3750(5)	P(1) – Rh(1) – P(2)	172.518(19)
P(2) – Rh(1)	2.3686(5)	C(3) – C(2) – C(1)	145.5(2)
		P(3) – C(3) – C(2)	123.43(15)

Complex **60** adopts a distorted square planar geometryin the solid state, with the P^iPr_3 found to be bent back from the allene ligand slightly (P(1)–Rh(1)–P(2) = 172.518(19)°) presumably due to steric clashes with the PPh_3 group. The bound allene double bond is predictably longer (C(1)-C(2) = 1.394(3) Å) than the unbound one (C(2)-C(3) = 1.341(3) Å), and longer than the C=C bonds in the free allene structure (C(1)-C(2) = 1.3025(18) Å, C(2)-C(3) = 1.294(2) Å). This is due to back-bonding from the metal centre into the π* orbital of the allene and more detail can be found in Chapter 1. Evidence for this back-bonding is also seen in the non-linear nature allene moiety with the non-bonded alkene bent away from the metal centre (C(3)–C(2)–C(1) = 145.5(2)°). This type of bonding was also observed in the structural data for ruthenium allene complex **45a**. Comparison between the two structures showed that they were remarkably similar and therefore the $[RhCl(P^iPr_3)_2]$ and $[Ru(\kappa^2\text{-}OAc)_2(PPh_3)_2]$ fragments must provide similar environments for the stabilisation of allene ligands.

One other rhodium phosphino-allene complex has been synthesised previously, $[Rh(acac)\{\eta^2\text{-}CH(PCy_3)=C=CPh_2\}(PCy_3)][BF_4]$, although in that case the allene was bound to the metal through the 1,2-double bond.[234] Despite this, the structural characterisitcs are very similar (Rh-C(1) 2.130(7) Å, Rh-C(2) 1.969(7) Å, C(1)-C(2) 1.401(10) Å, C(2)-C(3) 1.344(10) Å). Werner has reported many rhodium allene complexes, and has also observed formation of similar mixtures of allene and vinylidene isomers. In his case treatment of the acetylide $[RhCl(C{\equiv}CCO_2Et)(P^iPr_3)_2][NBu_4]$ with methyl iodide gave a mixture of the allene complex $[RhCl(\eta^2\text{-}H_2C=C=C\{H\}CO_2Et)(P^iPr_3)_2]$ and the vinylidene $[RhCl(=C=C\{H\}CO_2Et)(P^iPr_3)_2]$ (Scheme 4-21).[239] The structural characterisation of this rhodium allene complex (Rh-C(1) = 2.120(5) Å, Rh-C(2) = 1.991(5) Å, C(1)-C(2) = 1.390(7) Å, C(2)-C(3) =1.338(7) Å) compared well with the two phosphine-substituted allene complexes, suggesting that the presence of the PPh_3 substituent has little effect on the bonding.

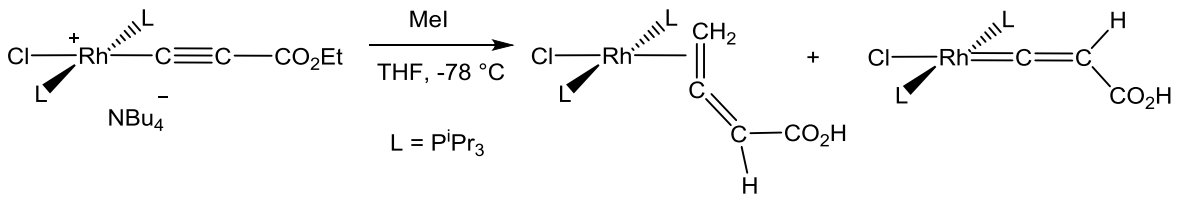

Scheme 4-21 Literature Formation of a Vinylidene Allene Mixture

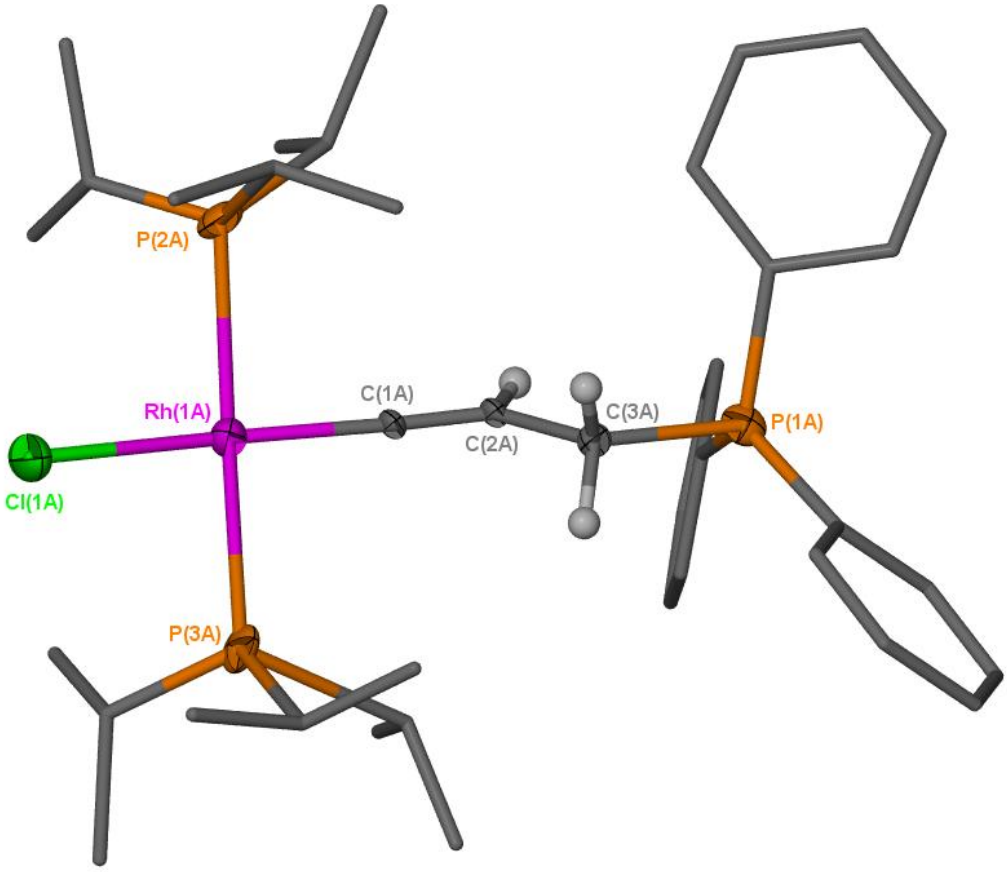

Figure 4-20 ORTEP Representation of Complex **63**; Thermal Ellipsoids, where shown, are at 50% Probability, Hydrogen Atoms, and the Counter Ion have been Omitted for Clarity. This is the Minor (ca. 15%) Component.

Table 4-9 Selected Bond Lengths and Angles for Complex **63**

Bond	Bond Length (Å)	Angle	Bond Angle (°)
C(1a) – Rh(1a)	1.866(18)	C(1a) – Rh(1a) – Cl(1a)	171.1(6)
C(1a) – C(2a)	1.15(2)	C(1a) – Rh(1a) – P(2a)	88.2(5)
C(2a) – C(3a)	1.47(3)	Rh(1a) – C(1a) – C(2a)	176.9(17)
C(3a) – P(1a)	1.77(2)	Cl(1a) – Rh(1a) – P(2a)	92.5(3)
Cl(1a) – Rh(1a)	2.367(7)	P(3a) – Rh(1a) – P(2a)	178.7(3)
P(3a) – Rh(1a)	2.346(9)	C(3a) – C(2a) – C(1a)	126.8(19)
P(2a) – Rh(1a)	2.409(14)	P(1a) – C(3a) – C(2a)	118.1(14)

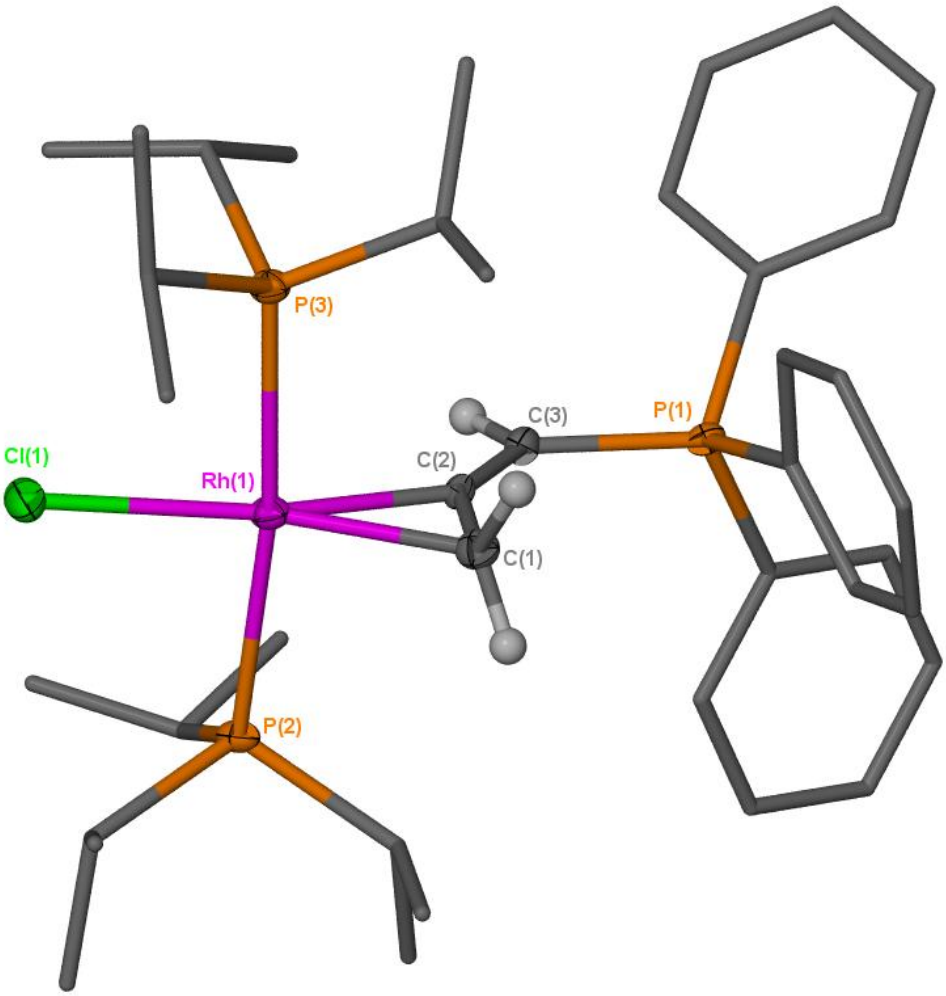

Figure 4-21 ORTEP Representation of Complex **60**; Thermal Ellipsoids, where shown, are at 50% Probability, Hydrogen Atoms, and the Counter Ion have been Omitted for Clarity. This is the Major (ca. 85%) Component.

Table 4-10 Selected Bond Lengths and Angles for Complex **60**

Bond	Bond Length (Å)	Angle	Bond Angle (°)
C(1) – Rh(1)	2.096(3)	C(1) – Rh(1) – Cl(1)	160.34(7)
C(2) – Rh(1)	1.965(3)	C(2) – Rh(1) – Cl(1)	159.38(8)
C(1) – C(2)	1.402(4)	C(1) – Rh(1) – P(2)	94.43(8)
C(2) – C(3)	1.47(3)	C(2) – Rh(1) – P(2)	93.72(8)
C(3) – P(1)	1.770(3)	C(1) – Rh(1) – C(2)	40.24(10)
Cl(1) – Rh(1)	2.3510(9)	Cl(1) – Rh(1) – P(2)	86.54(4)
P(3) – Rh(1)	2.3744(10)	P(3) – Rh(1) – P(2)	172.65(5)
P(2) – Rh(1)	2.3627(18)	C(3) – C(2) – C(1)	145.8(3)
		P(1) – C(3) – C(2)	123.1(2)

The allene component **60** of the co-crystal is essentially identical to that seen in the pure crystal (Figure 4-19). The vinylidene **63** component displayed the square planar

geometry expected for complexes of this type and the vinylidene moiety is approximately linear with Rh(1a) – C(1a) – C(2a) = 176.9(17)°. The bond lengths however compare less well with those previously reported by Werner $[RhCl(C=C=C\{H\}Me)(P^iPr_3)_2]$[80] and Lynam $[RhCl(C=C=C\{H\}Ur)(P^iPr_3)_2]$ (Ur = uracil).[240] The Rh-C bond length was found to be slightly longer than that observed in the two literature complexes with the bonds being 1.866(18) Å for **63**, 1.791(3) Å for Lynam's Ur complex and 1.775(6) Å for Werner's methyl analogue. The C(1)-C(2) bond length was significantly shorter than the corresponding literature bond lengths (1.15(2) Å for **63**, 1.319(4) Å for the Ur complex and 1.32(1) Å for the methyl analogue).

The structural metrics were compared with two analogous acetylide complexes reported by Werner, $[Rh(C{\equiv}CC(Ph)_2OPh)(CO)(P^iPr_3)_2]$[241] and $[RhH(C{\equiv}CC^iPr_2OH)_2(P^iPr_3)_2]$.[242] It can be seen that the Rh-C bond length of **63** (1.866(18) Å) is shorter than the acetylide complexes bond lengths of 2.037(4) Å being reported for the mono-acetylide, and 2.032(4) Å and 2.022(4) Å for the *bis*-acetylide complex. This suggests that there is significant double bond character, in line with the vinylidene structure. The C(1)-C(2) bond length (1.15(2) Å) of **63** was found to fall within the range observed for the acetylide complexes (1.205(5) Å for the mono-acetylide, 1.206(4) Å and 1.203(4) Å for the *bis*-acetylide) suggesting that this structure can be viewed as a vinylidene with acetylide character (Figure 4-22). This is corroborated by the ^{13}C-NMR data in which the α-carbon resonance observed for **63** is typical for a vinylidene (δ 283.1) whereas, in the acetylide complexes, the α-carbon resonances are observed at δ 127.0 and δ 114.8 respectively.

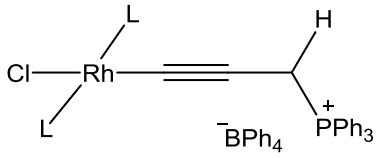

Figure 4-22 A Possible Rhodium Acetylide Complex

4.4.4 A Summary of the Isomerisation of Alkyne 39 to Allene 40

The isomerisation of propargylic alkynes to their allene isomers is a well-studied phenomenon and the generally accepted synthetic methods involving the use of strong base.[31, 233, 243] The phosphine-substituted propargylic alkyne $[HC{\equiv}CCH_2PPh_3]^+$ **39** has been observed by Hill to undergo spontaneous rearrangement to the allene $H_2C=C=CHPPh_3]^+$ **40**. The initial work involved reaction of alkyne **39** with organometallic species, leading to the formation of transition metal allene complexes (Scheme 4-5) and the isomerisation was therefore declared to be metal-mediated.[31, 32] However, subsequent investigations found that alkyne **39** isomerised to allene **40** on

standing in solution. This transformation was found to be highly solvent dependent and a small solvent screen was undertaken. No conversion was observed at all in CD_3CN and the half-life of conversion of **39** to **40** in $CDCl_3$ was found to be ~72 hours. With the use of anhydrous THF, the half-life dropped to ~60 minutes and in "benchtop" grade THF the conversion was complete within 60 minutes. As a result it was then suggested that the presence of water in the systems could lead to acid/base catalysis of the rearrangement. Theoretical calculations (using (RI-)PBE0/def2-TZVPP SCF) were also carried out and they showed that the allene isomer **40** is 27 kJ mol^{-1} more stable that the alkyne isomer **39** in the gas phase.[32]

This thermodynamic trend was confirmed in Section 4.3.5, and in Section 4.3.3 the effect of the counter ion on this isomerisation was investigated. The identity of the counter ion was found to have a large influence over the conversion from alkyne to allene, with faster reaction rates observed for more coordinating ions such as bromide. The more coordinating counter ions were also found to influence chemical shifts in ^{1}H-NMR spectra, suggesting that in solution the is a relatively strong ion pair interaction. This lends further weight to Hill's theory that external species such as halide ions or water maybe promoting the isomerisation.

In favour of the metal-mediated theory an enhancement in the rate in the reaction of alkyne **39** with ruthenium and rhodium complexes, over the metal free isomerisation reactions has been observed in these studies. However, the exact cause of this has not been established and it possible that the proton migration is being assisted by free acetate or chloride in the system.

However, further evidence against the rearrangement being metal-mediated was obtained though the observed product ratios in the reactions of alkyne **39** with the ruthenium and rhodium precursors reported in Sections 4.3 and 4.4.3 respectively. As reported by Hill, rearrangement to form the allene complex was observed in every case; but, alongside this, the vinylidene complexes were obtained in many cases. The ratio of products (allene and vinylidene complexes) formed varied enormously, suggesting that the isomerisation is not a simple metal-mediated process.

The fact that the vinylidene complexes are formed at all is the most compelling evidence against a metal-mediated process. No evidence for the rearrangement of the vinylidene complexes to their corresponding allenes was obtained, despite theoretical calculations showing the allene to be the thermodynamically most stable isomer. Therefore the vinylidene complex cannot be an intermediate in the metal-mediated isomerisation of the alkyne to the allene.

It would appear that coordination to a transition metal halts the isomerisation process, with the final ratio between the complexes merely representing the ratio of free allene **40** and alkyne **39** present in solution at the point of coordination.

4.5 Reactions of the Free Allene

4.5.1 Background

It was decided to investigate the reactivity of phosphino-allene **40** as very little data were present in the literature. It is known that this compound behaves like other allenes with electron-withdrawing substituents and is susceptible to nucleophilic attack at the central carbon.[232] It has been shown to react with protic nucleophiles such as amines in this manner with simple addition across the 1,2-double bond. When reacted with aprotic nucleophiles, such as phosphines a similar product is obtained but it is assumed that this proceeds via an unstable ylide species which then gains a proton from the reaction medium.[233] In Section 4.4.2 we have been able to shown that this is indeed the case and have presented evidence for the ylide intermediate **56**. We have also shown that in the case of triisopropylphosphine the ylide **58** is long lived.

With this knowledge it was decided to expand the known chemistry of allene **40** in the hope of forming some interesting and useful compounds. It was also hoped that the triphenylphosphine would prove to be a good leaving group, opening up the possibility for facile substitution chemistry.

4.5.2 Attempted Synthesis of a Phosphino-Enyne

The addition of phenylacetylene to form a phosphino-enyne **64** (Scheme 4-22) was investigated. Enynes are considered to be of great interest due to their presence in natural products with promising biological activity[244-246] and for their potential uses in electronic and photonic materials.[247]

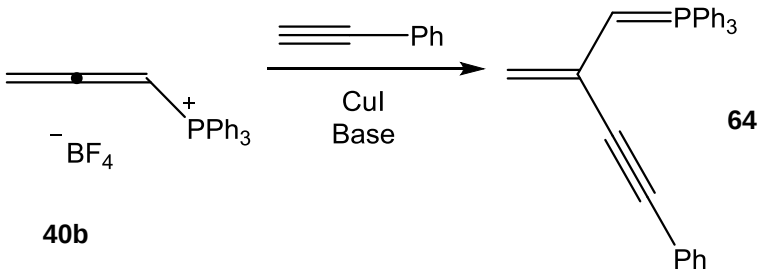

Scheme 4-22 Intended Enyne Formation

Phenylacetylene was added to a CD_2Cl_2 solution of allene **40b** and the reaction mixture monitored by NMR spectroscopy. No reaction was observed with just the allene and

alkyne, addition of copper iodide as catalyst for acetylide formation did not induce any reaction either. In an attempt to promote copper-acetylide formation, diisopropylamine was added as a base and an instant colour change from colourless to brown was observed, along with evidence in the NMR spectra of a selective reaction to form one species at δ 6.0 in the ^{31}P-NMR spectrum. The same reaction was observed if just diisopropylamine was added to a solution of **40b**. It became apparent that the diisopropylamine was adding to the central allene carbon in much the same way as previously reported in the literature.[233] No evidence for a reaction with phenylacetylene was observed. When the reaction was followed by NMR spectroscopy it was found that initial formation of a species at δ 6.0, **65** was observed in the ^{31}P-NMR spectrum. The resonance for this species was then found to reduce in intensity in favour of a species at δ 15.8, **66** (and phosphine oxide) with time, and this transformation was found to be faster in the presence of excess base.

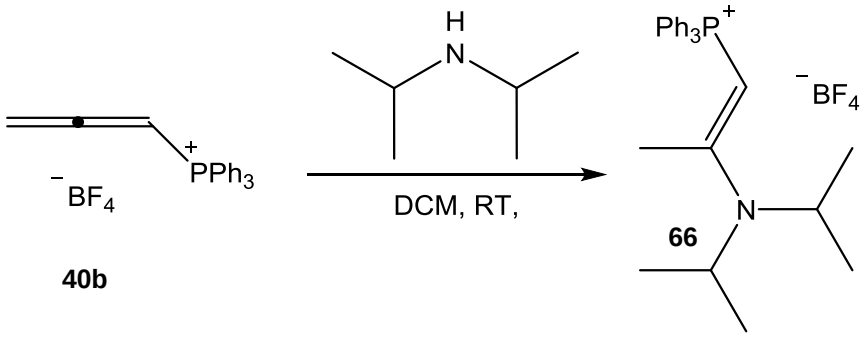

Scheme 4-23 Formation of Amine Addition Product **66**

Crystals of $[CH_3C(N(^iPr)_2)CHPPh_3][BF_4]$ **66** were obtained by layering DCM solutions of **65** with either toluene or pentane (Figure 4-23). The structural data for **66** shows the presence of the alkene with a short bond between C(1) and C(2) of 1.388(3) Å. In comparison the bond length between C(2) and C(3) was found to be 1.506(3) Å, which is representative of a single C-C bond length.

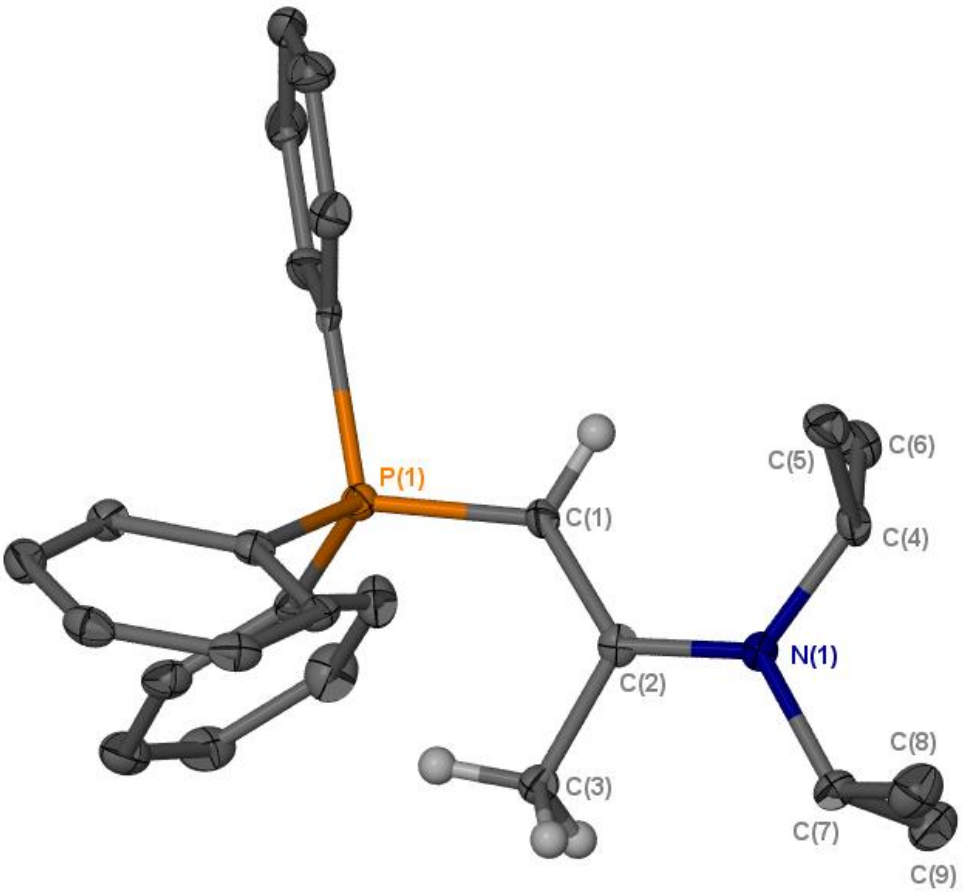

Figure 4-23 ORTEP Representation of Compound **66**; Thermal Ellipsoids, where shown, are at 50% Probability, Hydrogen Atoms (except those on the main scaffold) and the Counter Ion have been Omitted for Clarity.

Table 4-11 Selected Bond Lengths and Angles for Compound **66**

Bond	Bond Length (Å)	Angle	Bond Angle (°)
P(1) – C(1)	1.741(2)	P(1) – C(1) – C(2)	126.4(2)
C(1) – C(2)	1.388(3)	C(1) – C(2) – C(3)	118.9(2)
C(2) – C(3)	1.506(3)	C(1) – C(2) – N(1)	123.6(2)
C(2) – N(1)	1.346(3)	C(3) – C(2) – N(1)	117.54(19)
N(1) – C(4)	1.488(3)	C(2) – N(1) – C(4)	123.66(19)
N(1) – C(7)	1.492(3)	C(2) – N(1) – C(7)	121.6(2)
		C(4) – N(1) – C(7)	114.71(19)

The same crystals were obtained at any stage of the reaction. This enabled isolation of analytically pure material and allowed for full characterisation of this species (where the resonances of this species were observed at δ 15.8 in the ^{31}P-NMR spectra for

complex **66**). Importantly a methyl resonance was observed in the ^{1}H-NMR spectrum at δ 1.91 and a doublet at δ 3.98 which was assigned to the CH group ($^{2}J_{PH}$ = 14.1 Hz). The ^{13}C-NMR resonances all displayed phosphorus coupling with the methyl observed at δ 25.0 ($^{3}J_{PC}$ = 7.2 Hz), the methine at δ 62.2 ($^{1}J_{PC}$ = 122.4 Hz), and the central quaternary carbon observed as a broad resonance at δ 164.1.

The identity of the species observed in the ^{31}P-NMR spectrum at δ 6.0, **65** remains unknown and it's only known feature is a large doublet at δ 2.6 (J_{PH} = 4.6 Hz) in the ^{1}H-NMR which displayed a cross-peak in the ^{1}H-^{31}P HSQC spectrum. The corresponding resonance in the ^{13}C-NMR spectrum was at δ 7.4 (J_{PC} = 3.8 Hz) and was shown by a DEPT experiment to be a CH_2.

This species at δ 15.8 **66** in the ^{31}P-NMR spectrum could be transformed back to the species at δ 6.0 **65** by addition of $HBF_4.EtO_2$, suggesting that two could be related by a simple protonation-deprotonation mechanism. A crystal structure of the imine $[CH_3C(N(^{i}Pr)_2)CH_2PPh_3][BF_4]_2$ **67** was obtained during one of these reactions but no evidence has been obtained to directly relate it to the species at δ 6.0 **65**. When the crystals of **67** were subsequently analysed they were found to give NMR and MS data matching **66**.

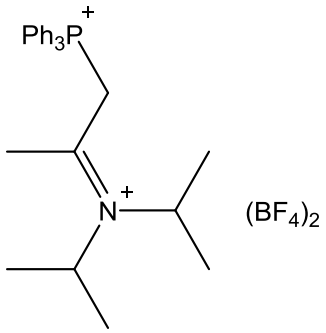

Figure 4-24 Imine **67** Isolated as Crystals

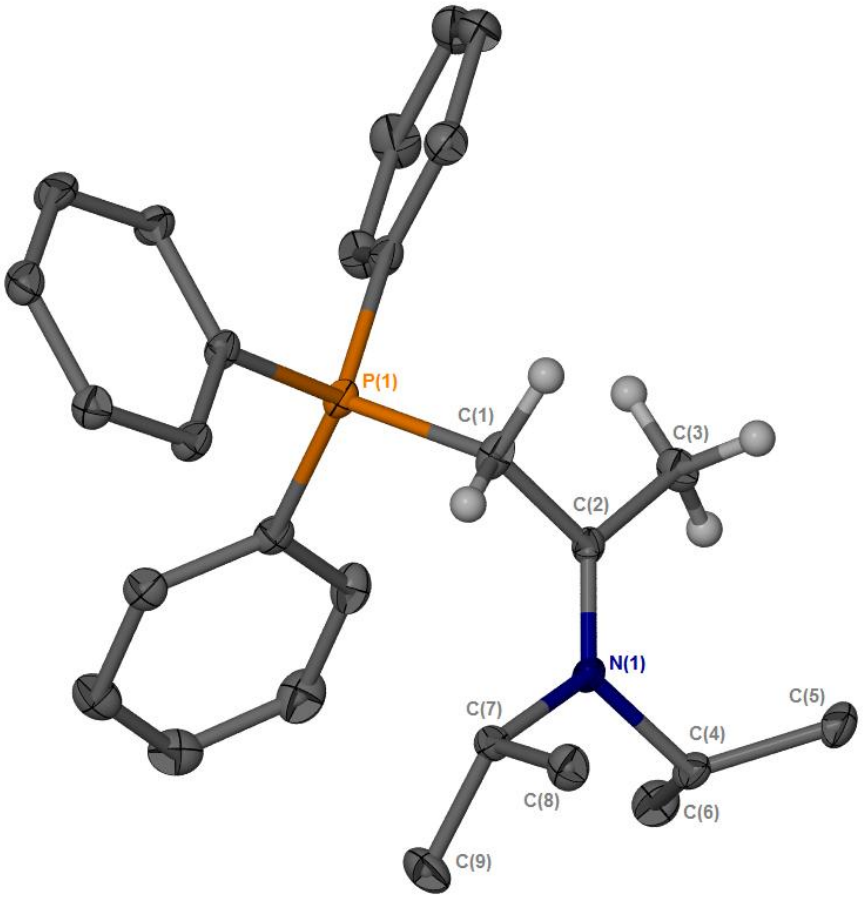

Figure 4-25 ORTEP Representation of Compound **67**; Thermal Ellipsoids, where shown, are at 50% Probability, Hydrogen Atoms (except those on the main scaffold), and the Counter Ions have been Omitted for Clarity. Only One Position for the Disordered Imine Moiety has been Shown.

Table 4-12 Selected Bond Lengths and Angles for Compound **67**

Bond	Bond Length (Å)	Angle	Bond Angle (°)
P(1) – C(1)	1.8391(14)	P(1) – C(1) – C(2)	115.24(10)
C(1) – C(2)	1.5063(19)	C(1) – C(2) – C(3)	113.85(12)
C(2) – C(3)	1.4939(18)	C(1) – C(2) – N(1)	120.57(13)
C(2) – N(1)	1.280(2)	C(3) – C(2) – N(1)	125.56(13)
N(1) – C(4)	1.520(2)	C(2) – N(1) – C(4)	124.17(14)
N(1) – C(7)	1.516(2)	C(2) – N(1) – C(7)	121.89(14)
		C(4) – N(1) – C(7)	113.68(15)

The crystal structure of **67** exhibited the presence of the imine moiety through a shortening of the C(2) to N bond length (1.280(2) Å versus 1.349(3) Å in **66**). The two C-C bonds were much more equal in length (C(1) – C(2) = 1.5063(19) Å and C(2) – C(3) = 1.4939(18) Å) with the relatively long bonds showing a single bond order.

Scheme 4-24 summarises the amine addition reactivity discussed in this section. Schweizer et al. have reported the addition of many amines to triphenylpropargylphosphonium bromide **39a** and have observed an equilibrium between the enamine **66** and imine **67**.[243] The data reported for the enamines matches that observed here for **66**, however the data reported for the imines (^{31}P-NMR shift range δ 20.3 - 22.5) suggests that **67** is not species **65** which was observed at δ 6.0 in the ^{31}P-NMR spectrum.

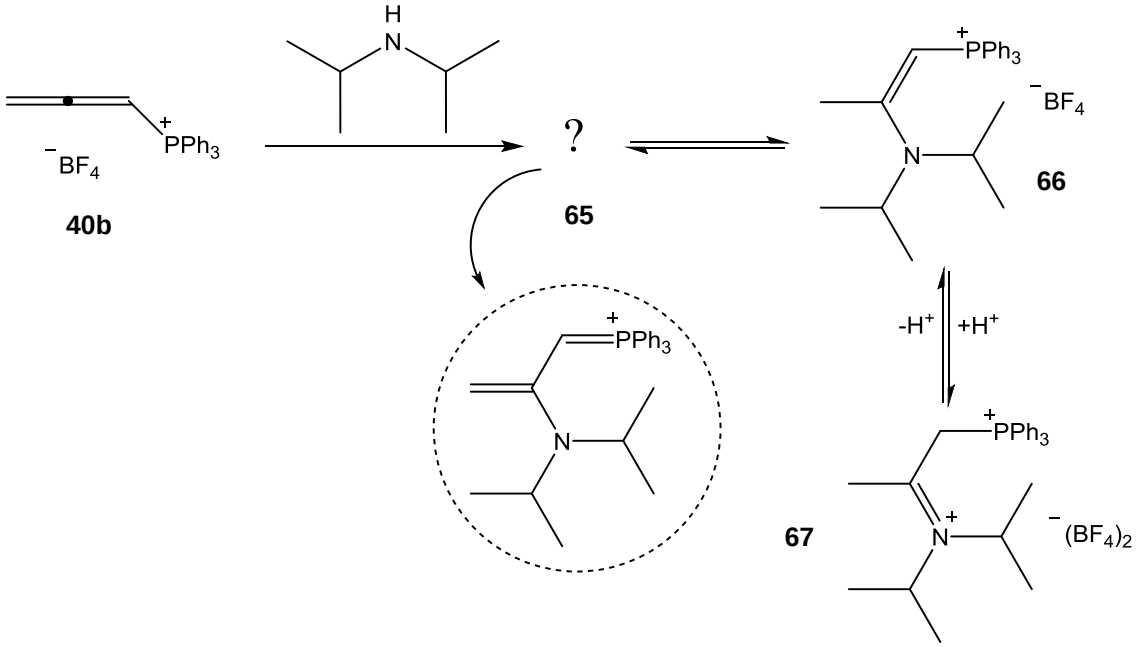

Scheme 4-24 Amine Addition Products

The logical identity of **65,** as postulated by Schweizer,[243] is the unsaturated ylide shown in the centre of Scheme 4-24, formed from the direct addition of deprotonated diisopropylamine to the central carbon of allene **40**. This does not however, allow for the observation that addition of acid to compound **66** leads to the formation of **65**.

4.5.3 Attempted Synthesis of Phosphine-Substituted Cyclobutanes

Allenes are known to undergo [2+2] cycloaddition reactions with alkenes and alkynes to form cyclobutane derivatives.[248] It was therefore decided to try these reactions in order to synthesise some phosphine-substituted cyclobutanes (Scheme 4-25).

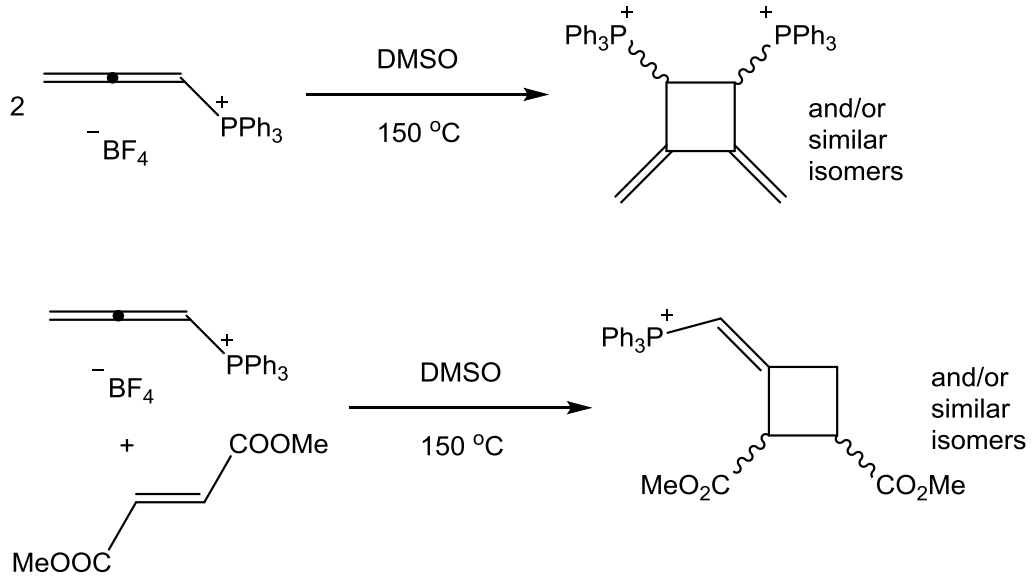

Scheme 4-25 Intended Synthesis of Phosphine-Substituted Cyclobutanes

No cycloaddition reactions were observed on the heating of **40b**, and if the reaction was heated for longer than one hour the only phosphorus-containing product observed in the ^{31}P-NMR spectrum was triphenylphosphine oxide.

However, if the reaction was halted after 30 minutes, selective formation of one product was observed. This product was found to be highly susceptible to oxidation (forming triphenylphosphine oxide) and therefore it could not be isolated. However, use of d_6-DMSO allowed observation by ^{1}H-NMR spectroscopy and it was deduced that the allene **40b** had reacted with the DMSO solvent to form $[S(CD_3)_2CH_2COCHPPh_3][BF_4]$ **68** (Scheme 4-26).

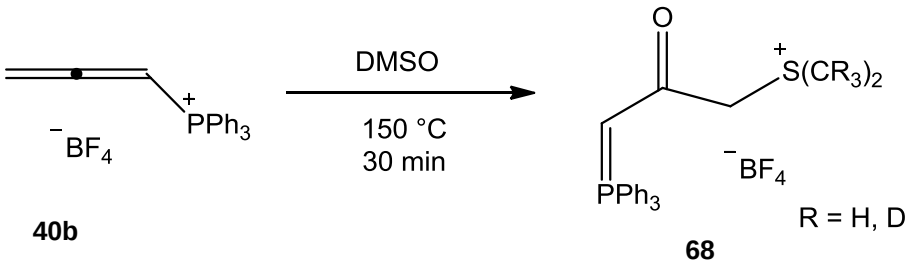

40b **68**

Scheme 4-26 Reaction of Allene **40b** with DMSO to form **68**

In the ^{1}H-NMR spectrum two major peaks were observed outside of the aromatic region. A doublet at δ 2.35 was found to integrate to two protons and have a small phosphorus coupling of 2.4 Hz, which was assigned to the CH_2 group next to the sulfur. The doublet at δ 5.49 however had a much larger phosphorus coupling (12.5 Hz) and integrated to one proton and was assigned to the CH group of the phosphorus ylide. Evidence for the carbonyl group was found in a ^{13}C-NMR resonance at δ 203.2 and a band observed at 1720 cm^{-1} in the IR spectrum.

This reaction highlights how susceptible phosphino-allene **40** is towards nucleophilic attack, even a weak nucleophile such as DMSO is capable of reacting. Scheme 4-27 presents a potential mechanism for this reaction, showing attack of the sulfoxide at the electron-deficient central allene carbon. The resulting cyclic intermediate can then be opened to form the observed product **68**.

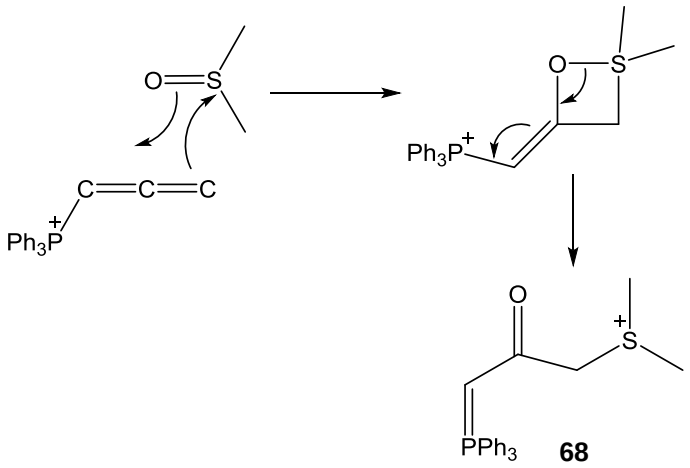

68

Scheme 4-27 Suggested Mechanism for the Formation of **68**

Conclusion

In Chapter 3 the successful synthesis and characterisation of vinyl carbenes **26** was discussed. Here in Chapter 4 attempts to isolate the unsubstituted analogue **26a** were presented. **26a** was found to be too reactive to be isolated, although evidence for its formation was obtained via NMR spectroscopy. Analysis of the data collected from the reaction mixtures showed evidence for many interesting products. The presence of triphenylethylphosphonium **43**, a coordination complex of **43** bound through the ethyl group **44** and phosphino-vinylidene $[Ru(\kappa^2\text{-}OAc)(\kappa^1\text{-}OAc)(PPh_3)_2(=C=CH\text{-}CH_2\text{-}PPh_3)]^+$ **38,** led to the conclusion that free triphenylphosphine must be attacking the vinyl moiety of **26a**.

Work towards the independent synthesis of vinylidene **38** was undertaken by reacting the commercially available triphenylpropargylphosphonium alkyne **39** with ruthenium and rhodium precursors. This led to the synthesis and full characterisation of some novel ruthenium and rhodium phosphino-allene complexes $[Ru(\kappa^2\text{-}OAc)(\kappa^1\text{-}OAc)(\eta^2\text{-}H_2C=C=CHPPh_3)(PPh_3)_2][BF_4]$ **45**, $[Ru(\kappa^2\text{-}O_2CPh)(\kappa^1\text{-}O_2CPh)(\eta^2\text{-}H_2C=C=CHPPh_3)(PPh_3)_2][BF_4]$ **49** and $[RhCl(\eta^2\text{-}H_2C=C=CHPPh_3)(P^iPr_3)_2][BPh_4]$ **60** via the isomerisation of **39** to its allene isomer **40**. A brief investigation into this isomerisation was found to not be metal-mediated and to occur spontaneously in solution. The rate of isomerisation was found to be counter-ion dependent and slowest rate was observed with the use of tetraphenylborate as the counter ion. Thus by slowing the isomerisation

it was now possible to observe some formation of the desired phosphino-vinylidene complexes. In the case of [Ru(κ^2-OAc)(κ^1-OAc)(PPh_3)$_2$(=C=CH-CH_2-PPh_3)][BPh_4] **38** and [RhCl(C=C=$CHCH_2PPh_3$)(P^iPr_3)$_2$][BPh_4] **63** these were formed alongside the allene isomers. [Ru(κ^2-O_2CPh)(κ^1-O_2CPh)(C=C=$CHCH_2PPh_3$)(PPh_3)$_2$][BPh_4] **47** however could be isolated as it was formed with very little contaminant allene complex. It is believed that these are the first examples of phosphorus-substituted vinylidene complexes to have been reported.

5. Conclusions and Future Work

An investigation has been carried out into the formation of a variety of C3 organometallic species via the isomerisation of alkynes mediated by ruthenium (II) and rhodium (I) complexes. It was already known that the $[Ru(OAc)_2(PPh_3)_2]$ scaffold is capable of stabilising a variety of π-accepting ligands. The known reactivity of this system has been extended and it has been shown that $[Ru(OAc)_2(PPh_3)_2]$ **1a** can stabilise and bind carbenes, vinylidenes, allenylidenes and η^2-allenes. These types of unsaturated organometallic species are of interest due to their roles as precursors and intermediates in a variety of catalytically relevant processes.[9, 111]

A range of analogues of **1** have been synthesised through the development of a new synthetic route. As the literature route to **1a** is only successful for triphenylphosphine the use of the half-sandwich complex $[Ru(\kappa^1\text{-OAc})(\kappa^2\text{-OAc})(p\text{-cymene})]$ **18** as a precursor was developed. This has allowed an investigation into the effects the phosphorus ligands have on the reactivity of **1**. In Chapter 2 it was shown that electron rich phosphines such as triisopropylphosphine promote vinylidene formation, whereas electron poor phosphites such as triisopropylphosphite did not promote formation of these ligands.

Novel synthetic routes have also been employed in the synthesis of the C3 organometallic species. In Chapter 3 vinyl carbenes **26** were formed by the use of a Lewis acid to abstract the hydroxy group of vinylidene **3** (Scheme 5-1). The resulting structure was then stabilised by the formation of a metallocyclic structure utilising the versatile binding modes of the acetate ligands.

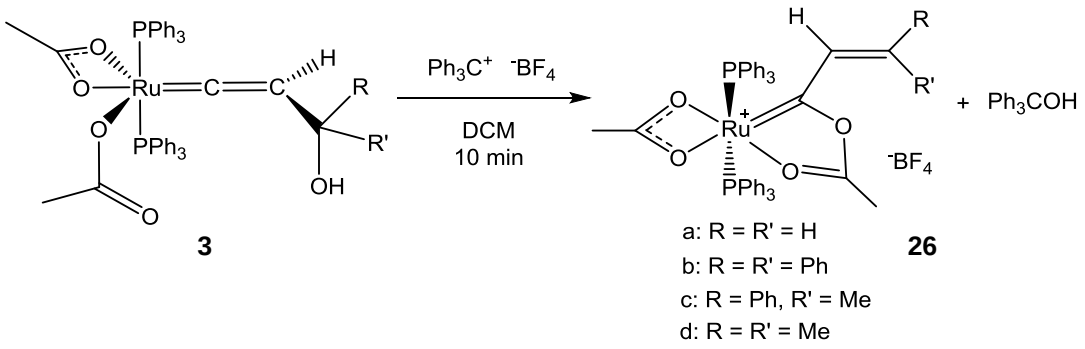

Scheme 5-1 Synthesis of $[Ru(\kappa^2\text{-OAc})(OC\{Me\}OCC\{H\}=CRR')(PPh_3)_2][BF_4]$ **26**

It was subsequently found that these carbenes could be deprotonated to form either an allenylidene **30** or vinylvinylidene **32** depending on the nature of the substituents on the vinyl moiety. Not only is this the only known route to allenylidenes for this ruthenium acetate system, it also suggests that vinyl carbenes could be intermediates in their formation. The versatility of the acetate ligands has allowed the isolation and full characterisation of a vinyl carbene structure which would otherwise have been unsaturated and highly unstable. Only one previous example of these cyclic vinyl carbenes has been reported,[202] and no investigations have been done into their wider reactivity. In the future it would be of interest to extend this deprotonation study to cover further reactivity. This is of particular interest considering the similarities of these structures to the widely used Hoveyda-Grubbs metathesis catalysts.

The synthesis of some novel phosphino-substituted organometallic species has also been presented in Chapter 4. These species were formed by the reaction of 1a and $[Rh(\mu^2\text{-}Cl)(P^iPr_3)_2]_2$ **59** with triphenylpropargylphosphonium salts **39**. There are a few reports of this alkyne in the literature which mainly serve to highlight the ease with which it rearranges to the allene isomer.[32, 233] In accordance with this, the synthesis of three new phosphino-allene complexes has been reported here. An investigation into the alkyne/allene isomerisation has shown that it is not metal mediated and strongly counter ion dependent. Therefore, use of the tetraphenylborate salt **39c** enabled the isomerisation to be slowed enough for phosphino-vinylidene complexes to be formed (Scheme 5-2).

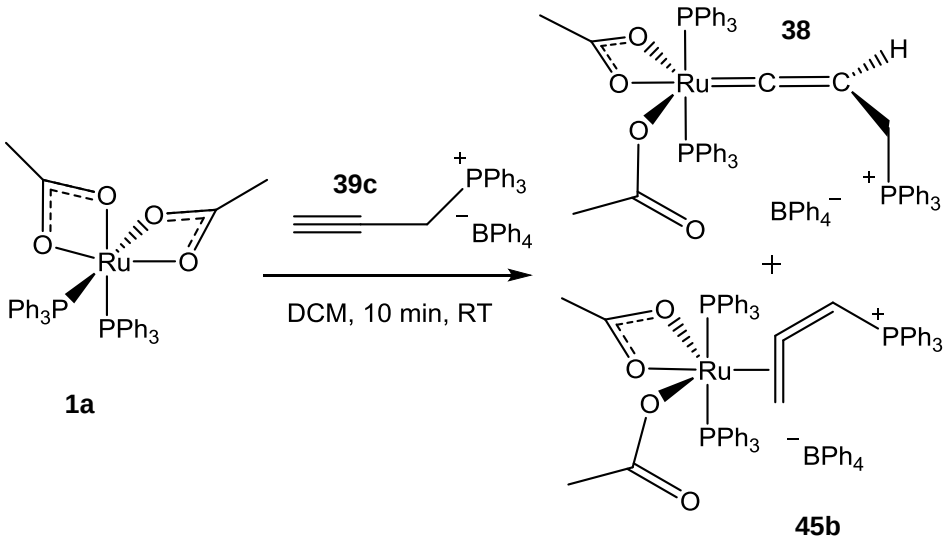

Scheme 5-2 Reaction of *cis*-$[Ru(\kappa^2\text{-}OAc)_2(PPh_3)_2]$ **1a** with Triphenylpropargylphosphonium Tetraphenylborate **39c**

These are the first phosphorus-substituted vinylidenes to have been synthesised and as a result future investigation into their properties and reactivity would be desirable. This would open the possibility of new synthetic and catalytic methodologies. One of

the initial ideas behind this project was the hope that the triphenylphosphine would prove to be a good leaving group allowing for some interesting substitution chemistry. Exploring this, and other types of reactivity such as elimination, would seem the next obvious step for this project.

A few examples of phosphino-allene complexes exist in the literature, but very few results have been reported as to their reactivity. Esteruelas has reacted a rhodium phosphino-allene complex with carbon monoxide and found that this displaces the allene ligand allowing for isolation of the free allene.[234] However, no results have been published concerning reactivity at the allene ligand and as to whether coordination of the presence of the phosphonium group ultimately affects the allene's reactivity at all.

In the future it would be of great interest to extend the known reactivity of the $[Ru(OAc)_2(PPh_3)_2]$ scaffold, in particular towards C3 moieties. In the introduction a number of alternative isomeric forms were discussed. Some of these, such as the alkyl ligands, are not capable of accepting electron density and so predicting their reactivity is not straight forward. However, those that are π-accepting ligands (such as the η^2-alkene or carbyne species) would be expected to bind well to this scaffold (Figure 5-1). This would then allow an exploration of the effects the non-innocent acetate ligands may have on those ligands classes and could open up whole new areas of chemistry.

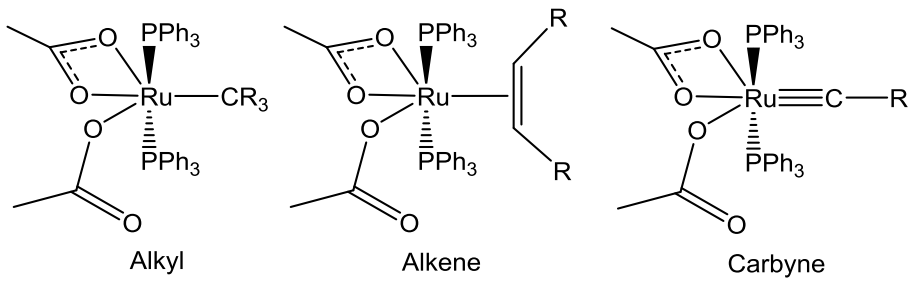

Figure 5-1 Future Work

In conclusion this thesis has been able to extend the known chemistry of the $[Ru(OAc)_2(PPh_3)_2]$ scaffold to a range of C3 organometallic species. The versatile binding modes of the acetate ligands have been exploited to enable novel synthesis of carbene, vinylidene, allenylidene and allene complexes. A new area of phosphorus-substituted vinylidene complexes has also been introduced and the reactivity of these provides encouraging scope for future work.

6. Experimental

General

All experimental procedures were performed under an atmosphere of dinitrogen using standard Schlenk Line and glovebox techniques. DCM, hexane, toluene and pentane were purified with the aid of an Innovative Technologies anhydrous solvent engineering system. Diethyl ether and toluene were distilled over sodium and methanol over Mg/I_2 (all under argon) before use. The CD_2Cl_2 used for NMR experiments was dried over CaH_2 and degassed with three freeze-pump-thaw cycles. NMR spectra were acquired on a Bruker AVANCE 500 (Operating frequencies; ^{1}H 500.23 MHz, ^{31}P 202.50 MHz, ^{13}C 125.77 MHz) or a Jeol ECS400 (Operating frequencies; ^{1}H 399.78 MHz, ^{13}C 100.53 MHz, ^{19}F 376.17 MHz, ^{11}B 128.27 MHz). ^{31}P, ^{19}F and ^{13}C spectra were recorded with proton decoupling. δ values are reported in ppm. Residual solvent peaks were identified by comparison with Fulmer and co-workers.[249] Mass spectrometry measurements were performed on a Bruker micrOTOF MS (ESI) instrument or a Waters GCT Premier Acceleration TOF MS (LIFDI) instrument. IR spectra were acquired on either a Mattson Research Series (CsCl a solution cell), a Thermo-Nicolet Avatar 370 FTIR spectrometer (CsCl a solution cell) or a Brüker Alpha spectrometer (CsCl solution cell and diamond crystal ATR). Reactions followed by IR used a Mettler Toledo ReactIR iC10 instrument. CHN measurements were performed using an Exeter Analytical Inc. CE-440 analyser and are reported for novel complexes and those that have not been previously isolated. Single crystal X-ray diffraction was carried out on an Oxford Diffraction SuperNova diffractometer with a molybdenum source. The crystals were kept at 110.00(10) K during data collection. Using Olex2,[250] the structures were solved with either the Superflip[251] structure solution program using Charge Flipping or the XS[252] structure solution program using Direct Methods or the Patterson Method. They were refined with the ShelXL[252] refinement package using Least Squares minimisation. $[Ru(p\text{-cymene})Cl_2]_2$ was either used as supplied from Sigma Aldrich or synthesised using the literature route.[253] *cis*-$[Ru(\kappa^2\text{-}OAc)_2(PPh_3)_2]$[168] was synthesised from $[Ru(Cl)_2(PPh_3)_3]$[254] both of which were prepared using the literature routes. Other chemicals were obtained from commercial sources and used as supplied with the exception of triisopropyl phosphine and triisopropyl phosphite which were distilled before use.

Key to NMR abbreviations

s (singlet), d (doublet), dd (doublet of doublets), t (triplet), bt (broad triplet), tt (triplet of triplets), q (quartet), hp (heptet), m (multiplet), at (apparent triplet), ad (apparent doublet), adt (apparent doublet of triplets).

Chapter 2 Experimental

Adapted Noyori Route to Complex 9: Formation of Complexes 12 and 14

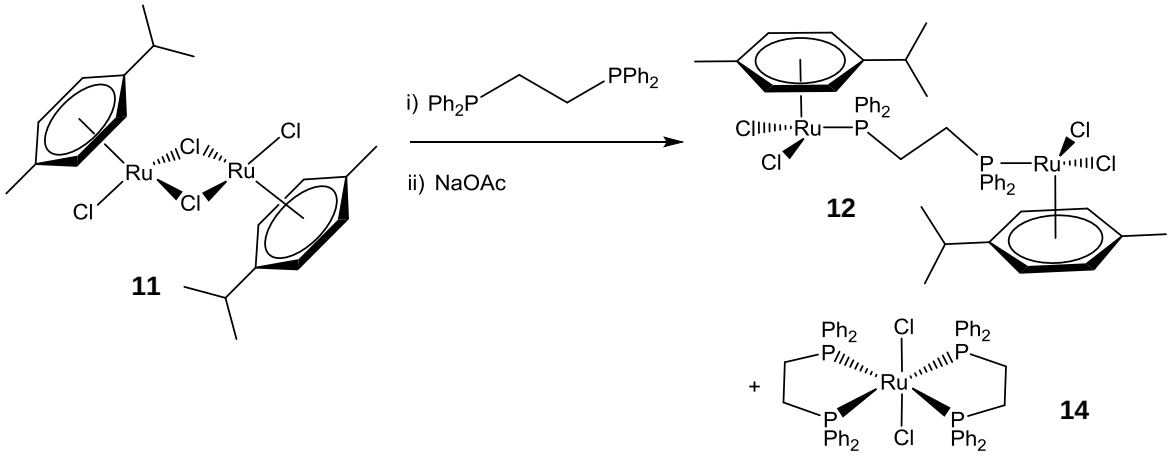

DMF (7.5 ml) was added to a Schlenk tube containing [Ru(*p*-cymene)Cl_2]$_2$ **11** (200 mg, 0.33 mmol) and dppe **8** (246 mg, 0.62 mmol). The resulting suspension was heated at 100 ˚C for 10 minutes. The red-brown solution was then cooled to room temperature and a solution of NaOAc (984 mg, 12 mmol) in methanol (13 ml) was added and stirred for 5 minutes. Toluene (6 ml) and water (12 ml) were added and mixed by vigorous stirring. The organic layer was then removed by cannula transfer and the aqueous layer washed with further portions of toluene (2 x 6 ml). The combined organic layers were then washed with water (3 x 4 ml) before removal of solvent and drying *in vacuo*. No evidence for the formation of [Ru(κ^2-OAc)$_2$(dppe)] **9** was observed, however crystals of [($RuCl_2$(*p*-cymene))$_2$(μ^2-dppe)] **12** and *trans*-[$RuCl_2$(dppe)$_2$] **14**[191] were obtained by slow diffusion of hexane into a toluene solution of the reaction mixture. These crystals were not isolated or characterised. All stages were carried out under an inert atmosphere. Adapted from Kitamura et al.[190]

Table 6-1 Crystal data and structure refinement for $[(RuCl_2(p\text{-cymene}))_2(\mu^2\text{-dppe})]$ **12**

Identification code	jml1102
Empirical formula	$C_{48}H_{56}Cl_8P_2Ru_2$
Formula weight	1180.61
Temperature / K	110.0
Crystal system	monoclinic
Space group	$P2_1/n$
a / Å, b / Å, c / Å	13.2923(4), 27.2545(13), 13.7758(3)
α/°, β/°, γ/°	90.00, 95.591(3), 90.00
Volume / Å^3	4966.9(3)
Z	4
ρ_{calc} / mg mm^{-3}	1.579
μ / mm^{-1}	1.136
F(000)	2392
Crystal size / mm^3	0.143 × 0.1084 × 0.0387
2Θ range for data collection	5.98 to 52.8°
Index ranges	-16 ≤ h ≤ 16, -21 ≤ k ≤ 34, -17 ≤ l ≤ 16
Reflections collected	22261
Independent reflections	10156[R(int) = 0.0332]
Data/restraints/parameters	10156/7/557
Goodness-of-fit on F^2	1.041
Final R indexes [I>2σ (I)]	R_1 = 0.0337, wR_2 = 0.0656
Final R indexes [all data]	R_1 = 0.0457, wR_2 = 0.0703
Largest diff. peak/hole / e Å^{-3}	0.500/-0.714

Synthesis of [Ru(p-cymene)(κ^2-OAc)(κ^1-OAc)] 18

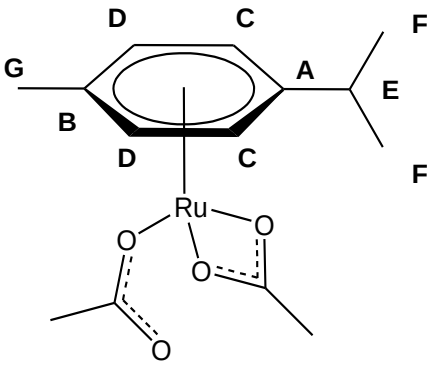

Silver acetate (2.3 g, 13.77 mmol) was added to a stirred solution of [Ru(*p*-cymene)Cl_2]$_2$ **11** (2 g, 3.23 mmol) in toluene (100 ml). The resultant suspension was protected from light with aluminium foil and stirred at room temperature for 20 hours. The reaction mixture was then filtered through celite before the solvent was removed to give [Ru(κ^1-OAc)(κ^2-OAc)(*p*-cymene)] **18** (1.65 g, 4.48 mmol, 69 % yield) as an orange solid.

^{1}H-NMR (399.78 MHz, CD_2Cl_2): δ_H 1.33 (d, $^3J_{HH}$ = 7.0 Hz, 6H, CHC*H*$_3$), 1.82 (s, 6H, COOC*H*$_3$), 2.21 (s, 3H, C*H*$_3$), 2.80 (hp, $^3J_{HH}$ = 7.0 Hz, 1H, C*H*CH$_3$), 5.55 (d, $^3J_{HH}$ = 6.0 Hz, 2H, AB pattern C_6H_4), 5.77 (d, $^3J_{HH}$ = 6.0 Hz, 2H, AB pattern C_6H_4);

^{13}C-NMR (100.52 MHz, CD_2Cl_2): δ_C 183.6 (s, *C*OOCH$_3$), 97.5 (s, A), 92.5 (s, B), 78.9 (s, C), 77.5 (s, D), 31.5 (s, E), 23.5 (s, COO*C*H$_3$), 22.3 (s, F), 18.4 (s, G);

IR (CsCl, solution in DCM) 1622 cm^{-1} (κ^1-OCO_{asym}), 1473 cm^{-1} (κ^2-OCO_{asym}), 1366 cm^{-1} (κ^2-OCO_{sym}), 1316 cm^{-1} (κ^1-OCO_{sym}), $\Delta\nu_{(uni)}$ 306 cm^{-1}, $\Delta\nu_{(chelate)}$ 107 cm^{-1};

MS (ESI), *m/z* 354.01 [M]$^+$.

Synthesis of [Ru(κ^2-OAc)$_2$(dppe)] 9

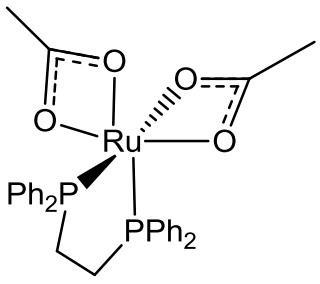

A solution of [Ru(*p*-cymene)(κ^1-OAc)(κ^2-OAc)] **18** (50 mg, 0.14 mmol) and 1,2-bis(diphenylphosphino)ethane (dppe) **8** (56 mg, 0.14 mmol) in DCM (5 ml) was stirred for 18 hours at room temperature. The solvent was then removed and the residue washed with pentane (3 x 10 ml). [Ru(κ^2-OAc)$_2$(dppe)] **9** was obtained as a

yellow powder (35 mg, 0.057 mmol, 40% yield). Crystals were obtained by slow diffusion of pentane into a DCM solution of **9**.

The product proved hard to isolate and was mainly observed via its peak at δ 89.5 in the ^{31}P-NMR spectrum. The following data has been obtained from crude product.

^{1}H-NMR (500.23 MHz, CD_2Cl_2): δ_H 1.22 (d, 6.9 Hz, 16H, (C*H*$_3$)$_2$ *p*-cymene), 1.34 (s, 6H, COOC*H*$_3$), 2.30 (s, 8H, C*H*$_3$ *p*-cymene), 2.54 (br, 4H, P-C*H*$_2$), 2.86 (hp, 2.5H, CH *p*-cymene), 7.10 (m, 10H, aromatic *p*-cymene), 7.30-7.57 (m, aromatic region);

^{31}P-NMR (202.49 MHz, CD_2Cl_2): δ_P 89.6 (dppe);

IR (CsCl, solution in DCM) 1433 cm^{-1} (P-Ph), 1372 cm^{-1} (κ^2-OCO$_{asym}$), 1319 cm^{-1} (κ^2-OCO$_{sym}$) $\Delta\nu_{(chelate)}$ 53 cm^{-1};

MS (LIFDI), *m/z* 618.05 [M]$^+$.

Table 6-2 Crystal data and structure refinement for [Ru(κ^2-OAc)$_2$(dppe)] 9

Identification code	jml1111
Empirical formula	$C_{30}H_{30}O_4P_2Ru$
Formula weight	617.55
Temperature / K	110.0
Crystal system	monoclinic
Space group	$P2_1/c$
a / Å, b / Å, c / Å	20.4154(6), 9.9402(5), 13.9464(6)
α/°, β/°, γ/°	90.00, 107.212(4), 90.00
Volume / Å^3	2703.45(19)
Z	4
ρ_{calc} / mg mm^{-3}	1.517
μ / mm^{-1}	0.733
F(000)	1264
Crystal size / mm^3	0.1093 × 0.0939 × 0.0407
2Θ range for data collection	5.84 to 54.98°
Index ranges	-26 ≤ h ≤ 25, -12 ≤ k ≤ 12, -15 ≤ l ≤ 17
Reflections collected	16084
Independent reflections	6173[R(int) = 0.0266]
Data/restraints/parameters	6173/70/363
Goodness-of-fit on F^2	1.102
Final R indexes [I>2σ (I)]	R_1 = 0.0304, wR_2 = 0.0609
Final R indexes [all data]	R_1 = 0.0380, wR_2 = 0.0633
Largest diff. peak/hole / e Å^{-3}	0.539/-0.485

Synthesis of [Ru(κ^2-OAc)$_2$(dppb)] 22

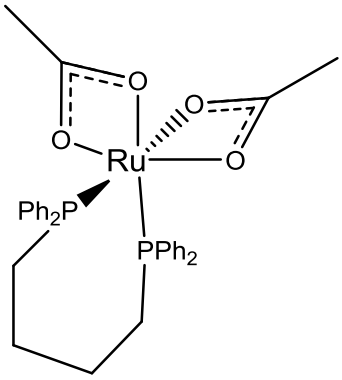

A solution of [Ru(*p*-cymene)(κ^1-OAc)(κ^2-OAc)] **18** (20 mg, 0.05 mmol) and 1,4-Bis(diphenylphosphino)butane (dppb) (23 mg, 0.05 mmol) in CD_2Cl_2 (0.5 ml) was placed in an NMR tube. Complete conversion to [Ru(κ^2-OAc)$_2$(dppb)] **22** was observed by ^{1}H-NMR and ^{31}P-NMR spectroscopy after 3 hours.

^{1}H-NMR (399.78 MHz, CD_2Cl_2): δ_H 1.26 (d, 7 Hz, 6H, *p*-cymene (C*H*$_3$)$_2$), 1.54 (s, 6H, COOC*H*$_3$), 1.70 (br, 4H, PCH$_2$C*H*$_2$), 2.34 (s, 3H, C*H*$_3$ *p*-cymene), 2.53 (br, 4H, P-C*H*$_2$), 2.90 (hp, 1H, CH *p*-cymene), 7.15 (m, 4H, aromatic *p*-cymene), 7.18-7.80 (m, aromatic region);

^{31}P-NMR (161.83 MHz, CD_2Cl_2): δ_P 63.5 (Ru-*P*Ph$_3$);

Synthesis of *cis*-[Ru(κ^2-OAc)$_2$(PPh$_3$)$_2$] 1a

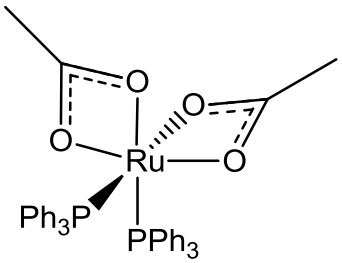

A solution of [Ru(*p*-cymene)(κ^1-OAc)(κ^2-OAc)] **18** (50 mg, 0.14 mmol) and triphenylphosphine (111 mg, 0.42 mmol) in DCM (10 ml) was stirred at room temperature for 18 hours. The solvent was then removed and the residue washed with pentane (2 x 5 ml) and then dried *in vacuo*. This yielded *cis*-[Ru(κ^2-OAc)$_2$(PPh$_3$)$_2$] **1a** as an orange powder (30 mg, 0.04 mmol, 39% yield). The following data matches that previously reported.[170]

^{1}H-NMR (500.23 MHz, CD_2Cl_2): δ_H 1.46 (s, 6H, COOC*H*$_3$), 7.10-7.34 (m, aromatic region);

^{13}C-NMR (125.81 MHz, CD_2Cl_2): δ_C 23.66 (s, COO*C*H_3), 128.08 (t, ΣJ = 9.4 Hz, $C_{2\text{ or }3}$ of PPh_3), 129.75 (s, C_4 of PPh_3), 134.66 (t, ΣJ = 10.2 Hz, $C_{2\text{ or }3}$ of PPh_3),135.52 (t, $^1J_{PC}+^3J_{PC}$ = 45.0 Hz, C_1 of PPh_3), 188.88 (s, *C*OOCH$_3$);

^{31}P-NMR (202.49 MHz, CD_2Cl_2): δ_P 63.6 (Ru-*P*Ph_3);

IR (CsCl, solution in DCM) 1434 cm^{-1} (P-Ph), 1460 cm^{-1} (κ^2-OCO_{asym}), 1506 cm^{-1} (κ^2-OCO_{sym}) $\Delta\nu_{(chelate)}$ 46 cm^{-1};

MS (LIFDI) *m/z* 744.08 [M]$^+$, 684.03 [M+H] –OAc.

Synthesis of *cis*-[Ru(κ^2-OAc)$_2$(P^{i}Pr$_3$)$_2$] 1b

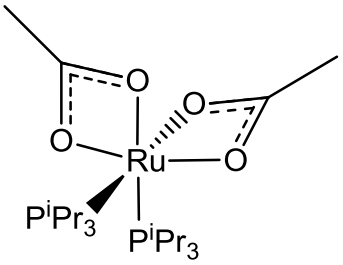

A solution of [Ru(*p*-cymene)(κ^1-OAc)(κ^2-OAc)] **18** 100 mg, 0.28 mmol) and triisopropyl phosphine (98 µl, 0.56 mmol) in DCM (10 ml) was stirred at room temperature for four hours. The solvent was then removed and the residue redissolved in pentane. This solution was then filtered (to remove residual *p*-cymene) before the volume was reduced to ~4 ml. Cooling the solution to -15 °C afforded red crystals of *cis*-[Ru(κ^2-OAc)$_2$(P^{i}Pr$_3$)$_2$] **1b** (25 mg, 0.05 mmol, 16 % yield).

^{1}H-NMR (500.23 MHz, CD_2Cl_2): δ_H 1.21 (dd, $^3J_{HH}$ = 7.1 Hz, $^3J_{PH}$ = 12.1 Hz, 36 H, CHC*H*$_3$)*, 1.72 (s, 6H, COOC*H*$_3$), 2.59 (m, $^3J_{HH}$ = 7.11 Hz, $^2J_{PH}$ = 9.8 Hz, 6H, C*H*CH$_3$)*.

^{1}H{^{31}P}-NMR, 1.21 (d, $^3J_{HH}$ = 7.2 Hz, 36H, CHC*H*$_3$), 1.72 (s, 6H, COOC*H*$_3$), 2.59 (hp, $^3J_{HH}$ = 7.2 Hz, 6H, C*H*CH$_3$).

^{31}P-NMR (202.49 MHz, CD_2Cl_2): δ_P 59.5 (s, $^2J_{PP}$ = 60.0 Hz, P(^{i}Pr)$_3$)*.

^{13}C -NMR (125.81 MHz, CD_2Cl_2): δ_C 20.0 (s, COO*C*H$_3$), 24.0 (s, CH*C*H$_3$), 28.8 (t, $^2J_{PC}+^4J_{PC}$ = 19.5 Hz, *C*HCH$_3$), 187.7 (s, *C*OOCH$_3$).

IR (CsCl, solution in DCM), 1522 cm^{-1} (κ^2-OCO_{asym}), 1455 cm^{-1} (P-^{i}Pr), 1413 cm^{-1} (κ^2-OCO_{sym}), $\Delta\nu_{(chelate)}$ 109 cm^{-1};

MS (LIFDI), *m/z* 540.26 [M]$^+$;

Anal. for $C_{22}H_{48}RuP_2O_4$, (calc) C 48.97, H 8.97; (found) C 49.04, H 8.90.

*Spectra simulated using gNMR[255] to determine these coupling constants.

Table 6-3 Crystal data and structure refinement for *cis*-[Ru(κ^2-OAc)$_2$(P^iPr_3)$_2$] 1b

Identification code	jml1119
Empirical formula	$C_{22}H_{48}O_4P_2Ru$
Formula weight	539.61
Temperature / K	109.7
Crystal system	monoclinic
Space group	$P2_1/n$
a / Å, b / Å, c / Å	10.81596(13), 17.4581(3), 14.16497(15)
α/°, β/°, γ/°	90.00, 100.2053(10), 90.00
Volume / Å^3	2632.40(6)
Z	4
ρ_{calc} / mg mm^{-3}	1.362
μ / mm^{-1}	0.740
F(000)	1144
Crystal size / mm^3	0.255 × 0.1935 × 0.127
2Θ range for data collection	6.04 to 64.38°
Index ranges	-15 ≤ h ≤ 16, -24 ≤ k ≤ 22, -21 ≤ l ≤ 15
Reflections collected	16355
Independent reflections	8322[R(int) = 0.0227]
Data/restraints/parameters	8322/0/276
Goodness-of-fit on F^2	1.049
Final R indexes [I>2σ (I)]	R_1 = 0.0262, wR_2 = 0.0580
Final R indexes [all data]	R_1 = 0.0319, wR_2 = 0.0615
Largest diff. peak/hole / e Å^{-3}	0.498/-0.470

Synthesis of *cis*-[Ru(κ^2-OAc)$_2$(P(O^{i}Pr)$_3$)$_2$] 1c

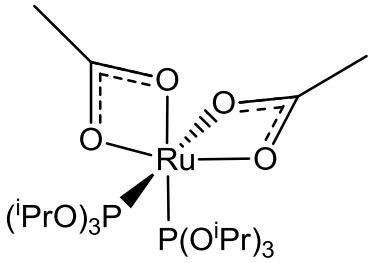

Triisopropylphosphite (26 µl, 0.1 mmol) was added to a solution of [Ru(*p*-cymene)(κ^1-OAc)(κ^2-OAc)] **18** (20 mg, 0.05 mmol) in CD_2Cl_2 (0.5 ml) and the reaction followed by ^{31}P-NMR. Ca. 95% conversion to [Ru(κ^2-OAc)$_2$(P(O^{i}Pr)$_3$)$_2$] **1c** was observed after 5 days. The product was not isolated and the reaction impurities are listed.

^{1}H-NMR (500.23 MHz, CD_2Cl_2): δ_H 1.16 (m, 7H unknown impurity), 1.20 (d, 15H (high due to overlapping unknown impurities), *p*-cymene), 1.24 (d, $^3J_{HH}$ = 6.8 Hz, 38H (high due to overlapping impurities), C*Me*$_2$ of P(O^{i}Pr)$_3$), 1.81 (s, 6H, COOC*H*$_3$), 1.88 (s, 1H, unknown impurity), 2.08 (s, 1H, unknown impurity), 2.28 (s, 6H, *p*-cymene), 2.84 (hp, 2H, *p*-cymene), 4.67 (m, 6H, C*H* of P(O^{i}Pr)$_3$), 7.08 (m, 8H, *p*-cymene);

^{31}P-NMR (202.51 MHz, CD_2Cl_2): δ_P 147.2 (s, P(O^{i}Pr)$_3$);

Synthesis of [Ru(κ^2-OAc)(κ^1-OAc)(P^{i}Pr$_3$)$_2$(=C=CHPh)] 7b

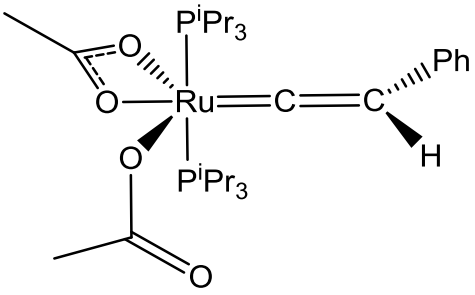

A solution of [Ru(*p*-cymene)(κ^1-OAc)(κ^2-OAc)] **18** (100 mg, 0.26 mmol) and triisopropyl phosphine (98 µl, 0.52 mmol) in DCM (10 ml) was stirred at room temperature for eighteen hours to give a red solution. The solvent was then removed and the residue dissolved in pentane. The solution was filtered and HC≡CPh **6** (28.5 µl, 0.26 mmol) was then added to the resulting deep red solution and the reaction stirred for 3 hours before being filtered again. The product was then crystallised from pentane (~5 ml) at -15 °C and [Ru(κ^2-OAc)(κ^1-OAc)(P^{i}Pr$_3$)$_2$(=C=CHPh)] **7b** (59 mg, 0.092 mmol, 33% yield) was obtained as square red crystals.

^{1}H-NMR (500.23 MHz, CD_2Cl_2): δ_H 1.24 (dd, 7.0 Hz, 36 H, CHC*H*$_3$), 1.92 (s, 6H, COOC*H*$_3$), 2.33 (m, $^{3}J_{HH}$ = 7.1, 6H, C*H*CH$_3$), 5.45 (t, 3.43 Hz, 1H, Ru=C=C*H*Ph), 6.85 (t, 7.35 Hz, H$_4$-CH*Ph*), 7.04 (d, 8.18 Hz, H$_2$-CH*Ph*), 7.12 (t, 7.35 Hz, H$_3$-CH*Ph*).

^{31}P-NMR (202.51 MHz, CD_2Cl_2): δ_P 27.9 (s, P(^{i}Pr)$_3$);

^{13}C-NMR (125.81 MHz, CD_2Cl_2): δ_C 19.8 (s, COO*C*H$_3$), 23.6 (t, $^{1}J_{PC}$+$^{3}J_{PC}$ = 17.07 Hz, *C*HCH$_3$), 24.2 (s, CH*C*H$_3$), 112.4 (t, $^{3}J_{PC}$ = 3.81 Hz, Ru=C=*C*), 123.6 (s, CH*Ph-C$_4$*), 125.2 (s, CH*Ph-C$_2$/C$_3$*), 128.5 (s, CH*Ph-C$_2$/C$_3$*), 135.3 (t, $^{4}J_{PC}$ = 2.3 Hz, CH*Ph-C$_1$*), 179.7 (s, *C*OOCH$_3$), 352.8 (t, $^{2}J_{PC}$ = 15.1 Hz, Ru=*C*).

IR (CsCl, solution in DCM), 1629 cm^{-1} (C=C), 1591 cm^{-1} (κ^1-OCO$_{asym}$), 1545 cm^{-1} (κ^2-OCO$_{asym}$), 1458 cm^{-1} (P-^{i}Pr), 1364 cm^{-1} (κ^2-OCO$_{sym}$), 1317 cm^{-1} (κ^1-OCO$_{sym}$), $\Delta\nu_{(uni)}$ 274 cm^{-1}, $\Delta\nu_{(chelate)}$ 181 cm^{-1};

MS (LIFDI), *m/z* 642.26 [M]$^+$, *m/z* 160.14 [P^{i}Pr$_3$]$^+$;

Anal. for $C_{30}H_{54}RuP_2O_4$, (calc) C 56.15, H 8.48; (found) C 56.13, H 8.44.

Table 6-4 Crystal data and structure refinement for $[Ru(\kappa^2\text{-}OAc)(\kappa^1\text{-}OAc)(P^iPr_3)_2(=C=CHPh)]$ **7b**

Identification code	jml1125
Empirical formula	$C_{30}H_{54}O_4P_2Ru$
Formula weight	641.74
Temperature / K	110.00(10)
Crystal system	monoclinic
Space group	$P2_1/n$
a / Å, b / Å, c / Å	12.6749(7), 14.7788(6), 17.0117(7)
α/°, β/°, γ/°	90.00, 90.298(4), 90.00
Volume / Å^3	3186.6(3)
Z	4
ρ_{calc} / mg mm^{-3}	1.338
μ / mm^{-1}	0.624
F(000)	1360
Crystal size / mm^3	0.1995 × 0.1591 × 0.0873
2Θ range for data collection	6.38 to 64.02°
Index ranges	$-18 \le h \le 17$, $-21 \le k \le 21$, $-21 \le l \le 24$
Reflections collected	21096
Independent reflections	9364[R(int) = 0.0626]
Data/restraints/parameters	9364/428/436
Goodness-of-fit on F^2	1.082
Final R indexes [I>2σ (I)]	R_1 = 0.0652, wR_2 = 0.1626
Final R indexes [all data]	R_1 = 0.0820, wR_2 = 0.1756
Largest diff. peak/hole / e Å^{-3}	1.452/-0.857

Synthesis of [Ru(κ^2-OAc)(κ^1-OAc)(CO)(PiPr$_3$)$_2$] 4b

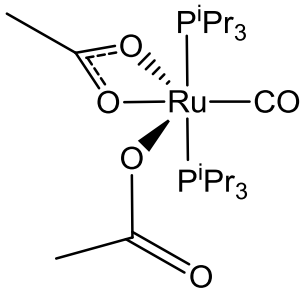

A solution of [Ru(*p*-cymene)(κ^1-OAc)(κ^2-OAc)] **18** (50 mg, 0.13 mmol) and triisopropyl phosphine (49 µl, 0.26 mmol) in DCM (5 ml) was stirred at room temperature for eighteen hours to give a red solution. The solvent was then removed and the residue redissolved in pentane. This was then filtered and the resulting pentane solution was then stirred under CO gas for 5 minutes during which time a colour change to dark green occured. The solution was then filtered to remove insoluble impurities. The product was then crystallised from pentane at -15 °C to give a small amount of [Ru(κ^2-OAc)(κ^1-OAc)(CO)(P^{i}Pr$_3$)$_2$] **4b** as green crystals. Too little product was obtained to allow a yield to be recorded or for full characterisation.

^{1}H-NMR (500.23 MHz, CD_2Cl_2): δ_H 1.29 (dd, $^3J_{PH}$ = 13.0 Hz, $^3J_{HH}$ = 7.2 Hz, 36H, CH(C*H*$_3$)$_2$), 1.77 (s, 6H, COOC*H*$_3$), 2.28 (m, 6H, C*H*CH$_3$);

^{31}P-NMR (202.53 MHz, CD_2Cl_2): δ_P 37.7 (s, P(^{i}Pr)$_3$)

IR (CsCl, solution in DCM), 1941 cm^{-1} (CO), 1640 cm^{-1} (κ^1-OCO$_{asym}$), 1539 cm^{-1} (κ^2-OCO$_{asym}$), 1461 cm^{-1} (P-^{i}Pr), 1380 cm^{-1} (κ^2-OCO$_{sym}$), 1312 cm^{-1} (κ^1-OCO$_{sym}$), $\Delta\nu_{(uni)}$ 328 cm^{-1}, $\Delta\nu_{(chelate)}$ 159 cm^{-1};

Alternatively **4b** could be synthesised via a reaction between **18** and phenyl propargyl ether.

A solution of [Ru(*p*-cymene)(κ^1-OAc)(κ^2-OAc)] **18** (200 mg, 0.56 mmol) and triisopropyl phosphine (196 µl, 1.12 mmol) in DCM (20 ml) was stirred at room temperature for four hours. The solvent was then removed from the resulting red solution and the residue extracted with pentane. Phenyl propargyl ether **24** (66 µl, 0.56 mmol) was then added and the solution stirred for 43 hours. The solvent was then removed from the resulting brown solution and the residue extracted with pentane. Neither this or further attempts at purification (such as crashing out at low temperature) were successful so the following data was collected for the crude reaction mixture. Many of the resonances in the resulting ^{1}H-NMR spectrum were overlapping and so integrations have not been reported.

^{1}H-NMR (500.23 MHz, CD_2Cl_2): δ_H 0.86 (t, 7.2 Hz), 1.17 (dd, J = 14.0 and 7.2 Hz), 1.19 (d, J = 6.8 Hz), 1.30 (dd, $^{3}J_{PH}$ = 13.0 Hz, $^{3}J_{HH}$ = 7.0 Hz, CH(C*H*$_3$)$_2$), 1.77 (s, COOC*H*$_3$), 2.10 (s), 2.27 (s), 2.28 (m, C*H*CH$_3$), 5.31 (s, *H*$_2$CC(Ph)$_2$), 5.44 (s), 7.10 (m, *p*-cymene aromatic), 7.31 (m, H$_2$CC(*Ph*)$_2$);

^{31}P-NMR (202.51 MHz, CD_2Cl_2): δ_P 36.2 (s, P(^{i}Pr)$_3$ of vinyl CO), 37.8 (s, P(^{i}Pr)$_3$ of product), 57.7 (s, P(^{i}Pr)$_3$ of starting material);

IR (CsCl, solution in DCM), 1927 cm^{-1} (CO), 1618 cm^{-1} (κ^1-OCO$_{asym}$), 1462 cm^{-1} (κ^2-OCO$_{asym}$), 1448 cm^{-1} (P-^{i}Pr), 1369 cm^{-1} (κ^2-OCO$_{sym}$), 1324 cm^{-1} (κ^1-OCO$_{sym}$), $\Delta\nu_{(uni)}$ 295 cm^{-1}, $\Delta\nu_{(chelate)}$ 94 cm^{-1};

MS (LIFDI), *m/z* 408.06 [M]$^+$ -P^{i}Pr$_3$, 568.20 [M]$^+$, 776.13 unknown;

Synthesis of [Ru(κ^2-OAc)(CO)(CH=CH$_2$)(P^{i}Pr$_3$)$_2$] 23b

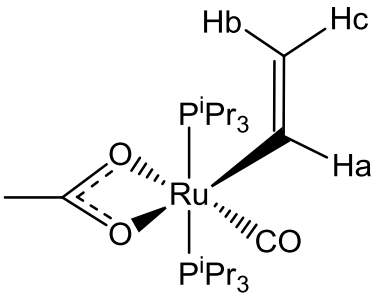

A solution of [Ru(*p*-cymene)(κ^1-OAc)(κ^2-OAc)] **18** (200 mg, 0.56 mmol) and triisopropyl phosphine (196 µl, 1.12 mmol) was stirred in DCM (20 ml) at room temperature for four hours. Phenyl propargyl ether (66 µl, 0.56 mmol) was then added to the red solution and stirred for two hours. The solvent was then removed from the resulting brown solution and the residue extracted with pentane. Neither this or further attempts at purification (such as precipitation at low temperature) were successful so the following data was collected for the crude reaction mixture. This has also lead to high integrations in the ^{1}H-NMR in some areas of the spectrum.

^{1}H-NMR (500.23 MHz, CD_2Cl_2): δ_H 1.24 (s, 3H), 1.26 (s, 3H), 1.33 (m, 37H, CHC*H*$_3$), 1.84 (s, 3H), 2.31 (s, 2H), 2.33 (s, 2H), 2.33 (m, 6H, C*H*CH$_3$), 2.89 (hp, 7 Hz, 1H), 4.91 (ddd, $^{3}J_{HaHb}$ = 16.5 Hz, $^{4}J_{PH}$ = 3.9 Hz , $^{2}J_{HbHc}$ = 2.0 Hz, 1H, Hb), 5.42 (ddd, $^{3}J_{HaHc}$ = 9.0 Hz, $^{4}J_{PH}$ = 4.2 Hz , $^{2}J_{HbHc}$ = 2.0 Hz, 1H, Hc), 6.74-7.45 (8H, aromatic), 7.92 (ddt, $^{3}J_{HaHb}$ = 16.5 Hz, $^{3}J_{HaHc}$ = 9.1 Hz , $^{3}J_{PH}$ = 1.3 Hz, 1H, Ha);

^{31}P-NMR (202.51 MHz, CD_2Cl_2): δ_P 37.5 (s, P(^{i}Pr)$_3$);

IR (CsCl, solution in DCM), 1909 cm^{-1} (CO), 1772 cm^{-1} (C=C), 1554 cm^{-1} (C=O of phenyl acetate), 1491 cm^{-1} (κ^2-OCO_{asym}), 1459 cm^{-1} (P-^{i}Pr), 1383 cm^{-1} (κ^2-OCO_{sym}), $\Delta\nu_{(chelate)}$ 103 cm^{-1};

MS (LIFDI), *m/z* 536.20 $[M-H]^+$;

Kinetic Experiments Run on the ReactIR

In order to get the best results it was found necessary to purge the instrument with nitrogen gas for 24 hours to remove all traces of water from the system. The experiment was then set up the usual way using a resolution of 8 wavenumbers), and a background of dry and degassed DCM taken. Spectra (256 scans) were taken at 1 minute intervals, though this was extended to 2 minutes overnight. It was also found that in order to view metal carbonyl peaks, a relatively high concentration was required, especially in the case of the tri-phenyl phosphine system. At the end of the experiments, ^{1}H-NMR and ^{31}P-NMR were taken of the reaction mixture to confirm the presence of the vinyl carbonyl product.

Reaction of *cis*-[Ru(κ^2-OAc)$_2$(P^{i}Pr$_3$)$_2$] 1b with Phenyl Propargyl Ether

cis-[Ru(κ^2-OAc)$_2$(P^{i}Pr$_3$)$_2$] **1b** was formed *in situ* prior to reaction with the alkyne (stoichiometry based on a 100% reaction). Therefore a solution of [Ru(*p*-cymene)(κ^1-OAc)(κ^2-OAc)] **18** (50 mg, 0.41 mmol) and triisopropyl phosphine (54 µl, 0.28 mmol) in DCM (10 ml) was stirred at room temperature for four hours. The solvent was then removed and the residue re-dissolved in pentane. This solution was then filtered (to remove residual *p*-cymene) before the pentane was removed. The product was then dissolved in DCM (40 ml) before being transferred to a three-necked 250 ml round-bottomed flask (B24 neck required for the ReactIR). Once the probe had been inserted into the reaction and the experiment begun, phenyl propargyl ether **24** (18 µl, 0.14 mmol) was added and the reaction followed for 4 hours.

Reaction of *cis*-[Ru(κ^2-OAc)$_2$(PPh$_3$)$_2$] 1a with Phenyl Propargyl Ether

A solution of *cis*-[Ru(κ^2-OAc)$_2$(PPh$_3$)$_2$] **1a** (50 mg, 0.067 mmol) in DCM (5 ml) under nitrogen was placed around the probe and the experiment begun. After 5 minutes phenyl propargyl ether **24** (8.5 µl, 0.067 mmol) was added to the Schlenk tube and the reaction followed for 20 hours.

Chapter 3 Experimental

General Procedure for the Synthesis of Species of the type [Ru(κ^2-O$_2$R)(OC{R}OCC{H}=CRR')(PPh$_3$)$_2$][BF$_4$] 26

cis-[Ru(κ^2-OAc)$_2$(PPh$_3$)$_2$] **1a** and an equivalent of the appropriate alkyne were dissolved in DCM and stirred at room temperature for 90 minutes. An equivalent of trityl carbenium tetrafluoroborate (the counter ion can be changed at this stage) was added and the resulting solution stirred for 15 minutes. The volume of DCM was the reduced to ~ 3 ml and the product precipitated by addition of pentane. After filtration the solid product was then re-dissolved in DCM (5 ml) and di-ethyl ether (7 ml) was carefully layered on top. After 2 days a crystalline product was obtained and the mother liquor was removed.

IR assignment for this class of compound was carried out with the aid of theoretical calculations performed by David Johnson. Structure vibrational spectrum calculations were performed using the TURBOMOLE v5.10 program. Geometry optimisations were performed on an initial trial structure using the (RI-)BP86/SV(P) functional and basis set, followed by a vibrational frequency calculation carried out at the same level.

CHN analysis of all of these species was obtained. However, all were found to have much lower percentage carbon than expected (some only by 0.6%, but others by as much as 2%). These results were found to be reproducible between batches. It is suspected that these complexes did not burn correctly, although no change in result was observed when a combustion aid (vanadium pentoxide) was used.

Synthesis of [Ru(κ^2-OAc)(OC{Me}OCC{H}=CPh$_2$)(PPh$_3$)$_2$][BF$_4$] 26b

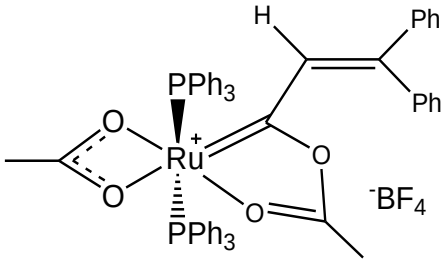

Reaction of *cis*-[Ru(κ^2-OAc)$_2$(PPh$_3$)$_2$] **1** (250 mg, 0.34 mmol),1,1-diphenylprop-2-yn-1-ol **2a** (70 mg, 0.34 mmol) and trityl carbenium tetrafluoroborate (111mg, 0.34 mmol) in DCM (20 ml) yielded

[Ru(κ^2-OAc)(OC{Me}OCC{H}=CPh$_2$)(PPh$_3$)$_2$][BF$_4$] **26b** (245 mg, 0.24 mmol, 71 % yield) as green crystals.

The diphenyl moiety has been assigned as Ph A and Ph B though the relative orientation of the rings is unknown. Peak assignment was completed with the aid of COSY, HSQC and HMBC experiments. The peak for the C_4 carbon of Ph B could not be located in the ^{31}C NMR spectrum, it is assumed that the peak is obscured under a resonance from the triphenyl phosphine.

^{1}H-NMR (700.13 MHz, CD_2Cl_2): δ_H 0.79 (s, 3H, COOC*H*$_3$), 1.31 (s, 3H, COOC*H*$_3$), 6.58 (m, 2H, *ortho*-Ph A), 7.26 (m, 2H, *ortho*-Ph B), 7.42 (m, 14H, *meta*-Ph B and the *ortho* or *meta*-PPh_3), 7.45 (m, 1H, *para*-Ph A), 7.49 (m, 12H, *ortho* or *meta*-PPh_3), 7.60 (m, 6H, *para*-PPh_3), 7.65 (m, 1H, *para*-Ph B), 8.37 (s, 1H, Ru=C-C*H*=CPh_2);

^{13}C-NMR (125.81 MHz, CD_2Cl_2): δ_C 17.7 (s, COO*C*H_3), 21.9 (s, COO*C*H_3), 127.7 (d, Ru=C-*C*H=CPh_2), 128.3 (s, C_3 of Ph A), 128.4 (t, $^{1}J_{PC}+^{3}J_{PC}$ = 45.5 Hz, C_1 of PPh_3), 128.8 (s, C_2 of Ph A), 129.6 (t, ΣJ = 11.5 Hz, $C_{2\text{ or }3}$ of PPh_3), 129.7 (s, C_3 of Ph B), 129.9 (s, C_4 of Ph A), 130.1 (s, C_2 of Ph B), 131.9 (s, C_4 of PPh_3), 134.4 (t, ΣJ = 10.1 Hz, $C_{2\text{ or }3}$ of PPh_3), 140.4 (s, C_1 of Ph A or B), 141.2 (s, C_1 of Ph A or B), 146.9 (s, Ru=CCH=*C*Ph_2), 183.2 (s, *C*$OOCH_3$), 186.6 (s, *C*$OOCH_3$), 279.8 (t, $^{2}J_{PC}$ = 9.3 Hz, Ru=*C*);

^{31}P-NMR (202.51 MHz, CD_2Cl_2): δ_P 32.4 (s, PPh_3);

^{11}B-NMR (128.27 MHz, CD_2Cl_2): δ_B -2.1 (s, BF_4);

^{19}F-NMR (376.17 MHz, CD_2Cl_2): δ_F -153.3 (s, $^{10}BF_4$), -153.4 (s, $^{11}BF_4$);

IR (CsCl, solution in DCM), 1630 cm^{-1} ν(C=O), 1542 cm^{-1} ν(C=C), 1530 cm^{-1} (κ^2-OCO_{asym}), 1481 cm^{-1} (P-Ph), 1434 cm^{-1} (κ^2-OCO_{sym}), 1095 cm^{-1} (B-F), $\Delta\nu_{(chelate)}$ 96 cm^{-1};

MS (ESI), *m/z* 935.1998 (Calculated for $C_{55}H_{47}{}^{102}RuP_2O_4$ $[M]^+$ = 935.2002, Δ = 0.4 mDa), *m/z* 673.1079 (Calculated for $C_{37}H_{32}{}^{102}RuPO_4$ $[M]^+$ -PPh_3 = 673.1086, Δ = 0.7 mDa), *m/z* 613.0861 (Calculated for $C_{35}H_{28}{}^{102}RuPO_2$ $[M\text{-}H]^+$ -PPh_3 -AcO = 613.0874, Δ = 1.5 mDa);

MS/MS showed that the lower mass species are observed due to fragmentation in the spectrometer.

Anal. for $C_{55}H_{47}$ $RuP_2O_4BF_4$, (calc) C 64.65, H 4.65; (found) C 64.00, H 4.67.

Table 6-5 Crystal data and structure refinement for $[Ru(\kappa^2\text{-}OAc)(OC\{Me\}OCC\{H\}=CPh_2)(PPh_3)_2][BF_4]$ **26b**

Identification code	jml1139
Empirical formula	$C_{56.0}H_{49.9}BCl_{2.9}F_4O_4P_2Ru$
Formula weight	1139.04
Temperature / K	110.00(10)
Crystal system	orthorhombic
Space group	$Pna2_1$
a / Å, b / Å, c / Å	21.0188(5), 11.7455(4), 22.0402(7)
α/°, β/°, γ/°	90.00, 90.00, 90.00
Volume / Å^3	5441.2(3)
Z	4
ρ_{calc} / mg mm^{-3}	1.390
μ / mm^{-1}	0.547
F(000)	2328
Crystal size / mm^3	0.1965 × 0.1423 × 0.1033
2Θ range for data collection	6.38 to 58.08°
Index ranges	-16 ≤ h ≤ 26, -14 ≤ k ≤ 11, -29 ≤ l ≤ 18
Reflections collected	23031
Independent reflections	10731[R(int) = 0.0269]
Data/restraints/parameters	10731/68/592
Goodness-of-fit on F^2	1.137
Final R indexes [I>2σ (I)]	R_1 = 0.0712, wR_2 = 0.1770
Final R indexes [all data]	R_1 = 0.0785, wR_2 = 0.1820
Largest diff. peak/hole / e Å^{-3}	1.322/-2.104
Flack Parameter	0.00(5)

Table 6-6 Crystal data and structure refinement for $[Ru(\kappa^2\text{-}OAc)(CH_2CPh_2)(CO)(PPh_3)_2]$ **29**

identification code	jml1142
Empirical formula	$C_{53}H_{44}O_3P_2Ru$
Formula weight	891.89
Temperature/K	110.00(10)
Crystal system	triclinic
Space group	P-1
a/Å, b/Å, c/Å	9.5876(6), 11.9448(8), 18.5587(13)
α/°, β/°, γ/°	78.810(6), 88.907(5), 86.189(5)
Volume/Å^3	2080.3(2)
Z	2
ρ_{calc}mg/mm^3	1.424
μ/mm^{-1}	0.499
F(000)	920
Crystal size/mm^3	0.2296 × 0.1555 × 0.0469
2Θ range for data collection	5.5 to 58.18°
Index ranges	-12 ≤ h ≤ 12, -15 ≤ k ≤ 15, -24 ≤ l ≤ 21
Reflections collected	14802
Independent reflections	9408[R(int) = 0.0286]
Data/restraints/parameters	9408/0/537
Goodness-of-fit on F^2	1.052
Final R indexes [I>=2σ (I)]	R_1 = 0.0400, wR_2 = 0.0813
Final R indexes [all data]	R_1 = 0.0516, wR_2 = 0.0883
Largest diff. peak/hole / e Å^{-3}	0.492/-0.434

Synthesis of [Ru(κ²-OAc)(OC{Me}OCC{H}=CPhMe)(PPh₃)₂][BF₄] 26c

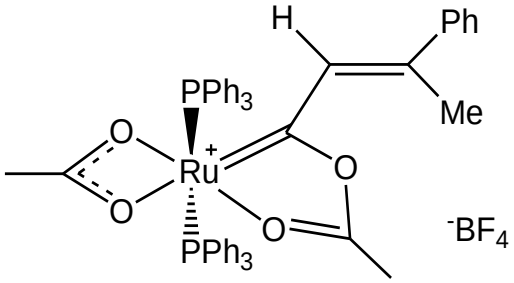

Reaction of *cis*-[Ru(κ²-OAc)₂(PPh₃)₂] **1** (250 mg, 0.336 mmol), 2-phenyl-3-butyn-2-ol **2b** (49 mg, 0.336 mmol) and trityl carbenium tetrafluoroborate (111 mg, 0.336 mmol) in DCM (20 ml) yielded

[Ru(κ²-OAc)(OC{Me}OCC{H}=CPhMe)(PPh₃)₂][BF₄] **26c** (170 mg, 0.177 mmol, 53 % yield) as a dark green powder.

^{1}H-NMR (500.23 MHz, CD_2Cl_2): δ_H 0.86 (s, 3H, COOC*H*$_3$), 1.82 (s, 3H, CPhC*H*$_3$), 1.92 (s, 3H, COOC*H*$_3$), 7.46 (m, 12H, *ortho* or *meta*-PPh_3), 7.52 (t, $^{3}J_{HH}$ = 7.6 Hz, 12H, *ortho* or *meta*-PPh_3), 7.57 (d, $^{3}J_{HH}$ = 7.0 Hz, 2H, *ortho* or *meta* Ph), 7.62 (m, 8H, *para*-PPh_3 and the *ortho* or *meta* Ph), 7.67 (t, $^{3}J_{HH}$ = 7.0 Hz, 1H, *para*-Ph), 8.10 (s, 1H, Ru=C-C*H*=CPh_2);

^{13}C-NMR (125.81 MHz, CD_2Cl_2): δ_C 19.6 (s, COO*C*H$_3$), 22.9 (s, COO*C*H$_3$), 23.2 (s, CPh*C*H$_3$), 128.6 (s, Ru=C-*C*H=CPh_2), 129.4 (t, $^{1}J_{PC}+^{3}J_{PC}$ = 46.0 Hz, C_1 of PPh_3), 130.6 (t, ΣJ = 10.1 Hz, $C_{2\text{ or }3}$ of PPh_3), 130.9 (s, Ph), 131.5 (s, Ph), 132.4 (s, Ph), 133.1 (s, C_4 of PPh_3), 135.4 (t, ΣJ = 12.0 Hz, $C_{2\text{ or }3}$ of PPh_3), 144.0 (s, C_1 of Ph), 148.7 (s, Ru=CCH=*C*PhMe), 184.7 (s, *C*OOCH$_3$), 187.7 (s, *C*OOCH$_3$), 284.3 (t, $^{2}J_{PC}$ = 8.6 Hz, Ru=*C*);

^{31}P-NMR (202.51 MHz, CD_2Cl_2): δ_P 32.3 (s, PPh_3);

^{11}B-NMR (128.27 MHz, CD_2Cl_2): δ_B -2.2 (s, BF_4);

^{19}F-NMR (376.17 MHz, CD_2Cl_2): δ_F -153.3 (s, $^{10}BF_4$), -153.4 (s, $^{11}BF_4$);

IR (CsCl, solution in DCM), 1631 cm^{-1} ν(C=O), 1579 cm^{-1} (κ²-OCO_{asym}), 1554cm^{-1} ν(C=C), 1481 cm^{-1} (P-Ph), 1433 cm^{-1} (κ²-OCO_{sym}), 1098 cm^{-1} (B-F), $\Delta\nu_{(chelate)}$ 146 cm^{-1};

MS (ESI), *m/z* 873.1830 (Calculated for $C_{50}H_{45}{}^{102}RuP_2O_4$ $[M]^+$ = 873.1845, Δ = 1.5 mDa), *m/z* 813.1624 (Calculated for $C_{48}H_{41}{}^{102}RuP_2O_2$ $[M\text{-}H]^+$ -AcO = 813.1632, Δ = 1.0 mDa), *m/z* 611.0912 (Calculated for $C_{32}H_{30}{}^{102}RuPO_4$ $[M]^+$ -PPh_3 = 611.0929, Δ = 1.7

mDa), *m/z* 551.0695 (Calculated for $C_{30}H_{26}{}^{102}RuPO_2$ $[M-H]^+$ -PPh_3 -AcO = 551.0717, Δ = 2.2 mDa);

Anal. for $C_{50}H_{45}RuP_2O_4BF_4$, (calc) C 62.58, H 4.73; (found) C 60.27, H 4.52.

Synthesis of [Ru(κ²-OAc)(OC{Me}OCC{H}=CMe₂)(PPh₃)₂][BF₄] 26d

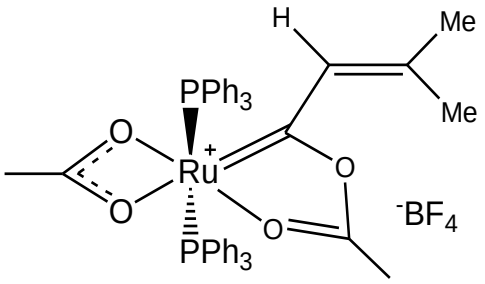

Reaction of *cis*-[Ru(κ²-OAc)₂(PPh₃)₂] **1** (250 mg, 0.34 mmol), 2-methyl-3-butyn-2-ol **2c** (32.5 µl, 0.34 mmol)and trityl carbenium tetrafluoroborate (111 mg, 0.34 mmol) in DCM (20 ml) yielded

[Ru(κ²-OAc)(OC{Me}OCC{H}=CMe₂)(PPh₃)₂][BF₄] **26d** (175 mg, 0.20 mmol, 58 % yield) as purple crystals.

^{1}H-NMR (500.23 MHz, CD_2Cl_2): δ_H 0.77 (s, 3H, κ²-COOC*H*3), 1.40 (s, 3H, COOC*H*$_3$), 1.74 (s, 3H, C*Me*$_2$), 1.80 (s, 3H, C*Me*$_2$), 7.37 (m, 12H, *ortho* or *meta*-PPh_3), 7.45 (m, 12H, *ortho* or *meta*-PPh_3), 7.54 (m, 6H, *para*-PPh_3), 7.69 (s, 1H, Ru=C-C*H*=CMe_2);

^{13}C-NMR (125.81 MHz, CD_2Cl_2): δ_C 18.5 (s, COO*C*H_3), 22.1 (s, COO*C*H_3), 24.1 (s, C*Me*$_2$), 30.4 (s, C*Me*$_2$), 128.3 (t, $^1J_{PC}+{}^3J_{PC}$ = 44.8 Hz, C_1 of PPh_3), 129.5 (t, ΣJ = 9.9 Hz, $C_{2\ or\ 3}$ of PPh_3), 130.9 (s, Ru=C-*C*H=CMe_2), 131.9 (s, C_4 of PPh_3), 134.3 (t, ΣJ = 11.8 Hz, $C_{2\ or\ 3}$ of PPh_3), 152.7 (s, Ru=CCH=*C*Me_2), 183.5 (s, *C*OOCH_3), 186.4 (s, *C*OOCH_3), 284.9 (t, $^2J_{PC}$ = 9.2 Hz, Ru=*C*);

^{31}P-NMR (202.51 MHz, CD_2Cl_2): δ_P 32.6 (s, PPh_3);

^{11}B-NMR (128.27 MHz, CD_2Cl_2): δ_B -2.1 (s, BF_4);

^{19}F-NMR (376.17 MHz, CD_2Cl_2): δ_F -153.3 (s, $^{10}BF_4$), -153.4 (s, $^{11}BF_4$);

IR (CsCl, solution in DCM), 1631 cm^{-1} ν(C=O), 1590 cm^{-1} (κ²-OCO_{asym}), 1527cm^{-1} ν(C=C), 1482 cm^{-1} (P-Ph), 1435 cm^{-1} (κ²-OCO_{sym}), 1096 cm^{-1} (B-F), $\Delta\nu_{(chelate)}$ 155 cm^{-1};

MS (ESI), *m/z* 811.1684 (Calculated for $C_{45}H_{43}{}^{102}RuP_2O_4$ $[M]^+$ = 811.1687, Δ = 0.3 mDa), $[M]^+$, *m/z* 549.0772 (Calculated for $C_{27}H_{28}{}^{102}RuPO_4$ $[M]^+$ -PPh_3 = 549.0770, Δ = 0.2 mDa);

Anal. for $C_{45}H_{43}$ $RuP_2O_4BF_4$, (calc) C 60.21, H 4.83; (found) C 59.53, H 5.08.

Table 6-7 Crystal data and structure refinement for $[Ru(\kappa^2\text{-}OAc)(OC\{Me\}OCC\{H\}=CMe_2)(PPh_3)_2][BF_4]$ **26d**

Identification code	jml1157_twin1_hklf4
Empirical formula	$C_{48.1}H_{49.6}BF_4O_4P_2Ru$
Formula weight	958.04
Temperature/K	110.00(10)
Crystal system	triclinic
Space group	P-1
a/Å, b/Å, c/Å	13.7465(5), 18.7040(7), 19.7169(6)
α/°, β/°, γ/°	109.732(3), 90.580(3), 107.771(3)
Volume/Å^3	4507.8(3)
Z	4
ρ_{calc}mg/mm^3	1.412
m/mm^{-1}	0.481
F(000)	1974.0
Crystal size/mm^3	0.2626 × 0.193 × 0.1579
2Θ range for data collection	5.78 to 52.22°
Index ranges	-15 ≤ h ≤ 16, -22 ≤ k ≤ 23, -24 ≤ l ≤ 24
Reflections collected	24811
Independent reflections	24811[R(int) = 0.0000]
Data/restraints/parameters	24811/72/1118
Goodness-of-fit on F^2	1.021
Final R indexes [I>=2σ (I)]	R_1 = 0.0460, wR_2 = 0.1211
Final R indexes [all data]	R_1 = 0.0647, wR_2 = 0.1280
Largest diff. peak/hole / e Å^{-3}	1.30/-1.21

Synthesis of [Ru(κ^2-O_2CPh)(OC{Ph}OCC{H}=CPh_2)(PPh_3)$_2$][BF_4] 27

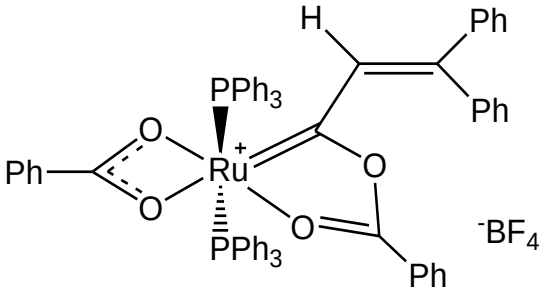

Reaction of *cis*-[Ru(κ^2-O_2CPh)$_2$(PPh_3)$_2$] **28** (250 mg, 0.29 mmol), 1,1-diphenylprop-2-yn-1-ol **2a** (60 mg, 0.29 mmol) and trityl carbenium tetrafluoroborate (95mg, 0.29 mmol) in DCM (20 ml) yielded [Ru(κ^2-O_2CPh)(OC{Ph}OCC{H}=CPh_2)(PPh_3)$_2$][BF_4] **27** (275 mg, 0.27 mmol, 80 % yield) as dark green crystals.

The diphenyl moiety has been assigned as Ph A and Ph B though the relative orientation of the rings is unknown. Peak assignment was completed with the aid of COSY, NOESY, DEPT, HSQC and HMBC experiments. Some resonances in the ^{13}C-NMR spectrum could not be unequivocally assigned.

^{1}H-NMR (700.13 MHz, CD_2Cl_2): δ_H 6.52 (br s, 2H, Ph), 6.74 (m, 2H, *ortho*-Ph A), 7.11 (m, 2H, Ph), 7.22 (m, 6H, two assigned as *ortho*-Ph B, two assigned as *ortho*-COOPh and two Ph), 7.32 (m, 13H, *ortho* or *meta*-PPh_3 and one Ph), 7.40 (m, 8H, *para*-PPh3 and *meta*-Ph A), 7.45 (m, 15H, *ortho* or *meta*-PPh_3 and Ph), 7.57 (tt, 1H, *para*-COOPh), 7.64 (tt, 1H, *para*-Ph A), 7.69 (tt, 1H, Ph), 8.56 (s, 1H, Ru=C-C*H*=CPh_2);

^{13}C-NMR (125.81 MHz, CD_2Cl_2): δ_C 123.8 (s, C_1 of COO*Ph*), 128.9 (s, Ph), 129.5 (t, $^1J_{PC}+^3J_{PC}$ = 45.4 Hz, C_1 of PPh_3), 129.5 (s, Ru=C-*C*H=CPh_2), 129.7 (s, C_2 of COOPh), 130.1 (s, $C_{3\text{ or }4}$ of Ph A), 130.3 (s, C_2 of Ph A), 130.4 (s, Ph), 130.5 (t, ΣJ = 9.7 Hz, $C_{2\text{ or }3}$ of PPh_3), 130.8 (s, Ph), 130.9 (s, Ph), 131.3 (s, Ph),132.2 (s, C_1 of COOPh), 132.2 (s, Ph), 132.7 (s, C_4 of PPh_3), 133.0 (s, Ph), 133.7 (s, Ph), 135.5 (t, ΣJ = 11.2 Hz, $C_{2\text{ or }3}$ of PPh_3), 138.1 (s, C4 of COOPh), 142.5 (s, C_1 of Ph), 143.1 (C_1 of Ph), 147.7 (s, Ru=CCH=*C*PhMe), 179.7 (s, *C*OOPh), 182.0 (s, *C*OOPh), 281.1 (t, $^2J_{PC}$ = 9.6 Hz, Ru=*C*);

^{31}P-NMR (202.51 MHz, CD_2Cl_2): δ_P 31.5 (s, PPh_3);

^{11}B-NMR (128.27 MHz, CD_2Cl_2): δ_B -2.1 (s, BF_4);

^{19}F-NMR (376.17 MHz, CD_2Cl_2): δ_F -153.4 (s, $^{10}BF_4$), -153.5 (s, $^{11}BF_4$);

IR (CsCl, solution in DCM), 1602 cm^{-1} ν(C=O), 1575 cm^{-1} (κ^2-OCO_{asym}), 1541cm^{-1} ν(C=C), 1481 cm^{-1} (P-Ph), 1434 cm^{-1} (κ^2-OCO_{sym}), 1095 cm^{-1} (B-F), $\Delta\nu_{(chelate)}$ 141 cm^{-1};

MS (ESI), *m/z* 1059.2280 (Calculated for $C_{65}H_{51}{}^{102}RuP_2O_4$ $[M]^+$ = 1059.2319, Δ = 3.9 mDa), *m/z* 797.1371 (Calculated for $C_{47}H_{36}{}^{102}RuPO_4$ $[M]^+$ -PPh_3 = 797.1402, Δ = 3.1 mDa), *m/z* 675.1028 (Calculated for $C_{40}H_{30}{}^{102}RuPO_2$ $[M-H]^+$ -PPh_3 -AcO = 675.1032, Δ = 0.4 mDa);

Anal. for $C_{65}H_{51}$ $RuP_2O_4BF_4$, (calc) C 68.12, H 4.49; (found) C 66.70, H 4.44.

Table 6-8 Crystal data and structure refinement for $[Ru(\kappa^2\text{-}COOPh)(OC\{Ph\}OCC\{H\}=CMe_2)(PPh_3)_2][BF_4]$ **29**

Identification code	jml1216
Empirical formula	$C_{66.1}H_{53.1}BCl_{2.1}F_4O_4P_2Ru$
Formula weight	1235.69
Temperature/K	110.00(10)
Crystal system	triclinic
Space group	P-1
a/Å, b/Å, c/Å	12.9840(4), 14.1298(5), 18.1180(6)
α/°, β/°, γ/°	89.703(3), 81.511(3), 63.313(3)
Volume/$Å^3$	2930.28(19)
Z	2
$\rho_{calc}mg/mm^3$	1.401
m/mm^{-1}	0.480
F(000)	1264.2
Crystal size/mm^3	0.1444 × 0.0839 × 0.0735
2Θ range for data collection	5.8 to 58.22°
Index ranges	-14 ≤ h ≤ 16, -17 ≤ k ≤ 19, -22 ≤ l ≤ 24
Reflections collected	20612
Independent reflections	13085[R(int) = 0.0290]
Data/restraints/parameters	13085/9/771
Goodness-of-fit on F^2	1.035
Final R indexes [I>=2σ (I)]	R_1 = 0.0458, wR_2 = 0.0950
Final R indexes [all data]	R_1 = 0.0625, wR_2 = 0.1044
Largest diff. peak/hole / e $Å^{-3}$	1.15/-0.85

General Method for the Reaction of [Ru(κ^2-OAc)(OC{Me}OCC{H}=CRR')(PPh$_3$)$_2$][BF$_4$] 26 with various nucleophiles and bases.

These reactions were carried out using 0.027 mmol of the starting organometallic reagent and an appropriate amount of organic reagent in 0.5 ml of CD_2Cl_2 in Young's NMR tubes. NMR spectra were recorded on the Brüker AV 500 spectrometer soon after addition and every few hours (or days depending on the speed of reaction) until the reaction was deemed complete. Organic products were then identified via comparison with a standard sample or literature values.[249, 256]

Synthesis of [Ru(κ^2-OAc)(κ^1-OAc)(PPh$_3$)$_2$(=C=C=CPh$_2$)] 30

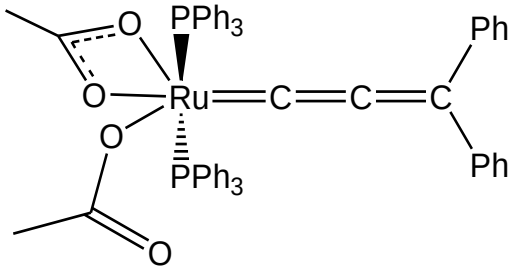

[Ru(κ^2-OAc)(OC{Me}OCC{H}=CPh$_2$)(PPh$_3$)$_2$][BF$_4$] **26b** (100 mg, 0.10 mmol) and sodium *tert*-butoxide (19 mg, 0.15 mmol) were dissolved in DCM and stirred at RT for 15 minutes. The DCM was then removed and the residue extracted with ether. The resulting solution was then reduced slightly before being placed in the freezer overnight. This either produced a red solid of approximately 83% purity by ^{31}P-NMR (20 mg, 0.02 mmol, 22% yield), or analytically pure red needle like crystals (5 mg, 0.005 mmol, 5% yield).

Peak assignment was completed with the aid of COSY, DEPT, HSQC, HMBC and ^{1}H-^{31}P HMQC experiments.

^{1}H-NMR (500.23 MHz, CD_2Cl_2): δ_H 0.91 (s, 6H, COO*C*H$_3$), 6.93 (at, 7.8 Hz, 4H, *ortho*-Ph), 7.15 (ad, 8.2 Hz, 4H, *meta*-Ph), 7.29 (at, 7.3 Hz, 12H, *ortho* or *meta*-PPh$_3$), 7.33 (ad, 7.0 Hz, 6H, *para*-PPh$_3$), 7.36 (m, 6H, *para*-Ph and impurities), 7.52 (m, 12H, *ortho* or *meta*-PPh$_3$);

^{13}C-NMR (125.78 MHz, CD_2Cl_2): δ_C 23.9 (s, COO*C*H$_3$), 129.2 (s, C$_4$ of Ph), 129.4 (t, ΣJ = 9.6 Hz, C$_{2\text{ or }3}$ of PPh$_3$), 129.9 (s, C$_3$ of Ph), 130.0 (s, C$_2$ of Ph), 131.4 (s, C$_4$ of PPh$_3$), 132.6 (t, $^1J_{PC}$+$^3J_{PC}$ = 41.3 Hz, C$_1$ of PPh$_3$), 136.2 (t, ΣJ = 12.0 Hz, C$_{2\text{ or }3}$ of PPh$_3$), 147.3 (s, Ru=C=C=*C*), 181.7 (s, *C*OOCH$_3$), 232.8 (t, $^3J_{PC}$ = 5.5 Hz, Ru=C=*C*), 305.0 (t, $^2J_{PC}$ = 17.3 Hz, Ru=*C*);

^{31}P-NMR (202.49 MHz, CD_2Cl_2): δ_P 32.6 (s, PPh_3);

IR (CsCl, solution in DCM), 1911 cm^{-1} ν(C=C=C), 1624 cm^{-1} (κ^1-OCO_{asym}), 1537 cm^{-1} (κ^2-OCO_{asym}), 1459 cm^{-1} (κ^2-OCO_{sym}), 1435 cm^{-1} (P-Ph), 1366 cm^{-1} (κ^1-OCO_{sym}), $\Delta\nu_{(uni)}$ 258 cm^{-1}, $\Delta\nu_{(chelate)}$ 78 cm^{-1};

MS (ESI), *m/z* 957.1781 (Calculated for $C_{55}H_{46}{}^{102}RuP_2O_4Na$ $[M+Na]^+$ = 957.1822, Δ = 4.1 mDa), *m/z* 935.1993 (Calculated for $C_{55}H_{47}{}^{102}RuP_2O_4$ $[M+H]^+$ = 935.2002, Δ = 0.9 mDa);

MS (LIFDI) *m/z* 934.13 $[M]^+$, *m/z* 892.14 $[M+H]^+$ -OAc;

Anal. for $C_{55}H_{46}RuP_2O_4$, (calc) C 70.73, H 4.96; (found) C 70.33, H 5.00.

Table 6-9 Crystal data and structure refinement for $[Ru(\kappa^2\text{-}OAc)(\kappa^1\text{-}OAc)(PPh_3)_2(=C=C=CPh_2)]$ **30**

Identification code	jml1226
Empirical formula	$C_{114}H_{102}O_9P_4Ru_2$
Formula weight	1941.98
Temperature/K	110.00(10)
Crystal system	triclinic
Space group	P-1
a / Å, b / Å, c / Å	11.1443(3), 13.0096(3), 18.0739(6)
α/°, β/°, γ/°	105.546(2), 105.975(3), 100.147(2)
Volume/Å^3	2337.02(11)
Z	1
ρ_{calc}mg/mm^3	1.380
m/mm^{-1}	0.453
F(000)	1006.0
Crystal size/mm^3	0.2586 × 0.1761 × 0.137
2Θ range for data collection	5.84 to 64.54°
Index ranges	-16 ≤ h ≤ 15, -19 ≤ k ≤ 19, -26 ≤ l ≤ 26
Reflections collected	43066
Independent reflections	15076[R(int) = 0.0273]
Data/restraints/parameters	15076/0/608
Goodness-of-fit on F^2	1.040
Final R indexes [I>=2σ (I)]	R_1 = 0.0295, wR_2 = 0.0676
Final R indexes [all data]	R_1 = 0.0365, wR_2 = 0.0719
Largest diff. peak/hole / e Å^{-3}	0.51/-0.82

Deprotonation of [Ru(κ^2-O_2CPh)(OC{Ph}OCC{H}=CPh_2)(PPh_3)$_2$][BF_4] 27

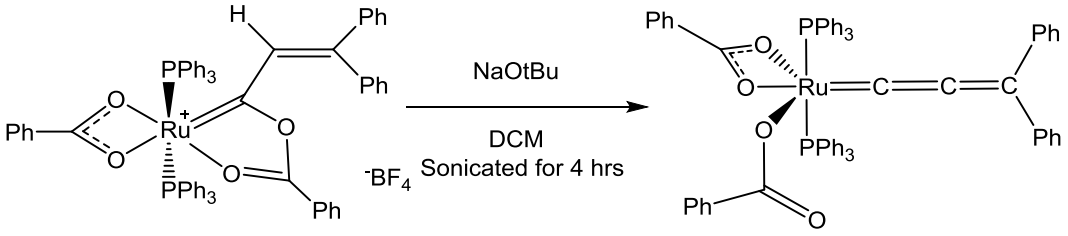

One equivalent of base was added to a DCM (5 ml) solution of [Ru(κ^2-O_2CPh)(OC{Ph}OCC{H}=CPh_2)(PPh_3)$_2$][BF_4] **27** (100 mg, 0.087 mmol). The resulting suspension was sonicated until a colour change from green to red was observed. The solvent was then removed *in vacuo* and the residue extracted with ether. Removal of the solvent yielded **27** as a dark red powder (23 mg, 0.022 mmol, 25% yield).

This data is from reaction with butoxide:

^{1}H-NMR (500.23 MHz, CD_2Cl_2): δ_H 6.87-7.75 (aromatic);

^{13}C-NMR (125.78 MHz, CD_2Cl_2): δ_C 126-145 (aromatic), 147.4 (t, $^4J_{PC}$ = 2.7 Hz Ru=C=C=*C*), 175.8 (d, J_{PC} = 2.7 Hz, by-product), 176.8 (s, *C*OOPh of by-product), 177.5 (s, *C*OOPh), 179.4 (s, unknown), 209.7 (d, J_{PC} = 4.5 Hz, by-product), 232.0 (t, $^3J_{PC}$ = 5.1 Hz, Ru=C=*C*), 281.9 (d, J_{PC} = 14.8 Hz, by-product), 304.4 (t, $^2J_{PC}$ = 18.6 Hz, Ru=*C*);

^{31}P-NMR (202.49 MHz, CD_2Cl_2): δ_P -5.5 (s, free PPh_3), 31.6 (s, PPh_3) allenylidene, 55.6 (s) unknown impurity;

MS (ESI), *m/z* 1059.2327 (Calculated for $C_{65}H_{51}{}^{102}RuP_2O_4$ $[M+H]^+$ = 1059.2318, Δ = 0.9 mDa), *m/z* 937.1964 (Calculated for $C_{58}H_{45}{}^{102}RuP_2O_4$ $[M]^+$ -COOPh = 673.1086, Δ = 26 mDa);

MS (LIFDI) *m/z* 1059.21 $[M+H]^+$, *m/z* 954.21 $[M]^+$ unknown;

Anal. for $C_{65}H_{50}RuP_2O_4$, (calc) C 73.78, H 4.76; (found) C 70.79, H 4.63.

Synthesis of [Ru(κ^2-OAc)(κ^1-OAc)(PPh$_3$)$_2$(=C=CH-C(Ph)=CH$_2$)] 32a

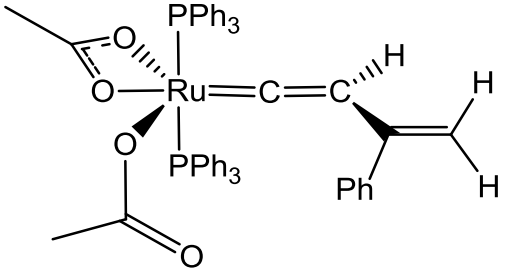

[Ru(κ^2-OAc)(OC{Me}OCC{H}=C(Me)Ph)(PPh$_3$)$_2$][BF$_4$] **26c** (100 mg, 0.104 mmol) and tetramethylammonium acetate (15 mg, 0.114 mmol) were suspended in DCM (10 ml). 2 minutes of sonication aided dissolution and the subsequent reaction was observed by a colour change from dark green to orange. After 10 minutes of stirring at RT the solvent was removed and the residue extracted with diethyl ether. Removal of the solvent yielded **32a** as an impure orange powder (15 mg, 0.017 mmol, 16% yield).

^{1}H-NMR (500.23 MHz, CD_2Cl_2): δ_H 0.86 (s, 6H, COOC*H*$_3$), 4.72 (s, 1H, Ru=C=C(H)C(Ph)C*H*$_2$), 4.90 (s, 1H, Ru=C=C(H)C(Ph)C*H*$_2$), 5.22 (t, 3.8 Hz, 1H, Ru=C=C(*H*), 6.90-7.56 (aromatic, 39H);

^{31}P-NMR (202.49 MHz, CD_2Cl_2): δ_P 34.6 (s, PPh_3);

IR (CsCl, solution in DCM), 1932 cm^{-1} ν(C=C), 1617 cm^{-1} (κ^1-OCO$_{asym}$, appears as a shoulder on the vinylidene resonance, a high resolution spectrum of a sample at much lower concentration enabled them to be resolved), 1534 cm^{-1} (κ^2-OCO$_{asym}$), 1465 cm^{-1} (κ^2-OCO$_{sym}$), 1436 cm^{-1} (P-Ph), 1366 cm^{-1} (κ^1-OCO$_{sym}$), Δν$_{(uni)}$ 251 cm^{-1}, Δν$_{(chelate)}$ 69 cm^{-1};

MS (ESI), *m/z* 873.1848 (Calculated for $C_{50}H_{45}{}^{102}RuP_2O_4$ [M+H]$^+$ = 873.1845, Δ = 0.3 mDa), *m/z* 812.1744 (Calculated for $C_{48}H_{41}{}^{102}RuP_2O_2$ [M-H]$^+$ -AcO = 812.1555, Δ = 18.9 mDa);

MS (LIFDI) *m/z* 872.20 [M]$^+$, *m/z* 812.06 [M-H]$^+$ -OAc.

Synthesis of [Ru(κ^2-OAc)(κ^1-OAc)(PPh$_3$)$_2$(=C=CH-C(Me)=CH$_2$)] 32b

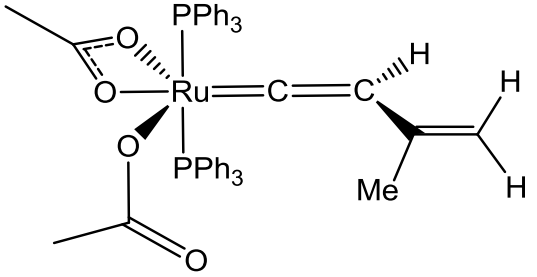

[Ru(κ^2-OAc)(OC{Me}OCC{H}=C(Me)$_2$)(PPh$_3$)$_2$][BF$_4$] **26d** (100 mg, 0.111 mmol) and tetramethylammonium acetate (17 mg, 0.125 mmol) were suspended in DCM (10 ml). 2 minutes of sonication aided dissolution and the subsequent reaction was observed by a colour change from dark purple to orange. After 10 minutes of stirring at RT the solvent was removed and the residue extracted with diethyl ether. Removal of the solvent yielded **32b** as an impure orange powder (18 mg, 0.022 mmol, 20% yield).

Peak assignment was completed with the aid of COSY, NOESY, HSQC and HMBC experiments.

^{1}H-NMR (500.23 MHz, CD_2Cl_2): δ_H 0.84 (s, 6H, COO*C*H$_3$), 1.31 (s, 3H, Ru=C=C(H)C(C*H*$_3$)CH$_2$), 3.75 (s, 1H, Ru=C=C(H)C(CH$_3$)C*H*$_2$), 3.48 (s, 1H, Ru=C=C(H)C(CH$_3$)C*H*$_2$), 5.21 (t, 3.8 Hz, 1H, Ru=C=C*H*), 7.40 (t, 7.2 Hz, 12H, *ortho* or *meta*-PPh$_3$), 7.44-7.54 (m, 18H, *ortho* or *meta*-PPh$_3$ and *para*-PPh$_3$);

^{13}C-NMR (125.78 MHz, CD_2Cl_2): δ_C 23.5 (s, COO*C*H$_3$), 23.7 (Ru=C=C(H)C(*C*H$_3$)CH$_2$), 104.6 (s, Ru=C=C(H)C(Ph)*C*H$_2$), 117.4 (s, Ru=C=*C*H), 129.5 (t, ΣJ = 10.1 Hz, C$_{2\text{ or }3}$ of PPh$_3$), 131.0 (t, $^1J_{PC}+^3J_{PC}$ = 43.3 Hz, C$_1$ of PPh$_3$), 131.6 (s, C$_4$ of PPh$_3$), 136.4 (t, ΣJ = 10.8 Hz, C$_{2\text{ or }3}$ of PPh$_3$), 137.4 (s, Ru=C=C(H)*C*(CH$_3$)CH$_2$), 181.0 (s, *C*OOCH$_3$), 360.4 (t, $^2J_{PC}$ = 17.0 Hz, Ru=*C*);

^{31}P-NMR (202.50 MHz, CD_2Cl_2): δ_P 33.4 (s, PPh$_3$);

IR (CsCl, solution in DCM), 1628 cm^{-1} ν(C=C), 1617 cm^{-1} (κ^1-OCO$_{asym}$, appears as a shoulder on the vinylidene resonance, a high resolution spectrum of a sample at much lower concentration enabled them to be resolved), 1552 cm^{-1} (κ^2-OCO$_{asym}$), 1466 cm^{-1} (κ^2-OCO$_{sym}$), 1434 cm^{-1} (P-Ph), 1367 cm^{-1} (κ^1-OCO$_{sym}$), Δν$_{(uni)}$ 250 cm^{-1}, Δν$_{(chelate)}$ 86 cm^{-1};

MS (ESI), *m/z* 811.1637 (Calculated for $C_{45}H_{43}{}^{102}RuP_2O_4$ $[M+H]^+$ = 811.1687, Δ = 5.0 mDa);

MS (LIFDI) *m/z* 810.19 $[M]^+$.

DFT Calculation Methods

Initial optimisations were performed at the (RI-)BP86/SV(P) level, followed by frequency calculations at the same level. Transition states were located by initially performing a constrained minimisation (by freezing internal coordinates that change most during the reaction) of a structure close to the anticipated transition state. This was followed by a frequency calculation to identify the transition vector to follow during a subsequent transition state optimisation. A final frequency calculation was then performed on the optimised transition-state structure. All minima were confirmed as such by the absence of imaginary frequencies and all transition states were identified by the presence of only one imaginary frequency. Energies, geometries and vibrational frequencies are presented.

Single-point calculations on the (RI-)BP86/SV(P) optimised geometries were performed using the hybrid PBE0 functional and the flexible def2-TZVPP basis set. The (RI-)PBE0/def2-TZVPP SCF energies were corrected for their zero point energies, thermal energies and entropies (obtained from the (RI-)BP86/SV(P)-level frequency calculations). In all calculations, a 28 electron quasi-relativistic ECP replaced the core electrons of Ru. No symmetry constraints were applied during optimisations. All calculations were performed using the TURBOMOLE V6.4 package using the resolution of identity (RI) approximation.[211-217, 219, 220]

Transition states were verified using the DRC module of TURBOMOLE 6.4. The DRC was run using an initial distortion length of 20, and all transition states were shown to be related to their adjacent minima.

Determination of pK_a

The calculation of pK_a values were undertaken as described by Lledós and co-workers.[221]

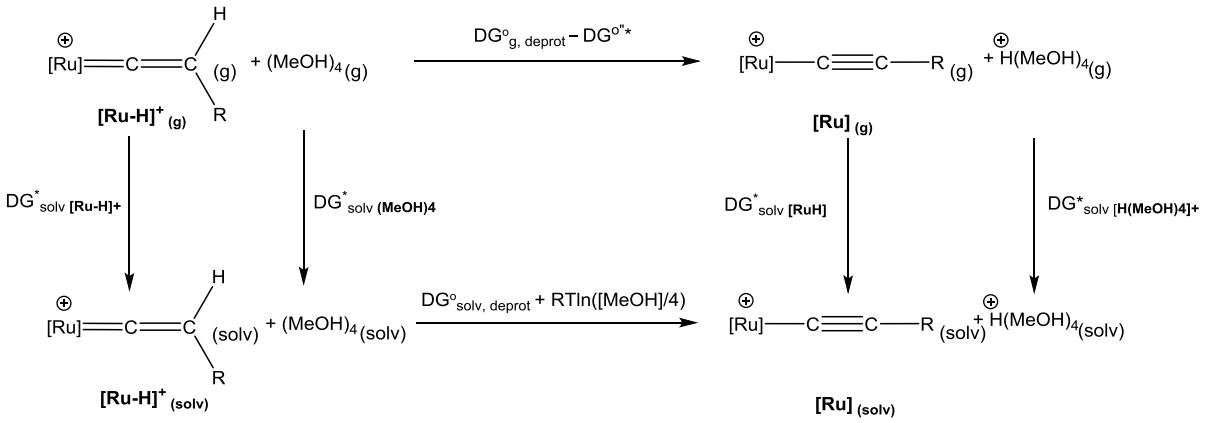

Scheme 6-1 Thermodynamic cycle for the evaluation of the free energy change association with deprotonation in solution. $\Delta G^{o\rightarrow *}$ is a conversion factor from 1 atm (ideal gas) to standard state of 1M. The RTln([MeOH]/4) term is a correction for the Gibbs energy change of one mole of $(MeOH)_4$ from liquids state to 1 M.

$$\Delta G°_{solv,deprot} = \Delta G°_{g,deprot} - \Delta G^{o\rightarrow *} + \Delta G^{*}_{solv[\boldsymbol{Ru}]} + \Delta G^{*}_{solv[H(\boldsymbol{MeOH})\boldsymbol{4}]+} - \Delta G^{*}_{solv[\boldsymbol{Ru-H}]+} - \Delta G^{*}_{solv\,(\boldsymbol{MeOH})\boldsymbol{4}} - RTln(\frac{[MeOH]}{4})$$

And

$$pKa = \frac{\Delta G_{sol,deprot}}{2.303\ RT}$$

An additional series of calculations were performed in order to benchmark the pK_a calculations against experimental data. The predicted and experimental pK_a values are in Table 6-10.

Table 6-10 pK_a Comparison

Complex	**Experimental pK_a**	**Calculated pK_a (MeOH)**	**Ref**
[Fe(η^5-C$_5$H$_5$)(=C=CHMe)(dppe)]$^+$	7.74 ± 0.05 (2:1 THF-H_2O)	8	[257]
[Fe(η^5-C$_5$H$_5$)(=C=CHBu^t)(CO)(PMe$_3$)]$^+$	13.6 ± 0.3 (CH_3CN)	3	[258]
[Ru(η^5-C$_5$H$_5$)(=C=CHBu^t)(PMe$_3$)$_2$]$^+$	20.8 ± 0.2 (CH_3CN)	13	[258]
[Ru(η^5-C$_5$H$_5$)(=C=CHSMe)(PMe$_3$)$_2$]$^+$	<6.35	11	[95]

Although this method predicts the pK_a of $[Fe(\eta^5\text{-}C_5H_5)(=C=CHMe)(dppe)]^+$ to a high degree of accuracy, the predicted acidity of the two complexes reported by Bullock[258] are modelled far less well. There may be a number of reasons for this, for example, the solvents used are different (CH_3CN for experiment and MeOH for the calculations). In addition, a difference of pKa of 1 correlates to an energy difference of only *ca.* 5 kJ mol^{-1}.

It is probably also unreasonable to suggest that the absolute calculated values are accurate, however, considering $[Fe(\eta^5\text{-}C_5H_5)(=C=CH^tBu)(CO)(PMe_3)]^+$ and $[Ru(\eta^5\text{-}C_5H_5)(=C=CH^tBu)(PMe_3)_2]^+$ (whose pK_a values were determined under identical conditions) it should be noted that the ordering of acidity is correct, and the difference is similar (experimental, 7.2; predicted 10). Therefore, we can gain confidence for the fundamental conclusion proposed regarding the difference in behaviour between the cationic vinylvinylidene/allenylidene complexes and their neutral analogues. Here the difference in pK_a is predicted to be *ca*. 17-19, supporting the far greater acidity of the cationic species.

Chapter 4 Experimental

Synthesis of $[Ru(\kappa^2\text{-}OAc)(OC\{Me\}OCC\{H\}=CH_2)(PPh_3)_2][BF_4]$ 26a

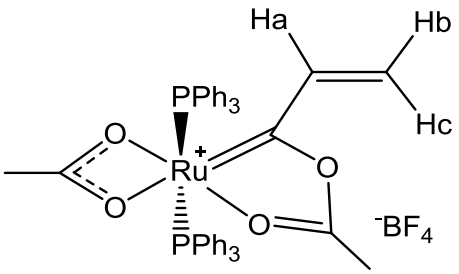

cis-$[Ru(\kappa^2\text{-}OAc)_2(PPh_3)_2]$ **1a** (150 mg, 0.20 mmol) and propargyl alcohol **2** (11 µl, 0.20 mmol) were dissolved in DCM (10 ml) and stirred at room temperature for 30 minutes. The DCM was then reduced to ~2 ml, and the hydroxy vinylidene **3a** precipitated by addition of pentane. The resulting pale orange solid was isolated by filtration and dried *in vacuo*. It was then redissolved in DCM (10 ml) and the solution frozen in liquid nitrogen. Tritylcarbenium tetrafluoroborate (66 mg, 0.20 mmol) was added and the solution was thawed and refrozen as quickly as possible. At this point the solution was partially thawed and an NMR sample taken (and kept frozen as much as practical). The remaining material was then thawed and layered with pentane. On one occasion crystals of $[Ru(\kappa^2\text{-}OAc)(CH_2CH_2PPh_3)(CO)(PPh_3)_2][BF_4]$ **44** were obtained.

$[Ru(\kappa^2\text{-}OAc)(OC\{Me\}OCC\{H\}=CH_2)(PPh_3)_2][BF_4]$ **26a** was found to be short lived and formed with a major impurity, only the peaks due to **26a** are reported.

^{1}H-NMR (500.23 MHz, CD_2Cl_2): δ_H 0.82 (s, 3H, COOC*H*$_3$) and 1.86 (s, 3H, COOC*H*$_3$). 6.32 (d, 1H, $^{3}J_{HH}$ = 11.0 Hz, Hb), 6.50 (d, 1H, $^{3}J_{HH}$ = 17.3 Hz, Hc), a 2D-COSY experiment showed cross-peaks that showed the resonance for Ha to be in the aromatic region.

^{31}P-NMR (202.50 MHz, CD_2Cl_2): δ_P 31.1 (s, PPh_3);

Table 6-11 Crystal data and structure refinement for $[Ru(\kappa^2\text{-}OAc)(CH_2CH_2PPh_3)(CO)(PPh_3)_2][BF_4]$ **44**

Identification code	jml1144
Empirical formula	$C_{59}H_{52}BF_4O_3P_3Ru$
Formula weight	1089.80
Temperature / K	110.00(10)
Crystal system	triclinic
Space group	P-1
a / Å, b / Å, c / Å	14.0432(11), 14.2540(10), 15.1618(11)
α/°, β/°, γ/°	76.741(6), 77.713(6), 69.227(7)
Volume / Å^3	2733.0(3)
Z	2
ρ_{calc} / mg mm^{-3}	1.324
m / mm^{-1}	0.431
F(000)	1120
Crystal size / mm^3	0.2488 × 0.1373 × 0.0917
2Θ range for data collection	5.82 to 51.92°
Index ranges	-16 ≤ h ≤ 16, -14 ≤ k ≤ 16, -12 ≤ l ≤ 18
Reflections collected	13675
Independent reflections	8278[R(int) = 0.0321]
Data/restraints/parameters	8278/32/657
Goodness-of-fit on F^2	1.060
Final R indexes [I>2σ (I)]	R_1 = 0.0486, wR_2 = 0.1157
Final R indexes [all data]	R_1 = 0.0642, wR_2 = 0.1242
Largest diff. peak/hole / e Å^{-3}	0.752/-0.655

Reaction of [Ru(κ^2-OAc)(κ^1-OAc)(C=C=CHCH$_2$OH)(PPh$_3$)$_2$] 3a with [CPh$_3$][BF$_4$] and PPh$_3$.

cis-[Ru(κ^2-OAc)$_2$(PPh$_3$)$_2$] **1a** (150 mg, 0.20 mmol) and propargyl alcohol (11 µl, 0.20 mmol) were dissolved in DCM (10 ml) and stirred at room temperature for 30 minutes. The DCM was then reduced to ~2 ml, and the hydroxy vinylidene **3a** precipitated by addition of pentane. The resulting pale orange solid was isolated by filtration and dried *in vacuo*. It was then redissolved in DCM (10 ml) and the solution frozen in liquid nitrogen. The solution was partially thawed before the addition of trityl carbenium tetrafluoroborate (66 mg, 0.20 mmol). The mixture was shaken and then triphenylphosphine (53 mg, 0.20 mmol) added to give a yellow solution which was refrozen. At this point the solution was partially thawed and an NMR sample taken (and kept frozen as much as practical). The major product was found to be *cis*-[Ru(κ^2-OAc)$_2$(PPh$_3$)$_2$] **1a**.

Synthesis of [Ph$_3$C–PPh$_3$][BF$_4$] 42

Tritylcarbenium tetrafluoroborate (50 mg, 0.15 mmol) was added to a DCM (10 ml) solution of triphenylphosphine (39 mg, 0.15 mmol). After 5 minutes stirring at room temperature the product was precipitated by addition of pentane and isolated by filtration. After drying *in vacuo*, [Ph$_3$C–PPh$_3$][BF$_4$] **42** was obtained as a white solid (60 mg, 0.10 mmol, 68% yield). Synthesis taken from Sanders where analytical data is presented.[226]

^{1}H-NMR (500.23 MHz, CD_2Cl_2): δ_H 6.89 (add, $^3J_{PH}$ = 11.4 Hz, $^3J_{HH}$ = 7.9 Hz, 6H, *ortho*-PPh$_3$), 7.05 (ad, $^3J_{HH}$ = 7.9 Hz, 6H, *ortho*-CPh$_3$), 7.34 (m, 2H, free PPh$_3$), 7.40 (at, $^3J_{HH}$ = 8.0 Hz, 7H, *meta*-CPh$_3$, the high integration is presumably due to contaminant free PPh$_3$.), 7.54 (atd, $^3J_{HH}$ = 8.0 Hz, 6H, *meta*-PPh$_3$), 7.60 (at, $^3J_{HH}$ = 7.4 Hz, 3H, *para*-CPh$_3$), 7.87 (at, $^3J_{HH}$ = 7.4 Hz, 3H, *para*-PPh$_3$);

^{13}C-NMR (125.78 MHz, CD_2Cl_2): δ_C 70.2 (d, $^1J_{PC}$ = 40.0 Hz, *C*Ph$_3$), 121.9 (d, $^1J_{PC}$ = 74.9 Hz, C_1 of PPh$_3$), 130.9 (d, $^4J_{PC}$ = 1.9 Hz, C_3 of CPh$_3$), 131.9 (d, $^5J_{PC}$ = 2.4 Hz, C_4 of CPh$_3$), 132.1 (d, $^3J_{PC}$ = 12.0 Hz, C_3 of PPh$_3$), 133.7 (d, $^3J_{PC}$ = 5.5 Hz, C_2 of CPh$_3$), 136.8 (d, $^2J_{PC}$ = 8.6 Hz, C_2 of PPh$_3$), 137.1 (d, $^4J_{PC}$ = 3.4 Hz, C_4 of PPh$_3$), 137.7 (d, $^2J_{PC}$ = 2.8 Hz, C_1 of CPh$_3$);

^{31}P-NMR (202.50 MHz, CD_2Cl_2): δ_P -5.5 (s, free PPh$_3$), 24.4 (s, Ph$_3$CPPh$_3$);

^{11}B-NMR (123.27 MHz, CD_2Cl_2): δ_B -2.1 (s, BF$_4$);

^{19}F-NMR (376.17 MHz, CD_2Cl_2): δ_F -152.9 (s, ^{10}BF$_4$), -152.8 (s, ^{11}BF$_4$);

IR (CsCl, solution in DCM), 1495 cm^{-1} (Ph C-H bend), 1484 cm^{-1} (Ph C-H bend), 1439 cm^{-1} (P-Ph), 1436 cm^{-1} (C-P), 1060 cm^{-1} (BF_4);

MS (ESI), *m/z* 243.1124 (Calculated for $C_{19}H_{15}$ $[CPh_3]^+$ = 243.1168, Δ = 4.4 mDa), *m/z* 263.0960 (Calculated for $C_{18}H_{15}P$ $[PPh_3+H]^+$ = 263.0984, Δ = 2.4 mDa);

Table 6-12 Crystal data and structure refinement for $[Ph_3C–PPh_3][BF_4]$ **42**

Identification code	jml1318
Empirical formula	$C_{37.4}H_{30}BCl_{0.8}F_4P$
Formula weight	627.00
Temperature / K	110.00(10)
Crystal system	orthorhombic
Space group	$Pna2_1$
a / Å, b / Å, c / Å	19.4505(7), 21.3891(9), 7.8748(3)
α/°, β/°, γ/°	90, 90, 90
Volume / $Å^3$	3276.1(2)
Z	4
ρ_{calc} / mg mm^{-3}	1.271
m / mm^{-1}	0.200
F(000)	1299.0
Crystal size / mm^3	0.2404 × 0.0692 × 0.0232
2Θ range for data collection	MoKα (λ = 0.71073)
Index ranges	5.898 to 55.842°
Reflections collected	-14 ≤ h ≤ 25, -27 ≤ k ≤ 15, -5 ≤ l ≤ 10
Independent reflections	8308
Data/restraints/parameters	4392 [R_{int} = 0.0331, R_{sigma} = 0.0597]
Goodness-of-fit on F^2	4392/65/432
Final R indexes [I>2σ (I)]	1.358
Final R indexes [all data]	R_1 = 0.1227, wR_2 = 0.3322
Largest diff. peak/hole / e $Å^{-3}$	R_1 = 0.1526, wR_2 = 0.3594

Synthesis of [Ru(κ^2-OAc)(κ^1-OAc)(η^2-H_2C=C=CHPPh_3)(PPh_3)$_2$][BF_4] 45a

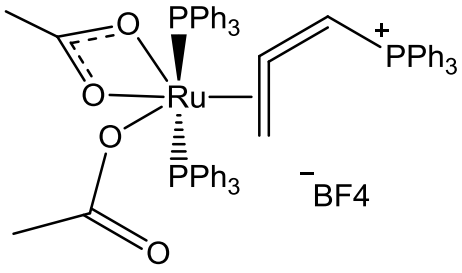

Triphenylpropargylphosphonium bromide **39a** (51 mg, 0.13 mmol) and silver tetrafluoroborate (26 mg, 0.23 mmol) were stirred in DCM (5 ml) for 5 minutes. The resulting precipitate was allowed to settle and the solution filtered into a solution of *cis*-[Ru(κ^2-OAc)$_2$(PPh_3)$_2$] **1a** (100 mg, 0.13 mmol) in DCM (5 ml). This solution was stirred for 15 minutes before the DCM was reduced to ~2 ml, and the product precipitated by addition of pentane. Filtration yielded [Ru(κ^2-OAc)(κ^1-OAc)(η^2-H_2C=C=CHPPh_3)(PPh_3)$_2$][BF_4] **45a** as a yellow solid (65 mg, 0.07 mmol, 50% yield) which was crystallised by slow diffusion of pentane into a DCM solution.

Peak assignment was completed with the aid of COSY, NOESY, HSQC and HMBC experiments.

^{1}H-NMR (500.23 MHz, CD_2Cl_2): δ_H 1.07 (s, 6H, COOC*H*$_3$), 2.81 (m, 2H, *H*$_2$C=C=CHPPh_3), 6.46 (ad, 1H, H_2C=C=C*H*PPh_3), 7.16 (m, 6H, *ortho* or *meta*-CHPPh_3), 7.37 (m, 27H, *ortho* and *meta*-PPh_3), 7.52 (m, 7H, *para*-PPh_3), 7.62 (m, 7H, *ortho* or *meta*-CHPPh_3), 7.86 (m, 3H *para*-CHPPh_3). The high integrations are presumably due to contaminant starting material.

^{13}C-NMR (125.78 MHz, CD_2Cl_2): δ_C 24.7 (s, COO*C*H$_3$), 27.3 (s, H_2*C*=C=CHPPh_3), 86.5 (d, $^1J_{PC}$ = 88.5 Hz, H_2C=C=*C*HPPh_3), 120.5 (d, $^1J_{PC}$ = 89.5 Hz, C_1 of CHPPh_3), 129.1 (t, $^1J_{PC}$+$^3J_{PC}$ = 41.9 Hz, C_1 of PPh_3), 129.9 (t, ΣJ = 10.1 Hz, $C_{2\text{ or }3}$ of PPh_3), 131.6 (d, ΣJ = 12.1 Hz, $C_{2\text{ or }3}$ of CHPPh_3), 132.3 (s, C_4 of PPh_3), 135.2 (d, ΣJ = 10.4 Hz, $C_{2\text{ or }3}$ of CHPPh_3), 136.1 (t, ΣJ = 10.9 Hz, $C_{2\text{ or }3}$ of PPh_3), 136.5 (d, $^4J_{PC}$ = 3.4 Hz, C_4 of CHPPh_3), 189.9 (s, *C*OOCH$_3$), 218.7 (s, H_2C=*C*=CHPPh_3);

^{31}P-NMR (202.50 MHz, CD_2Cl_2): δ_P 13.77 (t, $^4J_{PP}$ = 3.0 Hz, CHPPh_3), 29.05 (d, $^4J_{PP}$ = 3.0 Hz, PPh_3);

^{11}B-NMR (128.27 MHz, CD_2Cl_2): δ_B -2.1 (s, BF_4);

^{19}F-NMR (376.17 MHz, CD_2Cl_2): δ_F -153.1 (s, $^{10}BF_4$), -153.2 (s, $^{11}BF_4$);

IR (ATR), 3066 cm^{-1} (aromatic C-H stretch), 1692 cm^{-1} (allene and κ^1 combination), 1645 cm^{-1} (allene and κ^1 combination), 1586 cm^{-1} (κ^2-OCO_{asym}), 1518 cm^{-1} (κ^2-OCO_{sym}), 1435 cm^{-1} (P-Ph), 1054 cm^{-1} (BF_4), $\Delta\nu_{(chelate)}$ 107 cm^{-1};

MS (ESI), *m/z* 1045.2290 (Calculated for $C_{61}H_{54}{}^{102}RuP_3O_4$ $[M]^+$ = 1045.2289, Δ = 0.0 mDa);

Anal. for $C_{61}H_{54}BF_4O_4P_3Ru$ • 0.7 $C_{59}H_{51}BBrF_4O_2P_3Ru$, (calc) C 63.37, H 4.66; (found) C 63.36, H 4.69. The XRD and MS data suggest that the κ^1 acetate ligand can exchange with residual bromide and varying levels have been observed.

Table 6-13 Crystal data and structure refinement for $[Ru(\kappa^2\text{-}OAc)(\kappa^1\text{-}OAc)(\eta^2\text{-}H_2C{=}C{=}CHPPh_3)(PPh_3)_2][BF_4]$ **45a**

Identification code	jml1303
Empirical formula	$C_{61.9}H_{55.8}BBr_{0.1}Cl_2F_4O_{3.8}P_3Ru$
Formula weight	1219.82
Temperature / K	110.00(10)
Crystal system	triclinic
Space group	P-1
a / Å, b / Å, c / Å	11.7606(6), 15.4442(7), 17.4519(8)
α/°, β/°, γ/°	94.638(4), 92.883(4), 103.829(4)
Volume / $Å^3$	3059.9(3)
Z	2
ρ_{calc} / mg mm^{-3}	1.324
m / mm^{-1}	0.529
F(000)	1250.3
Crystal size / mm^3	0.3103 × 0.1944 × 0.06
2Θ range for data collection	MoKα (λ = 0.71073)
Index ranges	5.694 to 60.612°
Reflections collected	-16 ≤ h ≤ 15, -17 ≤ k ≤ 21, -24 ≤ l ≤ 22
Independent reflections	28846
Data/restraints/parameters	15990 [R_{int} = 0.0370, R_{sigma} = 0.0666]
Goodness-of-fit on F^2	15990/25/749
Final R indexes [I>2σ (I)]	1.090
Final R indexes [all data]	R_1 = 0.0725, wR_2 = 0.1979
Largest diff. peak/hole / e $Å^{-3}$	R_1 = 0.0935, wR_2 = 0.2130

Table 6-14 Crystal data and structure refinement for $[RuCl(\kappa^2\text{-}OAc)(\eta^2\text{-}H_2C{=}C{=}CHPPh_3)(PPh_3)_2][BF_4]$ **45a'** and $[Ru(\kappa^2\text{-}OAc)(CH_2CH_2PPh_3)(CO)(PPh_3)_2][BF_4]$ **44**

Identification code	jml1320
Empirical formula	$C_{60}H_{53.7}BCl_{2.3}F_4O_{2.7}P_3Ru$
Formula weight	1180.53
Temperature / K	109.95(10)
Crystal system	triclinic
Space group	P-1
a / Å, b / Å, c / Å	14.0007(5), 14.3027(5), 15.1862(7)
α/°, β/°, γ/°	76.224(4), 77.324(4), 69.030(4)
Volume / $Å^3$	2727.6(2)
Z	2
ρ_{calc} / mg mm^{-3}	1.437
m / mm^{-1}	0.547
F(000)	1209.0
Crystal size / mm^3	0.3366 × 0.1889 × 0.0229
2Θ range for data collection	MoKα (λ = 0.71073)
Index ranges	5.762 to 62.14°
Reflections collected	-19 ≤ h ≤ 20, -20 ≤ k ≤ 18, -16 ≤ l ≤ 20
Independent reflections	23580
Data/restraints/parameters	15168 [R_{int} = 0.0330, R_{sigma} = 0.0631]
Goodness-of-fit on F^2	15168/5/700
Final R indexes [I>2σ (I)]	1.036
Final R indexes [all data]	R_1 = 0.0672, wR_2 = 0.1703
Largest diff. peak/hole / e $Å^{-3}$	R_1 = 0.0903, wR_2 = 0.1878

Synthesis of $[HC{\equiv}CCH_2PPh_3][BF_4]$ 39b

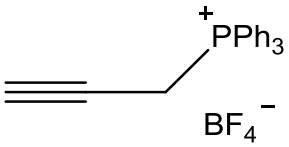

Triphenylpropargylphosphonium bromide **39a** (500 mg, 1.3 mmol) was dissolved in dry methanol (5 ml) and added to a solution of sodium tetrafluoroborate (175 mg, 1.3 mmol) in dry methanol (5 ml). The resulting white precipitate was filtered and washed with water and methanol. This gave triphenylpropargylphosphonium tetrafluoroborate **39b** (295 mg, 0.76 mmol, 46 % yield).

This compound was found to isomerise very readily to allene **40b** in solution. As a result the ^{13}C-NMR spectrum and the IR spectrum contained peaks for both species (those for the allene have not been reported here) and we were unable to observe the quaternary alkyne resonance in the ^{13}C-NMR spectrum.

^{1}H-NMR (399.78 MHz, CD_2Cl_2): δ_H 2.46 (dt, $^{4}J_{PH}$ = 6.7 Hz, $^{4}J_{HH}$ = 2.8 Hz, 1H, C*H*), 4.32 (dd, $^{2}J_{PH}$ = 15.1 Hz, $^{4}J_{HH}$ = 2.8 Hz, 2H, CH_2), 7.77 (m, 12H, *ortho* and *meta* PPh_3), 7.93 (m, 3H, *para*-PPh_3);

^{13}C-NMR (100.53 MHz, CD_2Cl_2): δ_C 17.4 (d, $^{1}J_{PC}$ = 58.0 Hz, *C*H_2), 77.4 (d, $^{3}J_{PC}$ = 9.2 Hz, H*C*CCH_2), 117.1 (d, $^{1}J_{PC}$ = 89.9 Hz, C_1 of PPh_3), 130.9 (d, $^{3}J_{PC}$ = 13.0 Hz, C_3 of PPh_3), 134.1 (d, $^{2}J_{PC}$ = 10.2 Hz, C_2 of PPh_3), 136.2 (d, $^{4}J_{PC}$ = 3.1 Hz, C_4 of PPh_3);

^{31}P-NMR (161.83 MHz, CD_2Cl_2): δ_P 22.0 (s, PPh_3);

^{11}B-NMR (123.27 MHz, CD_2Cl_2): δ_B -2.2 (s, BF_4);

^{19}F-NMR (376.17 MHz, CD_2Cl_2): δ_F -152.8 (s, $^{10}BF_4$), -152.9 (s, $^{11}BF_4$);

IR (CsCl, solution in DCM), 3300 cm^{-1} (alkyne C-H stretch), 3054 cm^{-1} (aromatic C-H stretch), 1440 cm^{-1} (P-Ph), 1423 cm^{-1} (C-P), 1268 cm^{-1} ($OPPh_3$), 1060 cm^{-1} (BF_4);

MS (ESI), *m/z* 301.1143 (Calculated for $C_{21}H_{18}P$ $[M]^+$ = 301.1141, Δ = 0.2 mDa);

Synthesis of $[H_2C=C=CHPPh_3][BF_4]$ 40b

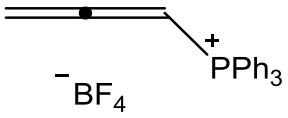

Triphenylpropargylphosphonium bromide **39a** (500 mg, 1.3 mmol) and sodium tetrafluoroborate (175 mg, 1.3 mmol) were stirred in DCM (25 ml) for 6 days. The resulting suspension was then filtered and the filtrate reduced and dried to give $[H_2C=C=CHPPh_3][BF_4]$ **40b** as a white powder (506 mg, 1.3 mmol, 99% yield).

^{1}H-NMR (399.78 MHz, CD_2Cl_2): δ_H 5.39 (dd, $^4J_{PH}$ = 12.7 Hz, $^4J_{HH}$ = 6.6 Hz, 2H, C*H*$_2$), 6.52 (dt, $^2J_{PH}$ = 8.0 Hz, $^4J_{HH}$ = 6.6 Hz, 1H, C*H*), 7.65 (m, 6H, *ortho* or *meta* PPh_3), 7.76 (m, 6H, *ortho* or *meta* PPh_3), 7.92 (3H, *para*-PPh_3);

^{13}C-NMR (100.53 MHz, CD_2Cl_2): δ_C 74.7 (d, $^1J_{PC}$ = 96.1 Hz, *C*H), 80.9 (d, $^3J_{PC}$ = 14.4 Hz, *C*H$_2$), 118.1 (d, $^1J_{PC}$ = 92.1 Hz, C_1 of PPh_3), 130.8 (d, $^3J_{PC}$ = 13.3 Hz, C_3 of PPh_3), 134.1 (d, $^2J_{PC}$ = 10.6 Hz, C_2 of PPh_3), 136.0 (d, $^4J_{PC}$ = 2.9 Hz, C_4 of PPh_3), 218.7 (d, $^2J_{PC}$ = 1.3 Hz, H$_2$C*C*CH);

^{31}P-NMR (161.83 MHz, CD_2Cl_2): δ_P 18.8 (s, PPh_3);

^{11}B-NMR (123.27 MHz, CD_2Cl_2): δ_B -2.1 (s, BF_4);

^{19}F-NMR (376.17 MHz, CD_2Cl_2): δ_F -152.8 (s, $^{10}BF_4$), -152.9 (s, $^{11}BF_4$);

IR (CsCl, solution in DCM), 3053 cm^{-1} (aromatic C-H stretch), 1960 cm^{-1} (allene C=C stretch), 1440 cm^{-1} (P-Ph), 1422 cm^{-1} (C-P), 1268 cm^{-1} ($OPPh_3$), 1060 cm^{-1} (BF_4);

MS (ESI), *m/z* 301.1140 (Calculated for $C_{21}H_{18}P$ $[M]^+$ = 301.1141, Δ = 0.1 mDa);

Anal. for $C_{21}H_{18}BF_4P$, (calc) C 64.98, H 4.67; (found) C 64.80, H 4.66.

Synthesis of $[HC{\equiv}CCH_2PPh_3][BPh_4]$ 39c

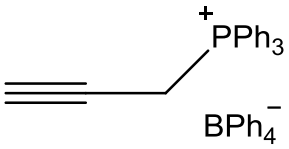

Triphenylpropargylphosphonium bromide **39a** (500 mg, 1.3 mmol) was dissolved in dry methanol (5 ml) was added to a solution of sodium tetraphenylborate (500 mg, 1.45 mmol) in dry methanol (5 ml). The resulting white precipitate was filtered and washed with water and methanol. It was then dried under vacuum overnight at 40 ˚C to give triphenylpropargylphosphonium tetraphenylborate **39c** (783 mg, 1.26 mmol, 97 % yield).

^{1}H-NMR (399.78 MHz, CD_2Cl_2): δ_H 2.36 (dt, $^4J_{PH}$ = 6.7 Hz, $^4J_{HH}$ = 2.8 Hz, 1H, C*H*), 3.08 (dd, $^2J_{PH}$ = 14.9 Hz, $^4J_{HH}$ = 2.8 Hz, 2H, CH_2), 6.83 (m, 4H, *para*-BPh_4), 6.99 (m, 8H, *meta*-BPh_4), 7.38 (m, 8H, *ortho*-BPh_4, displays complex B coupling), 7.47 (m, 6H, *ortho* or *meta* PPh_3), 7.69 (m, 6H, *ortho* or *meta* PPh_3), 7.89 (3H, *para*-PPh_3);

^{13}C-NMR (100.53 MHz, CD_2Cl_2): δ_C 16.7 (d, $^1J_{PC}$ = 58.0 Hz, *C*H_2), 71.1 (d, $^2J_{PC}$ = 12.8 Hz, HC*C*CH_2), 77.5 (d, $^3J_{PC}$ = 9.8 Hz, H*C*CCH_2), 116.8 (d, $^1J_{PC}$ = 87.9 Hz, C_1 of PPh_3), 122.1 (s, C_4 of BPh_4), 126.1 (m, $C_{2\text{ or }3}$ of BPh_4), 130.9 (d, $^3J_{PC}$ = 13.1 Hz, C_3 of PPh_3), 133.9 (d, $^2J_{PC}$ = 10.0 Hz, C_2 of PPh_3), 136.3 (br d, $^4J_{PC}$ = 2.8 Hz, C_4 of PPh_3 and $C_{2\text{ or }3}$ of BPh_4), 164.5 (q, $^1J_{PB}$ = 49.6 Hz, C_1 of BPh_4);

^{31}P-NMR (161.83 MHz, CD_2Cl_2): δ_P 21.5 (s, PPh_3);

^{11}B-NMR (123.27 MHz, CD_2Cl_2): δ_B -7.4 (s, BPh_4);

IR (CsCl, solution in DCM), 3300 cm^{-1} (alkyne C-H stretch), 3055 cm^{-1} (aromatic C-H stretch), 1580 cm^{-1} (BPh_4), 1440 cm^{-1} (P-Ph), 1427 cm^{-1} (C-P), 1270 cm^{-1} ($OPPh_3$);

MS (ESI, positive mode), *m/z* 301.1134 (Calculated for $C_{21}H_{18}P$ $[M]^+$ = 301.1141, Δ = 0.7 mDa), (ESI, negative mode), *m/z* 319.1680 (Calculated for $C_{24}H_{20}B$ $[M]^-$ = 319.1668, Δ = 1.2 mDa);

Anal. for $C_{45}H_{38}BP$, (calc) C 87.09, H 6.17; (found) C 87.07, H 6.18.

Synthesis of $[H_2C=C=CHPPh_3][BPh_4]$ 40c

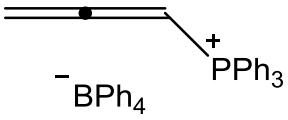

Triphenylpropargylphosphonium bromide **39a** (500 mg, 1.3 mmol) and sodium tetraphenylborate (449 mg, 1.3 mmol) were stirred in DCM (25 ml) for 3 weeks. The resulting suspension was then filtered and the filtrate reduced and dried to give $[H_2C=C=CHPPh_3][BPh_4]$ **40c** as a white powder (731 mg, 1.18 mmol, 90% yield).

^{1}H-NMR (399.78 MHz, CD_2Cl_2): δ_H 5.27 (dd, $^4J_{PH}$ = 12.7 Hz, $^4J_{HH}$ = 6.6 Hz, 2H, C*H*$_2$), 6.05 (dt, $^2J_{PH}$ = 8.3 Hz, $^4J_{HH}$ = 6.6 Hz, 1H, C*H*), 6.87 (m, 4H, *para*-BPh_4), 7.01 (m, 8H, *meta*-BPh_4), 7.33 (m, 8H, *ortho*-BPh_4, displays complex B coupling), 7.52 (m, 6H, *ortho* or *meta* PPh_3), 7.70 (m, 6H, *ortho* or *meta* PPh_3), 7.88 (3H, *para*-PPh_3);

^{13}C-NMR (100.53 MHz, CD_2Cl_2): δ_C 74.7 (d, $^1J_{PC}$ = 95.5 Hz, *C*H), 81.2 (d, $^3J_{PC}$ = 14.6 Hz, *C*H$_2$), 117.8 (d, $^1J_{PC}$ = 91.6 Hz, C_1 of PPh_3), 122.1 (s, C_4 of BPh_4), 126.0 (m, $C_{2\text{ or }3}$ of BPh_4), 130.9 (d, $^3J_{PC}$ = 13.1 Hz, C_3 of PPh_3), 134.0 (d, $^2J_{PC}$ = 10.5 Hz, C_2 of PPh_3), 136.2 (br d, $^4J_{PC}$ = 3.1 Hz, C_4 of PPh_3), 136.3 (m, $C_{2\text{ or }3}$ of BPh_4), 164.4 (q, $^1J_{PB}$ = 49.5 Hz, C_1 of BPh_4), 218.6 (d, $^2J_{PC}$ = 1.5 Hz, H_2CCCH);

^{31}P-NMR (161.83 MHz, CD_2Cl_2): δ_P 18.5 (s, PPh_3);

^{11}B-NMR (123.27 MHz, CD_2Cl_2): δ_B -7.6 (s, BPh_4);

IR (ATR), 3053 cm^{-1} (PPh_3 aromatic C-H stretch), 2959 cm^{-1} (BPh_4 aromatic C-H stretch), 1954 cm^{-1} (allene), 1587 cm^{-1} (BPh_4), 1436 cm^{-1} (P-Ph), 1425 cm^{-1} (P-C), 730 cm^{-1} (BPh_4),;

MS (ESI, positive mode), *m/z* 301.1139 (Calculated for $C_{21}H_{18}P$ $[M]^+$ = 301.1141, Δ = 0.2 mDa), (ESI, negative mode), *m/z* 319.1678 (Calculated for $C_{24}H_{20}B$ $[M]^-$ = 319.1668, Δ = 1.0 mDa);

Table 6-15 Crystal data and structure refinement for $[H_2C=C=CHPPh_3][BPh_4]$ **40c**

Identification code	jml1315
Empirical formula	$C_{45}H_{38}BP$
Formula weight	620.53
Temperature / K	110.00(10)
Crystal system	triclinic
Space group	P-1
a / Å, b / Å, c / Å	9.4574(3), 12.9884(4), 14.7736(5)
α/°, β/°, γ/°	92.701(3), 91.115(3), 109.029(3)
Volume / Å^3	1712.48(10)
Z	2
ρ_{calc} / mg mm^{-3}	1.203
m / mm^{-1}	0.112
F(000)	656.0
Crystal size / mm^3	0.3269 × 0.2405 × 0.0955
2Θ range for data collection	6.28 to 64.44°
Index ranges	-11 ≤ h ≤ 13, -19 ≤ k ≤ 18, -14 ≤ l ≤ 21
Reflections collected	16929
Independent reflections	10772[R(int) = 0.0227]
Data/restraints/parameters	10772/0/432
Goodness-of-fit on F^2	1.026
Final R indexes [I>2σ (I)]	R_1 = 0.0474, wR_2 = 0.1088
Final R indexes [all data]	R_1 = 0.0613, wR_2 = 0.1169
Largest diff. peak/hole / e Å^{-3}	0.42/-0.35

NMR Data for [HC≡CCH$_2$PPh$_3$][Br] 39a

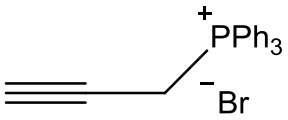

[HC≡CCH$_2$PPh$_3$][Br] was used as received from TCI.

^{1}H-NMR (399.78 MHz, CD_2Cl_2): δ_H 2.42 (dt, $^4J_{PH}$ = 6.8 Hz, $^4J_{HH}$ = 2.8 Hz, 1H, C*H*), 5.20 (dd, $^2J_{PH}$ = 15.4 Hz, $^4J_{HH}$ = 2.8 Hz, 2H, C*H$_2$*), 7.75 (m, 6H, *ortho* or *meta* PPh$_3$), 7.91 (m, 9H, *ortho* or *meta* PPh$_3$ and *para*-PPh$_3$);

^{13}C-NMR (100.53 MHz, CD_2Cl_2): δ_C 18.5 (d, $^1J_{PC}$ = 56.7 Hz, *C*H$_2$), 72.0 (d, $^2J_{PC}$ = 12.9 Hz, HC*C*CH$_2$), 76.9 (d, $^3J_{PC}$ = 9.70 Hz, H*C*CCH$_2$), 117.7 (d, $^1J_{PC}$ = 88.4 Hz, C_1 of PPh$_3$), 130.7 (d, $^3J_{PC}$ = 13.0 Hz, C_3 of PPh$_3$), 134.5 (d, $^2J_{PC}$ = 10.2 Hz, C_2 of PPh$_3$), 135.9 (d, $^4J_{PC}$ = 3.1 Hz, C_4 of PPh$_3$);

^{31}P-NMR (161.83 MHz, CD_2Cl_2): δ_P 22.6 (s, PPh$_3$);

Synthesis of [H$_2$C=C=CHPPh$_3$][Br] 40a

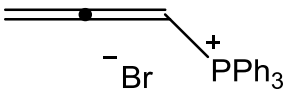

This data was obtained after monitoring a CD_2Cl_2 solution of [HC≡CCH$_2$PPh$_3$][Br] **39a** over the course of 5 days.

^{1}H-NMR (399.78 MHz, CD_2Cl_2): δ_H 5.35 (dd, $^4J_{PH}$ = 12.9 Hz, $^4J_{HH}$ = 6.6 Hz, C*H$_2$*, overlaps solvent peak so can't integrate, but shows HSQC to the peak at 80 ppm which was shown to be CH$_2$ using a DEPT experiment), 7.68 (dt, $^2J_{PH}$ = 7.1 Hz, $^4J_{HH}$ = 6.6 Hz, 1H, C*H*), 7.75 (m, 12H, *ortho* and *meta* PPh$_3$), 7.88 (3H, *para*-PPh$_3$);

^{13}C-NMR (100.53 MHz, CD_2Cl_2): δ_C 75.6 (d, $^1J_{PC}$ = 93.6 Hz, *C*H), 80.4 (d, $^3J_{PC}$ = 14.8 Hz, *C*H$_2$), 118.5 (d, $^1J_{PC}$ = 91.6 Hz, C_1 of PPh$_3$), 130.7 (d, $^3J_{PC}$ = 13.0 Hz, C_3 of PPh$_3$), 134.3 (d, $^2J_{PC}$ = 10.7 Hz, C_2 of PPh$_3$), 135.8 (d, $^4J_{PC}$ = 3.2 Hz, C_4 of PPh$_3$), 218.5 (d, $^2J_{PC}$ = 1.5 Hz, H$_2$C*C*CH);

^{31}P-NMR (161.83 MHz, CD_2Cl_2): δ_P 19.3 (s, PPh$_3$);

Synthesis of [Ru(κ^2-OAc)(κ^1-OAc)(C=C=CHCH$_2$PPh$_3$)(PPh$_3$)$_2$][BPh$_4$] 38

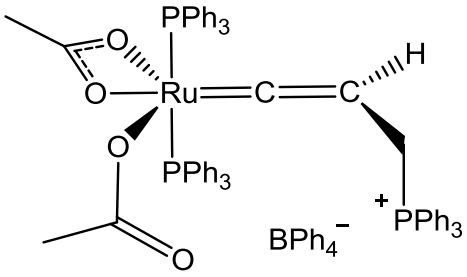

cis-[Ru(κ^2-OAc)$_2$(PPh$_3$)$_2$] **1a** (100 mg, 0.13 mmol) and [HC≡CCH$_2$PPh$_3$][BPh$_4$] **39c** (84 mg, 0.13 mmol) were dissolved in DCM (15 ml) and stirred at RT for 2 minutes. The solvent was then removed *in vacuo* and the residue washed with pentane (2 x 20 ml). This yielded [Ru(κ^2-OAc)(κ^1-OAc)(C=C=CHCH$_2$PPh$_3$)(PPh$_3$)$_2$][BPh$_4$]

38 (found to be a 60:40 mixture with the allene isomer [Ru(κ^2-OAc)(κ^1-OAc)(η^2-H$_2$C=C=CHPPh$_3$)(PPh$_3$)$_2$][BPh$_4$] **45b**) as a dark yellow powder (80 mg, 0.06 mmol, 44% yield).

IR data was collected but due to overlapping bands from the two species the spectrum is not reported. NMR resonances due to the allene complex are not reported.

^{1}H-NMR (500.23 MHz, CD_2Cl_2): δ_H 1.03 (s, 6H, COOC*H*$_3$), 3.94 (dd, $^2J_{PH}$ = 12.42 Hz, $^3J_{HH}$ = 6.0 Hz, 2H, C*H*$_2$), 4.74 (td, $^3J_{HH}$ = 6.0 Hz, $^3J_{PH}$ = 2.32 Hz, 1H, C*H*), 6.95-7.90 (112H (high due to a large number of very low level impurities), aromatic region);

^{13}C-NMR (125.78 MHz, CD_2Cl_2): δ_C 22.0 (s, COO*C*H$_3$), 22.8 (d, $^1J_{PC}$ = 51.5 Hz *C*H$_2$PPh$_3$), 96.5 (m, *C*HCH$_2$PPh$_3$), 119.9 (d, $^1J_{PC}$ = 85.6 Hz, C_1 of CH$_2$PPh$_3$), 123.6 (s, C_4 of BPh$_4$), 127.4 (m, $C_{2\text{ or }3}$ of BPh$_4$), 129.8 (t, ΣJ = 9.1 Hz, $C_{2\text{ or }3}$ of PPh$_3$), 131.8 (s, C_4 of PPh$_3$), 132.2 (d, ΣJ = 12.3 Hz, $C_{2\text{ or }3}$ of CH$_2$PPh$_3$), 133.1 (t, $^1J_{PC}$+$^3J_{PC}$ = 40.1 Hz, C_1 of PPh$_3$), 134.9 (d, ΣJ = 9.6 Hz, $C_{2\text{ or }3}$ of CHPPh$_3$), 136.3 (t, ΣJ = 11.9 Hz, $C_{2\text{ or }3}$ of PPh$_3$), 136.9 (d, $^4J_{PC}$ = 3.5 Hz, C_4 of CH$_2$PPh$_3$), 137.8 (br s, $C_{2\text{ or }3}$ of BPh$_4$), 165.8 (q, $^1J_{PB}$ = 49.2 Hz, C_1 of BPh$_4$), 182.9 (s, *C*OOCH$_3$), 254.0 (br, Ru*C*=CH);

^{31}P-NMR (202.50 MHz, CD_2Cl_2): δ_P 19.6 (t, $^4J_{PP}$ = 3.4 Hz, CH$_2$PPh$_3$), 37.5 (d, $^4J_{PP}$ = 3.4 Hz, PPh$_3$);

^{11}B-NMR (128.27 MHz, CD_2Cl_2): δ_B -7.5 (s, BPh$_4$);

MS (ESI), *m/z* 1045.2287 (Calculated for $C_{61}H_{54}{}^{102}RuP_3O_4$ $[M]^+$ = 1045.2289, Δ = 0.2 mDa), *m/z* 783.1367 (Calculated for $C_{43}H_{39}{}^{102}RuP_2O_4$ $[M]^+$ -PPh$_3$ = 783.1374, Δ = 0.7 mDa);

Anal. for $C_{85}H_{74}BO_4P_3Ru$, (calc) C 74.83, H 5.47; (found) C 74.72, H 5.47.

Synthesis of [Ru(κ^2- O_2CPh)(κ^1- O_2CPh)(C=C=CH$_2$PPh$_3$)(PPh$_3$)$_2$][BPh$_4$] 47

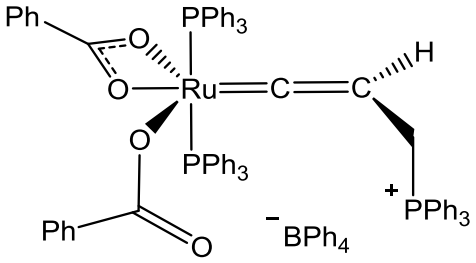

cis-[Ru(κ^2-COOPh)$_2$(PPh$_3$)$_2$] **34** (200 mg, 0.23 mmol) and [HC≡CCH$_2$PPh$_3$][BPh$_4$] **39c** (143 mg, 0.23 mmol) were dissolved in DCM (205 ml) and stirred at RT for 30 minutes. The solvent was then reduced *in vacuo* to ~5 ml and the product crashed out with pentane (40 ml). The yellow solution was then filtered off and the remaining orange oil dried to give **47** as an orange powder (232 mg, 0.15 mmol, 68% yield). Small amounts of allene complex **50** were also observed in the NMR data.

^{1}H-NMR (500.23 MHz, CD_2Cl_2): δ_H 4.06 (dd, $^2J_{PH}$ = 13.1 Hz, $^3J_{HH}$ = 6.3 Hz, 2H, C*H*$_2$), 4.84 (td, $^3J_{HH}$ = 6.3 Hz, $^3J_{PH}$ = 2.8 Hz, 1H, C*H*), 6.88-7.88 (92H (high due to the presence small amounts of allene complex), aromatic region);

^{13}C-NMR (125.78 MHz, CD_2Cl_2): δ_C 22.9 (d, $^1J_{PC}$ = 52.6 Hz *C*H$_2$PPh$_3$), 96.7 (m, *C*HCH$_2$PPh$_3$), 120.0 (d, $^1J_{PC}$ = 85.8 Hz, C_1 of CH$_2$PPh$_3$), 123.4 (s, C_4 of BPh$_4$), 127.3 (m, $C_{2\text{ or }3}$ of BPh$_4$), 128.9 (s, benzoate), 129.6 (t, ΣJ = 8.9 Hz, $C_{2\text{ or }3}$ of PPh$_3$), 129.9 (s, benzoate), 131.5 (s, C_4 of PPh$_3$), 132.1 (d, ΣJ = 12.4 Hz, $C_{2\text{ or }3}$ of CH$_2$PPh$_3$), 132.6 (t, $^1J_{PC}$+$^3J_{PC}$ = 39.4 Hz, C_1 of PPh$_3$), 133.2 (s, benzoate), 134.9 (d, ΣJ = 10.3 Hz, $C_{2\text{ or }3}$ of CHPPh$_3$), 136.1 (t, ΣJ = 11.5 Hz, $C_{2\text{ or }3}$ of PPh$_3$), 136.9 (d, $^4J_{PC}$ = 2.6 Hz, C_4 of CH$_2$PPh$_3$), 137.6 (s, $C_{2\text{ or }3}$ of BPh$_4$), 165.7 (q, $^1J_{PB}$ = 49.4 Hz, C_1 of BPh$_4$), 177.9 (s, *C*OOPh), 259.4 (only observed in the HMBC, Ru*C*=CH);

^{31}P-NMR (202.50 MHz, CD_2Cl_2): δ_P (20.00 (t, $^4J_{PP}$ = 3.0 Hz, CH$_2$PPh$_3$), 35.85 (d, $^4J_{PP}$ = 3.0 Hz, PPh$_3$);

^{11}B-NMR (128.27 MHz, CD_2Cl_2): δ_B -7.5 (s, BPh$_4$);

IR (ATR), 3054 cm^{-1} (PPh$_3$ aromatic C-H stretch), 2983 cm^{-1} (BPh$_4$ aromatic C-H stretch), 1634 cm^{-1} (C=C and κ^1 combination), 1602 cm^{-1} (C=C and κ^1 combination), 1578 cm^{-1} (κ^2-OCO$_{asym}$), 1516 cm^{-1} (κ^2-OCO$_{sym}$), 1480 cm^{-1} (BPh$_4$), 1434 cm^{-1} (P-Ph), 1417 cm^{-1} (P-C), 731 cm^{-1} (BPh$_4$), $\Delta\nu_{(chelate)}$ 62 cm^{-1};

MS (ESI), *m/z* 1169.2650 (Calculated for $C_{71}H_{58}{}^{102}RuP_3O_4$ [M]$^+$ = 1169.2605, Δ = 4.5 mDa), *m/z* 907.1725 (Calculated for $C_{53}H_{43}{}^{102}RuP_2O_4$ [M]$^+$ -PPh$_3$ = 907.1689, Δ = 3.6 mDa), (ESI, negative mode), *m/z* 319.1673 (Calculated for $C_{24}H_{20}B$ [M]$^-$ = 319.1668, Δ = 0.5 mDa);

Anal. for $C_{95}H_{78}BO_4P_3Ru$, (calc) C 76.66, H 5.28; (found) C 76.44, H 5.55.

Table 6-16 Crystal data and structure refinement for $[Ru(\kappa^1\text{-}OAc)(\kappa^2\text{-}OAc)(=C=CHCH_2PPh_3)(PPh_3)_2][BPh_4]$ **47**

Identification code	jml1382
Empirical formula	$C_{96}H_{80}BCl_2O_4P_3Ru$
Formula weight	1573.03
Temperature/K	110.00(14)
Crystal system	triclinic
Space group	P-1
a/Å, b/Å, c/Å	12.5833(4), 13.1462(4), 25.7463(9)
α/°, β/°, γ/°	100.054(3), 92.041(3), 110.548(3)
Volume/Å^3	3905.1(2)
Z	2
ρ_{calc}mg/mm^3	1.338
m/mm^{-1}	0.385
F(000)	1632.0
Crystal size/mm^3	0.1465 × 0.078 × 0.0329
Radiation	MoKα (λ = 0.7107)
2Θ range for data collection	6.16 to 56.12°
Index ranges	-16 ≤ h ≤ 16, -17 ≤ k ≤ 17, -33 ≤ l ≤ 21
Reflections collected	27562
Independent reflections	15480 [R_{int} = 0.0400, R_{sigma} = 0.0808]
Data/restraints/parameters	15480/70/1040
Goodness-of-fit on F^2	1.031
Final R indexes [I>=2σ (I)]	R_1 = 0.0516, wR_2 = 0.0995
Final R indexes [all data]	R_1 = 0.0762, wR_2 = 0.1120
Largest diff. peak/hole / e Å^{-3}	0.67/-0.60

Synthesis of [Ru(κ^2- O_2CPh)(κ^1- O_2CPh)(η^2-H_2C=C=CHPPh_3)(PPh_3)$_2$][BF_4] 49

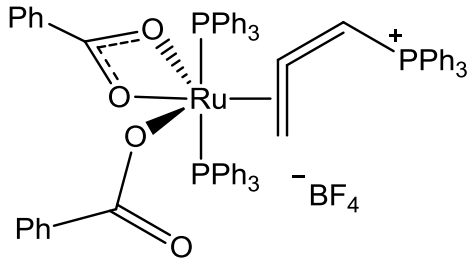

This was prepared in a similar manner to **45** by reaction of triphenylpropargylphosphonium bromide **39a** (88 mg, 0.23 mmol), silver tetrafluoroborate (26 mg, 0.23 mmol) and *cis*-[Ru(κ^2-COOPh)$_2$(PPh_3)$_2$] **34** (200 mg, 0.23 mmol). This yielded [Ru(κ^2- O_2CPh)(κ^1- O_2CPh)(η^2-H_2C=C=CHPPh_3)(PPh_3)$_2$][BF_4] **49** as a yellow solid (140 mg, 0.11 mmol, 48% yield).

^{1}H-NMR (500.23 MHz, CD_2Cl_2): δ_H 2.52 (ad, 1H, unknown), 3.04 (m, 2H, C*H*$_2$), 6.73 (ad, $^2J_{PH}$ = 23.8 Hz, 1H, C*H*), 7.14-7.97 (85H (high due to impurities), aromatic region);

^{13}C-NMR (125.78 MHz, CD_2Cl_2): δ_C 28.7 (br s, *C*H$_2$), 87.2 (d, $^1J_{PC}$ = 88.4 Hz, *C*H), 121.6 (d, $^1J_{PC}$ = 91.7 Hz, C_1 of $CHPPh_3$), 128.7 (s, benzoate), 129.2 (t, $^1J_{PC}$ + $^3J_{PC}$ = 42.1 Hz, C_1 of PPh_3), 129.9 (t, ΣJ = 9.1 Hz, $C_{2\ or\ 3}$ of PPh_3), 130.0 (s, benzoate), 131.6 (d, J_{PC} = 12.9 Hz, $C_{2\ or\ 3}$ of $CHPPh_3$), 132.1 (s, C_4 of PPh_3), 134.3 (s, benzoate), 132.9 (s, benzoate), 135.3 (d, J_{PC} = 10.3 Hz, $C_{2\ or\ 3}$ of $CHPPh_3$), 136.0 (t, ΣJ = 10.6 Hz, $C_{2\ or\ 3}$ of PPh_3), 136.5 (d, $^4J_{PC}$ = 2.7 Hz, C_4 of $CHPPh_3$), 178.8 (br s, *C*OOPh), 218.0 (m, H_2C=*C*=$CHPPh_3$);

^{31}P-NMR (202.50 MHz, CD_2Cl_2): δ_P 14.2 (t, $^4J_{PP}$ = 3.3 Hz, $CHPPh_3$), 27.9 (d, $^4J_{PP}$ = 3.3 Hz, PPh_3), 62.96 (s, bis-benzoate);

^{11}B-NMR (128.27 MHz, CD_2Cl_2): δ_B -2.1 (s, BF_4);

^{19}F-NMR (376.17 MHz, CD_2Cl_2): δ_F -152.9 (s, $^{10}BF_4$), -152.9 (s, $^{11}BF_4$);

IR (ATR), 30573 cm^{-1} (aromatic C-H stretch), 1695 cm^{-1} (allene and κ^1 combination), 1635 cm^{-1} (allene and κ^1 combination), 1575 cm^{-1} (κ^2-OCO_{asym}), 1504 cm^{-1} (κ^2-OCO_{sym}), 1434 cm^{-1} (P-Ph), 1051 cm^{-1} (BF_4), $\Delta\nu_{(chelate)}$ 71 cm^{-1};

MS (ESI), *m/z* 1169.2622 (Calculated for $C_{71}H_{58}{}^{102}RuP_3O_4$ [M]$^+$ = 1169.2605, Δ = 1.7 mDa), *m/z* 907.1694 (Calculated for $C_{53}H_{43}{}^{102}RuP_2O_4$ [M]$^+$ -PPh_3 = 907.1689, Δ = 0.5 mDa), 867.0566 (Calculated for $C_{46}H_{38}{}^{81}Br^{102}RuP_2O_2$ [M]$^+$ -PPh_3 -COOPh +Br = 867.0572, Δ = 0.6 mDa);

Anal. for $C_{71}H_{58}BF_4O_4P_3Ru$ • 1.05 $C_{64}H_{53}BBrF_4O_2P_3Ru$, (calc) C 65.57, H 4.52; (found) C 65.42, H 4.71. The XRD and MS data show that the κ^1 benzoate ligand exchanges readily with residual bromide.

Synthesis of [Ru(κ^2- O_2CPh)Br(η^2-H_2C=C=CHPPh_3)(PPh_3)$_2$][BF_4] 50

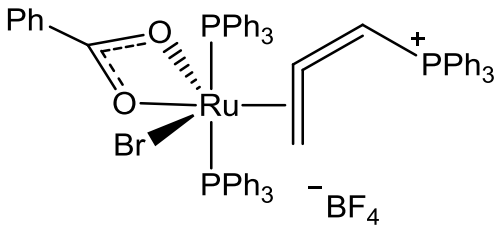

A DCM solution of [Ru(κ^2-O_2CPh)(κ^1-O_2CPh)(η^2-H_2C=C=CHPPh_3)(PPh_3)$_2$][BF_4] **49** was layered with diethyl ether and dark brown crystals of [Ru(κ^2- O_2CPh)Br(η^2-H_2C=C=CHPPh_3)(PPh_3)$_2$][BF_4] **50** obtained.

There is one benzoate resonance missing in the ^{13}C-NMR, presumably it is obscured by another peak.

^{1}H-NMR (500.13 MHz, CD_2Cl_2): δ_H 2.14 (m, 2H, C*H*$_2$), 6.85 (ad, $^2J_{PH}$ = 23.9 Hz, 1H, C*H*), 7.11-7.91 (53H (high due to a small number of low level impurities), aromatic region);

^{13}C-NMR (125.76 MHz, CD_2Cl_2): δ_C 28.1 (d, $^3J_{PC}$ = 3.6 Hz, *C*H$_2$), 84.8 (d, $^1J_{PC}$ = 87.6 Hz, *C*H), 119.6 (d, $^1J_{PC}$ = 89.6 Hz, C_1 of $CHPPh_3$), 127.2 (d, J_{PC} = 9.4 Hz, $C_{2\text{ or }3}$ of $CHPPh_3$), 128.0 (t, $^1J_{PC}$ + $^3J_{PC}$ = 42.4 Hz, C_1 of PPh_3), 128.1 (t, ΣJ = 9.2 Hz, $C_{2\text{ or }3}$ of PPh_3), 130.0 (d, J_{PC} = 13.7 Hz, $C_{2\text{ or }3}$ of $CHPPh_3$), 130.6 (s, C_4 of PPh_3), 132.6 (s, benzoate), 133.5 (s, benzoate), 133.6 (s, benzoate), 134.5 (t, ΣJ = 9.6 Hz, $C_{2\text{ or }3}$ of PPh_3), 134.9 (d, $^4J_{PC}$ = 3.0 Hz, C_4 of $CHPPh_3$), 180.9 (s, *C*OOPh), 214.9 (m, H_2C=*C*=CHPPh_3);

^{31}P-NMR (202.50 MHz, CD_2Cl_2): δ_P 14.6 (t, $^4J_{PP}$ = 3.1 Hz, $CHPPh_3$), 25.4 (d, $^4J_{PP}$ = 3.1 Hz, PPh_3);

^{11}B-NMR (128.27 MHz, CD_2Cl_2): δ_B -2.0 (s, BF_4);

^{19}F-NMR (376.17 MHz, CD_2Cl_2): δ_F -152.9 (s, $^{10}BF_4$), -153.0 (s, $^{11}BF_4$);

IR (ATR), 3053 cm^{-1} (aromatic C-H stretch), 1697 cm^{-1} (allene), 1553 cm^{-1} (κ^2-OCO_{asym}), 1504 cm^{-1} (κ^2-OCO_{sym}), 1433 cm^{-1} (P-Ph), 1052 cm^{-1} (BF_4), $\Delta\nu_{(chelate)}$ 48 cm^{-1};

MS (ESI), *m/z* 1129.1477 (Calculated for $C_{64}H_{53}{}^{81}Br^{102}RuP_3O_2$ $[M]^+$ = 1129.1490, Δ = 1.3 mDa);

Table 6-17 Crystal data and structure refinement for $[Ru(\kappa^2\text{-}O_2CPh)Br(\eta^2\text{-}H_2C{=}C{=}CHPPh_3)(PPh_3)_2][BF_4]$ **50**.

Identification code	jml1368
Empirical formula	$C_{66}H_{57}BBrCl_4F_4O_2P_3Ru$
Formula weight	1384.61
Temperature/K	110.05(10)
Crystal system	triclinic
Space group	P-1
a/Å, b/Å, c/Å	11.8805(3), 13.4688(3), 20.1628(5)
α/°, β/°, γ/°	95.303(2), 104.015(2), 97.399(2)
Volume/Å^3	3078.56(13)
Z	2
ρ_{calc}mg/mm^3	1.494
m/mm^{-1}	1.212
F(000)	1404.0
Crystal size/mm^3	0.2 × 0.178 × 0.1073
Radiation	MoKα (λ = 0.710)
2Θ range for data collection	5.676 to 64.342°
Index ranges	-17 ≤ h ≤ 16, -20 ≤ k ≤ 19, -30 ≤ l ≤ 30
Reflections collected	30601
Independent reflections	19292 [R_{int} = 0.0246, R_{sigma} = 0.0505]
Data/restraints/parameters	19292/85/862
Goodness-of-fit on F^2	1.039
Final R indexes [I>=2σ (I)]	R_1 = 0.0565, wR_2 = 0.1322
Final R indexes [all data]	R_1 = 0.0797, wR_2 = 0.1463
Largest diff. peak/hole / e Å^{-3}	2.41/-2.19

Reaction of $[H_2C=C=CHPPh_3][BF_4]$ 40b with PPh_3

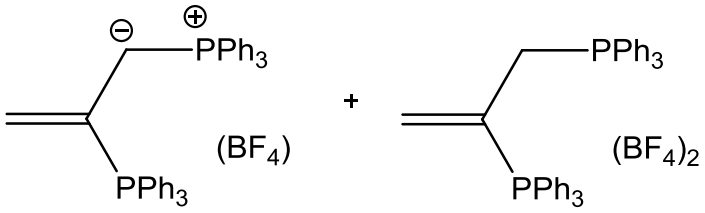

A solution of $[H_2C=C=CHPPh_3][BF_4]$ **40b** (20 mg, 0.05 mmol) and triphenylphosphine (13 mg, 0.05 mmol) in CD_2Cl_2 was followed by NMR spectroscopy. Two major species were formed, $[CH_2C(PPh_3)CH_2PPh_3][BF_4]_2$ **55** (identified by comparison with an authentic sample) and the ylide $[CH_2C(PPh_3)CHPPh_3][BF_4]$ **56** in approximately 1:2 ratio (by ^{31}P-NMR).

The ylide was found to be short lived with a half-life of ~4 hours. The following data was obtained ASAP after addition. Peak assignment was completed with the aid of $^1H\{^{31}P\}$, COSY, DEPT, HSQC, HMBC and ^1H-^{31}P HMQC experiments.

^{1}H-NMR (500.23 MHz, CD_2Cl_2): δ_H 2.24 (td, J_{PH} = 15.7 Hz, J_{HH} = 1.9 Hz, 1H, **56** CH), 3.71 (d, 0.5H, unknown), 4.01(dt, J_{PH} = 23.7 Hz, J_{HH} = J_{HH} = 1.7 Hz, 1H, **56** alkene H), 4.74 (dd, J_{PH} = 52.0 Hz, J_{HH} = 1.4 Hz, 1H, **56** alkene H), 5.34 (dd, J_{PH} = 14.8 Hz, J_{PH} = 10.7 Hz, 2H, **55** C*H*$_2$), 6.48 (ddd, $^3J_{PH}$ = 22.0 Hz, $^4J_{PH}$ = 3.0 Hz, $^2J_{HH}$ = 2.2 Hz, 1H, **55** alkene H), 6.83 (adt, $^3J_{PH}$ = 46.1 Hz, $^4J_{PH}$ = $^2J_{HH}$ = 3.1 Hz, 1H, **55** alkene H), 7.28 – 7.89 (aromatic);

^{31}P-NMR (202.51 MHz, CD_2Cl_2): δ_P -6.0 (s, free PPh_3), 11.3 (d, $^3J_{PP}$ = 67.1 Hz, PPh_3, **56**), 13.6 (s, unknown), 26.0 (d, $^3J_{PP}$ = 67.1 Hz, PPh_3, **56**), 22.4 (d, $^3J_{PP}$ = 19.3 Hz, PPh_3, **55**), 26.7 (d, $^3J_{PP}$ = 19.3 Hz, PPh_3, **55**);

Synthesis of $[CH_2C(PPh_3)CH_2PPh_3][BF_4]_2$ 55

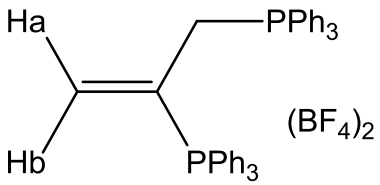

Triphenylphosphine (65 mg, 0.25 mmol), followed by tetrafluoroboric acid ($HBF_4.EtO_2$ complex, 34 µl, 0.25 mmol) was added to a stirred solution of $[H_2C=C=CHPPh_3][BF_4]$ **40b** (100 mg, 0.25 mmol) in DCM (20 ml). Diethyl ether (30 ml) was added after 5 minutes and the resulting white precipitate collect by filtration and washed with diethyl ether (2 x 10 ml). After drying *in vacuo* $[CH_2C(PPh_3)CH_2PPh_3][BF_4]_2$ **55** was obtained as a white powder (138 mg, 0.19 mmol, 75% yield). Crystals suitable for elemental

analysis and X-Ray diffraction were grown by slow diffusion of n-pentane into a DCM solution of the product.

^{1}H-NMR (500.23 MHz, CD_2Cl_2): δ_H 4.87 (dd, J_{PH} = 15.0 Hz, J_{PH} = 10.6 Hz, 2H, C*H*$_2$), 6.47 (ddd, $^{3}J_{PH}$ = 21.8 Hz, $^{4}J_{PH}$ = 3.8 Hz, $^{2}J_{HH}$ = 2.8 Hz, 1H, *Hb*), 6.78 (adt, $^{3}J_{PH}$ = 45.8 Hz, $^{4}J_{PH}$ = $^{2}J_{HH}$ = 2.8 Hz, 1H, *Ha*), 7.66 (m, 6H, PPh_3), 7.75 (18H, PPh_3), 7.92 (m, 6H, PPh_3);

^{13}C-NMR (125.81 MHz, CD_2Cl_2): δ_C 27.0 (dd, $^{1}J_{PC}$ = 51.7 Hz, $^{2}J_{PC}$ = 13.4 Hz, *C*H_2), 116.4 (d, $^{1}J_{PC}$ = 88.1 Hz, C_1 of PPh_3), 117.9 (d, $^{1}J_{PC}$ = 86.7 Hz, C_1 of PPh_3), 121.7 (dd, $^{1}J_{PC}$ = 78.1 Hz, $^{2}J_{PC}$ = 7.3 Hz, *C*), 132.6 (d, $^{3}J_{PC}$ = 12.8 Hz, C_3 of PPh_3), 132.6 (d, $^{3}J_{PC}$ = 12.8 Hz, C_3 of PPh_3), 135.7 (d, $^{2}J_{PC}$ = 10.4 Hz, C_2 of PPh_3), 136.4 (d, $^{2}J_{PC}$ = 10.4 Hz, C_2 of PPh_3), 137.7 (d, $^{4}J_{PC}$ = 3.0 Hz, C_4 of PPh_3), 137.8 (d, $^{4}J_{PC}$ = 3.0 Hz, C_4 of PPh_3), 148.9 (at, $^{2}J_{PC}$ = $^{3}J_{PC}$ = 7.0 Hz, alkene *C*H_2);

^{31}P-NMR (202.51 MHz, CD_2Cl_2): δ_P 23.0 (d, $^{3}J_{PP}$ = 20.0 Hz, PPh_3), 28.0 (d, $^{3}J_{PP}$ = 20.0 Hz, PPh_3);

^{11}B-NMR (123.27 MHz, CD_2Cl_2): δ_B -2.1 (s, BF_4);

^{19}F-NMR (376.17 MHz, CD_2Cl_2): δ_F -152.5 (s, $^{10}BF_4$), -152.6 (s, $^{11}BF_4$);

IR (KBr), 3080 cm^{-1} (geminal alkene C-H stretch), 3059 cm^{-1} (aromatic C-H stretch), 1584 cm^{-1} (alkene stretch), 1482 cm^{-1} (P-Ph stretch), 1437 cm^{-1} (P-C stretch), 1059 cm^{-1} (BF_4);

MS (ESI), *m/z* 263.0984 (Calculated for $C_{18}H_{16}P$ $[M]^+$ = 263.0984, Δ = 0 mDa), *m/z* 282.1050 (Calculated for $C_{39}H_{34}P_2$ $[M]^{2+}$ = 282.1062, Δ = 1.2 mDa), *m/z* 301.1142 (Calculated for $C_{21}H_{19}P$ $[M\text{-}H]^+$ -PPh_3 = 301.1141, Δ = 0.1 mDa), *m/z* 319.1242 (Calculated for $C_{21}H_{20}OP$ $[M]^+$ -PPh_3 + HO^- = 319.1246, Δ = 0.4 mDa), *m/z* 333.1405 (Calculated for $C_{22}H_{22}OP$ $[M]^+$ -PPh_3 + MeO^- = 333.1403, Δ = 0.2 mDa);

Anal. for $C_{39}H_{34}B_2F_8P_2$, (calc) C 63.45, H 4.64; (found) C 63.32, H 4.53.

Table 6-18 Crystal data and structure refinement for $[CH_2C(PPh_3)CH_2PPh_3][BF_4]_2$ 55.

Identification code	jml1345
Empirical formula	$C_{39}H_{34}B_2F_8P_2$
Formula weight	738.22
Temperature/K	110.05(10)
Crystal system	triclinic
Space group	P-1
a/Å, b/Å, c/Å	9.9081(4), 13.7516(7), 14.6581(8)
α/°, β/°, γ/°	65.358(5), 75.008(4), 83.678(4)
Volume/Å^3	1753.52(17)
Z	2
ρ_{calc}mg/mm^3	1.398
m/mm^{-1}	0.196
F(000)	760.0
Crystal size/mm^3	0.3396 × 0.0895 × 0.0229
Radiation	MoKα (λ = 0.71073)
2Θ range for data collection	5.8 to 58.38°
Index ranges	-13 ≤ h ≤ 12, -18 ≤ k ≤ 17, -20 ≤ l ≤ 20
Reflections collected	11775
Independent reflections	7817 [R_{int} = 0.0225, R_{sigma} = 0.0554]
Data/restraints/parameters	7817/68/496
Goodness-of-fit on F^2	1.079
Final R indexes [I>=2σ (I)]	R_1 = 0.0765, wR_2 = 0.1706
Final R indexes [all data]	R_1 = 0.0981, wR_2 = 0.1828
Largest diff. peak/hole / e Å^{-3}	1.33/-0.99

Synthesis of $[CH_2C(P^iPr_3)CHPPh_3][BPh_4]$ 58

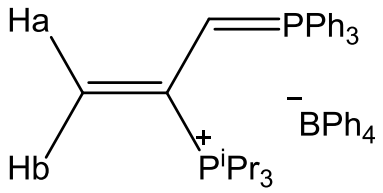

Triisopropylphosphine (6 µl, 0.032 mmol) was added to a CD_2Cl_2 (0.5 ml) solution of triphenylpropargylphosphonium tetraphenylborate **39c** (20 mg, 0.032 mmol) in a Youngs NMR tube. The initial products were found to be $[H_2C=C=CHPPh_3][BPh_4]$ **40c** and $[CH_2C(P^iPr_3)CHPPh_3][BPh_4]$ **58** but after three days the major product was found to be $[CH_2C(P^iPr_3)CHPPh_3][BPh_4]$ **58** (along with some unknown impurities and excess BPh_4 which have led to high integrations in some regions).

^{1}H-NMR (500.23 MHz, $CDCl_3$): δ_H 1.46 (dd, $^3J_{PH}$ = 15.5 Hz, $^3J_{HH}$ = 7.2 Hz, 18H, ^{i}Pr-C*H*$_3$), 2.13 (ddd, J_{PH} = 15.0 Hz, J_{PH} = 12.0 Hz, $^3J_{HH}$ = 2.3 Hz, 1H, C*H*), 2.74 (m, 3H, ^{i}Pr-C*H*), 4.09 (dt, $^3J_{PH}$ = 18.6 Hz, $^2J_{HH}$ = $^4J_{HH}$ = 2.0 Hz, 1H, *H*b), 4.49 (dd, $^3J_{PH}$ = 43.9 Hz, $^2J_{HH}$ = 2.0 Hz, 1H, *H*a), 6.91 (t, $^3J_{HH}$ = 7.2 Hz, 6H, p-BPh_4), 7.06 (t, $^3J_{HH}$ = 7.3 Hz, 12H, m-BPh_4), 7.37 (m, 13H, o-BPh_4), 7.56-7.92 (m, 21H, PPh_3);

^{13}C-NMR (125.81 MHz, $CDCl_3$): δ_C 18.6 (d, $^2J_{PC}$ = 2.6 Hz, ^{i}Pr-*C*H$_3$), 22.6 (d, $^1J_{PC}$ = 42.9 Hz, ^{i}Pr-CH), 33.4 (dd, $^1J_{PC}$ = 118.1 Hz, $^2J_{PC}$ = 15.4 Hz, *C*H), 102.0 (at, ΣJ_{PC} = 14.6 Hz, *C*H$_2$), 123.4 (s, C_4 of BPh_4), 126.0 (dd, $^1J_{PC}$ = 57.1 Hz, $^2J_{PC}$ = 9.4 Hz, *C*), 127.3 (m, C_3 of BPh_4), 127.3 (d, $^1J_{PC}$ = 89.4 Hz, C_1 of PPh_3), 131.0 (d, *J* = 12.2 Hz, $C_{2\text{ or }3}$ of PPh_3), 134.4 (d, $^3J_{PC}$ = 10.3 Hz, $C_{2\text{ or }3}$ of PPh_3), 134.4 (d, $^4J_{PC}$ = 2.8 Hz, C_4 of PPh_3), 137.6 (s, C_2 of BPh_4), 165.7 (q, $^1J_{BC}$ = 49.3 Hz, C_1 of BPh_4);

^{31}P-NMR (202.51 MHz, $CDCl_3$): δ_P 12.1 (d, $^3J_{PP}$ = 55.5 Hz, PPh_3), 40.6 (d, $^3J_{PP}$ = 55.5 Hz, P^iPr_3);

^{11}B-NMR (123.27 MHz, $CDCl_3$): δ_B -7.5 (s, BPh_4);

IR (ATR), 3052 cm^{-1} (PPh_3 aromatic C-H stretch), 2984 cm^{-1} (BPh_4 aromatic C-H stretch), 1580 cm^{-1} (BPh_4), 1514 cm^{-1} (P-C stretch), 1479 cm^{-1} (P-C stretch), 1435 cm^{-1} (P-C stretch), 1399 cm^{-1} (P-C stretch), 732 cm^{-1} (BPh_4);

MS (ESI), *m/z* 461.2513 (Calculated for $C_{30}H_{39}P_2$ $[M]^+$ = 461.2522, Δ = 0.9 mDa), *m/z* 301.1134 (Calculated for $C_{21}H_{19}P$ $[M\text{-}H]^+$ -P^iPr_3 = 301.1141, Δ = 0.7 mDa);

Synthesis of [RhCl(η^2-H_2C=C=CHPPh_3)(P^{i}Pr_3)$_2$][BPh_4] 60

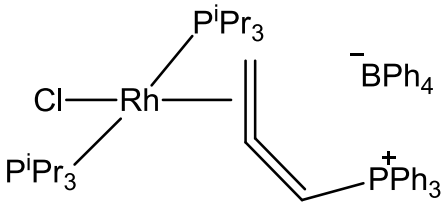

[HC≡CCH_2PPh_3][BPh_4] **39c** (27 mg, 0.044 mmol) was added to a red THF (0.5 ml) solution of [Rh(μ^2-Cl)(P^{i}Pr_3)$_2$]$_2$ **59** (20 mg, 0.022 mmol) to give a yellow solution. This was then layered with pentane and the resulting crystals isolated by filtration and dried to give [RhCl(η^2-H_2C=C=CHPPh_3)(P^{i}Pr_3)$_2$][BPh_4] **60** as a yellow crystalline solid (17 mg, 0.016 mmol, 71 % yield).

The integrations show that there is more than one equivalent of BPh_4 present. 2D experiments have shown that the CH allene proton is at 6.85, obscured by the BPh_4 meta-resonance.

^{1}H-NMR (500.23 MHz, CD_2Cl_2): δ_H 1.28 (aq, $^3J_{PH}$ = 20.6 Hz, $^3J_{HH}$ = 7.6 Hz, 19.5H, ^{i}Pr C*H*$_3$), 1.36 (aq, $^3J_{PH}$ = 20.6 Hz, $^3J_{HH}$ = 7.6 Hz, 19.5H, ^{i}Pr C*H*$_3$), 1.76 (m, observed as a shoulder on the THF peak, C*H*$_2$), 2.37 (m, 6H, ^{i}Pr C*H*), 6.71 (t, $^3J_{HH}$ = 7.2 Hz, 6H, para-BPh_4), 6.85 (t, $^3J_{HH}$ = 7.2 Hz, 13H, meta-BPh_4), 7.31 (m, 12H, ortho-BPh_4), 7.63 (td, $^3J_{HH}$ = 7.3 Hz, $^3J_{PH}$ = 3.2 Hz, 7H, meta-PPh_3), (dd, $^3J_{HH}$ = 7.3 Hz, $^3J_{PH}$ = 12.5 Hz, 7H, ortho-PPh_3), (t, $^3J_{HH}$ = 7.3 Hz, 3H, para-PPh_3),

^{13}C-NMR (125.78 MHz, CD_2Cl_2): δ_C 12.39 (ad, $^1J_{RhC}$ = 13.2 Hz *C*H$_2$), 21.04 (s, ^{i}Pr *C*H$_3$), 21.57 (s, ^{i}Pr *C*H$_3$), 24.64 (t, $^{2+4}J_{PC}$ = 19.7 Hz, ^{i}Pr *C*H, 85.49 (d, $^1J_{PC}$ = 80.5 Hz, *C*H), 122.50 (d, $^1J_{PC}$ = 88.9 Hz, C_1 of PPh_3), 122.50 (s, C_4 of BPh_4), 126.38 (m, $C_{2\text{ or }3}$ of BPh_4), 131.73 (d, J_{PC} = 12.9 Hz, $C_{2\text{ or }3}$ of PPh_3), 135.28 (d, J = 9.8 Hz, $C_{2\text{ or }3}$ of PPh_3), 136.51 (d, J = 2.7 Hz, C_4 of PPh_3), 137.93 (s, $C_{2\text{ or }3}$ of BPh_4), 165.9 (q, $^1J_{PB}$ = 49.3 Hz, C_1 of BPh_4), 210.7 (d, $^1J_{RhC}$ = 26.5 Hz, *C*);

^{31}P-NMR (202.50 MHz, CD_2Cl_2): δ_P 8.2 (dt, $^3J_{PRh}$ = 12.2 Hz, $^4J_{PP}$ = 2.1 Hz, PPh_3), 34.8 (dd, $^1J_{PRh}$ = 111.9 Hz, $^4J_{PP}$ = 2.1 Hz, P^{i}Pr_3);

^{11}B-NMR (128.27 MHz, CD_2Cl_2): δ_B -7.50 (s, BPh_4);

IR (ATR), 3055 cm^{-1} (PPh_3 aromatic C-H stretch), 2959 cm^{-1} (BPh_4 aromatic C-H stretch),1653 cm^{-1} (allene), 1580 cm^{-1} (BPh_4), 1480 cm^{-1} (P-^{i}Pr), 1455 cm^{-1} (P-Ph), 1436 cm-1, (P-C), 730 cm^{-1} (BPh_4);

MS (LIFDI) *m/z* 759.47 [M]$^+$, *m/z* 333.22 [alkyne + MeOH]$^+$;

Anal. for $C_{63}H_{80}BClP_3Rh$, (calc) C 70.10, H 7.47; (found) C 69.97, H 7.66.

Synthesis of [RhCl(C=C=CHCH$_2$PPh$_3$)(P^{i}Pr$_3$)$_2$][BPh$_4$] 63

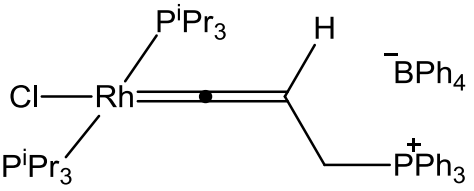

[Rh(μ^2-Cl)(P^{i}Pr$_3$)$_2$]$_2$ **59** (20 mg, 0.022 mmol) and [HC≡CCH$_2$PPh$_3$][BPh$_4$] **39c** (27 mg, 0.044 mmol) were mixed in a vial before addition of d$_8$-THF (0.5 ml). This resulted in a yellow solution and the reaction was the followed by NMR spectroscopy. Allene complex **60** and alkyne complex **61** were observed immediately. **61** was then found to transform into vinylidene **63** via alkynyl hydride **62** over the course of ~ 7 hours with a maximum ratio of 37:63 vinylidene:allene complex. At this point the following data was recorded.

Only NMR resonances due to the vinylidene are reported. Some integrations are not reported due to overlap with the allene resonances.

^{1}H-NMR (500.23 MHz, CD_2Cl_2): δ_H 0.39 (m, appears as a triplet in the $^1H\{^{31}P\}$ spectrum with $^3J_{HH}$ = 6.3 Hz, 1H, CH), 1.33 (d, $^3J_{HH}$ = 7.2 Hz, ^{i}Pr C*H*$_3$), 2.72 (m, 6H, ^{i}Pr C*H*), 4.46 (ddt, $^2J_{PH}$ = 13.1 Hz, $^3J_{HH}$ = 6.3 Hz, $^5J_{PH}$ = 2.0 Hz, 2H, C*H*$_2$), 4.06 (dd, $^2J_{PH}$ = 13.2 Hz, $^3J_{HH}$ = 6.3 Hz, $^5J_{PH}$ = 2.0 Hz, 2H, C*H*$_2$);

^{13}C-NMR (125.78 MHz, CD_2Cl_2): δ_C 8.3 (d, $^1J_{PC}$ = 52.6 Hz, *C*H$_2$), 21.0 (s, ^{i}Pr *C*H$_3$), 21.2 (s, ^{i}Pr *C*H$_3$), 25.0 (t, $^{2+4}J_{PC}$ = 10.0 Hz, ^{i}Pr *C*H), 94.0 (br d, $^2J_{RhC}$ = 15.5 Hz, *C*H), 283.1 (br, $^1J_{RhC}$ ~ 60 Hz, *C*);

^{31}P-NMR (202.50 MHz, CD_2Cl_2): δ_P 20.9 (t, $^4J_{PP}$ = 3.4 Hz, PPh$_3$), 43.2 (dd, $^1J_{PRh}$ = 132.1 Hz, $^4J_{PP}$ = 3.4 Hz, P^{i}Pr$_3$);

An IR spectrum was recorded of the mixture but it was found to be dominated by bands due to the allene complex.

MS (LIFDI) *m/z* 759.26 [M]$^+$;

Table 6-19 Crystal data and structure refinement for $[RhCl(\eta^2\text{-}H_2C{=}C{=}CHPPh_3)(P^iPr_3)_2][BPh_4]$ **60**

Identification code	2014ncs0021
Empirical formula	$C_{67}H_{88}BClOP_3Rh$
Formula weight	1151.45
Temperature/K	100
Crystal system	triclinic
Space group	P-1
a/Å, b/Å, c/Å	11.6843(4), 12.6555(4), 21.5962(15)
α/°, β/°, γ/°	99.886(7), 90.287(6), 106.837(8)
Volume/Å^3	3006.1(3)
Z	2
ρ_{calc}mg/mm^3	1.272
m/mm^{-1}	0.45
F(000)	1220.0
Crystal size/mm^3	0.13 × 0.06 × 0.02
Radiation	MoKα (λ = 0.7107)
2Θ range for data collection	6.132 to 54.906°
Index ranges	-15 ≤ h ≤ 15, -16 ≤ k ≤ 16, -27 ≤ l ≤ 27
Reflections collected	40506
Independent reflections	13740 [R_{int} = 0.042, R_{sigma} = 0.060]
Data/restraints/parameters	13740/0/687
Goodness-of-fit on F^2	1.050
Final R indexes [I>=2σ (I)]	R_1 = 0.0366, wR_2 = 0.0781
Final R indexes [all data]	R_1 = 0.0487, wR_2 = 0.0827
Largest diff. peak/hole / e Å^{-3}	0.93/-0.52

Table 6-20 Crystal data and structure refinement for [RhCl(η^2-H_2C=C=CHPPh_3)(P^iPr_3)$_2$][BPh_4] **60** and [RhCl(C=C=CH_2PPh_3)(P^iPr_3)$_2$][BPh_4] **63**.

Identification code	jml1393
Empirical formula	$C_{67}H_{88}BClOP_3Rh$
Formula weight	1151.45
Temperature/K	110.00(14)
Crystal system	triclinic
Space group	P-1
a/Å, b/Å, c/Å	11.6846(4), 12.6788(4), 21.6243(8)
α/°, β/°, γ/°	99.684(3), 90.372(3), 106.822(3)
Volume/Å^3	3017.62(19)
Z	2
ρ_{calc}mg/mm^3	1.267
m/mm^{-1}	0.448
F(000)	1220.0
Crystal size/mm^3	0.3097 × 0.1891 × 0.0587
Radiation	MoKα (λ = 0.71073)
2Θ range for data collection	5.676 to 64.532°
Index ranges	-16 ≤ h ≤ 16, -18 ≤ k ≤ 18, -31 ≤ l ≤ 22
Reflections collected	31962
Independent reflections	19003 [R_{int} = 0.0273, R_{sigma} = 0.0486]
Data/restraints/parameters	19003/1/757
Goodness-of-fit on F^2	1.119
Final R indexes [I>=2σ (I)]	R_1 = 0.0517, wR_2 = 0.1163
Final R indexes [all data]	R_1 = 0.0650, wR_2 = 0.1231
Largest diff. peak/hole / e Å^{-3}	1.54/-0.63

Synthesis of $[CH_3C(N(^iPr)_2)CHPPh_3][BF_4]$ 66

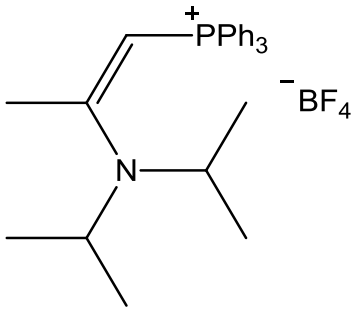

Diisopropylamine (144 µl, 1.03 mmol) was added to a stirred colourless solution of $[H_2C=C=CHPPh_3][BF_4]$ **40b** (400 mg, 1.03 mmol) in DCM (5 ml). The resulting brown solution was layered with toluene and crystals of $[CH_3C(N(^iPr)_2)CHPPh_3][BF_4]$ **66** and diisopropylammonium salts were obtained. Crystal picking allowed $[CH_3C(N(^iPr)_2)CHPPh_3][BF_4]$ **66** (222 mg, 0.45 mmol, 44%) to be isolated as a brown crystalline solid.

^{1}H-NMR (500.23 MHz, $CDCl_3$): δ_H 1.40 (br s, 12H, ^{i}Pr-C*H*$_3$), 1.91 (s, 3H, C*H*$_3$), 3.98 (d, $^2J_{PH}$ = 14.1 Hz, 1H, C*H*), 4.10 (br s, 2H, ^{i}Pr-CH), 7.58-7.79 (m, 15H, aromatic region);

^{13}C-NMR (125.81 MHz, $CDCl_3$): δ_C 22.0 (br s, ^{i}Pr-*C*H$_3$), 25.0 (d, $^3J_{PC}$ = 7.2 Hz, *C*H$_3$), 51.7 (br, ^{i}Pr-CH), 62.2 (d, $^1J_{PC}$ = 122.4 Hz, *C*H), 125.4 (d, $^1J_{PC}$ = 91.4 Hz, C_1 of PPh_3), 131.9 (d, *J* = 12.2 Hz, $C_{2\ or\ 3}$ of PPh_3), 134.5 (d, $^3J_{PC}$ = 10.3 Hz, $C_{2\ or\ 3}$ of PPh_3), 135.7 (d, $^4J_{PC}$ = 2.0 Hz, C_4 of PPh_3), 164.1 (br, *C*);

^{31}P-NMR (202.51 MHz, $CDCl_3$): δ_P 15.8 (s, PPh_3);

^{11}B-NMR (123.27 MHz, $CDCl_3$): δ_B -1.9 (s, BF_4);

^{19}F-NMR (376.17 MHz, $CDCl_3$): δ_F -151.8 (s, $^{10}BF_4$), -151.9 (s, $^{11}BF_4$);

MS (ESI), *m/z* 402.2339 (Calculated for $C_{27}H_{33}NP$ $[M]^+$ = 402.2345, Δ = 0.6 mDa);

Anal. for $C_{27}H_{33}BF_4NP$, (calc) C 66.27, H 6.80. N 2.86; (found) C 65.83, H 6.75, N 2.87.

Table 6-21 Crystal data and structure refinement for $[CH_3C(N(^iPr)_2)CHPPh_3][BF_4]$ **66**

Identification code	jml1351
Empirical formula	$C_{27}H_{33}BNF_4P$
Formula weight	489.32
Temperature / K	110
Crystal system	orthorhombic
Space group	$P2_12_12_1$
a / Å, b / Å, c / Å	7.48275(20), 11.5608(3), 28.6323(13)
α/°, β/°, γ/°	90.00, 90.00, 90.00
Volume / Å^3	2476.89(14)
Z	4
ρ_{calc} / mg mm^{-3}	1.312
m / mm^{-1}	0.157
F(000)	1032.0
Crystal size / mm^3	0.1744 × 0.1385 × 0.028
2Θ range for data collection	6.14 to 55.74°
Index ranges	-9 ≤ h ≤ 8, -13 ≤ k ≤ 14, -35 ≤ l ≤ 18
Reflections collected	10197
Independent reflections	5017[R(int) = 0.0399]
Data/restraints/parameters	5017/0/312
Goodness-of-fit on F^2	1.056
Final R indexes [I>2σ (I)]	R_1 = 0.0464, wR_2 = 0.0833
Final R indexes [all data]	R_1 = 0.0592, wR_2 = 0.0892
Largest diff. peak/hole / e Å^{-3}	0.28/-0.28
Flack parameter	-0.01(10)

Addition of Acid to $[CH_3C(N(^iPr)_2)CHPPh_3][BF_4]$ 66

$HBF_4.OEt_2$ (5.6 µl, 0.041 mmol) was added to a $CDCl_3$ (0.5 ml) solution of $[CH_3C(N(^iPr)_2)CHPPh_3][BF_4]$ **66**. On one occasion crystals of $[CH_3C(N(^iPr)_2)CH_2PPh_3][BF_4]_2$ **67** were obtained.

Table 6-22 Crystal data and structure refinement for $[CH_3C(N(^iPr)_2)CH_2PPh_3][BF_4]_2$ **67**

Identification code	jml1381
Empirical formula	$C_{27}H_{34}B_2F_8NP$
Formula weight	577.14
Temperature / K	109.9(6)
Crystal system	triclinic
Space group	P-1
a / Å, b / Å, c / Å	8.1578(3), 11.6995(4), 14.8483(6)
α/°, β/°, γ/°	85.959(3), 76.514(3), 80.952(3)
Volume / Å^3	1360.10(9)
Z	2
ρ_{calc} / mg mm^{-3}	1.409
m / mm^{-1}	0.174
F(000)	600.0
Crystal size / mm^3	0.2545 × 0.1684 × 0.0514
2Θ range for data collection	MoKα (λ = 0.71073)
Index ranges	5.646 to 60.162°
Reflections collected	-11 ≤ h ≤ 11, -16 ≤ k ≤ 16, -20 ≤ l ≤ 20
Independent reflections	12239
Data/restraints/parameters	7886 [R_{int} = 0.0199, R_{sigma} = 0.0409]
Goodness-of-fit on F^2	7886/99/464
Final R indexes [I>2σ (I)]	1.035
Final R indexes [all data]	R_1 = 0.0465, wR_2 = 0.1072
Largest diff. peak/hole / e Å^{-3}	R_1 = 0.0616, wR_2 = 0.1161
Flack parameter	0.41/-0.39

Synthesis of $[S(CD_3)_2CH_2COCHPPh_3][BF_4]$ 68

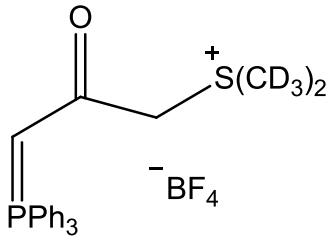

$[H_2C{=}C{=}CHPPh_3][BF_4]$ **40b** (30 mg, 0.075 mmol) was dissolved in d_6-DMSO (0.5 ml) and the resulting solution heated at 150 °C for 30 minutes. At this point no starting material remained and the following data for **68** was obtained although the prodect not isolated.

^{1}H-NMR (500.23 MHz, d^6-DMSO): δ_H 2.35 (d, $^4J_{PH}$ = 2.4 Hz, 2H, C*H*$_2$), 5.49 (d, $^2J_{PH}$ = 12.5 Hz, 1H, C*H*), 7.53-7.90 (16H (high due to oxidation impurity), aromatic);

^{13}C-NMR (125.81 MHz, d^6-DMSO): δ_C 33.7 (d, $^3J_{PC}$ = 6.8 Hz, *C*D$_3$), 39.8 (d, $^1J_{PC}$ = 58.5 Hz, *C*H), 120.8 (d, $^1J_{PC}$ = 89.1 Hz, C_1 of PPh_3), 131.1 (d, J_{PC} = 12.1 Hz, $C_{2\text{ or }3}$ of $OPPh_3$), 132.2 (d, J_{PC} = 12.9 Hz, $C_{2\text{ or }3}$ of PPh_3), 133.6 (d, J_{PC} = 9.9 Hz, $C_{2\text{ or }3}$ of $OPPh_3$), 134.3 (d, $^4J_{PC}$ = 2.1 Hz, C_4 of $OPPh_3$), 134.4 (d, $^1J_{PC}$ = 103.0 Hz, C_1 of PPh_3), 135.6 (d, J_{PC} = 10.7 Hz, $C_{2\text{ or }3}$ of PPh_3), 137.0 (d, $^4J_{PC}$ = 2.7 Hz, C_4 of PPh_3), 203.2 (d, $^2J_{PC}$ = 7.1 Hz, C=O);

^{31}P-NMR (202.51 MHz, d^6-DMSO): δ_P 12.1 (s, unknown), 19.4 (s, PPh_3), 26.6 (s, $OPPh_3$);

^{11}B-NMR (123.27 MHz, d^6-DMSO): δ_B -2.3 (s, BF_4);

^{19}F-NMR (376.17 MHz, d^6-DMSO): δ_F -148.1 (s, $^{10}BF_4$), -148.2 (s, $^{11}BF_4$);

IR (CsCl, solution in DCM), 3054 cm^{-1} (aromatic C-H stretch), 2986 cm^{-1} (alkyl CH stretch), 2306 cm^{-1} (alkyl CD stretch), 1720 cm^{-1} (C=O), 1439 cm^{-1} (P-Ph stretch), 1423 cm^{-1} (P-C stretch), 1269 cm^{-1} ($OPPh_3$), 1057 cm^{-1} (BF_4);

DFT Calculation Methods

Initial optimisations were performed at the (RI-)BP86/SV(P) level, followed by frequency calculations at the same level. Transition states were located by initially performing a constrained minimisation (by freezing internal coordinates that change most during the reaction) of a structure close to the anticipated transition state. This was followed by a frequency calculation to identify the transition vector to follow during a subsequent transition state optimisation. A final frequency calculation was then performed on the optimised transition-state structure. All minima were confirmed as

such by the absence of imaginary frequencies and all transition states were identified by the presence of only one imaginary frequency. Energies, geometries and vibrational frequencies are presented.

Single-point calculations on the (RI-)BP86/SV(P) optimised geometries were performed using the hybrid PBE0 functional and the flexible def2-TZVPP basis set. The (RI-)PBE0/def2-TZVPP SCF energies were corrected for their zero point energies, thermal energies and entropies (obtained from the (RI-)BP86/SV(P)-level frequency calculations). In all calculations, a 28 electron quasi-relativistic ECP replaced the core electrons of Ru and Rh. No symmetry constraints were applied during optimisations. All calculations were performed using the TURBOMOLE V6.4 package using the resolution of identity (RI) approximation.[211-217, 219, 220]

Transition states were verified using the DRC module of TURBOMOLE 6.4. The DRC was run using an initial distortion length of 20, and all transition states were shown to be related to their adjacent minima.

Abbreviations

Å	Angstrom
ADMET	Acyclic Diene Metathesis
Ar	Aryl
ASAP	As Soon As Possible
ATR	Attenuated Total Reflectance
AVR	Acetylene-Vinylidene Rearrangement
BAr^F_4	$[B[3,5\text{-}(CF_3)_2C_6H_3]_4]^-$
bbtp	t-butyl-bis(2-thienyl)phosphine
BINAP	2,2'-Bis(diphenylphosphino)-1,1'-binaphthyl
bpy	Bispyridine
Bu	Butyl
° C	Degrees Celsius
ca.	Circa
CM	Cross Metathesis
cm^{-1}	Wavenumber
COD	1,5-Cyclooctadiene
Cp	Cyclopentadienyl
Cp*	Pentamethylcyclopentadienyl
Cp’	Methylcyclopentadienyl
CP-MAS	Cross-Polarisation Magic Angle Spinning
Cy	Cyclohexyl
DABCO	1,4-Diazabicyclo[2.2.2]octane
DCM	Dicholoromethane
δ	Chemical shift in ppm
DEPT	Distortionless Enhancement by Polarisation Transfer
DFT	Density Functional Theory
dippe	1,2-Bis(diisopropylphosphino)ethane
dmpe	1,2-Bis(dimethylphosphino)ethane
dppb	1,4-Bis(diphenylphosphino)butane
dppe	1,2-Bis(diphenylphosphino)ethane
dppf	1,1'-Bis(diphenylphosphino)ferrocene
dppm	1,1-Bis(diphenylphosphino)methane
dppp	1,3-Bis(diphenylphosphino)propane
ESD	Estimated Standard Deviation

ESI	Electrospray Ionisation
Et	Ethyl
Et_2O	Diethyl ether
EtOH	Ethanol
FTIR	Fourier Transform Infrared
g	Gram
(g)	Gas
HOMO	Highest Occupied Molecular Orbital
IMes	1,3-Dimesityl-imidazol-2-ylidene
^{i}Pr	Isopropyl
IR	Infrared
J	Joules
J	Coupling constant (in Hertz)
kJ	kilojoules
(l)	Liquid
LAPS	Ligand-Assisted Proton Shuttle
LIFDI	Liquid Injection Field Desorption Ionisation
LUMO	Lowest Unoccupied Molecular Orbital
Me	Methyl
MeO-BIPHEP	(6,6'-Dimethoxybiphenyl-2,2'-diyl)bis(diphenylphosphine)
MeOH	Methanol
mg	Milligram
mL	Millilitre
mmol	Millimol
m.p.	Melting Point
MS	Mass Spectrometry
m/z	Mass/Charge Ratio
$NaBAr^F$	Sodium tetrakis[3,5-bis(trifluoromethyl)phenyl]borate
NMR	Nuclear Magnetic Resonance
OAc	Acetate
Ph	Phenyl
PhOH	Phenol
pic	Picoline
PCA	Principle Component Analysis
Pr	Propyl
PTFE	Polytetrafluoroethylene (Teflon)

Py	Pyridine
RCM	Ring Closing Metathesis
ROM	Ring Opening Metathesis
ROMP	Ring Opening Metathesis Polymerisation
(s)	Solid
^{t}Bu	*tert*-Butyl
THF	Tetrahydrofuran
TOF	Time-of-Flight
Tol	Tolyl
Tp	Trispyrazolylborate [$HB(C_3N_2H_3)_3$]
µL	Microliter
µmol	Micromole
ur	Uracil
VT	Variable Temperature
w.r.t	With respect to
XRD	X-ray diffraction

References

1. R. H. Crabtree, *Chem. Rev.*, 1985, **85**, 245.
2. J. McMurry, *Organic Chemistry*, Thomson Brooks/Cole, 7th edn., 2008.
3. C.-H. Jun, *Chem. Soc. Rev.*, 2004, **33**, 610.
4. M. Tobisu and N. Chatani, *Chem. Soc. Rev.*, 2008, **37**, 300.
5. J. March, *Advanced Organic Chemistry*, John Wiley & Sons Inc, New York, 4th edn., 1992.
6. R. Chinchilla and C. Nájera, *Chem. Rev.*, 2007, **107**, 874.
7. J. E. Hein and V. V. Fokin, *Chem. Soc. Rev.*, 2010, **39**, 1302.
8. R. Castarlenas, C. Fischmeister, C. Bruneau and P. H. Dixneuf, *J. Mol. Catal. A: Chem.*, 2004, **213**, 31.
9. Y. Nishibayashi and S. Uemura, in *Metal Vinylidenes and Allenylidenes in Catalysis*, eds. C. Bruneau and P. H. Dixneuf, Wiley-VCH, Weinheim, 2008, ch. 7, pp. 217.
10. J. Uddin, C. M. Morales, J. H. Maynard and C. R. Landis, *Organometallics*, 2006, **25**, 5566.
11. J. F. Hartwig, *Organotransition Metal Chemistry: From Bonding to Catalysis*, University Science Books, 2010.
12. A. E. Shilov and G. B. Shul'pin, *Chem. Rev.*, 1997, **97**, 2879.
13. D. D. Wick and W. D. Jones, *Organometallics*, 1999, **18**, 495.
14. P. E. M. Siegbahn, *J. Phys. Chem.*, 1995, **99**, 12723.
15. D. Balcells, E. Clot and O. Eisenstein, *Chem. Rev.*, 2010, **110**, 749.
16. V. W.-W. Yam, *Acc. Chem. Res.*, 2002, **35**, 555.
17. P. J. Low, *Coord. Chem. Rev.*, 2013, **257**, 1507.
18. N. J. Long and C. K. Williams, *Angew. Chem. Int. Ed.*, 2003, **42**, 2586.
19. J. E. McGrady, T. Lovell, R. Stranger and M. G. Humphrey, *Organometallics*, 1997, **16**, 4004.
20. M. I. Bruce and R. C. Wallis, *J. Organomet. Chem.*, 1978, **161**, C1.
21. J. Chatt and L. A. Duncanson, *J. Chem. Soc.*, 1953, 2939.
22. C. P. Casey and J. T. Brady, *Organometallics*, 1998, **17**, 4620.
23. C. P. Casey, J. T. Brady, T. M. Boller, F. Weinhold and R. K. Hayashi, *J. Am. Chem. Soc*, 1998, **120**, 12500.
24. K. M. Brummond, *Beilstein J. Org. Chem*, 2011, **7**, 394.
25. D. Xu, M. A. Drahl and L. J. Williams, *Beilstein J. Org. Chem*, 2011, **7**, 937.
26. F. Acree and F. B. LaForge, *J. Org. Chem.*, 1939, **04**, 569.
27. P. Maitland and W. H. Mills, *Nature*, 1935, **135**, 994.
28. D. Tejedor, G. Mendez-Abt, L. Cotos and F. Garcia-Tellado, *Chem. Soc. Rev.*, 2013, **42**, 458.
29. J. H. Wotiz and R. J. Palchak, *J. Am. Chem. Soc*, 1951, **73**, 1971.
30. V. B. Kobychev, N. M. Vitkovskaya, N. S. Klyba and B. A. Trofimov, *Russ. Chem. Bull., Int. Ed.*, 2002, **51**, 774.
31. W. H. Ang, R. L. Cordiner, A. F. Hill, T. L. Perry and J. Wagler, *Organometallics*, 2009, **28**, 5568.
32. A. L. Colebatch, I. A. Cade, A. F. Hill and M. M. Bhadbhade, *Organometallics*, 2013, **32**, 4766.
33. T. J. Brown, B. D. Robertson and R. A. Widenhoefer, *J. Organomet. Chem.*, 2014, **758**, 25.
34. B. L. Shaw and A. J. Stringer, *Inorg. Chim. Acta Rev.*, 1973, **7**, 1.

35. V. V. Krivykh, E. S. Taits and M. I. Rybinskaya, *Russ Chem Bull*, 1987, **36**, 2663.
36. C. Elschenbroich, *Organometallics*, Wiley-VCH, Weinheim, 3rd edn., 2005.
37. G. Wilke, B. Bogdanović, P. Hardt, P. Heimbach, W. Keim, M. Kröner, W. Oberkirch, K. Tanaka, E. Steinrücke, D. Walter and H. Zimmermann, *Angew. Chem. Int. Ed.*, 1966, **5**, 151.
38. L. S. Hegedus and Y. Inoue, *J. Am. Chem. Soc*, 1982, **104**, 4917.
39. A. Baeza and C. Nájera, *Synthesis*, 2014, **46**, 0025.
40. J. M. Howell, W. Liu, A. J. Young and M. C. White, *J. Am. Chem. Soc*, 2014.
41. A. Furstner, *Chem. Commun.*, 2011, **47**, 6505.
42. S. Díez-González, N. Marion and S. P. Nolan, *Chem. Rev.*, 2009, **109**, 3612.
43. S. T. Nguyen, L. K. Johnson, R. H. Grubbs and J. W. Ziller, *J. Am. Chem. Soc*, 1992, **114**, 3974.
44. S. T. Diver and A. J. Giessert, *Chem. Rev.*, 2004, **104**, 1317.
45. S. T. Diver, *Coord. Chem. Rev.*, 2007, **251**, 671.
46. C. Fischmeister and C. Bruneau, *Beilstein J. Org. Chem.*, 2011, **7**, 156.
47. C. S. Poulsen and R. Madsen, *Synthesis*, 2003, 1.
48. T. E. Wilhelm, T. R. Belderrain, S. N. Brown and R. H. Grubbs, *Organometallics*, 1997, **16**, 3867.
49. A. Fürstner, P. W. Davies and C. W. Lehmann, *Organometallics*, 2005, **24**, 4065.
50. R. Dussel, D. Pilette, P. H. Dixneuf and W. P. Fehlhammer, *Organometallics*, 1991, **10**, 3287.
51. Y. Nishibayashi, I. Wakiji and M. Hidai, *J. Am. Chem. Soc*, 2000, **122**, 11019.
52. C. Bruneau and P. H. Dixneuf, *Angew. Chem. Int. Ed.*, 2006, **45**, 2176.
53. A. B. Antonova, *Coord. Chem. Rev.*, 2007, **251**, 1521.
54. M. C. Puerta and P. Valerga, *Coord. Chem. Rev.*, 1999, **193-195**, 977.
55. H. Werner, *J. Organomet. Chem.*, 1994, **475**, 45.
56. Y. Wakatsuki, *J. Organomet. Chem.*, 2004, **689**, 4092.
57. M. I. Bruce, *Chem. Rev.*, 1991, **91**, 197.
58. J. M. Lynam, *Chem. Eur. J.*, 2010, **16**, 8238.
59. C. E. Dykstra and H. F. Schaefer, *J. Am. Chem. Soc*, 1978, **100**, 1378.
60. O. J. S. Pickup, I. Khazal, E. J. Smith, A. C. Whitwood, J. M. Lynam, K. Bolaky, T. C. King, B. W. Rawe and N. Fey, *Organometallics*, 2014, **33**, 1751.
61. J. Silvestre and R. Hoffmann, *Helv. Chim. Acta*, 1985, **68**, 1461.
62. J. Zhu and Z. Lin, in *Metal Vinylidenes and Allenylidenes in Catalysis*, eds. C. Bruneau and P. H. Dixneuf, Wiley-VCH, Weinheim, 2008, ch. 4, p. 129.
63. N. M. Kostic and R. F. Fenske, *Organometallics*, 1982, **1**, 974.
64. C. Slugovc, V. N. Sapunov, P. Wiede, K. Mereiter, R. Schmid and K. Kirchner, *J. Chem. Soc., Dalton Trans.*, 1997, 4209.
65. A. N. Nesmeyanov, G. G. Aleksandrov, A. B. Antonova, K. N. Anisimov, N. E. Kolobova and Y. T. Struchkov, *J. Organomet. Chem.*, 1976, **110**, C36.
66. A. B. Antonova, N. E. Kolobova, P. V. Petrovsky, B. V. Lokshin and N. S. Obezyuk, *J. Organomet. Chem.*, 1977, **137**, 55.
67. M. H. Chisholm and H. C. Clark, *J. Am. Chem. Soc*, 1972, **94**, 1532.

68. Y. Wakatsuki, N. Koga, H. Werner and K. Morokuma, *J. Am. Chem. Soc*, 1997, **119**, 360.
69. M. Olivan, O. Eisenstein and K. G. Caulton, *Organometallics*, 1997, **16**, 2227.
70. M. Olivan, E. Clot, O. Eisenstein and K. G. Caulton, *Organometallics*, 1998, **17**, 3091.
71. Y. Wakatsuki, N. Koga, H. Yamazaki and K. Morokuma, *J. Am. Chem. Soc*, 1994, **116**, 8105.
72. F. De Angelis, A. Sgamellotti and N. Re, *Organometallics*, 2002, **21**, 2715.
73. F. De Angelis, A. Sgamellotti and N. Re, *Dalton Trans.*, 2004, 3225.
74. I. de los Ríos, M. J. Tenorio, M. C. Puerta and P. Valerga, *J. Am. Chem. Soc*, 1997, **119**, 6529.
75. C. Bianchini, M. Peruzzini, A. Vacca and F. Zanobini, *Organometallics*, 1991, **10**, 3697.
76. T. Rappert, O. Nuernberg, N. Mahr, J. Wolf and H. Werner, *Organometallics*, 1992, **11**, 4156.
77. H. Werner, M. Baum, D. Schneider and B. Windmueller, *Organometallics*, 1994, **13**, 1089.
78. C. Bianchini, A. Meli, M. Peruzzini, F. Zanobini and P. Zanello, *Organometallics*, 1990, **9**, 241.
79. C. Bianchini, D. Masi, A. Meli, M. Peruzzini, J. A. Ramirez, A. Vacca and F. Zanobini, *Organometallics*, 1989, **8**, 2179.
80. F. J. G. Alonso, A. Höhn, J. Wolf, H. Otto and H. Werner, *Angew. Chem. Int. Ed.*, 1985, **24**, 406.
81. A. Hohn, H. Otto, M. Dziallas and H. Werner, *J. Chem. Soc., Chem. Commun.*, 1987, 852.
82. A. Höhn and H. Werner, *J. Organomet. Chem.*, 1990, **382**, 255.
83. J. Wolf, H. Werner, O. Serhadli and M. L. Ziegler, *Angew. Chem. Int. Ed.*, 1983, **22**, 414.
84. H. Werner and U. Brekau, *Z. Naturforsch.*, 1989, **44b**, 1438.
85. D. B. Grotjahn, X. Zeng and A. L. Cooksy, *J. Am. Chem. Soc*, 2006, **128**, 2798.
86. D. B. Grotjahn, X. Zeng, A. L. Cooksy, W. S. Kassel, A. G. DiPasquale, L. N. Zakharov and A. L. Rheingold, *Organometallics*, 2007, **26**, 3385.
87. M. J. Cowley, J. M. Lynam and J. M. Slattery, *Dalton Trans.*, 2008, 4552.
88. H. Katayama, K. Onitsuka and F. Ozawa, *Organometallics*, 1996, **15**, 4642.
89. N. G. Connelly, W. E. Geiger, C. Lagunas, B. Metz, A. L. Rieger, P. H. Rieger and M. J. Shaw, *J. Am. Chem. Soc*, 1995, **117**, 12202.
90. H. Werner, R. W. Lass, O. Gevert and J. Wolf, *Organometallics*, 1997, **16**, 4077.
91. M. V. Jiménez, E. Sola, F. J. Lahoz and L. A. Oro, *Organometallics*, 2005, **24**, 2722.
92. K. Ilg, M. Paneque, M. L. Poveda, N. Rendón, L. L. Santos, E. Carmona and K. Mereiter, *Organometallics*, 2006, **25**, 2230.
93. K. Venkatesan, O. Blacque, T. Fox, M. Alfonso, H. W. Schmalle, S. Kheradmandan and H. Berke, *Organometallics*, 2005, **24**, 920.
94. K. Venkatesan, T. Fox, H. W. Schmalle and H. Berke, *Eur. J. Inorg. Chem.*, 2005, 901.
95. D. C. Miller and R. J. Angelici, *Organometallics*, 1991, **10**, 79.

96. T. Miura, H. Murata, K. Kiyota, H. Kusama and N. Iwasawa, *J. Mol. Catal. A: Chem.*, 2004, **213**, 59.
97. T. Miura and N. Iwasawa, *J. Am. Chem. Soc*, 2002, **124**, 518.
98. P. J. King, S. A. R. Knox, M. S. Legge, A. G. Orpen, J. N. Wilkinson and E. A. Hill, *J. Chem. Soc., Dalton Trans.*, 2000, 1547.
99. R. Castarlenas and P. H. Dixneuf, *Angew. Chem. Int. Ed.*, 2003, **42**, 4524.
100. M. J. Shaw, S. W. Bryant and N. Rath, *Eur. J. Inorg. Chem.*, 2007, 3943.
101. I. de los Ríos, E. Bustelo, M. C. Puerta and P. Valerga, *Organometallics*, 2010, **29**, 1740.
102. V. K. Singh, E. Bustelo, I. de los Rios, I. Macias-Arce, M. C. Puerta, P. Valerga, M. A. Ortuno, G. Ujaque and A. Lledos, *Organometallics*, 2011, **30**, 4014
103. Y. Ikeda, T. Yamaguchi, K. Kanao, K. Kimura, S. Kamimura, Y. Mutoh, Y. Tanabe and Y. Ishii, *J. Am. Chem. Soc*, 2008, **130**, 16856.
104. Y. Mutoh, Y. Kimura, Y. Ikeda, N. Tsuchida, K. Takano and Y. Ishii, *Organometallics*, 2012, **31**, 5150.
105. Y. Mutoh, Y. Ikeda, Y. Kimura and Y. Ishii, *Chem. Lett.*, 2009, **38**, 534.
106. M. Otsuka, N. Tsuchida, Y. Ikeda, Y. Kimura, Y. Mutoh, Y. Ishii and K. Takano, *J. Am. Chem. Soc*, 2012, **134**, 17746.
107. N. Iwasawa, in *Metal Vinylidenes and Allenylidenes in Catalysis*, eds. C. Bruneau and P. H. Dixneuf, Wiley-VCH, Weinheim, 2008, ch. 5, pp. 159.
108. S. H. Wiedemann and C. Lee, in *Metal Vinylidenes and Allenylidenes in Catalysis*, eds. C. Bruneau and P. H. Dixneuf, Wiley-VCH, Weinheim, 2008, ch. 9, pp. 276.
109. H. Katayama and F. Ozawa, *Coord. Chem. Rev.*, 2004, **248**, 1703.
110. V. Dragutan and I. Dragutan, *Platinum Metal Rev.*, 2004, **48**, 148.
111. C. Bruneau and P. H. Dixneuf, *Acc. Chem. Res.*, 1999, **32**, 311.
112. C. Bruneau, in *Metal Vinylidenes and Allenylidenes in Catalysis*, eds. C. Bruneau and P. H. Dixneuf, Wiley-VCH, Weinheim, 2008, ch. 10, pp. 313.
113. V. Cadierno, J. Francos and J. Gimeno, *Organometallics*, 2011, **30**, 852.
114. H. Doucet, J. Hofer, C. Bruneau and P. H. Dixneuf, *J. Chem. Soc., Chem. Commun.*, 1993, 850.
115. H. Doucet, B. Martin-Vaca, C. Bruneau and P. H. Dixneuf, *J. Org. Chem.*, 1995, **60**, 7247.
116. H. Doucet, N. Derrien, Z. Kabouche, C. Bruneau and P. H. Dixneuf, *J. Organomet. Chem.*, 1998, **551**, 151.
117. F. E. McDonald and A. K. Chatterjee, *Tetrahedron Lett.*, 1997, **38**, 7687.
118. B. M. Trost and A. McClory, *Angew. Chem. Int. Ed.*, 2007, **46**, 2074.
119. V. Cadierno and J. Gimeno, *Chem. Rev.*, 2009, **109**, 3512.
120. M. I. Bruce, *Chem. Rev.*, 1998, **98**, 2797.
121. P. Thaddeus, J. M. Vrtilek and C. A. Gottlieb, *Astrophys. J.*, 1985, **299**, L63.
122. J. Cernicharo, C. A. Gottlieb, M. Guelin, T. C. Killian, G. Paubert, P. Thaddeus and J. M. Vrtilek, *Astrophys. J.*, 1991, **368**, L39.
123. H. E. Matthews and W. M. Irvine, *Astrophys. J.*, 1985, **298**, L61.
124. W. J. Hehre, J. A. Pople, W. A. Lathan, L. Radom, E. Wasserman and Z. R. Wasserman, *J. Am. Chem. Soc*, 1976, **98**, 4378.
125. C. D. Sherrill, C. G. Brandow, W. D. Allen and H. F. Schaefer, *J. Am. Chem. Soc*, 1996, **118**, 7158.

126. J. F. Stanton, J. T. DePinto, R. A. Seburg, J. A. Hodges and R. J. McMahon, *J. Am. Chem. Soc*, 1997, **119**, 429.
127. M. A. Esteruelas, A. V. Gómez, A. M. López, J. Modrego and E. Oñate, *Organometallics*, 1997, **16**, 5826.
128. M. Drexler, T. Haas, S.-M. Yu, H. S. G. Beckmann, B. Weibert and H. Fischer, *J. Organomet. Chem.*, 2005, **690**, 3700.
129. N. E. Kolobova, L. L. Ivanov, O. S. Zhvanko, O. M. Khitrova, A. S. Batsanov and Y. T. Struchkov, *J. Organomet. Chem.*, 1984, **262**, 39.
130. M. A. Esteruelas, A. V. Gómez, A. M. López, J. Modrego and E. Oñate, *Organometallics*, 1998, **17**, 5434.
131. M. Jiménez-Tenorio, M. D. Palacios, M. C. Puerta and P. Valerga, *J. Organomet. Chem.*, 2004, **689**, 2776.
132. V. Cadierno, M. P. Gamasa, J. Gimeno, M. C. López-González, J. Borge and S. García-Granda, *Organometallics*, 1997, **16**, 4453.
133. V. Cadierno, M. P. Gamasa, J. Gimeno, J. Borge and S. GarcÃ-a-Granda, *Organometallics*, 1997, **16**, 3178.
134. V. Cadierno, S. Conejero, M. P. Gamasa, J. Gimeno and M. A. Rodriguez, *Organometallics*, 2002, **21**, 203.
135. V. Cadierno, S. Conejero, M. P. Gamasa, J. Gimeno, I. Asselberghs, S. Houbrechts, K. Clays, A. Persoons, J. Borge and S. García-Granda, *Organometallics*, 1999, **18**, 582.
136. V. Cadierno, M. Pilar Gamasa and J. Gimeno, *J. Chem. Soc., Dalton Trans.*, 1999, 1857.
137. V. Cadierno, M. P. Gamasa and J. Gimeno, *J. Organomet. Chem.*, 2001, **621**, 39.
138. B. E. R. Schilling, R. Hoffmann and D. L. Lichtenberger, *J. Am. Chem. Soc*, 1979, **101**, 585.
139. J. P. Selegue, *Organometallics*, 1982, **1**, 217.
140. M. Martin, O. Gevert and H. Werner, *J. Chem. Soc., Dalton Trans.*, 1996, 2275.
141. K. J. Harlow, A. F. Hill and J. D. E. T. Wilton-Ely, *J. Chem. Soc., Dalton Trans.*, 1999, 285.
142. A. Fürstner, J. Grabowski and C. W. Lehmann, *J. Org. Chem.*, 1999, **64**, 8275.
143. A. Fürstner, O. Guth, A. Düffels, G. Seidel, M. Liebl, B. Gabor and R. Mynott, *Chem. Eur. J.*, 2001, **7**, 4811.
144. H.-J. Schanz, L. Jafarpour, E. D. Stevens and S. P. Nolan, *Organometallics*, 1999, **18**, 5187.
145. R. Castarlenas, C. Vovard, C. Fischmeister and P. H. Dixneuf, *J. Am. Chem. Soc*, 2006, **128**, 4079.
146. V. Dragutan, I. Dragutan and F. Verpoort, *Platinum Metal Rev.*, 2005, **49**, 33.
147. H. Fischer and N. Szesni, *Coord. Chem. Rev.*, 2004, **248**, 1659.
148. V. Cadierno, P. Crochet and J. Gimeno, in *Metal Vinylidenes and Allenylidenes in Catalysis*, eds. C. Bruneau and P. H. Dixneuf, Wiley-VCH, Weinheim, 2008, ch. 2, pp. 61.
149. B. J. Teobald, *Tetrahedron*, 2002, **58**, 4133.
150. Y. Nishibayashi, M. D. Milton, Y. Inada, M. Yoshikawa, I. Wakiji, M. Hidai and S. Uemura, *Chem. Eur. J.*, 2005, **11**, 1433.
151. Y. Nishibayashi, I. Wakiji, Y. Ishii, S. Uemura and M. Hidai, *J. Am. Chem. Soc*, 2001, **123**, 3393.

152. Y. Inada, Y. Nishibayashi and S. Uemura, *Angew. Chem. Int. Ed.*, 2005, **44**, 7715.
153. H. Matsuzawa, Y. Miyake and Y. Nishibayashi, *Angew. Chem. Int. Ed.*, 2007, **46**, 6488.
154. M. Ikeda, Y. Miyake and Y. Nishibayashi, *Chem. Eur. J.*, 2012, **18**, 3321.
155. K. Motoyama, M. Ikeda, Y. Miyake and Y. Nishibayashi, *Organometallics*, 2012, **31**, 3426.
156. I. Dragutan and V. Dragutan, *Platinum Metal Rev.*, 2006, **50**, 81.
157. R. Malcea and P. H. Dixneuf, in *Metal Vinylidenes and Allenylidenes in Catalysis*, ed. P. H. D. C. Bruneau, Wiley-VCH, Weinheim, 2008, ch. 8, pp. 251.
158. A. Furstner, M. Picquet, C. Bruneau and P. H. Dixneuf, *Chem. Commun.*, 1998, 1315.
159. M. Picquet, D. Touchard, C. Bruneau and P. H. Dixneuf, *New J. Chem.*, 1999, **23**, 141.
160. A. Fürstner, M. Liebl, C. W. Lehmann, M. Picquet, R. Kunz, C. Bruneau, D. Touchard and P. H. Dixneuf, *Chem. Eur. J.*, 2000, **6**, 1847.
161. A. Furstner and P. W. Davies, *Chem. Commun.*, 2005, 2307.
162. A. Mortreux and O. Coutelier, *J. Mol. Catal. A: Chem.*, 2006, **254**, 96.
163. W. Zhang and J. S. Moore, *Adv. Synth. Catal.*, 2007, **349**, 93.
164. R. R. Schrock, *Angew. Chem. Int. Ed.*, 2006, **45**, 3748.
165. M. Bindl, R. Stade, E. K. Heilmann, A. Picot, R. Goddard and A. Fürstner, *J. Am. Chem. Soc*, 2009, **131**, 9468.
166. C. Deraedt, M. d'Halluin and D. Astruc, *Eur. J. Inorg. Chem.*, 2013, **2013**, 4881.
167. A. Fürstner and G. Seidel, *J. Organomet. Chem.*, 2000, **606**, 75.
168. R. W. Mitchell, A. Spencer and G. Wilkinson, *J. Chem. Soc., Dalton Trans.*, 1973, 846.
169. C. Welby, PhD, University of York, 2011.
170. J. M. Lynam, C. E. Welby and A. C. Whitwood, *Organometallics*, 2009, **28**, 1320.
171. S. D. Robinson and M. F. Uttley, *J. Chem. Soc., Dalton Trans.*, 1973, 1912.
172. G. B. Deacon and R. J. Phillips, *Coord. Chem. Rev.*, 1980, **33**, 227.
173. C. E. Welby, T. O. Eschemann, C. A. Unsworth, E. J. Smith, R. J. Thatcher, A. C. Whitwood and J. M. Lynam, *Eur. J. Inorg. Chem.*, 2012, 1493.
174. D. G. Johnson, J. M. Lynam, J. M. Slattery and C. E. Welby, *Dalton Trans.*, 2010, **39**, 10432.
175. O. J. S. Pickup, MSc by Research, University of York, 2012.
176. H. Katayama and F. Ozawa, *Organometallics*, 1998, **17**, 5190.
177. C. Grunwald, M. Laubender, J. Wolf and H. Werner, *J. Chem. Soc., Dalton Trans.*, 1998, 833.
178. X. L. Lu, S. Y. Ng, J. J. Vittal, G. K. Tan, L. Y. Goh and T. S. A. Hor, *J. Organomet. Chem.*, 2003, **688**, 100.
179. M. C. Barral, R. Jiménez-Aparicio, R. Kramolowsky and I. Wagner, *Polyhedron*, 1993, **12**, 903.
180. W.-K. Wong, K.-K. Lai, M.-S. Tse, M.-C. Tse, J.-X. Gao, W.-T. Wong and S. Chan, *Polyhedron*, 1994, **13**, 2751.
181. T. Arliguie, B. Chaudret, G. Chung and F. Dahan, *Organometallics*, 1991, **10**, 2973.
182. E. Bustelo and P. H. Dixneuf, *Adv. Synth. Catal.*, 2005, **347**, 393.

183. E. Bustelo and P. H. Dixneuf, *Adv. Synth. Catal.*, 2007, **349**, 933.
184. M. A. Fox and J. K. Whitesall, *Organic Chemistry*, Jones and Barlett Publishers, Sudbury, Massachusetts, 3rd edn., 2004.
185. H. A. van Kalkeren, A. L. Blom, F. P. J. T. Rutjes and M. A. J. Huijbregts, *Green Chem.*, 2013, **15**, 1255.
186. K. C. K. Swamy, N. N. B. Kumar, E. Balaraman and K. V. P. P. Kumar, *Chem. Rev.*, 2009, **109**, 2551.
187. *European Pat.,* WO2004018399 (A1) 2004.
188. P. B. Critchlow and S. D. Robinson, *Inorg. Chem.*, 1978, **17**, 1902.
189. T. Ohta, H. Takaya and R. Noyori, *Inorg. Chem.*, 1988, **27**, 566.
190. M. Kitamura, M. Tokunaga and R. Noyori, *J. Org. Chem.*, 1992, **57**, 4053.
191. M. Al-Noaimi, I. Warad, O. S. Abdel-Rahman, F. F. Awwadi, S. F. Haddad and T. B. Hadda, *Polyhedron*, 2013, **62**, 110.
192. T. V. Ashworth, D. C. Liles, D. J. Robinson, E. Singleton, N. J. Coville, E. Darling and A. J. Markwell, *S. Afr. J. Chem.*, 1987, **40**, 183.
193. M. A. Bennett and A. K. Smith, *J. Chem. Soc., Dalton Trans.*, 1974, 233.
194. D. A. Tocher, R. O. Gould, T. A. Stephenson, M. A. Bennett, J. P. Ennett, T. W. Matheson, L. Sawyer and V. K. Shah, *J. Chem. Soc., Dalton Trans.*, 1983, 1571.
195. T. J. Geldbach, C. J. den Reijer, M. Wörle and P. S. Pregosin, *Inorg. Chim. Acta*, 2002, **330**, 155.
196. V. F. Kuznetsov, G. R. Jefferson, G. P. A. Yap and H. Alper, *Organometallics*, 2002, **21**, 4241.
197. N. P. Hiett, J. M. Lynam, C. E. Welby and A. C. Whitwood, *J. Organomet. Chem.*, 2010, **696**, 378.
198. C. A. Tolman, *Chem. Rev.*, 1977, **77**, 313.
199. O. J. S. Pickup, I. Khazal, E. J. Smith, A. C. Whitwood, J. M. Lynam, K. Bolaky, T. C. King, B. W. Rawe and N. Fey, *Organometallics*, 2014.
200. D. G. Johnson, PhD, University of York, 2013.
201. B. Powała, M. Kubicki, G. Spólnik, W. Danikiewicz and C. Pietraszuk, *J. Organomet. Chem.*, 2014, **752**, 109.
202. E. A. Shaffer, C.-L. Chen, A. M. Beatty, E. J. Valente and H.-J. Schanz, *J. Organomet. Chem.*, 2007, **692**, 5221.
203. M. I. Bruce, M. G. Humphrey, M. R. Snow and E. R. T. Tiekink, *Journal of Organometallic Chemistry*, 1986, **314**, 213.
204. H. Hamidov, J. C. Jeffery and J. M. Lynam, *Chem. Commun.*, 2004, 1364.
205. M. J. Cowley, J. M. Lynam, R. S. Moneypenny, A. C. Whitwood and A. J. Wilson, *Dalton Transactions*, 2009, 9529.
206. R. K. Hocking and T. W. Hambley, *Organometallics*, 2007, **26**, 2815.
207. A. F. Hill, in *Comprehensive Organometallic Chemistry II*, eds. E. W. Abel, F. G. A. Stone and G. Wilkinson, Elsevier, Oxford, 1995, vol. 7, pp. 299.
208. S.-H. Choi, I. Bytheway, Z. Lin and G. Jia, *Organometallics*, 1998, **17**, 3974.
209. M. R. Torres, A. Perales, H. Loumrhari and J. Ros, *J. Organomet. Chem.*, 1990, **385**, 379.
210. http://webcsd.cds.rsc.org/, Accessed 1st September, 2013.
211. F. Weigend, *Phys. Chem. Chem. Phys.*, 2006, **8**, 1057.
212. K. Eichkorn, F. Weigend, O. Treutler and R. Ahlrichs, *Theor Chem Acc*, 1997, **97**, 119.

213. P. Deglmann, F. Furche and R. Ahlrichs, *Chem. Phys. Lett.*, 2002, **362**, 511.
214. M. von Arnim and R. Ahlrichs, *J. Chem. Phys.*, 1999, **111**, 9183.
215. O. Treutler and R. Ahlrichs, *J. Chem. Phys.*, 1995, **102**, 346.
216. K. Eichkorn, O. Treutler, H. Öhm, M. Häser and R. Ahlrichs, *Chem. Phys. Lett.*, 1995, **240**, 283.
217. R. Ahlrichs, M. Bär, M. Häser, H. Horn and C. Kölmel, *Chem. Phys. Lett.*, 1989, **162**, 165.
218. T. Koga and H. Kobayashi, *J. Chem. Phys.*, 1985, **82**, 1437.
219. P. Pulay, *Chem. Phys. Lett.*, 1980, **73**, 393.
220. P. Császár and P. Pulay, *J. Mol. Struct.*, 1984, **114**, 31.
221. M. Jiménez-Tenorio, M. C. Puerta, P. Valerga, M. A. Ortuño, G. Ujaque and A. Lledós, *Inorg. Chem.*, 2013, **52**, 8919.
222. K. S. Alongi and G. C. Shields, in *Annual Reports in Computational Chemistry*, ed. A. W. Ralph, Elsevier, 2010, vol. Volume 6, pp. 113.
223. M. D. Liptak, K. C. Gross, P. G. Seybold, S. Feldgus and G. C. Shields, *J. Am. Chem. Soc*, 2002, **124**, 6421.
224. M. D. Liptak and G. C. Shields, *J. Am. Chem. Soc*, 2001, **123**, 7314.
225. E. J. Smith, D. G. Johnson, R. J. Thatcher, A. C. Whitwood and J. M. Lynam, *Organometallics*, 2013, **32**, 7407.
226. J. R. Sanders, *J. Chem. Soc., Dalton Trans.*, 1973, 743.
227. S. Bajo, M. A. Esteruelas, A. M. López and E. Oñate, *Organometallics*, 2011, **30**, 5710.
228. Y.-S. Gal, *Eur. Polym. J.*, 1997, **33**, 169.
229. S. Abbott, S. G. Davies and P. Warner, *J. Organomet. Chem.*, 1983, **246**, c65.
230. B. Chin, A. J. Lough, R. H. Morris, C. T. Schweitzer and C. D'Agostino, *Inorg. Chem.*, 1994, **33**, 6278.
231. M. A. Fox, J. E. Harris, S. Heider, V. Pérez-Gregorio, M. E. Zakrzewska, J. D. Farmer, D. S. Yufit, J. A. K. Howard and P. J. Low, *J. Organomet. Chem.*, 2009, **694**, 2350.
232. K. Banert and J. Lehmann, in *Modern Allene Chemistry*, eds. N. A. Krause and S. K. Hashmi, Wiley-VCH, Weinheim, 2008, vol. 1, ch. 7, pp. 359
233. G. B. Bagdasaryan, P. S. Pogosyan, G. A. Panosyan and M. G. Indzhikyan, *Russ J Gen Chem*, 2008, **78**, 1177.
234. M. A. Esteruelas, F. J. Lahoz, M. Martín, E. Oñate and L. A. Oro, *Organometallics*, 1997, **16**, 4572.
235. J. Wolf and H. Werner, *Organometallics*, 1987, **6**, 1164.
236. M. J. Cowley, PhD, University of York, 2008.
237. H. Werner, J. Wolf, F. J. G. Alonso, M. L. Ziegler and O. Serhadli, *J. Organomet. Chem.*, 1987, **336**, 397.
238. M. Schäfer, J. Wolf and H. Werner, *Organometallics*, 2004, **23**, 5713.
239. H. Werner, D. Schneider and M. Schulz, *J. Organomet. Chem.*, 1993, **451**, 175.
240. M. J. Cowley, J. M. Lynam and A. C. Whitwood, *J. Organomet. Chem.*, 2010, **695**, 18.
241. H. Werner, R. Wiedemann, M. Laubender, B. Windmüller and J. Wolf, *Chem. Eur. J.*, 2001, **7**, 1959.
242. H. Werner, R. Wiedemann, N. Mahr, P. Steinert and J. Wolf, *Chem. Eur. J.*, 1996, **2**, 561.

243. E. E. Schweizer, S. D. Goff and W. P. Murray, *J. Org. Chem.*, 1977, **42**, 200.
244. N. Zein, A. Sinha, W. McGahren and G. Ellestad, *Science*, 1988, **240**, 1198.
245. A. Rudi, M. Schleyer and Y. Kashman, *J. Nat. Prod.*, 2000, **63**, 1434.
246. S. L. Iverson and J. P. Uetrecht, *Chem. Res. Toxicol.*, 2001, **14**, 175.
247. R. E. Martin and F. Diederich, *Angew. Chem. Int. Ed.*, 1999, **38**, 1350.
248. B. Alcaide, P. Almendros and C. Aragoncillo, *Chem. Soc. Rev.*, 2010, **39**, 783.
249. G. R. Fulmer, A. J. M. Miller, N. H. Sherden, H. E. Gottlieb, A. Nudelman, B. M. Stoltz, J. E. Bercaw and K. I. Goldberg, *Organometallics*, 2010, **29**, 2176.
250. L. J. B. O. V. Dolomanov, R. J. Gildea, J. A. K. Howard and H. Puschmann, *J. Appl. Cryst.* , 2009, **42**, 339.
251. C. G. Palatinus L., *J. Appl. Cryst.*, 2007, **40**, 786.
252. G. M. Sheldrick, *Acta Cryst.*, 2008, **A64**, 112.
253. M. A. Bennett, T. N. Huang, T. W. Matheson, A. K. Smith, S. Ittel and W. Nickerson, in *Inorganic Syntheses*, John Wiley & Sons, Inc., 1982, vol. 21, pp. 74.
254. P. S. Hallman, T. A. Stephenson and G. Wilkinson, in *Inorganic Syntheses*, John Wiley & Sons, Inc., 1970, vol. 12, pp. 237.
255. gNMR, Version 5.0.6.0, Ivory Software, 5.0.6.0 edn., 2006.
256. http://www.sigmaaldrich.com/spectra/fnmr/FNMR010119.PDF.
257. A. Davison and J. P. Selegue, *J. Am. Chem. Soc*, 1978, **100**, 7763.
258. R. M. Bullock, *J. Am. Chem. Soc*, 1987, **109**, 8087.